N8470176
8-5094

# DESIGN, MANUFACTURE AND TEST OF A PROTOTYPE POWERED WHEEL FOR AIRCRAFT

By Robert K. Van Ausdal

Prepared under Contract No. NAS1-13787 by
THE BENDIX CORPORATION
ELECTRODYNAMICS DIVISION
North Hollywood, Ca.

for

NATIONAL AERONAUTICS AND SPACE ADMINISTRATION

TABLE OF CONTENTS


| Section | Page No. |
|---|---|
| Summary | 1 |
| Introduction | 4 |
| Symbols and Units | 6 |
| Performance Requirements/Description and Operation | 12 |
| Performance Requirements | 12 |
| System Description | 13 |
| System Operation | 15 |
| Dynavector Principle of Operation | 16 |
| Design Analyses | 28 |
| Sizing | 28 |
| Pressure Loss | 34 |
| Static Performance | 42 |
| Dynamic Performance | 46 |
| Loads and Stress | 56 |
| Thermal Analysis Summary | 85 |
| Weight Summary | 88 |
| Results | 92 |
| Conclusions | 147 |
| Recommendations | 191 |
| Appendices | |
| A - Statement of Work | A-1 |
| B - Pressure Loss Analyses | B-1 |
| C - Dynamic Performance | C-1 |
| D - Clutch Torque Capability | D-1 |
| E - Thermal Analysis | E-1 |
| F - Parts List | F-1 |
| G - Test Plans (7-3266 & 7-3277) | G-1 |
| H - Testing Based on Recommendation No. 2 | H-1 |
| References | R-1 |




**Preceding Page Blank**

List of Figures


| Figure No. | Title | Page No. |
|---|---|---|
| 1 | Cross Section - Wheel Drive Installation, Typical 737-100 | 3 |
| 2a | Flight Worthy System Arrangement Schematic | 14 |
| 2b | Test System Arrangement Schematic | 14 |
| 3 | Low Ratio Orbiter Configuration | 17 |
| 4 | Powered Wheel Drive Motor, Drawing 3311870, Sheet 1 (Shown with Clutch Discs Removed) | 21 |
| 5 | Powered Wheel Drive Motor, Drawing 3311870, Sheet 2 | 22 |
| 6 | Powered Wheel Drive Motor, Isometric | 23 |
| 7 | Dynavector Actuator Epicyclic Transmission Arrangements | 28 |
| 8 | Geometry for Derivation of Orbit Motor Torque and Displacement Equations | 30 |
| 9 | Flow Channel Model Through One Motor (C2/C1 Circuit Shown) | 37 |
| 10 | Predicted Torque Vs. Speed in Parallel Operation | 43 |
| 11 | Predicted Torque Vs. Speed in Series Operation | 44 |
| 12 | Block Diagram - Directional Control Valve and Motor | 47 |
| 13 | Block Diagram - Clutch and Aircraft | 48 |
| 14 | Simplified Block Diagram | 50 |
| 15 | Bearing Spacing and Effective Spread | 65 |
| 16 | Equivalent Curves for Velocity and Pressure Differential at SOW Condition 2 (Braking) | 86 |

List of Figures (Continued)


| Figure No. | Title | Page No. |
|---|---|---|
| 17 | P/N 3311870 Powered Wheel Drive Actuator Assembly (Minus Four Clutch Plates) | 93 |
| 18 | Outboard View of P/N 3311870 Actuator Without Clutch Plates, Thrust Bearing Assembly and Drive Plate Assembly | 94 |
| 19 | Outboard View of P/N 3311870 Actuator Without Clutch Plates, Thrust Brg. Assembly, Drive Plate Assembly and Inner Race | 95 |
| 20 | Inboard View of P/N 3311870 Actuator Without Hydraulic Quills | 96 |
| 21 | View of P/N 3311870 Actuator Without Outboard Housing | 97 |
| 22 | View of P/N 3311870 Actuator Without Outboard Housing | 98 |
| 23 | Same View as Figure 22 Without Orbiter Ring, Output Shaft and Without Some Vanes | 99 |
| 24 | P/N 3311870 Actuator Subassembly and Components | 100 |
| 25 | Part of P/N 3311870 Actuator Components | 101 |
| 26 | Test Arrangement - No-Load (Front) | 102 |
| 27 | Test Arrangement - No-Load (Rear) | 103 |
| 28 | Test Arrangement - Close-Up | 104 |
| 29 | Load Test Setup | 105 |
| 30 | Inboard Housing Intercircuit Leakage Vs Differential Pressure | 106 |

List of Figures (Continued)


| Figure No. | Title | Page No. |
|---|---|---|
| 31 | Individual Motor Test Arrangement | 107 |
| 32 | Series Mode Flow Vs Pressure Loss With One Idle Motor | 109 |
| 33 | Test Arrangement Line Loss Vs Flow | 110 |
| 34 | Cycling and Static Test Arrangement | 111 |
| 35 | Individual Hydraulic Circuit Flow Vs Average Pressure Loss | 112 |
| 36 | Pressure Level Effect on Volumetric Efficiency | 113 |
| 37 | Total Chamber Flow Versus Speed | 115 |
| 38 | Total Chamber Flow and Case Drain Leakage Versus Supply Pressure | 116 |
| 39 | Output Shaft, Part No. 3311968 - Total Composite Error at Four Axial Locations | 119 |
| 40 | Orbiter Gear, Part No. 3311974 - Total Composite Error at Outboard Axial Location | 120 |
| 41 | Powered Wheel Drive Output Shaft Speef Versus Flow | 122 |
| 42 | Powered Wheel Drive Pressure Loss Versus Flow | 124 |
| 43 | Orbiter Ring, P/N 3311970, Showing Surface Damage | 125 |
| 44 | Close-Up of Orbiter Ring, P/N 3311970 Surface Damage | 126 |
| 45 | Inboard Housing, P/N 3311945, Showing Surface Damage | 127 |
| 46 | Close-Up of Inboard Housing, P/N 3311945, Surface Damage | 128 |
| 47 | Ring Orbiter, P/N 3311970, Sealing Surface Damage | 129 |

List of Figures (Continued)


| Figure No. | Title | Page No. |
|---|---|---|
| 48 | Outboard Housing, P/N 3311940, Metering Surface Damage | 130 |
| 49 | Outboard Housing, P/N 3311940, Metering Surface Damage | 131 |
| 50 | Ring Orbiter Sealing Pattern (Top Side as Tested) | 132 |
| 51 | Configuration 1 Mechanical Load Test Arrangement | 134 |
| 52 | Configuration 1 Mechanical Load Test Arrangement (Outboard Housing Removed for Clarity) | 135 |
| 53 | Orbiter Mechanical Load Test | 136 |
| 54 | Orbiter Mechanical Load Test | 137 |
| 55 | Orbiter Mechanical Load Test | 138 |
| 56 | Orbiter Ring/Ring gear/Output Shaft Assembly (Configuration 2) Load Test Results | 139 |
| 57 | Orbiter Ring Mechanical Load Test Arrangement | 140 |
| 58 | Ring Gear Load Test Results | 141 |
| 59 | Metering Slot/Orbiter Ring Overlap | 142 |
| 60 | Port Leakage Test Arrangement | 144 |
| 61 | Braze Assembly P/N 3311946 Heat Treat Cracks | 148 |
| 62 | Braze Assembly P/N 3311946 Heat Treat Cracks | 149 |
| 63 | Braze Assembly P/N 3311946 - Plates 4 and 5 Separation | 150 |
| 64 | Braze Assembly P/N 3311946 - Sketch Showing Heat Treat Cracks | 151 |
| 65 | Braze Assembly P/N 3311946, Showing Unbrazed Portion of Plates 4 and 5 and Corresponding Repair Welding | 152 |

List of Figures (Continued)


| Figure No. | Title | Page No. |
|---|---|---|
| 66 | Supply Pressure Effect on Volumetric Efficiency | 155 |
| 67 | Orbiter Ring Forces Diagram | 158 |
| 68 | 32 Pitch Gears Maximum Overlap | 159 |
| 69 | 24 Pitch Gears Maximum Overlap | 162 |
| 70 | Deflected Form of Orbiter/Gear at 4000 PSI | 164 |
| 71 | Concentrated Frictional Orbiter Ring Loading | 165 |
| 72 | Normal Porting Conditions Corresponding to Figure 71(a) Orientation | 172 |
| 73 | Inboard Housing Metering Slot | 175 |
| 74 | Same View as Figure 22 Without Orbiter Ring, Output Shaft and Without Some Vanes | 176 |
| 75 | Inboard Housing Metering Slot | 177 |
| 76 | Inboard Housing Metering Slot | 178 |
| 77 | Inboard Housing Metering Slot | 179 |
| 78 | Inboard Housing Metering Slot | 180 |
| 79 | Outboard Housing Metering Slot | 181 |
| 80 | Outboard Housing Metering Slot | 182 |
| 81 | Outboard Housing Metering Slot | 183 |
| 82 | Outboard Housing Metering Slot | 184 |
| 83 | Additional Vent Slots to Eliminate Erosion/Cavitation Damage to Metering Slot Edges | 189 |
| 84 | Recommended Orbiter Ring Slot With Change to Create Effective Venting Slots | 193 |
| 85 | Proposed Cams to Prevent Gear Disengagement | 195 |
| 86 | Inverted Vane Modification of Orbiter Ring P/N 3311952 | 197 |

List of Tables


| Table No. | Title | Page No. |
|---|---|---|
| 1 | Major Component Materials and Special Processing | 26 |
| 2 | Summary of Wheel Drive Parameters | 35 |
| 3 | $\sum \frac{K}{\frac{(A_{dn}Qt)2}{Q}}$ Determination for Flow Through One Motor (C2/C1 Flow) | 39 |
| 4 | Calculated Time and Distance to Reach Various Speeds | 53 |
| 5 | Summary of Bearing Loads, Speed and Time | 57 |
| 6 | Bearing Equivalent Dynamic Loads and Speed (Based on Required Test Cycles and Data from Table 5) | 58 |
| 7 | Equations 63/64 Parameters for Bearing No. 1 (INA NK105/26) | 60 |
| 8 | Equations 63/64 Parameters for Bearing No. 2 (INA NK95/26) | 60 |
| 9 | Results of Calculations for Gear Mesh Configuration No. 1 | 74 |
| 10 | Results of Calculations for Gear Mesh Configuration No. 2 | 76 |
| 11 | Results of Calculations for Gear Mesh Configuration No. 3 | 77 |
| 12 | Results of Calculations for Gear Mesh Configuration No. 4 | 78 |
| 13 | Margins of Safety - Summary | 87 |
| 14 | Summary of Thermal Analysis Showing Heat Input and Fluid Temperature for SOW Conditions | 89 |
| 15 | Estimated Wheel Drive Assembly Weight (Includes Clutch) | 90 |
| 16 | Estimated Weight of the Modified Wheel/Brake and the Weight Impact | 91 |
| 17 | Powered Wheel Drive Gear Disengagement Data | 117 |
| 18 | Component Size and Assembly Performance Parameter Changes | 121 |
| 19 | Port Leakage Test Results | 145 |
| 20 | Port Leakage Test Results After Plating Orbiter Ring Slots | 145 |
| 21 | Vane Leakage | 146 |

# DESIGN, MANUFACTURE AND TEST OF A PROTOTYPE POWERED WHEEL FOR AIRCRAFT

By Robert K. Van Ausdal
Bendix Electrodynamics Division

## SUMMARY

A hydraulically powered wheel drive motor, suitable for installation inside one wheel on each of the two main landing gears of the Boeing 737-100 type aircraft, was designed, manufactured and tested. The purpose of the program was to evaluate a hydromechanical means of driving the aircraft wheels for taxi operations (rather than the main engines) prior to initiating a flight test program that would demonstrate feasibility and evaluate handling qualities.

Dynamometer testing of the prototype unit to demonstrate the capability of the Bendix DYNAVECTOR® concept in meeting the design goals, stated in the Statement of Work, Appendix A, could not be accomplished because of design deficiencies encountered in the static and cyclic performance phase of the test program. The proven DYNAVECTOR® concept for rotary actuation, which consists of a captive-vane hydraulic motor and epicyclic gear transmission, was designed and implemented to meet the typical taxi operational requirements for the aircraft. These requirements are a 15 mph (24.14 km/h) maximum taxi speed, reverse operation, braking capability and 57,000 lb-in (6.44 kN-m) stall torque. These goals were to be attained during simulation of six landing-through-take-off cycles with the hydraulically actuated clutch of the assembly, disengaged above the maximum taxi speed, and 94 typical ground taxi operational cycles after landing-to-take-off. Simulation was to have been accomplished using a dynamometer with an applied drag equivalent of 2 percent and 4 percent runway grades, using MIL-H-5606 hydraulic fluid supplied at 4000 psi (27.58 $MN/m^2$) at a maximum flow rate of 45 GPM (170.37 lit/min).

To meet the required output torque and maximum speed within the confines of the restrictive envelope of the 737-100 wheel, it was determined necessary (through an installation design study, Figure 1) to modify the wheel and eliminate 60 percent of the brake discs. A previous computer study, conducted by the Bendix Energy Controls Division, demonstrated that adequate braking existed on a 10,000-ft (3.05 km) runway without any braking capability in one wheel of each main landing gear. Design modification of the wheel and brakes resulted in an estimated weight saving of 35.3 pounds (16.01 kg) for each of the two wheels containing the wheel drive unit. This partially compensates for the 142.0 pounds (64.41 kg) weight of the actuator/clutch assembly for a net estimated weight increase per wheel of only 106.7 pounds (48.40 kg). This weight impact does not include the weight of the necessary hydraulic lines, valving or power supply.

Also to overcome the restrictive envelope, it was necessary to design the hydraulic porting of the 12 chamber motors to provide parallel/series operation controlled by a selector valve. Parallel operation allows the motor to operate as two six-chamber motors to provide high torque for starting and up to 7.5 mph (12.7 km/h). Switching to series operation permits lower torque taxi operations from 7.5 to 15 mph (12 to 24 km/h) without the need for additional pump capacity.

The design deficiencies uncovered involved both the motor and the transmission. The motor deficiency is excessive internal leakage primarly caused by erosion and, or cavitation, of the edges of the self commutating metering slots. The erosion/cavitation damage was restricted to the tungsten-carbide flame plated wear coating on the metering faces of both housings. The leakage was so excessive that output torque was greatly affected. The transmission deficiency is caused by excessive compliance of the motor orbiting ring gear which allowed it to disengage from the output gear under hydraulic loading.

Both of these deficiencies can be overcome as covered in the section on Recommendations, but the additional costs of redesign, fabrication, and testing are beyond the current limitations existing for this program.

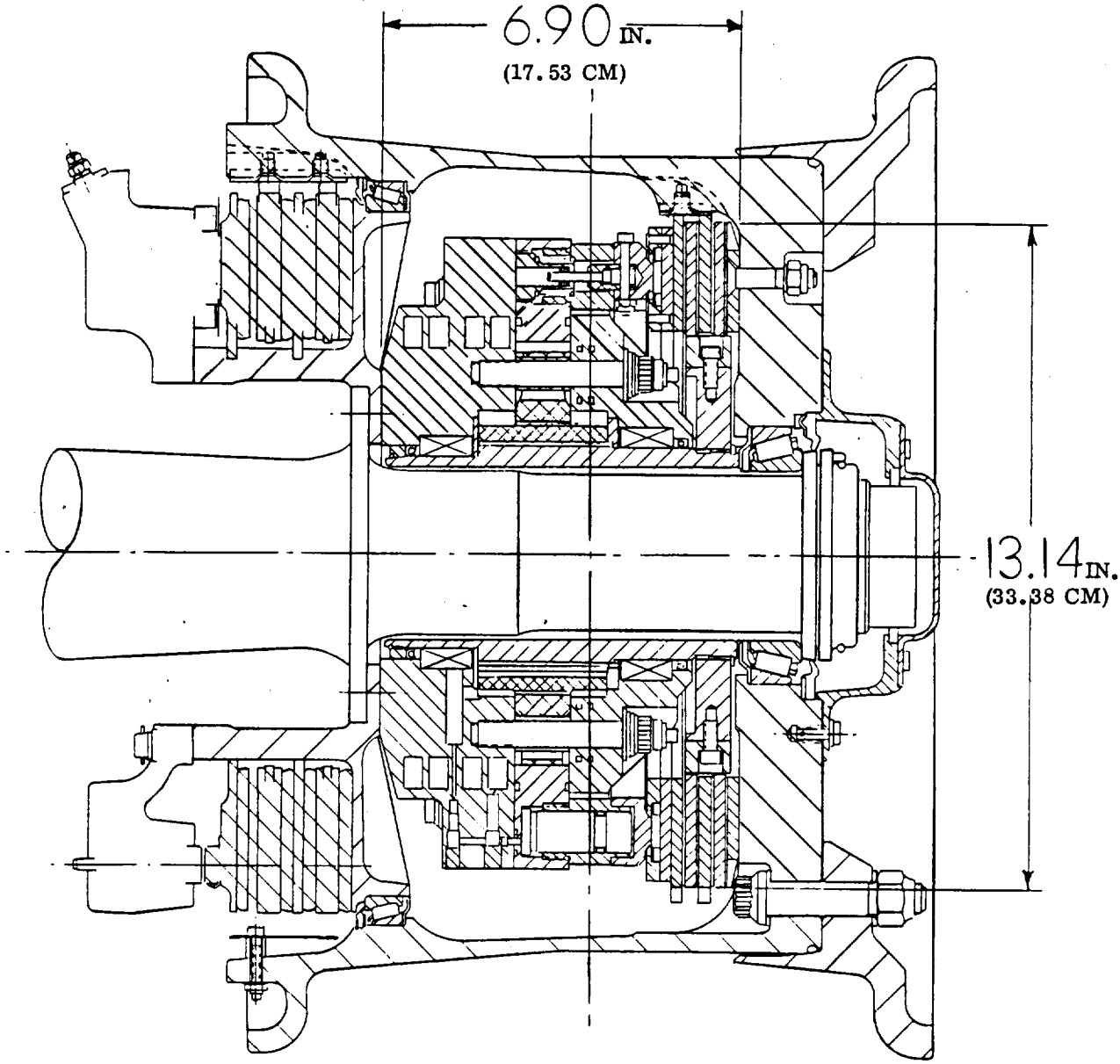


CROSSECTION - WHEEL DRIVE INSTALLATION TYPICAL 737-100

FIGURE 1

## INTRODUCTION

Energy conservation and ecological considerations have caused the transportation industry to review systems and operational procedures in an effort to achieve savings in energy and reductions in environmental pollution. The aircraft industry in particular has conducted studies to achieve greater operational efficiency in terms of energy. A number of their studies (Ref. 1) have centered around alternatives to the use of the primary power source (main engines) as a means of providing the power for taxiing aircraft. A specific alternative using a secondary power source involved the use of individually powered wheels in the main landing gear eliminating dependence on a ground based power source such as a tow tractor.

The main objective of the powered wheel program was the design, manufacture and test of a suitable, full scale, hydraulically powered motor that would be compatible with the outboard wheels of the Boeing 737-100 type aircraft, and capable of providing typical taxi performance. Compatibility included no interference with braking other than removal of three of the five plates in the outboard wheels and essentially no change in the ground check-out, removal and replacement for tires, anti-skid systems and brakes.

The powered wheel program was conducted by three divisions of The Bendix Corporation. Electrodynamics Division was responsible for management of the program, design, analyses, test plan, and manufacture of the actuator. Energy Controls Division had responsibility for establishing the installation requirements, wheel and brake modifications, providing the dynamometer equipment and conducting the testing. In addition, Energy Controls Division was responsible for design, analyses and manufacture of the clutch. Bendix Research Laboratories, provided the over-all technical guidance and expertise gained from their development of the DYNAVECTOR® concept into a practical motor-actuator mechanism for applications ranging from a prototype missile digital hydraulic fin control to a prototype high temperature airplane control surface secondary actuator.

Although the present program should have demonstrated (in dynamometer testing) the feasibility of using a DYNAVECTOR® and clutch assembly to drive a 737-100 type aircraft through simulated typical taxi operations, flight testing would have been required to fully evaluate the powered wheel performance. This type of follow-on program would require the manufacture of modified wheels and brakes and the installation of a practical hydraulic system using the existing or a dedicated APU for power. The satisfaction of all demands for a flight test application would go a long way in demonstrating the desirability and capability of powered wheels.

While powered wheel concepts are not new (Ref. 2-5). The mechanization presented in this paper is unique in that it is readily adaptable to a hollow center output for accommodation of the wheel axle. Also, the relative short length of the hydraulic motor is favorable in packaging the unit within the allowable wheel envelope. The accommodation of the drive unit internal to the wheel provides protection against external contamination and eliminates any necessity of providing additional space in the wheel wells.

The significance of the information and data disclosed in this report is that certain design and materials modifications are required for the present design to provide a practical hydraulic wheel drive motor/clutch assembly. However, the design effort clearly shows that it is technically feasible to provide a practical hydraulic wheel drive assembly within the restricted envelope of an aircraft wheel. Also the design analyses indicate the aircraft can meet typical taxi operations without the use of the main engines. Feasibility is indicated in the analyses with the use of a developed concept for rotary motion known as the Bendix DYNAVECTOR® in a form using conventional precision manufacturing methods and standard high quality aircraft materials. The desirability and practicality of applying this technology to the air transport industry as a possible means of saving energy and reducing pollution during ground operations must still be determined. These characteristics can be determined by additional evaluation involving flight testing, hydraulic system design studies, and operational trades analyses.

## SYMBOLS AND UNITS

| | |
|---|---|
| $A$ | Orifice Area, $in^2$ ($cm^2$) |
| $A_c$ | Clutch Disc Contact Area, $in^2$ ($cm^2$) |
| $A_i$ | Shaft Inboard Shoulder Bearing Area, $in^2$ ($cm^2$) |
| $A_o$ | Shaft Outboard Shoulder Bearing Area, $in^2$ ($cm^2$) |
| $A_p$ | Clutch Actuating Piston Area, $in^2$ ($cm^2$) |
| $a$ | Aircraft Acceleration in Series or Parallel Mode, $ft/sec^2$ ($m/sec^2$) or Number of Bearing Rollers. |
| $a_p$ | Aircraft Acceleration in the Parallel Mode, $ft/sec^2$ ($m/sec^2$) |
| $a_s$ | Aircraft Acceleration in the Series Mode, $ft/sec^2$ ($m/sec^2$) |
| BRR | Basic Radial Rating in Pounds (kg) for a 90% Expected Life of 3000 hours at 500 RPM. |
| BTR | Same as BRR Except Based on Thrust |
| $b$ | Displacement Chamber Face Width, in (cm) |
| $b_g$ | Gear Face Width, in (cm) |
| $C$ | Dynamic Bearing Rating, or Specific Heat, $Btu/lb/^oF$ |
| $c$ | Fraction of Gear Teeth Carrying Load |
| $D$ | Tubing Inside Diameter or Mean Bearing Roller Diameter, in (cm) |
| $D_h$ | Output Shaft Inboard Sealing Diameter, in (cm) |
| $D_o$ | Output Gear Pitch Diameter, in (cm) |
| $D_p$ | Diametral Pitch, $in^{-1}$ ($cm^{-1}$) |
| $D_r$ | Orbiter Gear Pitch Diameter, in (cm) |
| $D_S$ | Vane Socket Holes Pitch Diameter, in (cm) |
| $D_s$ | Output Shaft Outboard Sealing Diameter, in (cm) |
| $D_v$ | Vane Sealing Diameter, in (cm) |
| $D_1$ | Diameter of Curvature of Gear Tooth Concave Surface, in (cm) |
| $D_2$ | Diameter of Curvature of Gear Tooth Convex Surface, in (cm) |

| | |
|---|---|
| $d$ | Bearing Mean Diameter, in (cm) |
| $d_{ap}$ | Orbit Motor Displacement in Parallel Mode, $in^3$/rev. (cc/rev.) |
| $d_{as}$ | Orbit Motor Displacement in Series Mode, $in^3$rev. (cc/rev.) |
| $d_m$ | Orbit Motor Displacement in Series or Parallel Mode, $in^3$/rev. (cc/rev.) |
| $E$ | Young's Modulus of Elasticity, psi ($N/m^2$) |
| $e$ | Orbiter Eccentricity with Respect to Center Line of Output, in (cm) |
| $F$ | Bearing Load, lbs (kg) |
| $F_{b1}$ | Force on Outboard Bearing, lbs (kg) |
| $F_{b2}$ | Force on Inboard Bearing, lbs (kg) |
| $F_c$ | Force Applied by Clutch Pistons, lbs (kg) |
| $F_g$ | Force Reacted by Gear Teeth, lbs (kg) |
| $F_h$ | Gear Hold-in Force, lbs (kg) |
| $F_m$ | Dynavector Output Force in Series or Parallel mode, lbs (kg) |
| $F_{mb}$ | Developed Motor Force in Braking Mode, lbs (kg) |
| $F_{mp}$ | Dynavector Output Force in Parallel Mode, lbs (kg) |
| $F_{ms}$ | Dynavector Output Force in Series Mode, lbs (kg) |
| $F_n$ | Force Reacted by $n^{th}$ Gear Tooth, lbs (kg) |
| $F_o$ | Orbiter Force, lbs (kg) |
| $F_r$ | Orbiter Hydraulic Force, lbs (kg) |
| $F_{rr}$ | Rolling Resistance, lbs (kg) |
| $F_T$ | Output Shaft Total Thrust Force, lbs (kg) |
| $F_t$ | Thrust Force, lbs (kg) |
| $F_{tm}$ | Thrust Force Caused by Gear Teeth Misalignment, lbs (kg) |
| $F_{ty}$ | Allowable Tensile Yield Stress, psi (N/m) |
| $F_{UB}$ | Allowable Ultimate Bearing Stress, psi (N/m) |
| $f$ | Coefficient of Friction or Tube Internal Surface Roughness Factor |
| $g$ | Gravitational Constant, $in/sec^2$ ($cm/sec^2$) |

| | |
|---|---|
| $H$ | Bearing Material Factor (Radial) $lb/in^2$ ($kg/cm^2$) |
| $H'$ | Bearing Material Factor (Thrust) $lb/in^2$ ($kg/cm^2$) |
| $H_l$ | Head Loss in Height of Fluid, ft (m) |
| $h$ | Bearing Radial Thickness, in (cm) |
| $J_t$ | Total Inertia of Motor Moving Parts, $lb\text{-}in\text{-}sec^2$ ($kg\text{-}cm\text{-}sec^2$) |
| $J_w$ | Wheel Inertia, $lb\text{-}in\text{-}sec^2$ ($kg\text{-}cm\text{-}sec^2$) |
| $K$ | Flow Loss Factor $K \triangleq H_l 2g/V_s^2$, or $\frac{BRR}{BTR}$ for Bearing Load Computation |
| $K_h$ | Hydraulic Spring Rate, lb-in/rad (N-m/rad) |
| $K_s$ | Output Shaft Torsional Spring Rate, lb-in/rad (N-m/rad) |
| $k$ | Bearing Latest Uprating Factor |
| $L$ | Vane Sealing Effective Length, in (cm) |
| $L_s$ | Total Hydraulic Line Length, ft (m) |
| $L_h$ | $L_{10}$ Bearing Life, or Unit Operational Life, hrs |
| $l$ | Effective Roller Length, in (cm) |
| $l'$ | Roller Length, in (cm) |
| $l_c$ | Length of Gear Teeth Contact, in. (cm.) |
| $M_a$ | Aircraft Mass, $lb\text{-}sec^2/ft$ ($kg\text{-}sec^2/cm$) |
| $N$ | Bearing Equivalent Speed, RPM |
| $N_a$ | Number of Allowable Passes for Zero Wear |
| $N_s$ | Output Shaft Speed, RPM |
| $N_w$ | Aircraft Wheel Speed, RPM |
| $N_1$ | Number of Teeth on Ground Gear |
| $N_2$ | Number of Teeth on Ring Gear in Mesh with $N_1$ |
| $N_3$ | Number of Teeth on Ring Gear in Mesh with $N_4$ |
| $N_4$ | Number of Teeth on Output Gear |
| $\Delta N$ | Number of Teeth Difference |

| | |
|---|---|
| $n$ | Bearing Speed, RPM |
| $n_c$ | Number of Clutch Pistons |
| $n_i$ | Number of Fatigue Cycles @ Condition i |
| $n_s$ | Number of Clutch Friction Surfaces |
| $n_w$ | Number of Powered Wheels |
| $P$ | Equivalent Dynamic Loading Force, lbs (kg), or Load Per Unit Length, lbs/in. (N/m) |
| $P_b$ | Thrust Shoulder Bearing Stress, psi ($N/m^2$) |
| $P_c$ | Case Pressure, psi ($N/m^2$) |
| $P_{cc}$ | Clutch Disc Contact Pressure, psi ($N/m^2$) |
| $P_l$ | Pressure Loss, psi ($N/m^2$) |
| $P_n$ | Load Per Unit Length on $\eta^{th}$ Gear Tooth, lbs/in (N/m) |
| $P_r$ | Return Pressure, psi ($N/m^2$) |
| $P_s$ | Supply Pressure, psi ($N/m^2$) |
| $\Delta P_c$ | Clutch Actuation Pressure, psi ($N/m^2$) |
| $\Delta P_{lp}$ | Total Line Loss in Parallel Mode, psi ($in/m^2$) |
| $\Delta P_{ls}$ | Total Line Loss in Series Mode, psi ($N/m^2$) |
| $\Delta P_m$ | Pressure Loss Across the Orbit Motors in Either Series or Parallel Mode, psi ($N/m^2$) |
| $\Delta P_{mp}$ | Pressure Loss Across Each Motor in Parallel Mode, psi ($N/m^2$) |
| $\Delta P_{ms}$ | Pressure Loss Across Each Motor in Series Mode, psi ($N/m^2$) |
| $\Delta P_p$ | Dynavector Pressure Loss in Parallel Mode, psi ($N/m^2$) |
| $\Delta P_s$ | Dynavector Pressure Loss in Series Mode, psi ($N/m^2$) |
| $\Delta P_t$ | System Total Pressure Loss in Parallel or Series Pressure loss, psi ($N/m^2$) |
| $\Delta P_{tp}$ | System Total Pressure Loss in Parallel Mode, psi ($N/m^2$) |
| $\Delta P_{ts}$ | System Total Pressure Loss in Series Mode, psi ($N/m^2$) |
| $Q_{dp}$ | Dynavector Flow in Parallel Mode = 2 $Q_m$, gpm (lit/min) |

| | |
|---|---|
| $Q_{ds}$ | Dynavector Flow in Series Mode, gpm (lit/min) |
| $Q_m$ | Orbit Motor Flow, gpm (lit/min) |
| $Q_t$ | Orbit Motor Max. Flow = $(Q_m)$max, gpm (lit/min) |
| q | % of Total Time |
| $\bar{R}$ | Clutch Plate Average Radius, in (cm) |
| $R_b$ | Bearing Outside Radius, in (cm) |
| $R_I$ | Inboard Bearing Load from Load $W_w$, lbs (kg) |
| $R_i$ | Clutch Plate Inside Radius, in (cm) |
| $R_O$ | Outside Bearing Load from Load $W_w$, lbs (kg) |
| $R_o$ | Clutch Plate Outside Radius, in (cm) |
| $R_r$ | Aircraft Wheel Rolling Radius, in (cm) |
| $R_t$ | Transmission Ratio |
| $r_b$ | Bearing Inside Radius, in (cm) |
| $r_o$ | Output Gear Pitch Circle Radius, in (cm) |
| $S_c$ | Compressive Stress, psi ($N/m^2$) |
| $S_b$ | Bending Stress, psi ($N/m^2$) |
| $T_{cn}$ | Clutch Torque, lb-in (N-m) |
| $T_1$ | Load Torque, lb-in (N-m) |
| $T_{1p}$ | Load Torque in Parallel Mode, lb-in (N-m) |
| $T_{1s}$ | Load Torque in Series Mode, lb-in (N-m) |
| $T_m$ | Output Torque of Both Orbit Motors, lb-in (N-m) |
| $T_o$ | Output Torque, lb-in (N-m) |
| $T_s$ | Stall Torque, lb-in (N-m) |
| t | Time, Seconds or Hours |
| $t_p$ | Proportionate Amount of Time Under Certain Operating Conditions |
| $V_a$ | Aircraft Taxi Speed, mph (km/h) |

| | |
|---|---|
| $V_s$ | Fluid Velocity, Ft/min (m/min) |
| $V_t$ | Motor Fluid Total Volume Under Compression, $in^3$ (cc) |
| W | Aircraft Weight, lbs, (kg) or bearing width, in (cm) |
| $W_w$ | Weight on the Wheel, lbs (kg) |
| x | Distance Travelled, Ft. (m) |
| $\dot{X}$ | Gear Teeth Sliding Velocity, ft/min (m/min) or Aircraft Taxi Speed, ft/sec (m/sec) |
| Y | Lewis Factor |

GREEK

| | |
|---|---|
| $\alpha$ | Clutch Spin-up Acceleration or 1/2 Included Bearing Cup Angle deg (rad) |
| $\beta$ | Fluid Bulk Modulus, psi ($N/m^2$) or 1/2 Included Bearing Cone Angle, deg (rad) |
| $\gamma$ | Gear Pressure Angle, Deg (rad) or 1/2 Included Roller Angle, $\beta + \nu$, deg (rad) |
| $\eta_t$ | Torque Efficiency |
| $\eta_v$ | Volumetric Efficiency |
| $\theta$ | Misalignment Angle of Gear Teeth, deg (rad) |
| $\lambda_r$ | Zero Wear Factor |
| $\mu$ | Poisson's Ratio |
| $\rho$ | Fluid Specific Weight, $lb/in^3$ (g/cc) |
| $\nu$ | 1/2 Included Bearing Roller Angle, deg (rad) |
| $\phi$ | Angular Position of Contact Point on Output Gear |
| $\omega$ | Wheel Angular Velocity, deg (rad) |
| $\omega_m$ | Motor Angular Velocity, deg (rad) |

## PERFORMANCE REQUIREMENTS/DESCRIPTION AND OPERATION

### Performance Requirements

The following design and performance requirements and operating parameters have been specified for use with the Boeing 737-100 type aircraft (Ref. Statement of Work, Appendix A).

| | | |
|---|---|---|
| 1. | Weight and Inertia: | Minimum |
| 2. | Ambient Temperature: | $-65^{\circ}$ to $120^{\circ}$F ($-54^{\circ}$ to $+49^{\circ}$C) |
| 3. | Fluid: | |
| | Type: | Skydrol 500 |
| | Design Pressure: | 4000 PSI (27.58 $MN/m^2$) |
| | Flow Rate: | 45 GPM (170.34 lit/min.) |
| 4. | Aircraft Top Taxi Speed: | 15 mph (24.14 km/h) |
| 5. | 737-100 Top Wheel Speed: | 153 rpm |
| 6. | Stall Torque: | 57,000 lb-inch (6.44 kN - m) |
| 7. | Braking: | Capable of applying braking torque equivalent to stall value while not exceeding design pressure. |
| 8. | Dynamometer Test Envelope: | The tests shall demonstrate a typical use cycle including reverse for 100 yards (91.46 m); taxi 2.5 miles (4.02 km) at 15 mph (24.14 km/h); disengage drive unit; accelerate wheel to 180 mph (289.68 km/h); stop, pause and cool for an interval to simulate a short flight; accelerate very rapidly to 180 mph; slow to 15 mph, engage drive unit; taxi 2.5 miles at 15 mph, and then stop. |
| 9. | Dynamometer Test Cycles: | 100 cycles pursuant to item 8 above. |

System description. The wheel drive system includes a DYNAVECTOR® motor housed entirely within the outboard main wheel of a Boeing 737-100 aircraft. The motor drives the wheel through a multidisc clutch that can be disengaged to allow high speed take-off and landing without requiring the Dynavector to withstand the resulting high speeds. For this reason, there must be some interlock so that the wheel drive cannot be engaged when aircraft speed exceeds approximately 15 mph (24.14 km/h).

The wheel drive uses a "ratio change" to minimize the flow required at high speed. This approach was chosen since very high torque is required at stall speed and approximately 25 percent of stall speed torque is required at maximum speed. The ratio change was accomplished by porting every other motor chamber so that, in effect, two motors are contained in the same housing. During the high torque regime, the motors will be operated in parallel to achieve maximum possible torque; however, during high speed-low torque requirements, the motors will be driven in series to achieve maximum speed for a given flow rate while cutting the torque potential in half.

The hydraulic valving necessary to control the motor, effect the "ratio change," limit the braking torque, and actuate the clutch, is shown in the schematic of Figure 2a. One major design goal is to minimize the number of hydraulic and electric lines leading to the powered wheel itself. A flightworthy design would require only two 3/4-inch (1.91 cm) diameter hydraulic lines, one 3/8-inch (0.95 cm) diameter hydraulic line and two low voltage-low current electrical wires. However, since the purpose of this effort was to prove the feasibility of a wheel drive concept on a dynamometer (in lieu of initial implementation on the aircraft), extensive time and cost were saved by installing two additional 3/4-inch (1.91 cm) diameter hydraulic lines into the wheel. The use of four 3/4-inch (1.91 cm) diameter

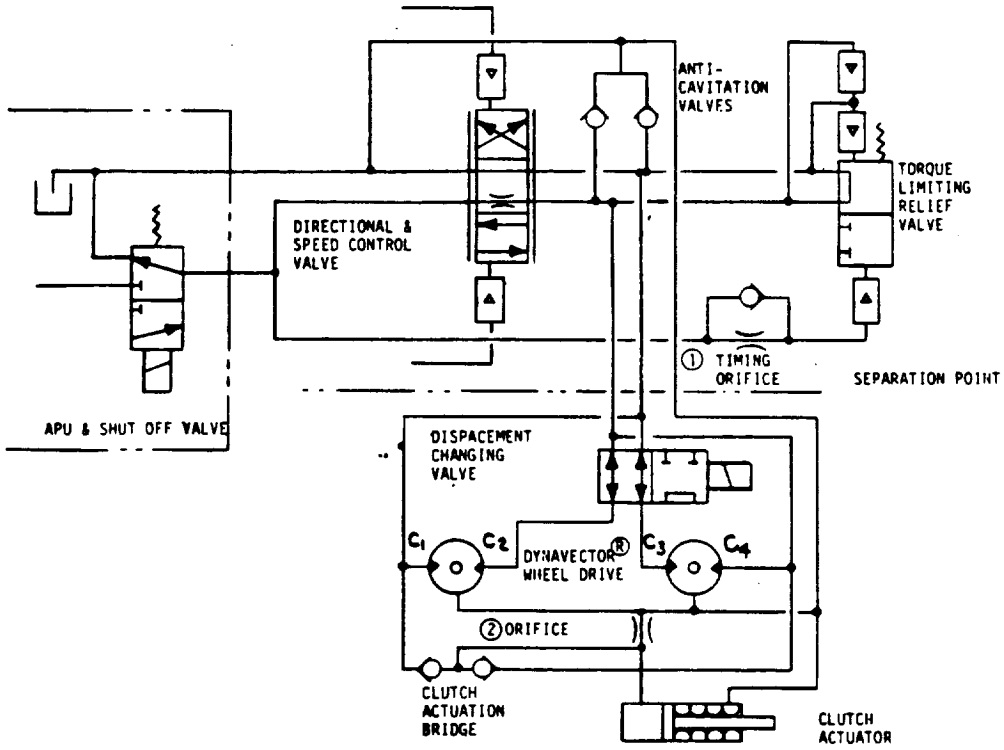


Figure 2a. Flight Worthy System Arrangement Schematic

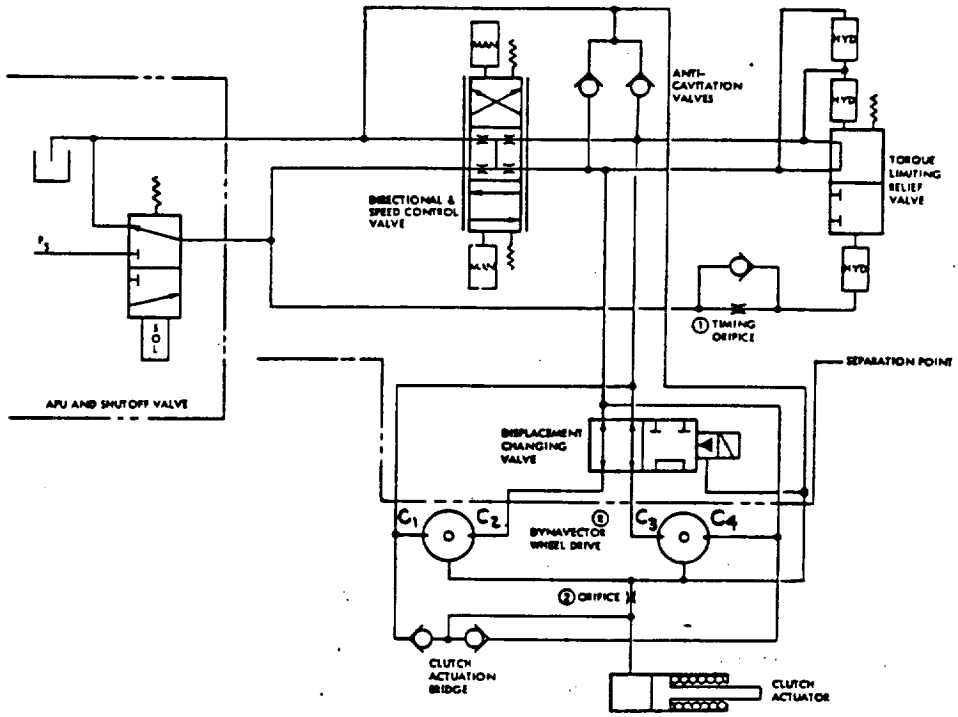


Figure 2b. Test System Arrangement Schematic

hydraulic lines allowed the "displacement changing valve" to be located with the other valves, and further allowed the use of a standard test unit precluding the need for a special valve design in the motor manifold. This expedient system development is shown in Figure 2b.

System operation. With reference to Figure 2, a or b, it is shown that when the system shut-off valve is in the deenergized position, all powered wheel system areas communicate with (or are linked to) system return; the directional and speed control valve is centered; the torque limiting relief valve is in the bypass position; the clutch is disengaged, and the displacement changing valve is in the "low speed-high-torque" full-displacement mode.

To pressurize the system, the aircraft system shut-off valve is energized, applying supply pressure to the directional and speed control valve at null. This action further applies partial supply pressure to each of the cylinder lines. Supply pressure to the torque limiting relief valve is lagged by the timing orifice. The clutch is engaged as soon as the cylinder pressures are applied (engagement occurs before the supply pressure can operate the torque limiting relief valve). Thus, the clutch is engaged fully before hydraulic torque can be applied.

Supply pressure builds up through orifice No. 1 and shifts the torque limiting relief valve to the running mode (nonbypassing). At this point, full torque is available to move the aircraft in forward or reverse. As the aircraft speed increases, the pilot may select high speed control by energizing the displacement changing valve which switches half of the motor chambers into series with the remaining half, thus doubling the output speed available for a given flow. It would not be possible to start the aircraft from a standstill with the system in its high speed mode due to the six percent breakaway torque requirement and the four percent maximum equivalent available motor torque in the high speed mode. During braking, the torque limiting relief valve will port excessive pressure from the high pressure motor line to the low pressure motor line, thus limiting the $\Delta P$ to approximately supply pressure.

Upon deenergizing the system, the clutch does not disengage immediately due to the throttling of orifice No. 2. As the system pressure drops, the torque limiting relief valve shifts to its bypassed position before the clutch disengages, thus removing hydraulic torque before clutch disengagement and limiting motor torque during the period of possible clutch slippage.

Dynavector Principle of Operation. The fluid power Dynavector motor is an integrated high speed-captive vane-orbit motor and epicyclic transmission without high velocity mechanical elements. The transmission and motor use components common to both, resulting in a simple and reliable design.

There are several different categories of Dynavector actuator configurations. They may be categorized by the manner in which they are powered — electrically, pneumatically or hydraulically — and by the type (or ratio) of transmission arrangement, either low ratio (approximately 10:1 to 100:1) or high ratio (50:1 or 1000:1).

Two features make the low ratio configuration (used in this program) small and light: 1) its transmission reduces the high speed input to a low speed output in one step, using only two moving gears; and 2) it has no physical motor —only a rotating force vector and hence the name "Dynavector." As the force vector rotates at high speed, it causes the input member of the transmission to orbit. This orbiting member is geared directly to the rotating output shaft. Because it orbits instead of rotates, gear tooth contact velocities are small and a large speed reduction is accomplished without complex gearing.

The operation of the low ratio Dynavector drive concept is illustrated by Figure 3. The basic components are the orbiter, orbiter gear, the sleeve spacers and bolts, housings and spacer, the center output gear, and the unique vanes. The displacement chambers are formed between the spacer and the orbiter/gear by the vanes. The orbiter/gear motion, which is purely orbital, is constrained by the stationary bolts and sleeve spacers (considered guide pins) located in each chamber.

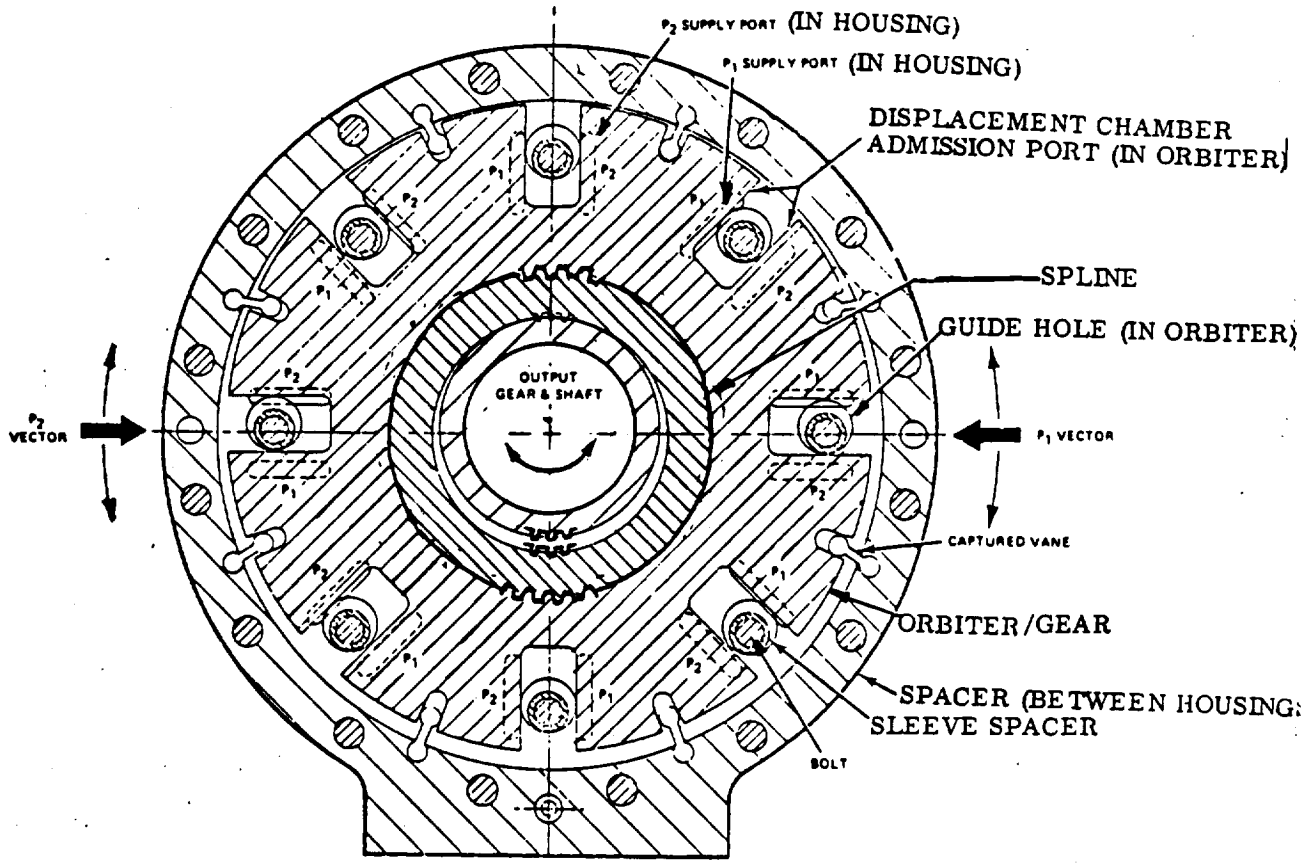


FIGURE 3. Low Ratio Orbiter Configuration

These guide pins contact the guide holes in the orbiter/gear. The difference in diameters between the guide pins and the orbiter/gear guide holes is twice the eccentricity of the orbit motion necessary for the gear mesh between the orbiter/gear and output shaft. The orbiting motion of the orbiter/gear causes rotation of the output shaft at a reduced speed.

The motor is a positive displacement, very low inertia, nonrotating vane motor. Its output is a radial force vector which rotates at high speed and in either direction of rotation. The displacement chambers formed by the vanes and the spacer expand and collapse at the same speed as the force vector, but do not rotate. The motor is self-commutating but does not contain a rotating porting plate or spindle. The absence of high-velocity members in the motor significantly reduces the inertia, resulting in high acceleration capability.

The force vector is generated by pressurizing four adjacent displacement chambers, while venting the remaining four. The vector is made to rotate by pressurizing a vented chamber adjacent to the original four pressurized chambers, while simultaneously venting the diametrically opposite pressurized chamber. At that instant, the force vector advances through an angle equal to the arc width of one displacement chamber. If the force vector on the orbiter/gear is located at approximately 90 degrees (1.57 rad.) to the orbiter/gear and output gear contact point, the orbiter/gear will move, causing the output gear to turn and the contact point to move. Movement of the orbiter/gear switches the porting causing the force vector to rotate so that it remains 90 degrees (1.57 rad.) to the contact point; thus, the motion is continuous and the output shaft turns continuously but at a much lower speed than the force vector. The ratio is determined by the difference in the number of teeth between the orbiter/gear and the number of teeth on the output gear.

For each of the two motors incorporated in the design, the available differential pressure in the form of two motor port pressures, $P_1$ and $P_2$ ($P_3$ and $P_4$ for the other motor) is commutated to the proper displacement chambers to produce a rotating force vector in phase with the orbiter/gear motion. To ensure that this phase relationship always holds true, the motion or position of the orbiter/gear is used to provide this commutation through a series of ports. Each displacement chamber has a pair of supply ports designated $P_1$ and $P_2$. The $P_1$ ports are all interconnected in the housing and brought out to a single inlet port, as are all the $P_2$ ports. These ports are in the housing and, therefore, are stationary with respect to the displacement chambers. They are also located under the orbiter/gear face, as shown in Figure 3, and a port connecting the displacement chamber to the orbiter/gear face is located opposite them.

By locating these $P_1$ and $P_2$ ports as shown in Figure 3, the orbiter/gear ports open $P_1$ ports to half the displacement chambers, and $P_2$ ports to the remaining half. The resulting pressure force on the orbiter/gear from the displacement chambers connected to $P_1$ is 180 degrees (3.14 rad.) opposite $P_2$ and 90 degrees (1.57 rad.) from the output gear contact point. Therefore, pressurizing $P_1$ and venting $P_2$ produces rotation in one direction while interchanging pressure and return reverses the orbiter/gear. This also satisfies the desired relationship between force vector and orbiter/gear position. Because this commutation is created by the displacement member or orbiter/gear itself, it always rotates in phase with the orbiter/gear, producing maximum efficiency.

There is a very low speed torque ripple which depends only on the number of vanes or displacement chambers. The number of chambers need not be odd or even since the starting torque is only a function of the force-vector angle which varies through an angle equal to the angle included by one displacement chamber.

Several limiting factors present in conventional rotary motors, plus transmission systems, are significantly improved by the Dynavector motor design and operation. The relative velocities between dynamic and static members are very small because of the small-amplitude orbital motion. In a Dynavector actuator, the relative velocity between the gears and housing is only a function of the eccentricity, which is 0.0833 inch (0.2117 cm) times the angular velocity, whereas in a conventional motor there are usually components with a radius of more than 1.00 inch (2.54 cm) rotating at the same angular velocity. Thus, for a force-vector speed of 3000 rpm, the rubbing velocity would not exceed 26 in/sec (66 cm/sec), whereas in a conventional motor rotating at 3000 rpm, rubbing velocities would be greater than 300 in/second (762 cm/sec). The relative tooth velocities correspond to those found only in the last stage of a conventional transmission. The absence of high relative velocities produces high mechanical efficiency by reducing friction losses at high motor speed.

Another factor that is significantly reduced is motor inertia. In conventional high speed motors, the motor inertia resulting from a rotor mass rotating at high angular velocities has always limited the motor response capabilities. The small volumes under compression have helped to compensate for the poor response due to inertia and have placed rotary servos in contention, with linear actuators provided high supply pressures are used.

The Dynavector motor, having no mass rotating at input speed and only a small reflected inertia due to the small eccentric rotation of the orbiter/gear and the low speed output shaft, is equivalent to the reflected inertia of a similar capacity piston-cylinder actuator. On the other hand, the volume under compression is equivalent to a rotary servo and is much less than that of a piston-cylinder actuator.

Wheel drive motor/clutch description and operation. The wheel drive motor/clutch assembly, Bendix P/N 3311870, is shown in Figures 4 through 6. Although the clutch discs are not included in Figure 4, they can be seen clearly in the cross sectional view (Section B-B) in Figure 5 and in the isometric cut-away view in Figure 6. A list of parts and the required quantities is included in Appendix F.

The basic configuration of the orbiter is one that is typical for a low ratio Dynavector actuator and is shown in Figure 6, which depicts the arrangement of the housings, vanes, orbiter/gear and output shaft. The orbiter/gear displacement chambers are on the outside of the epicyclic transmission and this mechanical arrangement is advantageous where high torque output and high output speed are required with high pressure. Thus, maximum motor displacement volume is provided (for any given package outside diameter) and the gear ratio is minimized. Normally in the case of high pressure and high torque systems, the face width of the transmission gear teeth rather than the motor displacement-chamber length determines the actuator package size. In cases where low output speed is required and high

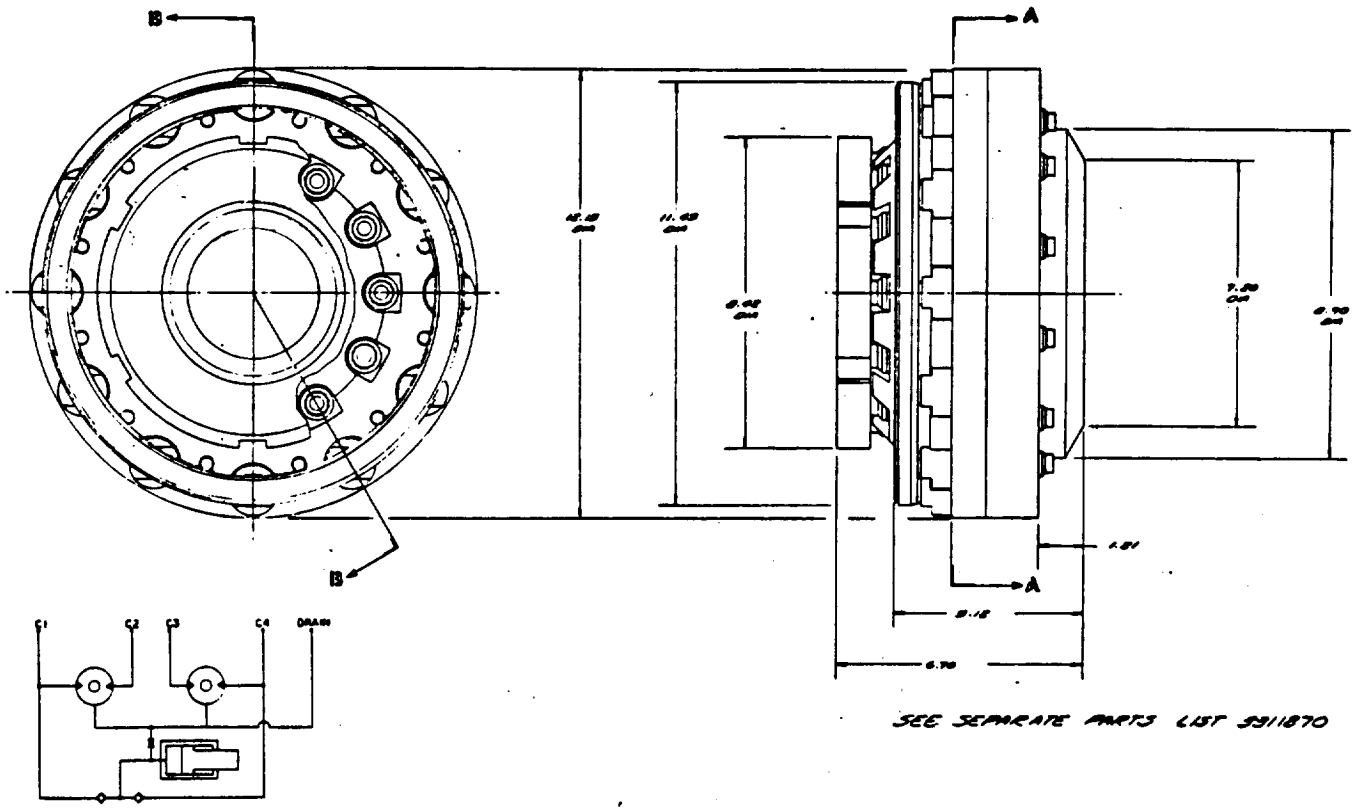


FIGURE 4. Powered Wheel Drive Motor, Drawing 3311870, Sheet 1
(Shown with clutch discs removed)

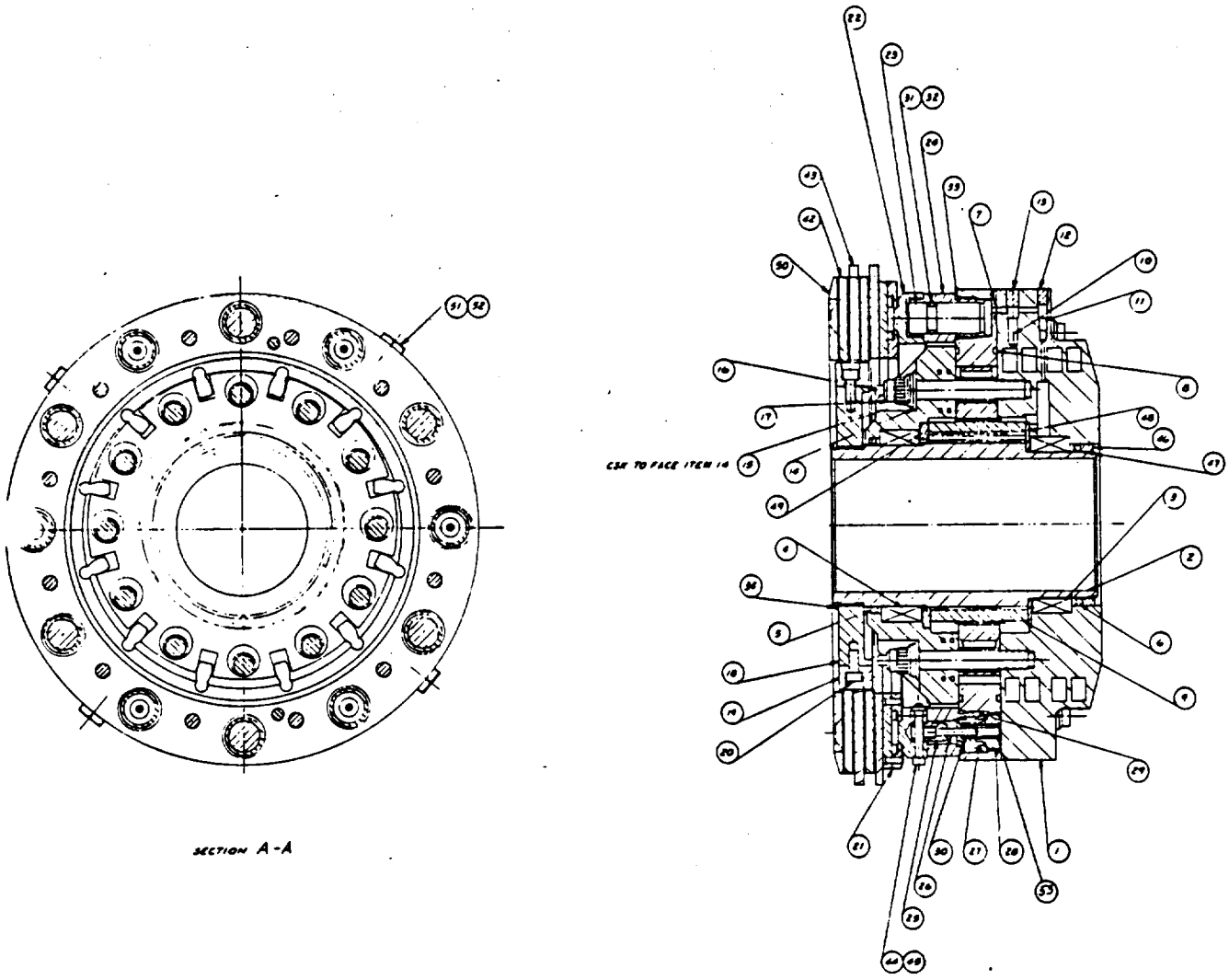


FIGURE 5. Powered Wheel Drive Motor Cross Section, Drawing 3311870, Sheet 2

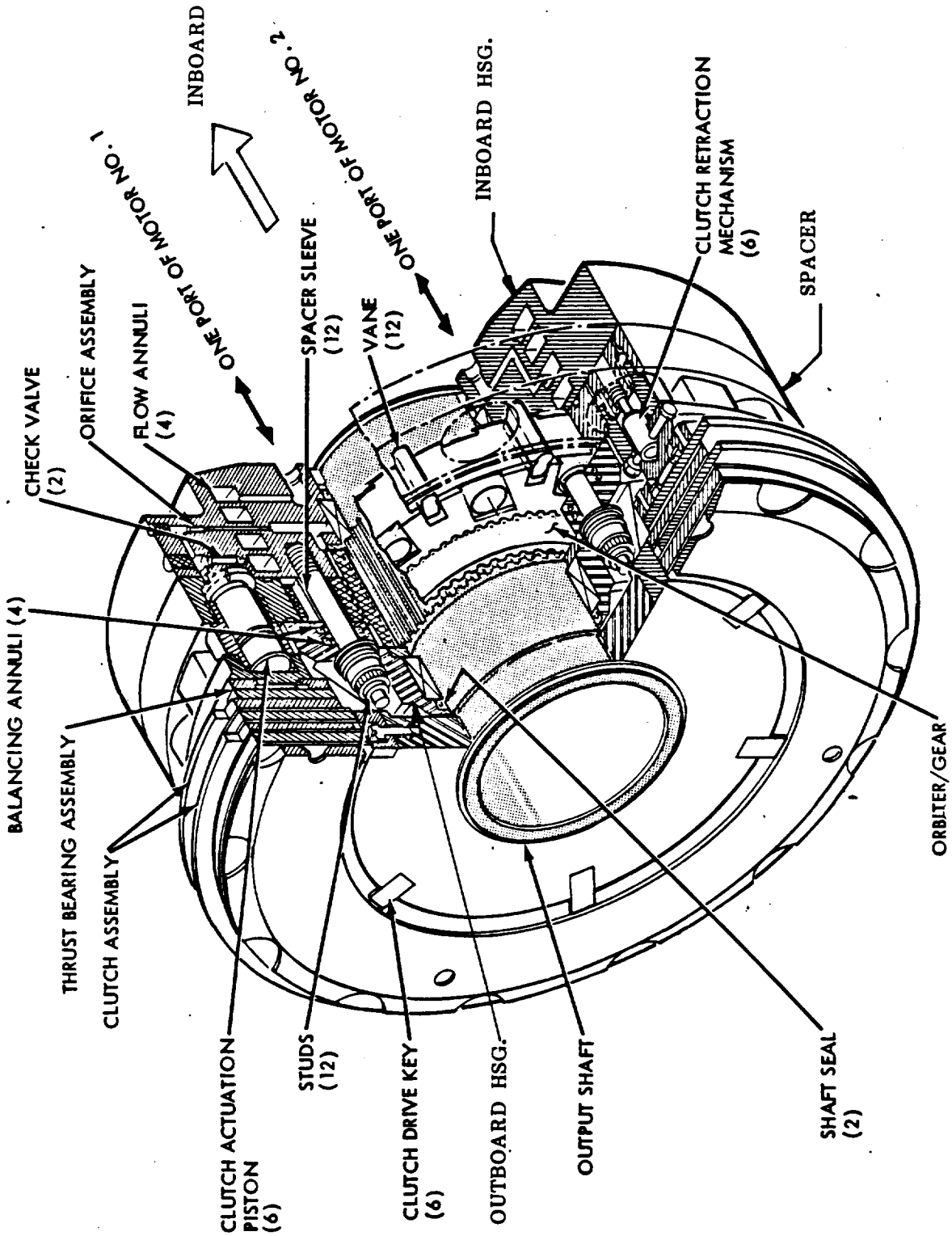


FIGURE 6. Powered Wheel Drive Motor Isometric

pressure supply is available, this arrangement could be reversed and the motor displacement chambers could be designed so that they would be inside the epicyclic ring gear and yet they would not experience high orbiting speeds. This arrangement would be similar to that shown as configuration (a) in Figure 7.

In Figure 6, one of the two ports of each motor is shown to illustrate the manner in which the four flow annuli are communicated through the quill type inlet ports with the displacement changing valve (not shown) for parallel/series operation. Flow passages (not shown) connect each annuli to the metering slots at the interface surface of the inboard housing and orbiter/gear combination. To pressure balance the orbiter/gear, the flow annuli pressures are conducted through the guide holes in the orbiter/gear to the four balancing annuli in the outboard housing which also has metering slots at the interface. On each side of the spacer sleeve holes in the orbiter/gear are metering edges (forming a port to the displacement chamber) that control the flow of fluid through the metering slots as the orbiter/gear moves in orbit to provide the self commutation and sustain the motion. As can be seen in Figure 6, a displacement chamber (there are 12) is created by the boundary components consisting of two vanes, spacer (separating the inboard and outboard housings) and the orbiter/gear. The pressure developed in the 12 chambers is such that six of them (in series mode) are at a higher pressure than the others, creating a hydraulic force (or vector) on the orbiter/gear. This force is developed at a nominal $90^{\circ}$ (1.57 rad.) to the eccentricity that exists between the orbiter/gear and output shaft centerlines to produce the force moment causing orbiter/gear orbiting motion and output shaft rotation.

Output shaft rotation produces rotation of the two clutch stator disc (Figure 5, item 42) which are keyed to the drive plate assembly (item 18). This assembly is attached to the output shaft by a spline fit. The two clutch rotor discs (item 43) are attached to the airplane wheel and made to move into contact with the

rotor discs until they are all stacked against the wheel-attached backing plate (item 50) so that the wheel rotates with the output shaft.

The clutch plates are compressed by six clutch actuation pistons (visible in Figure 6). The combined forces of the six pistons are distributed over the surface of the inboard rotor plate by the thrust bearing assembly. As explained previously and shown in Figure 2, the pistons are pressurized by opening the shut-off valve. One of the two check valves of the clutch actuation bridge can be seen in Figure 6 along with the orifice assembly that delays clutch deactivation until the motor torque decays at shut-down. The six clutch retraction mechanisms are spring operated to disengage the clutch. They incorporate circular push on retaining rings (Figure 5, item 30) to allow for automatic position adjustment as the clutch wears. This adjustment maintains the clutch actuation stroke constant along with its response time.

The moving parts of the motor (orbiter/gear and vanes) are secured within the stationary components (inboard and outboard housings and spacer) by a set of 12 studs (Figure 5, item 16) and 12 bolts. The heads of the bolts can barely be seen (Figure 5) on the exterior surface of the inboard housing. These bolts screw into the outboard housing and the bolt circle is such that the position of the bolts is beyond the two static metallic seals (Figure 5, item 8) in the spacer. The bolt circle of the studs is inside the static metallic seals so that a commercial sealing type washer (Figure 5, item 14) is used with the nut to prevent fluid leakage. The studs, in addition to reacting the motor portion of the separating load on the housing (caused by hydraulic pressure) act as guide pins to limit the orbit of the orbiter/gear.

Spacer/sleeves (Figure 6) are slip fitted on the studs to maintain the running clearance between the housings and the orbiter/gear to attain satisfactory volumetric and torque efficiencies. The spacer sleeve O.D. and the I.D. of the holes in the orbiter/gear are sized so their difference is twice the required eccentricity of the orbiter/gear orbit.

The output shaft shown in Figure 6 has an integral gear machined on the O.D. that meshes with the orbiter/gear to attain an epicyclic gear transmission of moderately large gear ratio (22.67/1) in a small space. The center of the output shaft is sufficiently large to provide clearance for the wheel axle (Figure 1). The shaft is supported in the housings with roller bearings and sealed with spring loaded, plastic lip-type shaft seals. Because the shaft is nearly hydraulically balanced, thrust washers (Figure 5, items 48 and 49) are used in lieu of bearings.

The materials used for the components of the drive motor/clutch assembly are considered consistent with good aerospace design practice. The materials and special processing for the major components are listed in Table 1.

TABLE 1 - MAJOR COMPONENT MATERIALS AND SPECIAL PROCESSING

| Component | Material | Special Processing | Bendix P/N |
|---|---|---|---|
| Ring Orbiter | 4330M (Vacuum Melt) IAW AMS6411 or MIL-S-8699 | 1, 2 | 3311970 |
| Vane | | 3 | 3311966 |
| Sleeve Spacer | | 1, 2 | 3311972 |
| Spacer | | 4 | 3311952 |
| Housing Inboard | | 5 | 3311945 |
| Housing Outboard | | 5 | 3311940 |
| Output Shaft | | 1, 2 | 3311968 |
| Orbiter Gear | | 1, 2 | 3311974 |
| Housing, Pin Assy | P/N's 3311940 and 3311945 | 6 | 3311967 |
| Backing Plate (Clutch) | Steel, Low Alloy, Heat Resistant IAW Bendix Specification ES 0789 | 7 | AXD28937 |
| Rotor (Clutch) | | 7 | AXD28936 |
| Inner Rotor (Clutch) | | 7 | AXD28933 |
| Stator Plate (Clutch) | 4130 Steel | 8 | AXD28934 |
| Stator | AXD28934 | 9 | AXD28935 |

NOTES: (TABLE 1) PROCESSING

1. H.T. IAW MIL-H-6875; temper @ 1050 $\pm 25^{\circ}$F (566 $\pm 14^{\circ}$C) 170,000 to 200,000 psi (1172 to 1379 $MN/m^2$)
2. Nitride IAW MIL-S-6090 floe process or equivalent (.010 to .015 thick) on all surfaces except as noted on the drawing.
3. Same as #1 except 220,000 to 240,000 psi (1517 to 1655 $MN/m^2$) ultimate tensile strength.
4. Same as #1 except 200,000 to 220,000 psi (1379 to 1517 $MN/m^2$) ultimate tensile strength.
5. Braze IAW MIL-B-7883, Type II, Grade A, using copper braze, Hardness after braze to be $R_c$ 28 to 34. Heat treat after rough machining IAW BEPS 9.035, type III 160,000 to 180,000 psi (1103 to 1241 $MN/m^2$).
6. Plate metering plate surfaces with .008 thick tungsten carbide. Finish surfaces to .003 - .005 thickness.
7. Heat treat to $R_c$ 42 - 52 IAW Bendix Specification AI - 280.
8. Heat treat to $R_c$ 30 - 35.
9. Flame spray material 4555 - 65 to 0.005 in. (0.127 mm) min. thick.

## DESIGN ANALYSES

### Sizing

The low ratio epicyclic transmission arrangement shown in Figure 3 is only one of four arrangements possible. The gears may be inverted from external meshes to internal, and vice versa so that the output may be either a center output shaft or an outer housing hinge design with either low ratio or high ratio configuration. The four possible transmission arrangements are shown in Figure 7.

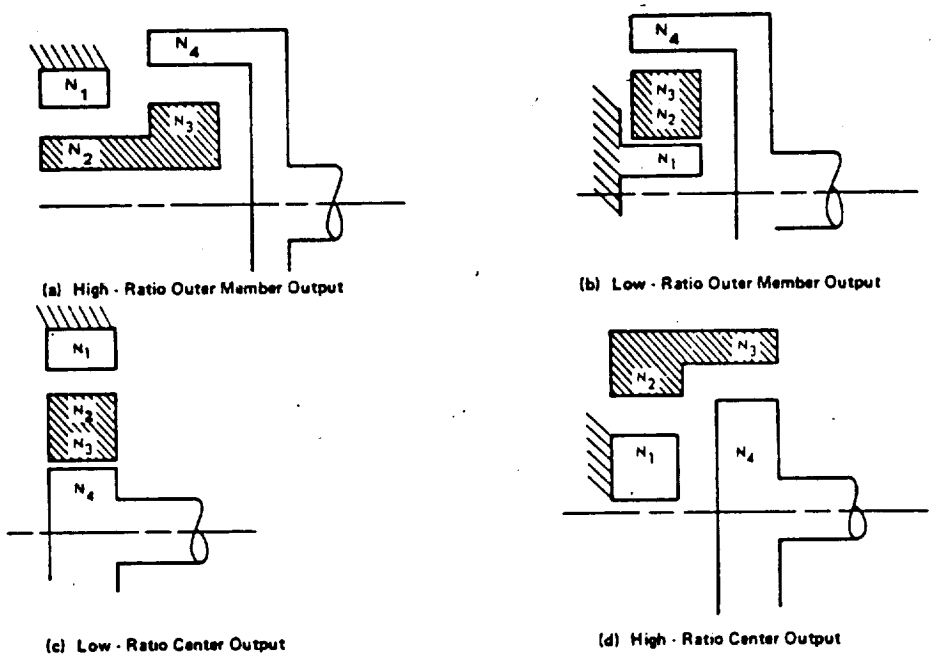


FIGURE 7. Dynavector Actuator Epicyclic Transmission Arrangements

For all the arrangements shown in Figure 7, the transmission ratio $R_t$, is given by:

$$R_t = \frac{N_2 N_4}{N_2 N_4 - N_1 N_3} \qquad (1)$$

where: $N_1$ = number of teeth on ground gear

$N_2$ = number of teeth on ring gear in mesh with ground gear

$N_3$ = number of teeth on ring gear in mesh with output gear

$N_4$ = number of teeth on output gear

The basic design shown in Figure 3 is a special case of arrangement (c) shown in Figure 7 in which $N_1 = N_2$. For this special case, the orbiter/gear orbits with respect to ground and does not rotate. In this case the transmission ratio is, with $N_1 = N_2$,

$$R_t = \frac{N_4}{N_4 - N_3} \qquad (2)$$

This type of differential transmission has formerly been considered an inefficient device. However, the inefficiencies in conventional differential gearing result from the high pitch-line velocities of the input member and planet gears, which also are heavily loaded. These factors are not present in the Dynavector actuator. A rotating force vector is used in place of an input gear, and the pitch diameter of the orbiter/gear is nearly equal to the pitch diameter of the output gear; therefore, no high velocities exist in the transmission.

An advantage of having the orbiter/gear pitch diameter nearly equal to the output gear pitch diameter is the resulting high load capacity. Under load, deflections quickly allow many teeth to share the load. This same feature provides high resistance to shock overloads and minimizes dynamic loading forces. The transmission has excellent torque transmitting capability because the dynamic loads are negligible and the static strength equals the dynamic strength.

In any fluid-powered Dynavector actuator, the orbit motor torque is developed when one-half of the pressurized displacement chambers exerts a hydraulic force against the rotor ring element through the effective center described by the vane sealing diameter, $D_v$, where $D_v \triangleq D_s - L$ (as shown in Figure 8). The magnitude of the hydraulic force is equal to the projected area formed by the vane sealing diameter, $D_v$; the rotor ring width, b; and the differential motor pressure, $\Delta P$. The vane sealing diameter is described as the effective orbiter diameter over which pressure acts to provide a force coincident with the stator-ring center, as shown in Figure 8.

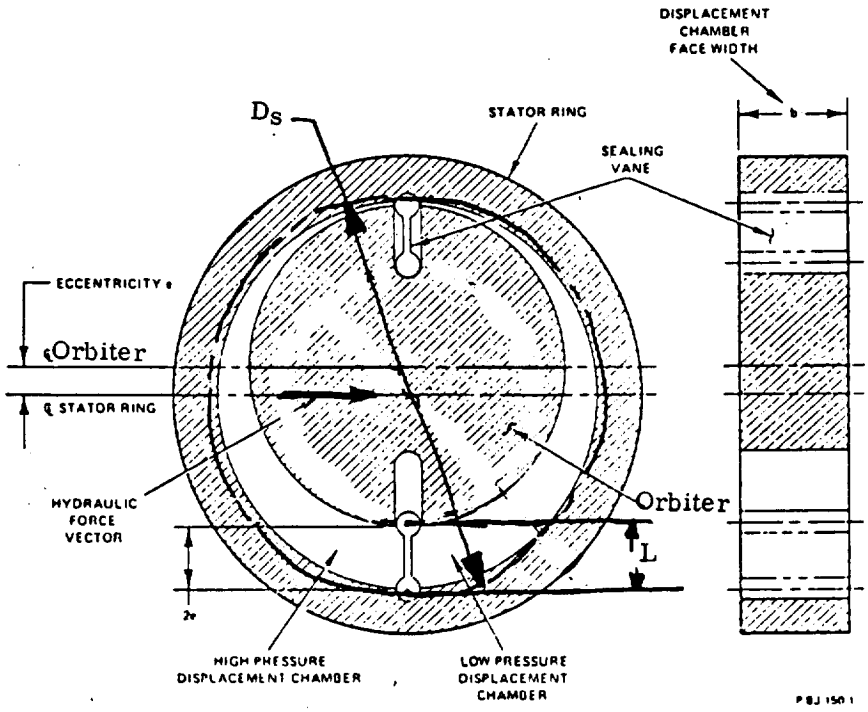


FIGURE 8. Geometry for Deriviation of Orbit Motor Torque and Displacement Equations

The product of the hydraulic force multiplied by the eccentricity is equal to the motor output torque. Therefore:

$$T_m = D_v \, b \, \Delta P_m \, e \, \eta_t \qquad (3)$$

where: $T_m$ = motor torque, in-lb (N - m)

$D_v$ = vane seal diameter, inch (m)

b = face width, inch (m)

$\Delta P_m$ = differential motor pressure, psi ($N/m^2$)

e = eccentricity, inch (m)

$\eta_t$ = torque efficiency

Motor torque can also be obtained from the classical torque equation

$$T_m = \frac{d_m \Delta P_m \eta_t}{2\pi} \qquad (4)$$

where: $d_m$ = motor displacement $in^3/rev$

Combining equations (3) and (4) gives

$$d_m = 2\pi D_v e\, b \tag{5}$$

Since load torque, $T_l$, is given by

$$T_l = R_t\, T_m \tag{6}$$

we can also write

$$T_l = D_v b \Delta P_m e R_t \eta_t \tag{7}$$

The wheel drive motor sizing calculations are based on the following assumptions:

a. Tire breakaway resistance, 6 percent.

b. Rolling resistance, 2 percent.

c. Maximum grade resistance, 2 percent.

d. Maximum breakaway resistance on grade, 8 percent.

e. Rolling resistance on grade, 4 percent.

f. Maximum taxi weight of aircraft, 85,600 pounds (38,827 kg).

g. Rolling radius, 16.5 in. (41.91 cm).

The motor displacement corresponding to the maximum allowable flow and output shaft speed may be calculated as follows:

$$d_{as} = \frac{231\, \eta_v Q}{N_s} \quad (1)$$

where: $d_{as}$ = actuator displacement, $in^3$/rev (cc/rev) - (with the two orbit motors in series)

$\eta_v$ = Volumetric efficiency

$Q_m$ = Flow gpm (lit/min)

$N_s$ = Output shaft speed, rpm

---

Footnote:

(1) 231 is the number of $in^3$ in the U.S. gallon. Use 1000 for the SI units.

With: $\eta_v$ = 0.85

$Q_m$ = 45 gpm (170 lit/min)

$N_s$ = 153 rpm

equation (8) gives $d_{as}$ = 57.75 $IN^3$/REV (946 cc/Rev)

This is the motor displacement with the displacement changing valve in the high speed position. With the displacement changing valve in the alternate position the displacement will be doubled.

$$d_{ap} = 2\, d_{as} \tag{9}$$

The stall torque required to overcome the maximum breakaway resistance on the grade may be calculated as follows:

$$T_s = \frac{R_r W\ .08}{n_w}\ ^{(1)} \tag{10}$$

where: $T_s$ = Stall torque in-lbs (N - m)

$R_r$ = Rolling radius, in. (m)

$W$ = Weight of aircraft pounds (kg)

$n_w$ = Number of powered wheels

with: $R_r$ = 16.5 in (41.9 cm)

$W$ = 86,500 lbs (39,271 kg)

$n_w$ = 2

equation (10) gives $T_s$ = 57,090 in-lbs (64.56 N - m)

Then, based on equation (4) the pressure differential in the parallel mode to produce the required output torque per wheel is:

$$\Delta P_{mp} = \frac{2\pi T_s}{\eta_t d_{ap}} \tag{11}$$

- - - - - - - - - - - - - - - - - - - - - - - - - - - - - - - - - - - - - - - -

Footnote:

(1) Multiply by 9.807 when using the S.I. units.

When: $T_s$ = =57,000 lb-in. (6441 N - m)

$\eta_t$ = 0.85

$d_{ap}$ = 2 (57.75 $IN^3$/REV) = 115.5 $IN^3$/REV. (1893 cc/Rev.)

equation (11) gives $\Delta P$ = 3649 PSI (25.16 $MN/m^2$) which is less than the 4000 PSI (27.58 $MN/m^2$) maximum value.

The motor transmission ratio was selected to keep the orbit motor speed to less than 3600 RPM. Hence, the transmission ratio must be less than 23.5. The relationship between gear ratio, eccentricity and output gear pitch diameter is:

$$R_t = \frac{D_o}{2e} \qquad (12)$$

From the layout, the maximum value of $D_o$ is 4.40 in. (11.18 cm). So from equation (12), if $R_t < 23.5$, then e = 0.09362 IN. (0.2378 cm).

An additional restriction on the design is that the gears should have integral numbers of teeth and use standard AGMA diametral pitches. The relationship between the diametral pitch, $D_p$, and the number of teeth difference is,

$$N_4 - N_3 = \Delta N = 2eD_p \qquad (13)$$

A convenient value of $\Delta N$ is 3 which normally gives enough wrap-around to ensure the gears do stay in mesh. Substitution of $\Delta N$ = 3 and e = 0.09362 IN. (0.2378 cm) into equation (13) gives $D_p$ = 16.022 $IN^{-1}$ (6.038 $cm^{-1}$). A standard AGMA value of 16 $IN^{-1}$ (6.299 $cm^{-1}$), if substituted into equation (13), gives e = 0.9375 IN (0.2381 cm).

With $D_p$ = 16 $IN^{-1}$ (6.299 $cm^{-1}$), the largest value of $D_o$ less than 4.40 IN (11.18 cm) which gives an integral number of teeth is 4.25 IN (10.795 cm) for which the number of output gear teeth is 68. Substitution of $D_o$ = 4.25 IN (10.795 cm) and e = 0.9375 IN (0.2381 cm) into equation (12) gives $R_t$ = 22.67.

With 153 RPM shaft speed, the orbit speed is 3469 RPM. Then from equation (13), $N_4 = 71$. However, as shown later in the Gear Mesh and Stress Analyses, using a diametral pitch ($D_p$) of 32 results in lower tooth bending and contact stresses. Therefore, $N_3$ and $N_4$ increase proportionately to 136 and 142, respectively, and $\Delta N = 6$.

Substituting into equation (6) and solving for $T_m$ give 2514 lb-in (284.08 N-m). Then solving for the product $D_v b$ in equation (3) establishes the effective orbiter size.

$$D_v b = \frac{T_m}{P_m e N_t} \qquad (14)$$

$$= \frac{2514}{3649(.09375).85} = 8.646 \text{ IN}^2 \ (55.78 \text{ cm}^2)$$

By difinition and the layout based on the geometry of Figure 8,

$$D_v = D_s - L \qquad (15)$$

$$= 8.330 - .375 = 7.955 \text{ IN } (20.206 \text{ cm}).$$

Then from the value of equation (14), b = 1.087 IN (2.761 cm).

Table 2 summarizes the wheel drive motor sizing parameters used in the detail design of the assembly as revised for coarser pitch gears.

## Pressure Loss

The pressure loss analysis presented in Appendix B was based on the schematic of Figure 2 and included losses from the displacement changing valve (DCV) through the motor assembly and back to the DCV. For the motor assembly, it was considered to consist of two orbit motors connected in series, or parallel. It was assumed that 10 feet (3.05 m) of 0.75 IN (1.905 cm) diameter by 0.070 IN (0.178 cm) wall thickness tubing is to be used for the four connections from the DCV to the motor assembly.

TABLE 2. SUMMARY OF WHEEL DRIVE PARAMETERS *

| Symbol | Parameter | Value |
|---|---|---|
| b | Displacement chamber face width | 1.087 in. (2.761 cm) |
| $D_o$ | Output gear pitch diameter | 4.2500 in. (10.7950 cm) |
| $D_p$ | Diametral pitch | 24 $in^{-1}$ (9.4488 $cm^{-1}$) |
| $D_r$ | Orbiter gear pitch diameter | 4.4167 in. (11.2184 cm) |
| $D_S$ | Vane socket holes pitch diameter | 8.33 in (21.16 cm) |
| $D_v$ | Vane sealing diameter | 7.955 in (20.206 cm) |
| $d_{ap}$ | Actuator displacement in parallel mode | 115.50 $in^3$rev (1893 cc/rev) |
| $d_{as}$ | Actuator displacement in series mode | 57.75 $in^3$/rev (946 cc/rev) |
| e | Orbiter eccentricity relative to output shaft center line | 0.08333 in. (0.21166 cm) |
| L | Vane sealing length | 0.375 in (0.953 cm) |
| $N_3$ | Number of orbiter gear teeth | 106 |
| $N_4$ | Number of output gear teeth | 102 |
| $\Delta P_{mp}$ | Parallel mode predicted differential pressure required at rated torque | 3649 psi (25.16 $MN/m^2$) |
| $R_p$ | Sleeve spacer (guide pin) radial location | 3.469 in (8.811 cm) |
| $R_t$ | Transmission ratio | 25.50 |
| $T_1$ | Required load torque at rated speed | 14,250 lb-in. (1.61 kN-m) |
| $T_s$ | Required stall torque | 57,000 lb-in. (6.44 kN-m) |
| $\eta_t$ | Predicted torque efficiency | .85 |
| $\eta_v$ | Predicted volumetric efficiency | .85 |

* Parameters revised pursuant with Table 18.

Since the flow to and from each orbit motor is distributed and collected in the four annuli visible in Figure 6, the analysis determined the maximum percentage chamber flow equivalent of double that for a 12-chamber motor (26.8%) or 53.6% to cover the series mode connection. A maximum annular flow of 72% of the maximum motor assembly flow was determined to occur in the series mode by a distribution analysis. This is shown in the flow channel model of Figure 9 for $Q/Q_t$ in the channel sections corresponding to the annuli. This flow model neglects passage length and treats flow resistance as a series of orifices including expansion, contractions and bends.

The pressure loss was determined on the basis of the total resistance through one motor. Since the flow passages are essentially identical for both motors, this makes it convenient for determining pressure loss for series and parallel modes of operation.

Based on the use of a velocity head loss factors for the various features of the flow passage,

$$Q = \sqrt{\frac{\frac{2g}{\rho}\Delta P_m}{\sum \frac{K}{A^2}}} \quad IN^3SEC\ (cc/sec)^{(1)} \qquad (15)$$

Where: $A$ = Orifice area, $IN^2$ ($cm^2$)

$g$ = Gravitational constant, $IN/SEC^2$ ($cm/sec^2$)

$K$ = Velocity head loss factor

$\Delta P_m$ = Orbit motor pressure loss, PSI ($MN/m^2$)

$\rho$ = Fluid specific weight $LB/IN^3$ ($g/cc$)

Solving equation (15) for pressure loss,

$$\Delta P_m = \frac{\sum \frac{K}{A^2} Q^2 \rho}{2g} \qquad (16)$$

---

Footnote:

(1) Multiply by 257 when using S.I. units to obtain cc/sec.

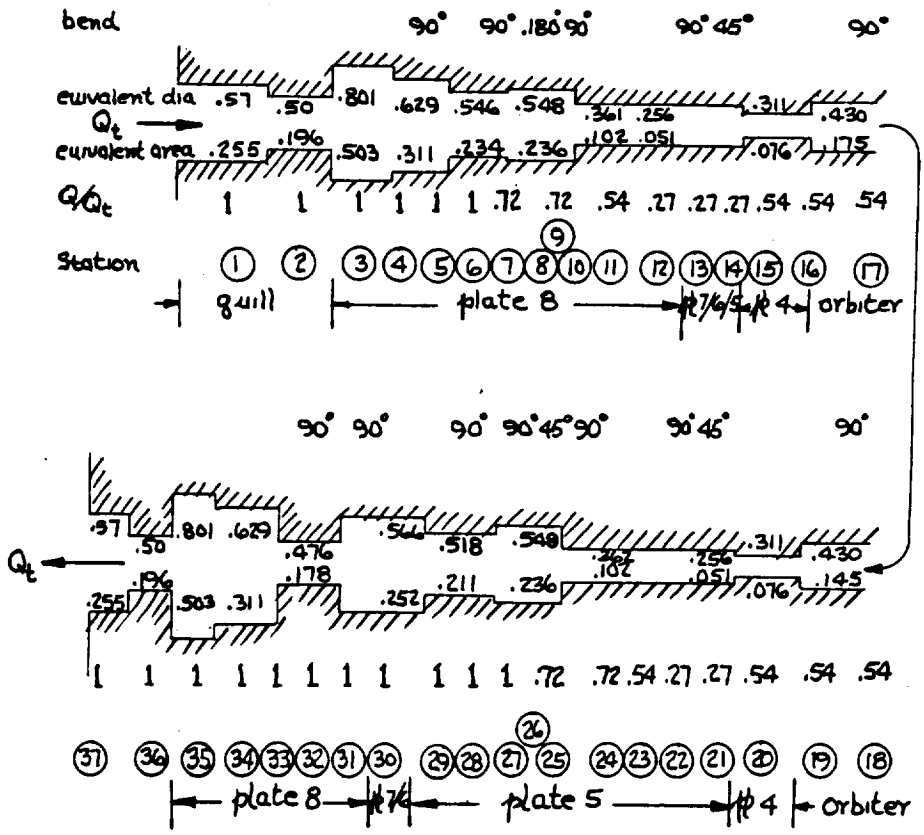


FIGURE 9. Flow Channel Model Through One Motor ($C_2/C_1$ Circuit Shown)

For convenience, the flow model indicates the normalized flow at each station and

$$\left(\frac{Q}{Q_t}\right)_{Max} = 1 \qquad (17)$$

Where: $Q$ = Flow at a given station, $IN^3/MIN$ (cc/min)

$Q_t$ = Maximum orbit motor flow, $IN^3/MIN$ (cc/min)

By substituting $Q/Q_t$ into (16) for Q and multiplying by $Q_t^2$, we obtain,

$$P_m = \Sigma \frac{\frac{K}{A^2}\left(\frac{Q}{Q_t}\right)^2 Q_t^2 \rho}{2g} \qquad (18)$$

$$= \Sigma \left[\frac{K}{\left(\frac{A\ Q_t}{Q}\right)^2}\right] \frac{Q_t^2 \rho}{2g}$$

Table 3 presents the calculated value of $\frac{K}{\left(\frac{A\ Q_t}{Q}\right)^2}$ for each station and the resultant summation for the 37 stations of 380.1 $IN^{-4}$ (9.13 $cm^{-4}$).

TABLE 3. $\sum \frac{K}{\left(\frac{A_{dn}Q_t}{Q}\right)^2}$ DETERMINATION FOR FLOW THROUGH ONE MOTOR ($C_2/C_1$ FLOW)

| Sta. No. | Resistance Type | Flow Ratio $Q/Q_t$ | (1) Area Ratio $A_{dn}/A_{up}$ | Press. Loss Factor $K^{(2)}$ | Downstream Velocity Ft/Sec | Downstream Area $A_{dn}$, $IN^2$ | $\left(\frac{A_{dn}Q_t}{Q}\right)^2$ | $\frac{K}{\left(\frac{A_{dn}Q_t}{Q}\right)^2}$ |
|---|---|---|---|---|---|---|---|---|
| 1 | Contract. | 1 | 0 | .44 | 56.6 | .255 | .065 | 6.767 |
| 2 | Contract. | 1 | .769 | .07 | 73.7 | .196 | .038 | 1.822 |
| 3 | Expansion | 1 | .390 (1) | .40 | 28.7 | .503 | .253 | 1.581 |
| 4 | Contract. | 1 | .618 | .18 | 46.4 | .311 | .097 | 1.861 |
| 5 | 90° Bend | 1 | - | 1.2 | 61.7 | .234 | .055 | 21.818 |
| 6 | Contract. | 1 | .752 | .08 | 61.7 | .234 | .055 | 1.455 |
| 7 | 90° Bend | .72 | - | 1.1 | 61.2 | .236 | .107 | 10.238 |
| 8 | Expansion | .72 | .992 (1) | 0 | 61.2 | .236 | .107 | 0 |
| 9 | 180° Bend | .72 | - | .2 | 61.2 | .236 | .107 | 1.869 |
| 10 | 90° Bend | .54 | - | 1.2 | 82.9 | .094 | .030 | 39.602 |
| 11 | Contract. | .54 | .576 | .21 | 76.4 | .102 | .036 | 5.88 |
| 12 | Flow Divide | .27 | 0 | .26 | 76.4 | .051 | .036 | 0 |
| 13 | 90° Bend | .27 | - | 1.2 | 76.4 | .051 | .036 | 33.33 |
| 14 | 45° Bend | .27 | .745 | .50 | 101.8 | .076 | .020 | 25.00 |
| 15 | Contract. | .536 | .745 | .08 | 101.8 | .076 | .020 | 3.979 |
| 16 | Expansion | .536 | .524 (1) | .25 | 53.4 | .145 | .073 | 3.416 |
| 17 | 90° Bend | .536 | - | 1.2 | 53.4 | .145 | .073 | 16.438 |
| 18 | 90° Bend | .536 | - | 1.2 | 53.4 | .145 | .073 | 16.438 |
| 19 | Contract. | .54 | .524 | .25 | 102.5 | .076 | .020 | 12.621 |

NOTE: (1) For expansions, the area ratio is $\frac{A_{up}}{A_{dn}}$

(2) K- Factors from Ref. 7

Where: $A_{up}$ = upstream area

Adn = downstream area

TABLE 3. $\sum \frac{K}{\left(\frac{A_{dn}Q_t}{Q}\right)^2}$ DETERMINATION FOR FLOW THROUGH ONE MOTOR ($C_2/C_1$ FLOW)

| Sta. No. | Resistance Type | Flow Ratio $Q/Q_t$ | (1) Area Ratio $A_{dn}/A_{up}$ | Press. Loss Factor $K^{(2)}$ | Downstream Velocity Ft/Sec | Downstream Area $A_{dn}$,IN$^2$ | $\left(\frac{A_{dn}Q_t}{Q}\right)^2$ | $\frac{K}{\left(\frac{A_{dn}Q_t}{Q}\right)^2}$ |
|---|---|---|---|---|---|---|---|---|
| 20 | Expansion | .27 | .745 (1) | .08 | 76.4 | .051 | .036 | 2.22 |
| 21 | 45° Bend | .27 | 1.342 | .5 | 76.4 | .051 | .036 | 13.88 |
| 22 | 90° Bend | .54 | 1.00 | 1.2 | 76.4 | .102 | .036 | 33.63 |
| 23 | 90° Bend | .72 | 1.74 | 1.2 | 44.0 | .236 | .107 | 11.169 |
| 24 | Expansion | .72 | .576 (1) | .21 | 44.0 | .236 | .107 | 1.963 |
| 25 | 45° Bend | .72 | - | .35 | 44.0 | .236 | .107 | 3.271 |
| 26 | 90° Bend | 1 | - | 1.2 | 68.4 | .211 | .045 | 26.954 |
| 27 | Contract. | 1 | .645 | .15 | 68.4 | .211 | .045 | 3.369 |
| 28 | 90° Bend | 1 | - | 1.2 | 57.3 | .252 | .064 | 18.896 |
| 29 | Expansion | 1 | .837 (1) | .03 | 57.3 | .252 | .064 | 0.472 |
| 30 | 90° Bend | 1 | - | 1.2 | 81.1 | .178 | .032 | 37.87 |
| 31 | Contract. | 1 | .706 | .10 | 81.1 | .178 | .032 | 3.16 |
| 32 | 90° Bend | 1 | - | 1.2 | 46.4 | .311 | .097 | 12.407 |
| 33 | Expansion | 1 | .572 (1) | .22 | 46.4 | .311 | .097 | 2.268 |
| 34 | Expansion | 1 | .618 (1) | .18 | 28.7 | .503 | .253 | 0.711 |
| 35 | Contract. | 1 | .390 | .31 | 73.7 | .196 | .038 | 1.628 |
| 36 | Expansion | 1 | .769 (1) | .07 | 56.6 | .255 | .065 | 1.077 |
| 37 | Expansion | 1 | .419 (1) | .37 | 23.7 | .609 | .371 | 0.998 |
| | | | | | | | $\sum =$ | 380.1 IN$^{-4}$ |
| | | | | | | | | (9.13 cm$^{-4}$) |

Series mode operation. For the series mode operation, maximum flow through each orbit motor is 45 gpm (170 lit/min), $\rho$ = 0.031 lbs/in$^3$ (0.86 gm/cc) and g = 386 in/sec (980 cm/sec$^2$), so from equation (18) for one orbit motor,

$$\Delta P_m = \frac{380.1\ [45(3.85)]^2\ .031}{2\ (386)}$$

$$= 458 \text{ PSI } (3.16 \text{ MN/m}^2)$$

The total series loss for both motors, $\Delta P_s$, is then double or 916 PSI (6.32 MN/m$^2$).

To this loss must be added that of the four lengths of 0.609 IN (1.549 cm) I.D. by 10 feet (3.05 m) tubing. The tubing pressure loss is

$$\Delta P_{1s} = \frac{12f\ L_s\ \rho V_s^2}{2Dg} \quad \text{lb/in}^2 \ (1) \quad (\text{MN/m}^2) \qquad (19)$$

Where: $f$ = Tube surface roughness factor = .03

$L_s$ = Total line length = 40.0 ft (12.19 m)

$V_s$ = Fluid velocity = $Q_s/A$

$$= \frac{173.25 \text{ in}^3/\text{sec}}{0.291 \text{ in}^2} = 594.77 \text{ in/sec } (1511 \text{ cm/sec})$$

$D$ = Tubing I.D. = 0.609 in (1.549 cm)

$$\Delta P_{1s} = \frac{.03(40)\ 12\ (.031)594.77^2}{2\ (.609)\ 386}$$

$$= 335.9 \text{ PSI } (2.32 \text{ MN/m}^2)$$

Thus for the series mode operation, the predicted pressure loss is

$$\Delta P_{ts} = \Delta P_s + \Delta P_{1s} \qquad (20)$$

$$= 916 + 336 = 1252 \text{ PSI } (8.63 \text{ MN/m}^2)$$

---

Footnote:

(1) The factor 12 is to convert feet into inches. For the S.I. units use 0.009807 $6.894(10^3)$

Parallel mode operation. For parallel operation, maximum orbit motor flow is 22.5 gpm (85 lit/min), or one-half of the series mode which, substituted in equation (18), results in one-fourth the pressure loss, or 114.5 PSI (0.789 $MN/m^2$). Since this is the total loss in the parallel mode, it is one-eighth of the loss for both orbit motors in series. Also, the total line length in parallel is half that for series and the velocity is one-fourth (since flow is half), so the product results again in one-eighth the pressure loss, or 42 PSI (0.289 $MN/M^2$). Consequently, the total parallel mode pressure loss is then one-eighth that predicted for the series mode, or 156.5 PSI (1,079 $MN/m^2$).

Summarizing, the total pressure loss for the two modes can be expressed as

$$\Delta P_t = kQ_t^2 \qquad (21)$$

So,

$$\Delta P_{ts} = 0.6183\ (45\ GPM)^2 = 1252\ PSI$$

$$= \left[0.0002986\ (170\ lit/min)^2 = 8.63\ MN/m^2\right]$$

and

$$\Delta P_{tp} = 0.07728\ (45)^2 = 156.5\ PSI$$

$$= \left[.00003734\ (170\ lit/min)^2 = 1.079\ MN/m^2\right]$$

## Static Performance

The static performance of the wheel drive motor can best be presented in the form of predicted torque-speed curves. The curves, one each for parallel and series operation, are displayed in Figures 10 and 11 respectively. The analysis for the plotting of the curves is based on the assumed efficiencies and predicted pressure losses.

With the previously assumed torque efficiency, $\eta_t = .85$, and the pertinent sizing parameters from Table 2, equation (7) becomes,

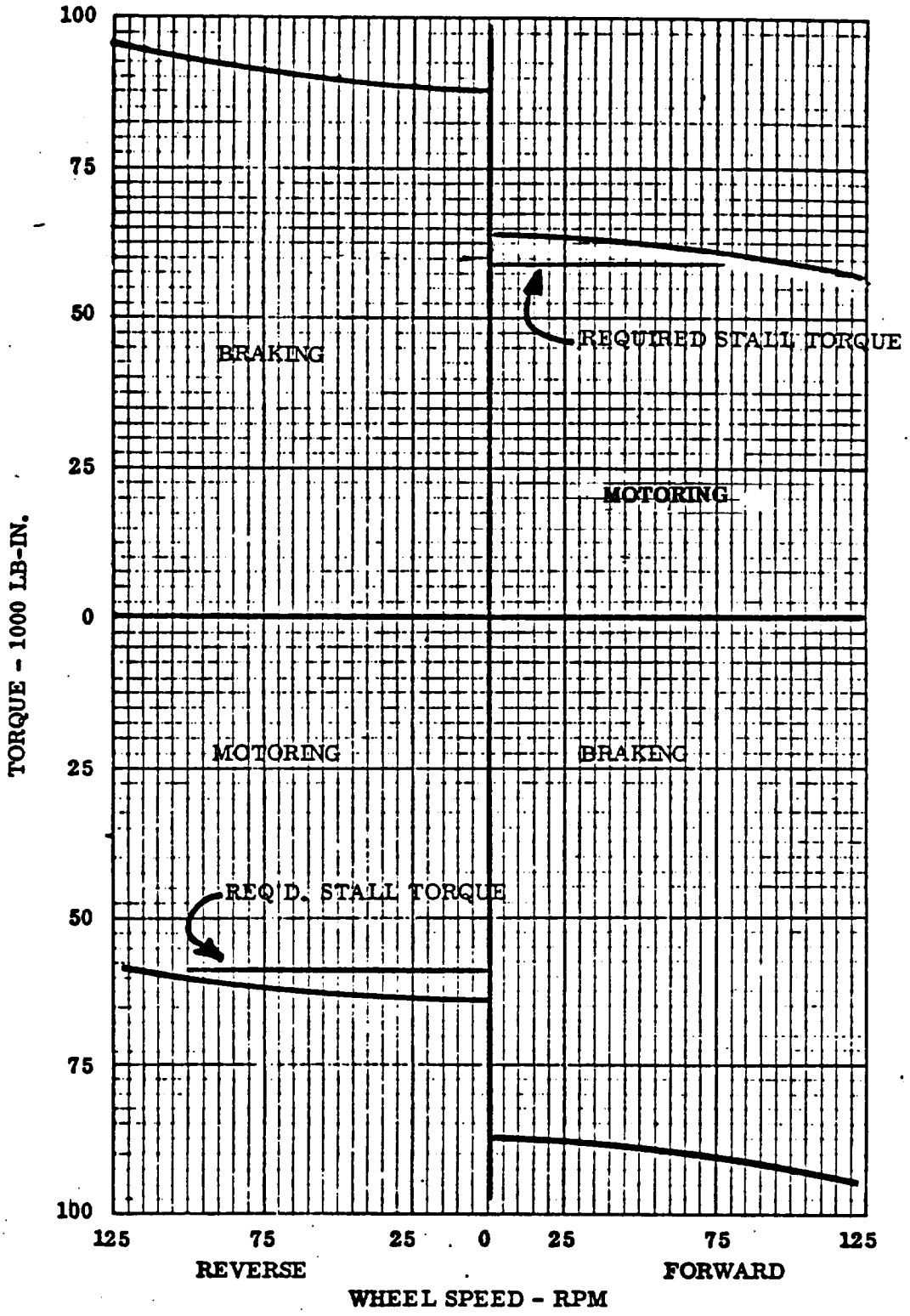


FIGURE 10. Predicted Torque Vs. Speed In Parallel Operation

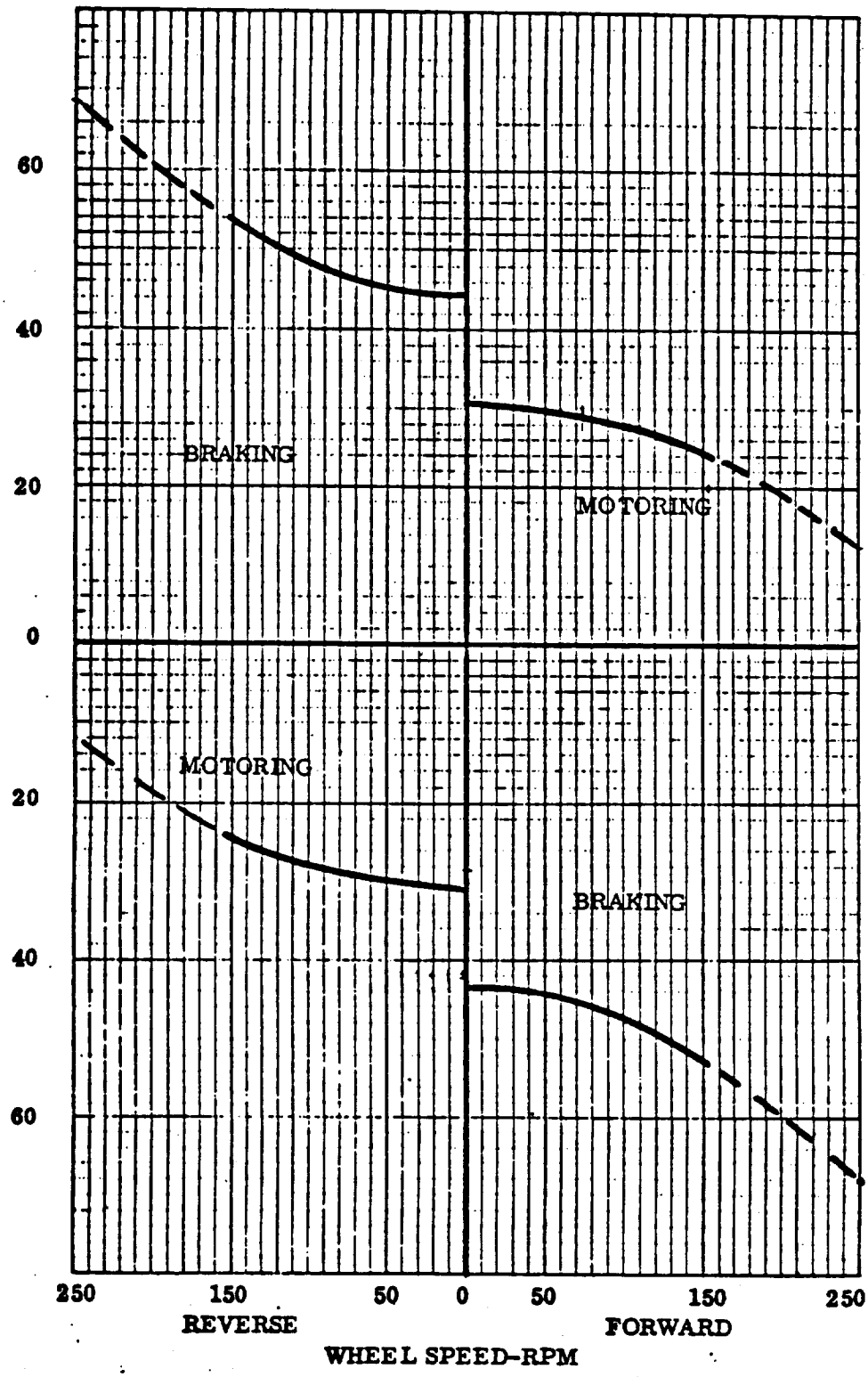


FIGURE 11. Predicted Torque Vs. Speed In Series Operation

$$T_{1p} = 15.62\Delta P \text{ Lb-In/psi in the parallel mode} \quad (22)$$

$$= (256\Delta P \text{ N-m/MN/m}^2)$$

$$T_{1s} = 7.81\Delta P \text{ Lb-In/psi in the series mode} \quad (23)$$

$$= (128\Delta P \text{ N-m/MN/m}^2$$

From the previous section on pressure loss and equation (20), the total pressure loss at 45 gpm (170 lit/min) flow is 1252 psi (8.62 $MN/m^2$) so at any flow Q,

$$\Delta P_{ts} = \frac{1252 \text{ psi } Q_{ds}^2}{(45 \text{ gpm})^2} = 0.618\ Q_{ds}^2 \text{ psi } (0.000299\ Q_d^2\ MN/m^2) \quad (24)$$

and from equation (21) for parallel mode,

$$\Delta P_{tp} = \frac{156.5 \text{ psi } Q_{dp}^2}{(45 \text{ gpm})^2} = 0.0773\ Q_{dp}^2 \text{ psi } (0.0000373\ Q^2\ MN/m^2) \quad (25)$$

Since at a maximum aircraft wheel speed of $N_w$ = 153 rpm, the flow is 45 gpm (170 lit/min),

$$N_w = 153\ \frac{Q_{ds}}{45} = 3.4\ Q_d\ \frac{\text{rpm}}{\text{gpm}}\ \ (0.9\ Q_d\ \frac{\text{rpm}}{\text{lit/min}})$$

Solving for $Q_d$,

$$Q_{ds} = 0.294\ N_w \text{ gpm } (1.11\ N_w \text{ lit/min) series mode} \quad (26)$$

$$Q_{dp} = 0.588\ N_w \text{ gpm } (2.22\ N_w \text{ lit/min parallel mode} \quad (27)$$

which substituting in equations (24) and (25)

$$\Delta P_{ts} = 0.0534\ N_w^2 \text{ psi } (0.000368\ N_w^2\ MN/m^2) \quad (28)$$

$$\Delta P_{tp} = 0.0267\ N_w^2 \text{ psi } (0.000184\ N_w^2\ MN/m^2) \quad (29)$$

The pressure available to produce torque,

$$\Delta P_t = P_s - P_r - P_1 \quad (30)$$

where: $\Delta P_s$ = supply pressure = 4000 psi (27.58 $MN/m^2$)

$\Delta P_1$ = pressure loss, equation (28) or (29)

$\Delta P_r$ = return pressure = 100 psi (0.6895 $MN/m^2$)

Therefore, the predicted motor output torque-speed relationship in the driving mode is,

$$T_{1p} = 15.62\ (3900 - 0.0267\ N_w^2)\ \text{Lb-In, parallel mode} \quad (31)$$

$$= [256\ (26.89 - 0.000184\ N_w^2)\ N - m]$$

$$T_{1s} = 7.81\ (3900 - 0.0534\ N_w^2)\ \text{Lb-In, series mode} \quad (32)$$

$$= [128\ (26.89 - 0.000368\ N_w^2)\ N - m]$$

For the torque-speed relation in the braking mode of operation, the torque efficiency is inverted so that equation (7) becomes,

$$T_1 = D_v b\ \Delta P_m \rho R_t / \eta_t \quad (33)$$

In the braking mode, the pressure loss increases the torque with speed over the relief valve setting, which will be set at 4100 psi (28.27 $MN/m^2$). Therefore, the expressions equivalent to equations (31) and (32) in braking are,

$$T_{1p} = 21.66\ (4100 + 0.0267\ N_w^2)\ \text{Lb-In} \quad (34)$$

$$= [354.33\ (28.27 + 0.000184\ N_w^2)\ N - m]$$

$$T_{1s} = 10.84\ (4100 + 0.0534\ N_w^2)\ \text{Lb-In} \quad (35)$$

$$= [177.16\ (28.27 + 0.000368\ N_w^2)\ N - m]$$

Figures 10 and 11 show the predicted torque versus speed for the parallel and series conditions, respectively, for both the motoring and braking modes based on equations (31), (32), (34), and (35). It is apparent from the required stall torque value shown in Figure 10 that the design has some positive margin performance of 6.9% for meeting the requirement.

## Dynamic Performance

The dynamic performance of the wheel drive motor consists of the static torque-speed curves presented in the previous section as applied to the aircraft in conjunction with the actuator inertia, oil volume under compression, and the control valving. A rigorous analysis of the powered wheel drive/aircraft system, shown by the block diagram in Figures 12 and 13, would require the use of a

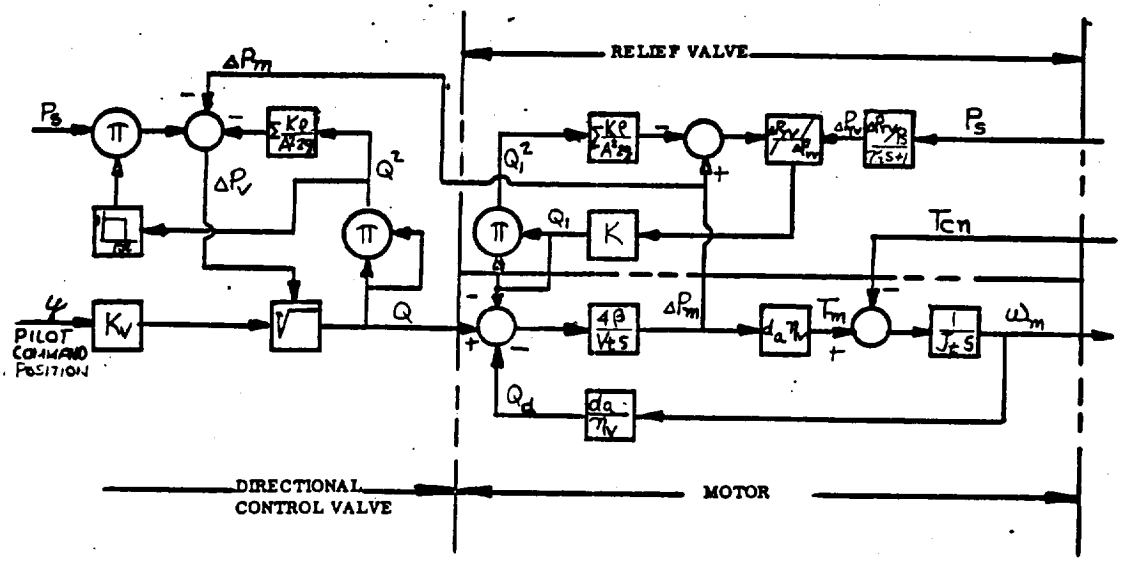


FIGURE 12. Block Diagram - Directional Control Valve and Motor

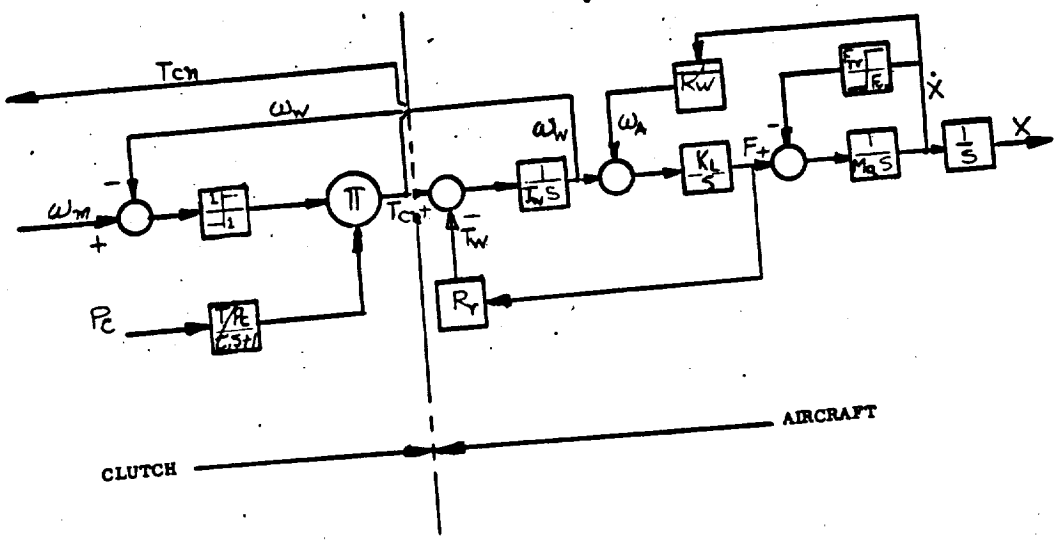


FIGURE 13. Block Diagram - Clutch and Aircraft

computer and considerable effort which was not considered economically justified for the program. Instead, various natural frequencies were determined and compared with known aircraft landing gear frequencies. Also, some parameters were evaluated, such as actuator spin-up time after clutch actuation and the spin-up load magnitude imposed on the output shaft bearings, etc. The lowest order response was determined by elimination of all higher order dynamics and considering only the aircraft wheel inertia with the pilot's control valve in some steady state condition.

Pursuant to the SOW (Appendix A) typical use cycle specified for dynamometer testing, there are five distinct operating conditions which are:

Condition 1 - Brake to 0 mph from 15 mph (24 km/h, series mode.

Condition 2 - Accelerate to 7.5 mph (12 km/h) from 0 mph, parallel mode.

Condition 3 - Accelerate to 15 mph from 7.5 mph, series mode

Condition 4 - Constant 15 mph for remainder of 2.5 mile (4 km) taxi.

Condition 5 - Reverse direction for 300 ft. (91 km) at 3 mph (4.8 km/h), parallel mode.

Acceleration performance. Consequently, as developed in Appendix C, acceleration equations for motoring and braking in both series and parallel modes of operation were derived before the accelerations associated with the above five conditions could be evaluated. Simplifying assumptions made in the manipulations of the block diagrams were:

Directional control valve gain, $K_v = \infty$

Landing gear spring rate, $K_1 = \infty$

Wheel inertia, $J_w = 0$

Actuator inertia, $J_t = 0$

Fluid volume under compression, $V_t = 0$

These assumptions result in the simplified block diagram shown below.

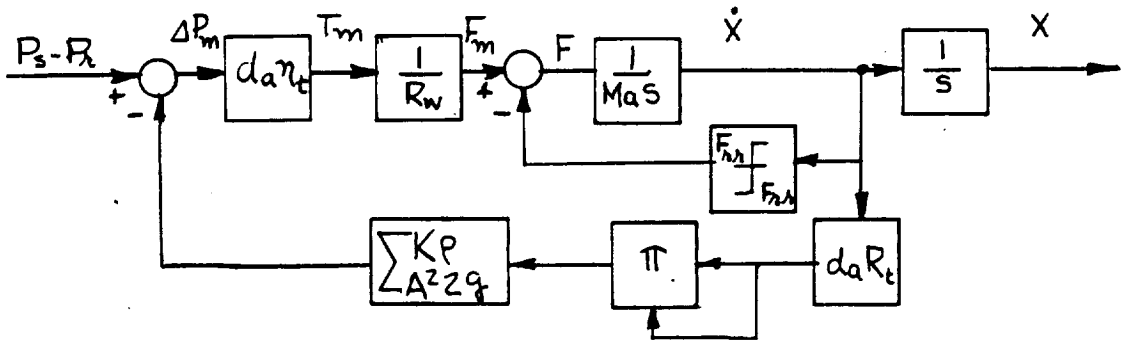


FIGURE 14. Simplified Block Diagram

Therefore, based on the following numerical values and definitions,

$$\Delta P_m \triangleq P_s - \Delta P_t \text{ @ } P_r = 0 \text{ in a motoring condition} \quad (36)$$

$$= P_s + \Delta P_t \text{ @ } P_r = 0 \text{ in a braking condition} \quad (37)$$

$$\Delta P_t \triangleq (\Delta P_{tp}) \text{ max } (\dot{X}/\dot{X}max)^2, \text{ in parallel mode} \quad (38)$$

$$= (\Delta P_{ts}) \text{ max } (\dot{X}/\dot{X}max)^2, \text{ in series mode} \quad (39)$$

$(\Delta P_{tp})$ max = 156.5 psi (1.079 $MN/m^2$) @ $\dot{X}max$ = 11 Ft/Sec (3.35 m/sec)

$(\Delta P_{ts})$ max = 1252 psi (8.63 $MN/m^2$) @ $\dot{X}max$ = 22 Ft/Sec (3.70 m/sec)

$M_a$ = 50% of aircraft mass = 1329 $lb\text{-}sec^2/ft$ (19.77 $kg\text{-}sec^2/cm$)

$d_a \triangleq d_{as}/2\pi$ = 9.19 $In^3$Rad (150.6 cc/rad) in series mode

$\triangleq d_{ap}/2\pi$ = 18.38 $In^3$/Rad (301.1 cc/rad) in parallel mode

$R_w$ = wheel radius = 16.48 In (41.86 cm)

$F_{rr}$ = % resistance times ($M_a$ g) = 856 lbs. (388.6 kg) for 2% resistance

= % resistance times ($M_a$ g) = 1712 lbs. (777.3 kg) for 4% resistance

$P_s$ = 3900 psi (26.89 $MN/m^2$) for driving conditions

= 4100 psi (28.27 $MN/m^2$) for braking conditions

and from the block diagram above, the expressions for the output force and resultant aircraft acceleration are,

$$F_m = (\Delta P_m \, d_a \, \eta_t / R_w) - F_{rr} \quad (40)$$

$$a = F_m / M_a \quad (41)$$

Therefore, based on the numerical values of parameters as presented above for the series mode,

$$F_{ms} = 1849 - 1.22 \dot{X}^2 - F_{rr} \text{ Lbs.} \quad (42)$$

$$= (838.5 - .553 \dot{X}^2 - F_{rr}) \text{ kg}$$

$$a_s = 1.391 - .000918\dot{X}^2 - .000752 F_{rr} \text{ Ft/Sec}^2 \quad (43)$$

$$= (.4240 - .0002798\dot{X}^2 - .000506 F_{rr}) \text{ m/Sec}^2$$

For the parallel mode, the two expressions are,

$$F_{mp} = 3698 - 1.22 \dot{X}^2 - F_{rr} \text{ Lbs.} \quad (44)$$

$$= (1677.6 - .533\dot{X}^2 - F_{rr}) \text{ kg}$$

$$a_p = 2.782 - .000918 \dot{X} - .000752 F_{rr} \text{ Ft/Sec}^2 \quad (45)$$

$$= (.8486 - .0002798 \dot{X}^2 - .000506 F_{rr}) \text{ m/sec}^2$$

Therefore, for the four motoring conditions and resistance combinations derived from equations (42) and (44)

at 2% resistance

$$a_{s2} = .747 - .000918\dot{X}^2 \text{ Ft/Sec}^2 \quad (46)$$

$$= (.2274 - .0002798\dot{X}^2) \text{ m/sec}^2$$

$$a_{p2} = 2.138 - .000918\dot{X}^2 \text{ Ft/Sec}^2 \quad (47)$$

$$= (.6520 - .0062798\dot{X}^2) \text{ m/sec}^2$$

At 4% resistance

$$a_{s4} = .1036 - .000918\dot{X}^2 \text{ In/Sec}^2 \quad (48)$$

$$= (.0307 - .0002798\dot{X}^2) \text{ m/sec}^2$$

$$a_{p4} = 1.4946 - .000918\dot{X}^2 \text{ In/Sec}^2 \quad (49)$$

$$= (.4553 - .0002798\dot{X}^2) \text{ m/sec}^2$$

For the braking condition, only the series mode operation is considered since output shaft bearing overload will occur if the parallel mode is used for braking at high taxi speeds. Overloading can occur even though the relief valve is set at 4100 psi (28.27 $MN/m^2$) because of the excessive line pressure loss that will occur (with twice the normal maximum flow) and which is additive to the relief valve set pressure. So from the block diagram again and equation (37) for the series mode, the output force and resultant aircraft acceleration expressions are,

$$F_m = (\Delta P_m \, d_a/\eta_t \, R_w) + F_{rr} \qquad (50)$$

Therefore, based on the numerical values, equation (50) for braking becomes,

$$F_{mb} = 2690 + 1.697 \, \dot{X}^2 + F_{rr} \text{ Lbs.} \qquad (51)$$

$$= (1220.2 + .7679 \, \dot{X}^2 + F_{rr}) \text{ kg}$$

$$a_b = 2.0241 + .001277 + .000752 \, F_{rr} \text{ Ft/Sec}^2 \qquad (52)$$

$$= (.6170 + .000388 \, \dot{X}^2 + .000506 \, F_{rr}) \text{ m/sec}^2$$

Table 4 shows the calculated time and distance required to attain the limiting speed during conditions 1 through 3 for both resistance values. The time values were determined by equating the appropriate acceleration equation to $d\dot{X}/dt$, solving for dt, then integrating to find t. The distance values were similarly determined by equating the acceleration equations to $\dot{X}d\dot{X}/dX$, solving for dX and integrating to find X. In the condition 3 case with 4% resistance, it was found that 7.5 mph (12 km/h) speed could not be sustained after shifting to the series mode. It was determined that the speed would decline approximately 4%. Naturally, the decline may be avoided by not shifting out of the parallel mode.

TABLE 4. CALCULATED TIME AND DISTANCE TO REACH VARIOUS SPEEDS

| Condition | Rolling Resistance % | Speed mph, (km/h) | Motor Mode | Reqd. Time Seconds | Reqd. Distance Ft. (m) |
|---|---|---|---|---|---|
| Braking | 2 | To zero from 15 (24) | Series | 7.7 | 82 (25) |
| Acceleration | 2 | Zero to 7.5 (12) | Parallel | 5.2 | 29 (8.8) |
| Acceleration | 2 | 7.5 (12) to 15 (24) | Series | 23.7 | 407 (124) |
| Braking | 4 | To zero from 15 (24) | Series | 6.3 | 67 (20.4) |
| Acceleration | 4 | Zero to 7.5 (12) | Parallel | 7.6 | 42 (12.8) |
| Acceleration | 4 | 7.5 (12) to 15 (24) | Series | * | * |

* Calculations indicate torque saturation will occur with only an attainable top speed of approximately 7.5 mph (12 km/h).

Clutch spin-load. In evaluation of the loading imposed on the output shaft bearings produced by engaging the clutch with a maximum wheel speed of 15 mph (24 km/h), it was necessary to calculate the total inertia of the rotating parts. This inertia is composed of the individual inertia of the orbiter/gear, output shaft, and rotating clutch parts. Fortunately, even though the orbiter/gear weights were computed to be a substantial 9.5 lbs. (4.3 kg), the inertia is very small because the assembly does not rotate but orbits in a very small diameter (2e) circle. The inertia multiplied by the transmission ratio (22.67) to reflect it to the output is less than 10% of the clutch inertia. The output shaft inertia is small also since it is less than 6% of that of the clutch. The total calculated inertia ($J_t$), as calculated in Appendix C, is only 1.5316 Lb-In-Sec$^2$ (1.765 kg-cm-sec$^2$) so that the spin-up acceleration with no differential applied to the motor (bypass load limiting valve in the bypass mode and the directional control valve is neutral) is,

$$\alpha = T_{cn}/J_t \qquad (53)$$

Where $T_{cn}$ = 44,744 Lb-In (51,550 kg - cm) torque developed by the clutch with 4000 psi (27.58 $MN/m^2$) pressure applied to the six actuating pistons and four clutch friction surfaces with .35 coefficient of friction (Ref. Appendix D).

$$= \frac{44,744}{1.5316} = 29213.9 \text{ Rad/Sec}^2$$

Then the time to reach 15 mph (24 km/h speed,

$$t = \frac{\omega}{\alpha} \qquad (54)$$

$$= \frac{2\pi \ 153 \text{ rpm}}{29213.9 \ (60)} = .00055 \text{ Sec}$$

A low spin-up time such as this suggests that full clutch torque cannot be applied while the clutch is slipping because of the slower hydraulic pressure response. Assuming a single order pressure rise time constant of .050 second, the time to reach maximum speed is determined (in Appendix C) to be .00758 second, at which time clutch torque developed is only 6294 lb-in (711 N - m). Of this amount, only that which is proportional to the ratio of the orbiter/gear inertia (at the output) to the total inertia is applied to the output shaft bearings, or only 457 lb-in (51.57 N - m).

Actuator natural frequency. The natural frequency of the actuator and wheel,

$$n = \sqrt{K_h \ K_s/(K_h + K_s) \ (J_w + J_t)} \quad \text{Rad/Sec}^{(1)} \qquad (55)$$

Where: $K_h$ = Hydraulic spring rate

$K_s$ = Output shaft spring rate

$J_w$ = Wheel inertia

$J_t$ = Actuator inertia

---

Footnote:

(1) When using S.I. units multiply by 3.193.

Since $K_s >>>> K_h$ and $J_w >>>> J_t$

$$\omega_n = \sqrt{K_h/J_w} \qquad (56)$$

Where: $K_h = 4\beta (d_{as})^2/V_t$

$\beta$ = Fluid bulk modulus = 100,000 psi (689.5 $MN/m^2$)

$d_{as}$ = 9.19 $In^3$/Rad (150.6 cc/rad)

$V_t$ = 231 $In^3$ (3785 cc)

$J_w$ = 84 Lb-In-$Sec^2$ (96.78 kg - cm - $sec^2$)

$$\omega_n = \sqrt{\frac{1.4624(10^5)\ \text{Lb-In}}{84\ \text{Lb-In-Sec}^2}} = 41.73\ \text{Rad/Sec}$$

$$= 6.64\ \text{HZ}$$

This frequency is about the same as that normally attributed to aircraft landing gears based on Bendix's experience so it seems that some coupling could occur with a resultant gear oscillation. However, since the torque generated is so small compared to the typical brake torque, oscillation would be small in magnitude. In addition, it is anticipated that for installation on the 737, the oil volume could be reduced to 40% of the 231 $In^3$ (3785 cc) estimated for dynamometer testing by eliminating 20 feet (6.098 m) of .75 in (1.905 cm) diameter tubing and using a much smaller displacement changing valve. This smaller volume, 92.4 $In^3$ (1514 cc), would increase the natural frequency to 10.50 Hertz. This is still quite near the normal gear frequencies so assuming that a further oil volume reduction to 30 $In^3$ (492 cc) can be achieved by packaging the displacement changing valve and relief valves together, the natural frequency would increase to 18.43 Hertz, which should be sufficiently high to preclude any noticeable coupling effects on the 737 landing gear.

In summary based on a simplified dynamic model of the powered wheel actuator - wheel - aircraft system, the lowest order dynamics indicates that no significant coupling of the actuator dynamics (during braking) with landing gear dynamics should occur. The analysis does indicate that a reasonable effort should be made to reduce the volume of oil under compression in the plumbing to a minimum to separate actuator and landing gear natural frequencies.

## Loads and Stress

Output shaft bearings load and life. An analysis of the loads on the output shaft bearings has to originate with the force on the orbiter. This force is,

$$\vec{F}_o = \vec{F}_h + \vec{F}_r \qquad (57)$$

Where: $F_h$ = Gear hold-in force

$F_r$ = Orbiter hydraulic force

It can be shown that for any condition, the wheel drive motor orbiter total force,

$$F_o = 8.62 \text{ Lb/psi } \Delta P_m \text{ Lbs.} \qquad (58)$$

$$= (567.07 \text{ kg/MN/m}^2)\, \Delta P_m \text{ kg.}$$

Then based on the location of the orbiter between the two shaft bearings, force distribution is as follows:

$$F_{b1} = .526\, F_o \qquad (59)$$

and

$$F_{b2} = .474\, F_o \qquad (60)$$

where: $F_{b1}$ = Clutch-end or outboard bearing force

$F_{b2}$ = Axle flange-end or inboard bearing force

During driving conditions, for which maximum $\Delta P_m$ = 3649 psi (25.16 MN/m$^2$), the values of the three forces are from equations (58) - (60).

$F_o$ = 31454 lbs (14267 kg)

$F_{b1}$ = 16545 lbs (7505 kg)

$F_{b2}$ = 14909 lbs (6763 kg)

For the five distinct operating conditions required by the SOW and previously enumerated, the summary of bearing loads, speed and time is presented in Table 5. Table 6 presents the accumulative time for one test cycle at 2% and 4% resistance. Since there are 50 cycles at each condition, the predicted total cycling time is 54.28 hours. Table 6 also shows the predicted percentage of total time spent at seven conditions of distinctly different loading conditions so that the $L_{10}$ bearing life must be determined from,

$$L_h = \frac{16666}{N} \left(\frac{C}{P}\right)^3 \qquad (61)$$

TABLE 5. SUMMARY OF BEARING LOADS, SPEED AND TIME

| Rolling Resistance % | Condition No. (Ref.: Page Number 49) | Time Seconds | Distance Travelled Ft (m) | Average Bearing Load Pounds (kN) | | Average Speed RPM |
|---|---|---|---|---|---|---|
| | | | | $F_{b1}$ | $F_{b2}$ | |
| 2 | 1 | 7.7 | 82 (25) | 14,172 (63.0) | 12,770 (56.8) | 74.06 |
| 2 | 2 | 5.2 | 29 (8.8) | 16,543 (73.6) | 14,907 (66.3) | 38.78 |
| 2 | 3 | 23.7 | 407 (124) | 9,068 (40.3) | 8,172 (36.4) | 119.40 |
| 2 | 4 | 594.4 | 13077 (3987) | 4,534 (20.2) | 4,085 (18.2) | 153.00 |
| 2 | 5 | 68.2 | 300 (91.5) | 4,094 (18.2) | 3,690 (16.4) | 30.59 |
| 4 | 1 | 6.3 | 67 (20.4) | 14,172 (63.0) | 12,770 (56.8) | 73.96 |
| 4 | 2 | 7.6 | 42 (12.8) | 16,543 (73.6) | 14,907 (66.3) | 38.43 |
| 4 | 3 | 1241 | 13158 (4012) | 7,482 (33.3) | 6,743 (30.0) | 73.73 |
| 4 | 4 | * | - | - | - | - |
| 4 | 5 | 68.2 | 300 (91.5) | 8,189 (36.4) | 7,379 (32.8) | 30.59 |

*Condition will not be met because of torque saturation.

TABLE 6. BEARING EQUIVALENT DYNAMIC LOADS AND SPEED

(BASED ON REQUIRED TEST CYCLES & DATA FROM TABLE 5)

| Rolling Resistance | Cond. No. (Ref.: Pg.# 49) | Accum. Time Sec. | Bearing Load Pounds (kN) | | Avg. Speed RPM | % of Total Accum. Time @ Each Cond. | Accum. % of Time @ Identical Loads and Speed |
|---|---|---|---|---|---|---|---|
| | | | $F_{h1}$ | $F_{h2}$ | | | |
| 2 | 1 | 7.7 | 14,172 (63.0) | 12,770 (56.8) | 74.06 | 0.197 | 0.72 |
| | 2 | 12.9 | 16,543 (73.6) | 14,907 (66.3) | 38.78 | 0.133 | 0.65 |
| | 3 | 36.6 | 9,068 (40.3) | 8,172 (36.4) | 119.40 | 0.506 | 1.01 |
| | 4 | 631.0 | 4,534 (20.2) | 4,085 (18.2) | 153.00 | 15.209 | 30.42 |
| | 1 | 638.7 | 14,172 (63.0) | 12,770 (56.8 | 74.06 | 0.197 | |
| | 5 | 706.9 | 4,094 (18.2) | 3,690 (16.4) | 30.59 | 1.745 | 1.75 |
| | 2 | 712.9 | 16,543 (73.6) | 14,907 (66.3) | 38.78 | 0.133 | |
| | 3 | 735.8 | 9,068 (40.3) | 8,172 (36.4) | 119.40 | 0.506 | |
| | 4 | 1330.2 | 4,534 (20.2) | 4,085 (18.2) | 153.00 | 15.209 | |
| 4 | 1 | 1336.5 | 14,172 (63.0) | 12,770 (56.8) | 73.96 | 0.161 | |
| | 2 | 1344.1 | 16,543 (73.6) | 14,907 (66.3) | 38.43 | 0.194 | |
| | 3 | 2585.1 | 7,482 (33.3) | 6,743 (30.0) | 73.73 | 31.754 | 63.51 |
| | 1 | 2591.4 | 14,172 (63.0) | 12,770 (56.8) | 73.96 | 0.161 | |
| | 5 | 2659.6 | 8,189 (36.4) | 7,379 (32.8) | 30.59 | 1.745 | 1.75 |
| | 2 | 2667.2 | 16,543 (73.6) | 14,907 (66.3) | 38.43 | 0.194 | |
| | 3 | 3908.2 | 7,482 (33.3) | 6,743 (30.0) | 73.73 | 31.754 | |

Where: C = Dynamic rating of bearing

P = Equivalent dynamic load

N = Equivalent speed

For variable loads and speeds,

$$P = \sqrt[3]{\frac{q_1 n_1 F_1^3 + q_2 n_2 F_2^3 + \text{---} q_n n_n F_n^3}{q_1 n_1 + q_2 n_2 + \text{---} q_n n_n}} \qquad (62)$$

Where: q = % of time

n = speed, rpm

F = load, lbs.

$$N = \frac{q_1 n_1 + q_2 n_2 \text{---} + q_n n_n}{100} \qquad (63)$$

From Tables 6 - 8, values of the parameters in equations (62) and (63) result in

Bearing No. 1 (INA NK 105/26) C = 6900 kg

P = 6609 lbs (3000 kg)

N = 96.614

$L_h$ = 2103 hours

Bearing No. 2 (INA NK 95/26) C = 6400 kg

P = 5956 lbs (2702 kg)

N = 96.614

$L_h$ = 2294 hours

The ratio of maximum predicted loads (at stall) to the static ratings of the bearings is

Bearing No. 1

Static Ratio = $\frac{7505 \text{ kg}}{8300 \text{ kg}} = .90$

Bearing No. 2

Static Ratio = $\frac{6763 \text{ kg}}{7400 \text{ kg}} = .91$

TABLE 7. EQUATIONS 63 AND 64 PARAMETERS FOR BEARING NO. 1

(INA NK 105/26)

| $q_n$ | $n_n$ RPM | $F_n$ Lbs. | $F_n^3$ $Lbs^3$ | $q_n n_n F_n^3$ RPM-$lbs^3$ | $q_n n_n$ RPM |
|---|---|---|---|---|---|
| 0.72 | 74.06 | 14,172 | 2.846 $(10^{12})$ | 1.518 $(10^{14})$ | 53.323 |
| 0.65 | 38.78 | 16,543 | 4.527 $(10^{12})$ | 1.141 $(10^{14})$ | 25.207 |
| 1.01 | 119.40 | 9.068 | 0.746 $(10^{12})$ | 0.900 $(10^{14})$ | 120.594 |
| 30.42 | 153.00 | 4,534 | 0.093 $(10^{12})$ | 4.328 $(10^{14})$ | 4654.260 |
| 1.75 | 30.59 | 4,094 | 0.069 $(10^{12})$ | 0.037 $(10^{14})$ | 53.533 |
| 63.51 | 73.73 | 7,482 | 0.419 $(10^{12})$ | 19.620 $(10^{14})$ | 4682.592 |
| 1.75 | 30.59 | 8,189 | 0.549 $(10^{12})$ | 0.294 $(10^{14})$ | 53.533 |
| 99.81 | | | | 27.838 $(10^{14})$ | 9.643 $(10^3)$ |

TABLE 8. EQUATIONS 63 AND 64 PARAMETERS FOR BEARING NO. 2

(INA NK 95/26)

| $q_n$ | $n_n$ RPM | $F_n$ Lbs. | $F_n^3$ $Lbs^3$ | $q_n n_n F_n^3$ RPM-$lbs^3$ | $q_n n_n$ RPM |
|---|---|---|---|---|---|
| 0.72 | 74.06 | 12,770 | 2.082 $(10^{12})$ | 1.110 $(10^{14})$ | 53.323 |
| 0.65 | 38.78 | 14,907 | 3.313 $(10^{12})$ | 0.835 $(10^{14})$ | 25.207 |
| 1.01 | 119.40 | 8,172 | 0.546 $(10^{12})$ | 0.658 $(10^{14})$ | 120.594 |
| 30.42 | 153.00 | 4,085 | 0.068 $(10^{12})$ | 3.173 $(10^{14})$ | 4654.260 |
| 1.75 | 30.59 | 3,690 | 0.050 $(10^{12})$ | 0.027 $(10^{14})$ | 53.533 |
| 63.51 | 73.73 | 6,743 | 0.307 $(10^{12})$ | 14.356 $(10^{14})$ | 4682.592 |
| 1.75 | 30.59 | 7,379 | 0.402 $(10^{12})$ | 0.215 $(10^{14})$ | 53.533 |
| 99.81 | | | | 20.374 $(10^{14})$ | 9.643 $(10^3)$ |

Based on the acceptable static ratio and predicted life of greater than 38 times that of the required 100 test cycles, bearing application was considered satisfactory.

If the two orbit motors are connected in the parallel mode during landing, each of them will develop 45 gpm (170 lit/min) flow at 15 mph (24 km/h) speed for twice the normal maximum flow, or 90 gpm (340 lit/min). Therefore, from equation (21),

$$\Delta P_{tp} = 0.07728\ (90\ \text{gpm})^2 = 626\ \text{psi}\ (4.32\ \text{MN/m}^2)$$

to which must be added the relief valve pressure of 4100 psi (28.27 $MN/m^2$) to obtain the torque resisting $\Delta P_c$ = 4726 psi (32.58 $MN/m^2$). Then from equation (58),

$$F_o = 8.62\ (4726) = 40738\ \text{lbs}\ (18478\ \text{kg})$$

and according to equation (59),

$$F_{b1} = .526\ (40738) = 21438\ \text{lbs}\ (9720\ \text{kg})$$

With a static rating for the No. 1 bearing of 8300 kg,

$$\text{Static ratio} = \frac{9720}{8300} = 1.17$$

or the bearing would be 17% overloaded.

For the No. 2 bearing,

$$F_{b2} = .474\ (40738) = 19310\ \text{lbs}\ (8759\ \text{kg})$$

and

$$\text{Static ratio} = \frac{8759}{7400} = 1.18$$

so the bearing would be 18% overloaded.

To prevent the overloading condition, it is feasible and desirable to prevent actuation of the wheel drive motor during landing with the motors parallel connected. During dynamometer testing, this was accomplished by the operating procedure and during flight testing it could be insured by pilot procedure or automatic switch sequencing from the landing gear operation.

Clutch torque capability. The force exerted by the clutch actuating pistons,

$$F_c = n_c A_p \Delta P_c \quad (64)$$

$$= 6\ (0.504\ In^2)\ \Delta P_c$$

$$= 3.02\ In^2\ \Delta P_c\ Lbs \quad (65)$$

$$= (198.97\ \frac{kg - m^2}{MN} \Delta P_c)\ kg$$

Therefore, at stall load, 4000 psi ( $\Delta P_c = 27.58\ MN/m^2$),

$F_{cs}$ = 12080 lbs

= (5488 kg)

and under braking conditions, 5352 psi ($\Delta P_c = 36.90\ MN/m^2$)

$F_{cb}$ = 16163 Lbs

= (7331 kg)

Since the torque developed by the clutch is,

$$T_c = F_c \bar{R} f n_s \quad (66)$$

where $\bar{R} = \sqrt{\frac{R_o^2 + R_i^2}{2}} = \sqrt{\frac{6.300^2 + 4.020^2}{2}} = 5.28$ In (13.42 cm)

$f$ = .35 (dry)

$n_s$ = 4

Then at stall,

$T_{cs}$ = 89488 lb-in

= (10.10 kN - m)

and under braking conditions,

$T_{cb}$ = 119736 lb-in

= (13.50 kN - m)

Since at stall only 57,000 lb-in (6.44 kN - m) is required, the assumed coefficient may diminish by 5.7% and still meet the required stall torque.

The clutch disc contact pressure which will be developed,

$$P_{cc} = F_c/A_c \quad (67)$$

where: $A_c = \pi (R_o^2 - R_i^2)$

$= \pi (6.300^2 - 4.020^2) = 73.92 \text{ In}^2 (476.90 \text{ cm}^2)$

$$P_{cc} = 0.01353 F_c \text{ psi } (.02097 \text{ MN/m}^2/\text{kN } F_c) \quad (68)$$

Under braking condition at 15 mph (24 km/h).

$F_{cb}$ = 16163 lbs (71.90 kN)

$P_{cc}$ = 218.69 psi (1.51 $MN/m^2$).

This is 55% of the manufacturer's recommended value for the maximum allowable.

Wheel bearing load and life. Part of the design task involved the layout design of a modified wheel for the 737-100 airplane that would provide sufficient space for the wheel drive motor. The modified wheel design proposed is shown in Figure 1 which requires replacement of the existing inboard bearing (Timken No. 492A/497) with a special bearing and continuation of the use of the existing outboard bearing (Timken No. 27620/27690). the evaluation of these bearings follows:

Inboard special bearing:

$R_b$, bearing outside radius = 7.16 In (18.19 cm)

$r_b$, bearing inside radius = 6.58 In (16.71 cm)

h, bearing radial thickness = 0.58 In (1.48 cm)

W, bearing width = 0.73 In (1.85 cm)

D, mean roller diameter = 0.25 In (0.635 cm)

d, bearing mean diameter = 13.74 In (34.90 cm)

a, number of rollers = 60

1, effective roller length = 0.44 In (1.118 cm)

| | | |
|---|---|---|
| l', roller length | = | 0.5 In (1.27 cm) |
| H, material factor (radial) | = | 1854 Lb/In$^2$ (130.5 kg/cm$^2$) |
| H', material factor (thrust) | = | 4761 Lb/In$^2$ (335.0 kg/cm$^2$) |
| K = BRR/BTR | = | H/H' cot $\alpha$ |
| k, Latest uprating factor | = | 1.39 |
| $\alpha$, One-half included cup angle | = | 15 deg (0.262 Rad) |
| $\beta$, One-half included cone angle | = | 14 deg (0.244 Rad) |
| $\gamma$, One-half included roller angle ($\beta + \nu$) | = | 14.5 deg (0.253) |
| $\nu$, One-half included roller angle | = | 0.5 deg (0.009 Rad) |
| BRR, Basic radial rating in lbs (kg) for a 90% expected life of 3000 hr at 500 rpm | = | 1854 lb (841.7 kg) |
| BTR, Basic thrust rating in lbs (kg) for a 90% expected life of 3000 hr at 500 rpm | = | 4761 lb (2161.5 kg) |
| o and i subscripts | = | Outboard and Inboard bearing, respectively |

It is accepted (Ref. 14) that the basic radial rating of a tapered roller bearing can be determined as follows:

$$(BRR)_i = kH\, a^{.7}\; 1\; D \left(\frac{\cos\alpha \sin\beta}{\cos 2\nu \sin\gamma}\right)\left(\frac{\sin\alpha + \sin\beta}{\sin\alpha}\right)^{.3} \qquad (69)$$

$$= (1.39)\; 1854\; (60)^{.7}\; 0.44(0.25)\left(\frac{\cos 15 \sin 14}{\cos 1 \sin 14.5}\right)\left(\frac{\sin 15 + \sin 14}{\sin 15}\right)^{.3}$$

$$= 5666 \text{ lbs } (2570 \text{ kg})$$

Since,

$$K_i \triangleq \frac{H_i}{H'_i} \text{Cot}\alpha_o = \frac{1854}{4761} \text{ Cot } 15 = 1.4 \qquad (70)$$

then,

$$(BTR)_i = \frac{(BRR)_i}{K_i} = \frac{5666}{1.4} = 4047 \text{ lb } (1835.7 \text{ kg}) \qquad (71)$$

Outboard bearing - Timken No. 27620/27690. -

D = .375 in (0.953 cm)

a = 18

l = .68 in (1.727 cm)

l' = .62 in (1.575 cm)

$\alpha$ = 15.5 deg (.271 rad)

$\beta$ = 14.5 deg (.253 rad)

$\gamma$ = 15 deg (.262 rad)

$\nu$ = 0.5 deg (.009 rad)

From equation (69)

$(BRR)_o$ = 1.39 (1854) $18^{.7}$ (0.62) 0.375 (1.13688)

= 5152 lbs (2337 kg)

$K_o$ = 1.4 (Timken rating revision supplement - 1962)

and from equation (71)

$(BTR)_o$ = $\frac{5152}{1.4}$ = 3680 lbs (1669 kg)

Based on a bearing spacing as shown in Figure 15.

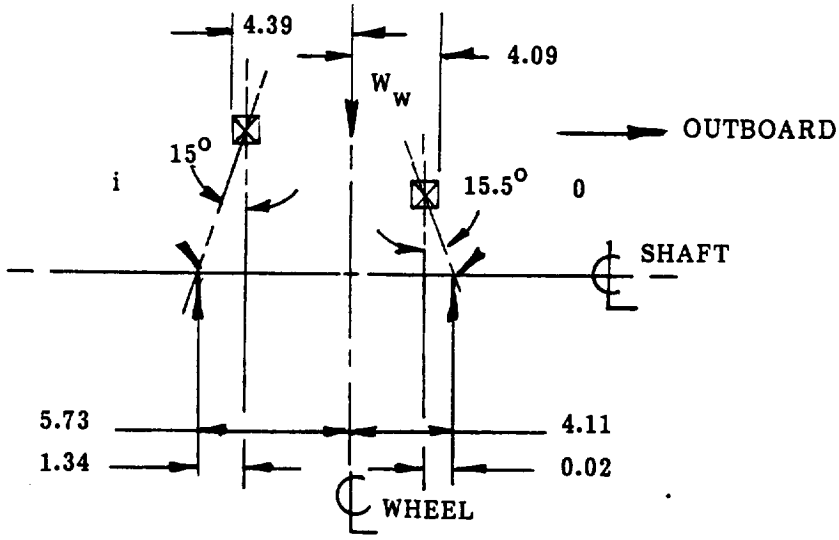


FIGURE 15. Bearing Spacing and Effective Spread

For a 20,000 lb roll condition (9072 kg)

$\Sigma M_i = 0$

$$W_w 5.73 - R_o 9.84 = 0 \quad (72)$$

Solving for $R_o$

$$R_o = W_w\ 5.73/9.84 = 20{,}000\ (.5823) \quad (73)$$

$$= 11646 \text{ lbs } (5283 \text{ kg})$$

and summing vertical forces,

$\Sigma F_y = 0$

$R_i = 20{,}000 - 11646 = 8354$ lbs (3789 kg)

Since, $K_o = K_i$, then

$$\frac{R_o}{K_o} = \frac{R_i}{K_i}$$

and the equivalent radial load for the outboard bearing,

$$RE_o \triangleq 1.25\ R_o = 1.25\ (11646) = 14558 \text{ lbs } (6603 \text{ kg}) \quad (74)$$

Where 1.25 is Timken empirical constant for a rotating cup application, for the inboard bearing,

$$RE_i \triangleq 0.78\ R_i + 0.47\ R_o\ K_i/K_o \quad (75)$$

$$= 0.78\ (8354) + 0.47\ (11646)\ 1.4/1.4 = 11990 \text{ lbs } (5438 \text{ kg})$$

The B-10 life of the inboard bearing,

$$(LB\text{-}10)_i = \left[(BRR)_i \cdot SF/(RE_i \cdot AF)\right]^{3.33}\ 3000 \text{ hours} \quad (76)$$

Where: SF = Speed Factor = 1.00 @ 500 rpm

AF = Application Factor = 1.2

$$(LB\text{-}10)_i = \left[5666\ X\ 1.00/(11990\ X\ 1.2)\right]^{3.33}\ 3000$$

$$= 134.71 \text{ hrs}$$

In terms of distance expectation at 500 rpm and the wheel radius of .419 m (16.5 in), the LB-10 life is,

$(LB\text{-}10)_i$ = 500 rpm (60 min/hr) $2\pi$ [16.48/12(5280)] 134.66

= 49.03 (134.66) = 6602 miles (10,628 km)

The B-10 life of the outboard bearing,

$$(LB\text{-}10)_o = [(BRR)_o \cdot SF/(RE_o \cdot AF)]^{3.33} \ 3000 \text{ hours} \qquad (77)$$

$$= [(5152) \cdot 1.00/(14558 \cdot 1.2)]^{3.33} \ 3000 = 51.43 \text{ hrs}$$

In terms of distance expectation at 500 rpm and the wheel radius, the LB-10 life is,

49.03 (51.43) = 2522 miles (4057 km)

For a 0.2 g right turn maneuver, assuming a tire lateral shift of 1.00 In (2.54 cm),

$\Sigma M_i$ = 0 (Ref. Figure 14)

$$W_w (5.73 + LS) + .2 W_w R_r - 9.84 R_o = 0 \qquad (78)$$

Solving for $R_o$,

$R_o$ = 20,000 [(5.73 + 1.00) + .2 (16.48)] /9.84

= 20,378 lbs (9243 kg)

Since

$\Sigma F_y$ = 0

$R_i$ = 20378 - 20,000 = 378 (171 kg)

From equation (73)

$RE_o$ = 1.25 (20378) = 25473 lbs (11554 kg)

From equation (76)

$(LB\text{-}10)_o$ = [(5152) 1.00/25473 (1.2)] $^{3.33}$ 3000

= 7.98 hrs

Again in terms of distance expectation at 500 rpm, the LB-10 life is,

49.03 (7.98) = 391 miles (630 m)

Now for a 0.2 g left turn maneuver,

$\Sigma M_o = 0$

$$W_w (4.11 + LS) + .2\ W_w\ R_r - 9.84\ R_i = 0 \qquad (79)$$

Solving for $R_i$

$R_i = 20{,}000\ [(4.11 + 1.00) + .2\ (16.48)]\ /9.84$

$= 17085$ lbs (7750 kg)

Since,

$\Sigma F_y = 0$

$R_o = 20{,}000 - 17085 = 2915$ lbs (1322 kg)

and from equation (74),

$RE_o = 0.78\ (2915) + 0.47\ (17085)\ 1.4/1.4$

$= 10303$ lbs (4674 kg)

The B-10 life in terms of hours and miles is,

$(LB\text{-}10)_o = [(5152)\ 1.00/10303\ (1.2)]^{3.33}\ 3000$

$= 162.61$ hrs

$= 49.03\ (162.61 = 7972$ miles (12829 km)

Considering a thrust condition of 11,000 lbs (4989.5 kg) induced by the clutch,

$$RE_o = K_o T \qquad (80)$$

$= 1.4\ (11{,}000) = 15{,}400$ lbs (6985 kg)

and

$(LB\text{-}10)_o = [(5152)\ 1.00/15400\ (1.2)]^{3.33}\ 3000$

$= 42.65$ hrs

$= 49.03\ (42.65) = 2091$ miles (3364 km)

Vectorially combining the 11,000 lbs (4989.5 kg) thrust and 20,000 lbs (9072 kg) roll condition loads:

$$RE_o = \sqrt{15400^2 + 14558^2} = 21192 \text{ lbs (9612 kg)}$$

$$(LB\text{-}10)_o = \left[(5152)\ 1.00/21192\ (1.2)\right]^{3.33}\ 3000$$

$$= 14.73 \text{ hrs}$$

$$= 49.03\ (14.73) = 722 \text{ miles (1162 km)}$$

Vectorially combining 11,000 lbs (4989.5 kg) thrust and a 0.2 g right turn loads:

$$RE_o = \sqrt{25473^2 + 14558^2} = 29340 \text{ lbs (13308 kg)}$$

$$(LB\text{-}10)_o = \left[(5152)\ 1.00/29340\ (1.2)\right]^{3.33}\ 3000 = 4.99 \text{ hrs}$$

$$= 49.03\ (4.99) = 244 \text{ miles (393 km)}$$

Vectorially combining 11,000 lbs (4989.5 kg) thrust and 0.2 g left turn loads:

$$RE_o = \sqrt{10303^2 + 14558^2} = 17835 \text{ lbs (8090 km)}$$

$$(LB\text{-}10)_o = \left[5152\ (1.00)\ /\ 17835\ (1.2)\right]^{3.33}\ 3000 = 26.16 \text{ hrs}$$

$$= 49.03\ (26.16) = 1282 \text{ miles (2064 km)}$$

Assuming 16 flights at 6 miles (9.66 km) each, plus an additional 100 miles (161 km) ground handling, the roll spectrum is:

| | | |
|---|---|---|
| 24 mi | ( 38.62 km) | No thrust (clutch disengaged) |
| 154 mi | (247.83 km) | Straight + thrust (clutch engaged) |
| 9 mi | (14.48 km) | 0.2 g right turn and thrust |
| 9 mi | (14.48 km) | 0.2 g left turn and thrust |
| 196 mi | (315.41 km) | |

The B-10 life of the outboard bearing at spectrum is:

$$\frac{196 \text{ miles}}{24 \text{ miles}/2522 \text{ miles} + 154 \text{ miles}/722 \text{ miles} + 9 \text{ miles}/244 \text{ miles} + 9 \text{ miles}/1282 \text{ miles}} =$$

$$\frac{196}{.267} = 734 \text{ miles (1181 km)} \quad (81)$$

Since the inboard special bearing does not resist thrust loading from the clutch, and because it carries less radial load and has a larger BRR, the life will be longer than that of the outboard bearing. Thus, the inboard bearing life is not as critical and will not be determined. Therefore, the anticipated life distance of the wheel bearings (734 miles) is 3.74 times greater than the assumed flight test distance required.

Gear mesh and stress analyses. The analyses of the gear mesh and stresses in this section are based on the design parameters established in the subsection on Sizing, as follows.

$D_o$ = output gear pitch diameter, 4.25 in (10.795 cm)

$D_r$ = orbiter gear pitch diameter, 4.4375 in (11.271 cm)

$R_t$ = transmission ratio, 22.67:1

In addition, the analyses use the values of the required torques and output velocity as shown below.

Stall torque, $T_s$ = 57,000 lb-in (6.44 kN-m) min.

Torque at maximum velocity, $T_o$ = 14,250 lb-in (1.61 kN-m) min.

Maximum wheel velocity, $N_w$ = 153 rpm

From detail design and manufacturing considerations, the following data is used.

Gear tooth face width, $b_g$ = 2.38 in (6.045 cm)

Material = Nitrided 4330 mod. steel

Ultimate tensile strength = 160,000-180,000 psi (1103-1241 $MN/m^2$)

Yield strength = 140,000-157,000 psi (965-1083 $MN/m^2$)

Minimum bearing strength (Nitride) = 500,000 psi (3448 $MN/m^3$) (Ref. 8)

Gear mesh: Twenty times size layouts of gear meshes of various pressure angles and diametral pitches were made. In these layouts, the relative positions of the internal and external gear teeth at various points around the pitch circles of

the gears were plotted. These layouts enable one to select modifications of the standard tooth profile to eliminate interference and also permit an estimate to be made of the number of teeth carrying the load. The approach used in preparing the gear layouts is similar to that described in Reference 9.

Layouts were prepared for the following combinations of pressure angle and diametral pitch.

| Config. No. | Press. Angle Deg. (Rad.) | | Dia Pitch $IN^{-1}$ ($cm^{-1}$) | | No. of Teeth* |
|---|---|---|---|---|---|
| 1 | 14-1/2 | (.2531) | 16 | (6.299) | 68/71 |
| 2 | 20 | (.3471) | 16 | (6.299) | 68/71 |
| 3 | 14-1/2 | (.2531) | 32 | (12.598) | 136/142 |
| 4 | 20 | (.3491) | 32 | (12.598) | 136/142 |

*Numerator = output shaft teeth

Denominator = orbiter gear teeth

Gear stress: The values of maximum tooth bending stress, maximum contact stress, and the maximum PV (pressure times velocity) were calculated for each of the four combinations of pressure angle and diametral pitch.

Configuration No. 1

From the layout, it is estimated that six teeth carry the load. The distribution of forces among the six teeth is assumed to be linear as shown in the figure.

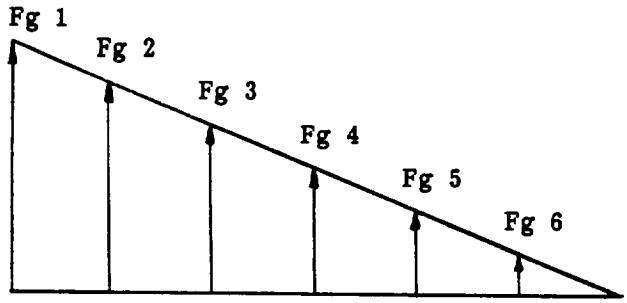

The output torque is given by:

$$T_o = (F_{g1}+F_{g2}+F_{g3}+F_{g4}+F_{g5}+F_{g6})r_o \cos \gamma \quad (82)$$

where

$T_o$ = output torque, in-lbs (N - m)

$F_{g1}$ through $F_{g6}$ = forces carried by individual teeth, lbs (N)

$r_o$ = radius of output gear pitch circle, in (m)

$\gamma$ = pressure angle, deg (rad)

For the assumed linear distribution of forces shown in the figure

$$F_{g2} = \frac{5F_{g1}}{6} \quad (83)$$

$$F_{g3} = \frac{2F_{g1}}{3} \quad (84)$$

$$F_{g4} = \frac{F_{g1}}{2} \quad (85)$$

$$F_{g5} = \frac{F_{g1}}{3} \quad (86)$$

$$F_{g6} = \frac{F_{g1}}{6} \quad (87)$$

Substituting equations (83) through (87) into (82) gives:

$$F_1 = \frac{T_o}{3.5\ r_o \cos \gamma} \quad (88)$$

If we assume a 90% gear efficiency, then $T_o$ = 14,250/0.9 = 15,833 in-lbs (1.79 kN-m) at rated conditions. For $\gamma = 14.5^o$ (.253 rad) and $r_o$ = 2.125 in (5.398 cm), equation (88) yields $F_{g1}$ = 2,199 pounds (9981 N). The corresponding values of $F_{g2}$ through $F_{g6}$ are tabulated in Table 9.

Gear mesh sliding velocity is given by:

$$\dot{x} = e\omega_m \cos \phi \quad (89)$$

where

$\dot{x}$ = sliding velocity, ft/min (m/s)

e = eccentricity, ft (m)

$\omega_m$ = motor speed, rad/min

$\phi$ = angular position of contact point on output gear = $90^o$ ($\Pi/2$ rad) at mesh point

The motor speed is given by:

$$\omega_m = 2 \Pi N_s R_t \quad (90)$$

where

$N_s$ = output shaft speed, rpm

$R_t$ = transmission ratio

for $N_s$ = 153 rpm and $R_t$ = 22.67, Equation (90) gives $\omega_m$ = 21,790 rad/min

Values of $\phi$ and $x$ are tabulated in Table 9 based on $\omega_m$ = 21,790 rad/min and e = 7.81 x $10^{-3}$ ft (2.38 x $10^{-3}$m)

The bearing stress for a convex cylindrical surface in contact with a concave cylindrical surface of identical material is given by Reference (10) as

$$S_c = 0.798 \sqrt{\frac{P_E (D_1 - D_2)}{2(1- \mu^2) D_1 D_2}} \quad (1) \quad (91)$$

where

$S_c$ = contact stress, psi (MN/$m^2$)

P = load per unit length, lb/in (MN/m)

E = Young's modulus, psi (TN/$m^2$)

$D_1$ = diameter of curvature of concave surface, in (m)

$D_2$ = diameter of curvature of convex surface, in (m)

$\mu$ = Poisson's ratio

The value of P is given by

$$P_n = \frac{F_n}{b_g} \quad (92)$$

where

$P_n$ = $P_{g1}$ through $P_{g6}$, lb/in (N/m)

$F_n$ = $F_{g1}$ through $F_{g6}$, lb/in (N)

$b_g$ = gear face width, in (m)

---

Footnote:

(1) When using S.I. units multiply by 32.929.

For the gear teeth:

$$D_1 = D_r \sin \gamma \quad (93)$$

$$D_2 = D_o \sin \gamma \quad (94)$$

where

$D_o$ = pitch diameter of output gear, in (m)

$D_r$ = pitch diameter of orbiter gear, in (m)

Substitution of equations (92) through (94) into equation (91) gives:

$$S_c = 0.798 \sqrt{\frac{F_n E (D_r - D_o)}{2b_g (1-\mu^2) D_r D_o \sin \gamma}} \quad (95)$$

The gears are to be made from 4330 steel for which $E = 29 \times 10^6$ psi ($0.20$ TN/m$^2$) and $\mu = 0.32$. For the gears, $D_r = 4.4375$ in (0.1127 m), $D_o = 4.250$ in (0.1080 m), $b_g = 2.38$ in (0.0605 m) and $\gamma = 14.5^o$ (.253 rad). Values of $S_c$ for each tooth are tabulated in Table 9.

Also tabulated in Table 9 is the product $\dot{x} S_c$ for each tooth. The average value of $\dot{x} S_c$ is 462,600 psi x fpm (16.18 MN/m-s).

TABLE 9.

RESULTS OF CALCULATIONS FOR CONFIGURATION NO. 1

| Tooth | $F_n$ lbs (kN) | $\phi$ deg (rad) | $\dot{x}$ fpm (m/s) | $P_n \frac{\text{lbs}}{\text{in}}$ (MN/m) | $S_c$ psi (MN/m$^2$) | $\dot{x} S_c \frac{\text{ft}}{\text{min}} \frac{\text{lb}}{\text{in}^2}$ (MN/m-s) |
|---|---|---|---|---|---|---|
| 1 | 2199 (9.782) | 90 (1.571) | 0 | 924 (0.162) | 20,093 (138.5) | 0 |
| 2 | 1832 (8.149) | 84.71 (1.478) | 15.32 (.0778) | 770 (0.135) | 18,342 (126.5) | 280,999 (9.84) |
| 3 | 1466 (6.521) | 79.42 (1.386) | 30.64 (.1557) | 616 (0.108) | 16,406 (113.1) | 502,680 (17.61) |
| 4 | 1100 (4.893) | 74.13 (1.294) | 45.95 (.2334) | 462 (0.081) | 14,208 (98.0) | 652,858 (22.87) |
| 5 | 733 (3.260) | 68.84 (1.201) | 61.27 (.3113) | 308 (0.054) | 11,601 (80.0) | 710,793 (24.90) |
| 6 | 366 (1.628) | 63.55 (1.109) | 76.59 (.3891) | 154 (0.027) | 8,203 (56.6) | 628,268 (22.01) |

The maximum bending stress for a single tooth and the maximum contact stress are calculated at stall conditions, again assuming a 90% torque efficiency.

The bending stress is given by:

$$S_b = \frac{4\ T_s}{\eta_t\ Yb_g c\ D_o^2} \qquad (96)$$

where

$S_b$ = bending stress, psi ($MN/m^2$)

$T_s$ = stall torque, in-lb (kN - m)

$\eta_t$ = torque efficiency

Y = Lewis factor

c = fraction of teeth driving load

For $T_s$ = 57,000 in-lbs (6.44 kN-m), $\eta_t$ = 0.90, Y 0.45, $b_g$ = 2.38 in (0.0605 m), c = 6/68 = 0.088, and $D_o$ = 4.25 in (0.10795 m), equation (15) gives $S_b$ = 149,000 psi (1027.4 $MN/m^2$).

From equations (88), (92), and (95), the maximum value of $S_c$ is 40,186 psi (277.1 $MN/m^2$) at stall.

Configuration No. 2

From the layout, it is estimated that six teeth carry the load. The results of calculations for $\dot{x}\ S_c$, similar to those described under Configuration No. 1, are summarized in Table 10. The average value of $\dot{x}\ S_c$ is 406,033 psi x fpm (14.22 MN/m-s).

Since none of the values of parameters used in equation (96) has changed from the previous case, the bending stress remains 149,000 psi (1027.4 $MN/m^2$). The value of $S_c$ is 37,204 psi (256.5 $MN/m^2$) at stall.

TABLE 10

RESULTS OF CALCULATIONS FOR GEAR MESH CONFIGURATION NO. 2

| Tooth | $F_n$ lbs (kN) | $\theta$ deg (rad) | $\dot{x}$ fpm (m/s) | $P_n \frac{lbs}{in}$ ($MN/m^2$) | $S_c$ psi ($MN/m^2$) | $\dot{x} S_c \frac{ft}{min} \frac{lb}{in^2}$ (MN/m-s) |
|---|---|---|---|---|---|---|
| 1 | 2266 (10.08) | 90 (1.571) | 0 | 952 (0.167) | 17,649 (121.7) | 0 |
| 2 | 1887 (8.39) | 84.71 (1.478) | 15.32 (.0778) | 793 (0.139) | 16,108 (111.1) | 246,775 (8.64) |
| 3 | 1510 (6.72) | 79.42 (1.386) | 30.64 (.1557) | 634 (.0111) | 14,403 (99.3) | 441,308 (15.46) |
| 4 | 1133 (5.04) | 74.13 (1.294) | 45.95 (.2334) | 476 (0.834) | 12,480 (86.0) | 573,456 (20.09) |
| 5 | 755 (3.36 | 68.84 (1.201) | 61.27 (.3113) | 317 (0.056) | 10,184 (70.2) | 623,974 (21.86) |
| 6 | 3377 (1.68) | 63.55 (1.109) | 76.59 (.3891) | 158 (0.028) | 7,190 (49.6) | 550,682 (19.29) |

Configuration No. 3

From the layout, it is estimated that 15 teeth carry the load. The results of calculations for $\dot{x} S_c$, similar to those described under Configuration No. 1, are summarized in Table 11. The average value of $\dot{x} S_c$ is 403,938 psi x fpm (14.15 MN/m-s).

For the finer teeth, c = 15/136 = 0.11 and Y 0.5 from equation (96) $S_b$ = 107, 145 psi (738.8 $MN/m^2$). The value of $S_c$ at stall = 28,016 psi (193.2 $MN/m^2$).

TABLE 11

RESULTS OF CALCULATIONS FOR GEAR MESH CONFIGURATION NO. 3

| Tooth | $F_n$ lbs (kN) | $\theta$ deg (rad) | $\dot{x}$ fpm (m/s) | $P_n$ $\frac{lbs}{in}$ (kN/m) | $S_c$ psi ($MN/m^2$) | $\dot{x} S_c$ $\frac{ft}{min} \frac{lb}{in}$ 2 (MN/m-s) |
|---|---|---|---|---|---|---|
| 1 | 962 (4.28) | 90 (1.51) | 0 | 404 (70.75) | 13,286 (91.6) | 0 |
| 2 | 898 (4.00) | 87.35 (1.525) | 8.51 (.0432) | 377 (66.02) | 12,834 (88.5) | 109,217 (3.83) |
| 3 | 834 (3.71) | 84.70 (1.478) | 15.32 (.0778) | 350 (61.29) | 12,366 (85.3) | 189,447 (6.64) |
| 4 | 770 (3.43) | 82.05 (1.432) | 23.83 (.1188) | 324 (56.74) | 11,898 (82.0) | 283,529 (9.93) |
| 5 | 705 (3.14) | 79.40 (1.386) | 30.64 (.1557) | 296 (51.84) | 11,372 (78.4) | 348,438 (12.20) |
| 6 | 641 (2.85) | 76.75 (1.340) | 39.15 (.1989) | 269 (47.11) | 10,841 (74.7) | 424,425 (14.87) |
| 7 | 577 (2.57) | 74.10 (1.293) | 45.95 (.2334) | 242 (42.38) | 10,283 (70.9) | 472,504 (16.55) |
| 8 | 513 (2.28) | 71.45 (1.247) | 54.47 (.2767) | 216 (37.83) | 9,715 (67.0) | 529,176 (18.54) |
| 9 | 449 (2.00) | 68.80 (1.201) | 61.27 (.3113) | 189 (33.10) | 9.087 (62.7) | 556,760 (19.50) |
| 10 | 385 (1.71) | 66.15 (1.155) | 68.08 (.3458) | 162 (28.37) | 8,413 (58.0) | 572,757 (20.06) |
| 11 | 321 (1.43) | 63.50 (1.108) | 76.59 (.3891) | 135 (23.64) | 7,680 (53.0) | 588,211 (20.60) |
| 12 | 257 (1.14) | 60.85 (1.062) | 83.40 (.4237) | 108 (18.91) | 6,869 (47.4) | 572,875 (20.07) |
| 13 | 192 (0.85) | 58.20 (1.016) | 90.21 (.4583) | 81 (14.19) | 5,949 (41.0) | 536,569 (18.79) |
| 14 | 128 (0.57) | 55.25 (.964) | 97.02 (.4929) | 54 (9.46) | 4,857 (33.5) | 471,226 (16.51) |
| 15 | 64 (0.29) | 52.90 (.923) | 102.12 (.5188) | 27 (4.73) | 3,435 (23.7) | 350,782 (12.29) |

Configuration No. 4

From the layout, it is estimated that again 15 teeth carry the load. The results of the calculations for $\dot{x} S_c$ are summarized in Table 12. The average value of $\dot{x} S_c$ is 400,394 psi x fpm (14.02 MN/m-s).

Since none of the values of parameters used in equation (96) has changed from the previous case, the bending stress, $S_b$, remains 107,145 psi (738.8 kN/m). The value of $S_c$ is 24,244 psi (167.2 $MN/m^2$) at stall.

TABLE 12

RESULTS OF CALCULATIONS FOR GEAR MESH CONFIGURATION NO. 4

| Tooth | $F_n$ lbs (kN) | $\theta$ deg (rad) | $\dot{x}$ fpm (m/s) | $P_n \frac{lbs}{in}$ (kN/m) | $S_c$ psi ($MN/m^2$) | $\dot{x} S_c \frac{ft}{min} \frac{lb}{in} 2$ (MN/m-s) |
|---|---|---|---|---|---|---|
| 1 | 991 (4.41) | 90 (1.571) | 0 | 416 (72.85) | 11,667 (80.4) | 0 |
| 2 | 925 (4.12) | 87.35 (1.525) | 8.51 (.0432) | 389 (68.12) | 11,282 (77.8) | 96,010 (3.36) |
| 3 | 859 (3.82) | 84.70 (1.478) | 15.32 (.0778) | 361 (63.22) | 10,868 (74.9) | 166,498 (5.83) |
| 4 | 793 (3.53) | 82.05 (1.432) | 28.83 (.1188) | 333 (58.14) | 10,438 (72.0) | 248,738 (8.71) |
| 5 | 727 (3.23) | 79.40 (1.386) | 30.64 (.1557) | 305 (53.42) | 9,990 (68.9) | 306,094 (10.72) |
| 6 | 661 (2.94) | 76.75 (1.340) | 39.15 (.1989) | 278 (48.69) | 9,537 (65.8) | 373,374 (13.08) |
| 7 | 595 (2.65) | 74.10 (1.293) | 45.95 (.2334) | 250 (43.78) | 9.044 (62.4) | 415,572 (14.56) |
| 8 | 529 (2.35) | 71.45 (1.247) | 54.47 (.2767) | 222 (38.88) | 8,523 (58.8) | 464,248 (16.26) |
| 9 | 462 (2.06) | 68.80 (1.201) | 61.27 (.3113) | 194 (33.98) | 7,967 (54.9) | 488,138 (17.10) |
| 10 | 396 (1.76) | 66.15 (1.155) | 68.08 (.3458) | 166 (29.07) | 7,370 (50.8) | 501,750 (17.57) |
| 11 | 330 (1.47) | 63.50 (1.108) | 76.59 (.3891) | 139 (24.34) | 6,744 (46.5) | 516,523 (18.09) |
| 12 | 264 (1.17) | 60.85 (1.067) | 83.40 (.4237) | 111 (19.44) | 6,026 (41.5) | 502,560 (17.60) |
| 13 | 198 (0.88) | 58.20 (1.016) | 90.21 (.4583) | 83 (14.54) | 5,211 (35.9) | 470,084 (16.47) |
| 14 | 132 (0.59) | 55.55 (.964) | 97.02 (.4929) | 55 (9.63) | 4,242 (29.2) | 411,559 (14.42) |
| 15 | 66 (0.29) | 52.90 (.923) | 102.12 (.5188) | 28 (4.90) | 3,027 (20.9) | 309,117 (10.83) |

The numerical calculations outlined for the four configurations clearly show that the bending and contact stress at stall and the value of $\dot{x}\, S_c$ at rated conditions are the least when the 32 (12.8 $cm^{-1}$) DP $20^{o}$ (.35 rad) PA gears are used.

Therefore, based on the calculated stresses and allowables, the margins of safeties are.

Ult. M.S. = 160,000/107,145 - 1 = .493

Yld. M.S. = 140,000/107,145 - 1 = .307

Brg. M.S. = 500,000/24,244 - 1 = 19.6

The chief significance of the estimated values of $\dot{x}\, S_c$ is that the parameter should be minimized. An estimate of the wear characteristics of the gearing may be made following the method suggested by Reference (11), which in turn is based on Reference (12). This method is based on a finding that if the maximum shear stress developed in two surfaces sliding together is less than a critical value, there will be "zero wear" for a given number of passes. "Zero wear" is defined as a wear having an order of magnitude equivalent to that of the surface finishes involved. By relating shearing yield stress to tensile yield stress and maximum shearing stress to compressive stress, the following equation for the number of passes for which there will be zero wear is derived in Reference (11).

$$N_a = 3.569 \times 10^4 \left( \frac{\lambda_r F_{ty}}{S_c} \right)^9 \qquad (97)$$

where

$N_a$ = allowable number of passes

$\lambda_r$ = zero wear factor

In this equation, a "pass" is defined as "a sliding distance equal to the contact area length. The parameter $\lambda_r$ has a value of either 0.2 or 0.54.

From Table (12), the maximum value of $S_c$ for the 32 $in^{-1}$ (12.6 $cm^{-1}$) DP $20^{o}$ (.35 rad) PA gearing is 11,667 psi (80.4 $MN/m^2$). Substituting this value, $F_{ty}$ = 260,000 psi (1793 $MN/m^2$)*, and $\lambda_r$ = 0.2 into equation (97) gives $N_a = 2.47 \times 10^{10}$.

(*This value of $F_{ty}$ is obtained from extrapolation based on a plot of the ultimate and yield strengths of steels at various heat treats from Reference (13) for a steel having an ultimate bearing strength, $F_{UB}$, of 500,000 psi (3448 $MN/m^2$).)

The contact length is given by Reference (9) as:

$$l_c = 2.26 \sqrt{\frac{P}{E} \frac{D_r D_o \sin\gamma (1 - \mu^2)}{(D_r - D_o)}} \qquad (98)$$

Substitution of P = 416 lb/in (1860 N/m), $D_r$ = 4.4375 in (.1127 m), $D_o$ = 4.250 in (.1080 m), $\gamma$ = 20° (.35 rad), E = 29 x $10^6$ psi (200 $TN/m^2$) and  = 0.32 into equation (88) gives $l_c$ = 0.048 in (0.122 cm).

From the gear layout, the total length of contact is approximately .050 in (0.127 cm). Hence there is approximately still one pass per orbit. Since there are 22.67 orbits per revolution, the number of passes per minute at the rated speed of 153 rpm is 153 x 22.67 = 3469. This number, divided into the 2.47 x $10^{10}$ allowable passes gives a prediction of 7.15 $(10)^6$ minutes of operating time at rated conditions before measurable wear will take place. This is in excess of 2860 hours and is much greater than the lives of the bearings.

The stall value of $S_c$ = 24,244 psi (167.2 $MN/m^2$), substituted into equation (87) gives: $N_a$ = 34.2 x $10^6$ passes. This value appears to be adequate since wheel speeds at near-stall conditions will be quite low.

Based on these calculations, it is concluded that a 32 $in^{-1}$ (12.6 $cm^{-1}$) DP 20° (.35 rad) PA gear set will have sufficient strength and wear resistance for this application.

Output shaft thrust loading. Because of the necessity of using two different sizes of shaft seals, an unbalanced hydraulic load occurs to impose a thrust load on the output shaft. This condition was mitigated by designing to rotate on the I.D. of one seal (outboard seal) and the O.D. of the other (inboard seal). In addition,

thrust can be generated through the output shaft and orbiter gear teeth misalignment. The following analysis evaluates the combined effect of these forces to establish the contact pressure that will occur between the thrust shoulders on the shaft and the two thrust washers.

The thrust loading occurring by use of the two different shaft seal sizes is,

$$F_t = P_c (D_x^2 - D_h^2)\pi /4 \qquad (99)$$

where

$P_c$ = 150 psig (1.034 MN/m$^2$)

$D_s$ = 4.122 in (.10470 m)

$D_h$ = 4.113 in (.10447 m)

$F_t = 150 (4.122^2 - 4.133^2)\pi /4 = 8.73$ lbs (38.81 N)

With maximum allowed misalignment of .001 in/in (.001 cm/cm) between shaft and orbiter gear teeth, the misalignment angle is

$$\theta = \tan^{-1} .001 = 0.05730 \text{ deg}$$

also,

$$\theta = \sin^{-1} F_{tm}/F_o \qquad (100)$$

where

$F_o$ = maximum orbiter load imposed on the output shaft gear

$= 2 T_{1p}/\eta_t D_o$

From equation (35) at $N_w$ = 153 rpm

$T_{1s}$ = 57,994 lb-in (6.534 kN-m)

So

$$F_o = \frac{2 (57994)}{.85(4.25)} = 32{,}107 \text{ lbs } (143 \text{ kN})$$

and from (100),

$F_{tm}$ = sin 0.05730 (32,107) = 32.11 lbs (.143 kN)

The maximum thrust load, then, is

$$F_T = F_t \pm F_{tm} = 8.73 \pm 32.11 \text{ lbs} \quad (101)$$

In the outboard direction

$$F_{Tmax} = 40.84 \text{ lbs } (.182 \text{ kN})$$

Consequently, the outboard thrust shoulder bearing pressure is,

$$P_{bo} = F_T/A_o \quad (102)$$

where $A_o$ = shaft outboard shoulder bearing area

$$= \frac{\pi}{4}(4.25^2 - 4.137^2) = 0.74 \text{ in}^2 \ (.477 \text{ cm}^2)$$

$$P_{bo} = \frac{40.84}{0.74} = 55.2 \text{ psi } (0.38 \text{ MN/m}^2$$

With a maximum surface speed of 170 ft/min (51.9 m/min) at a 4.25 in (0.0094 m) diameter and 153 rpm, the maximum PV value is,

$$PV = 55.2\ (170) = 9384 \text{ lb/in}^2 \text{ ft/min } (19.7 \text{ MN/m - min})$$

This value is approximately 5 percent of the value reported (Reference 15) for a similar aluminum bronze journal bearing and 4140 steel shaft in a compatibility test in which good performance was achieved. In addition, as indicated by equation (101), there may be no dynamic load at all on the outboard thrust washer if the misalignment angle is in the opposite direction from that assumed. In this case,

$$F_{Tmax} = 23.38 \text{ lbs } (-0.1 \text{ kN})$$

and is imposed on the inboard thrust washer as denoted by the minus sign.

The corresponding shaft shoulder,

$$A_i = \frac{\pi}{4}(4.25^2 - 3.754^2) = 3.12 \text{ in}^2 \ (.002 \text{ m}^2)$$

Therefore,

$$P_{bi} = \frac{23.38}{3.12} = 7.49 \text{ psi } (49 \text{ kN/m}^2)$$

With the same maximum surface speed as the outboard thrust shoulder of 170 ft/min (519 m/min), the maximum PV value is only,

PV = 7.49 (170) = 1274 lb/in$^2$ ft/min (2.68 MN/m - min),

which justifies the use of teflon for the inboard thrust washer which has a limiting PV value (Reference 16) of 1800 lb/in ft/min (3.78 kN/m - min) at a contact speed of 100 ft/min (30.48 m/min).

Margin of safety summary - The margin of safety results developed in the program are presented in Table 13 and show a plus value for all critical conditions based on published (Reference 17) ultimate and yield strengths. Much of the analyses for the various components involved defied rigorous solutions, or involved more effort than allowed, so different approaches to modeling were used in the Bendix digital computer stress programs to arrive at the margins of safety. A complete explanation and illustration of the models used, including computer input/output print-outs, have been previously documented (Reference 18) and is too voluminous for inclusion herein.

The design requirements and the material design allowables used in the design of the powered wheel unit were:

Pressure: Operating pressure - 4000 psi (27.58 MN/m$^2$)

Proof pressure - 6000 psi (41.37 MN/m$^2$)

Burst pressure - 10,000 psi (68.95 MN/m$^2$)

Design factors of safety: Ultimate S.F. = 2.50 maximum limit condition

Yield S.F. = 1.65 maximum limit condition

Fatigue life: In the absence of fatigue life requirements, the following spectrum was derived from the SOW test cycle (Appendix A) and the predicted life of approximately 2000 hours for the No. 2 output shaft bearing.

Condition A - 95% of the summation of time at a constant 15 mph (24 km/h), defined as condition 4 in the section on dynamic performance, with 2% rolling resistance and acceleration from 7 mph (12 km/h) to 15 mph, defined as condition 3 previously, with 4% rolling resistance. In the analysis, a chamber pressure range of 2500 to 1000 psi was used as representative of Condition A.

Condition B - 0.74% of the time will be assigned to the braking condition. Only that portion of total cycles occurring at 4400 psi (30.34 $MN/m^2$) are included for this condition (see Figure 16).

Condition C - Stall condition is considered to occur once each test cycle when the pressure is 4000 psi (27.58 $MN/m^2$) for a total of 100 times.

The operational life in hours corresponding to Conditions A and B were related to the fatigue cycles according to the following:

$$L_h = \frac{n_i (2\pi R_r}{12} / t_p V_a R_t 5280 \qquad (103)$$

Solving for the number of fatigue cycles, $n_i = \frac{L_h t_p V_a R_t}{R_r}$ (10,084 cycles (104)

where:

$L$ = life in hours (taken as 2000)

$t_p$ = proportionate amount of time at Condition A (.94) or Condition B (.0074)

$V_a$ = aircraft speed 15 mph (24 km/h) or 7.5 mph (12 km/h)

$R_t$ = transmission ratio, 22.67

$R_r$ = wheel rolling radius, 16.48 in (.419 m)

Therefore, for Condition A, at P = 2500 psi (44 $MN/m^2$) - 1000 psi (6.90 $MN/m^2$)

$$n_a = \frac{2000(.94)15(22.67)}{16.48} = (10,084)$$

$$= 39.12\ (10^7) \text{ cycles}$$

For Condition B from Figure 16, P = 4400 psi (30.34 $MN/m^2$) is considered to exist only 76.7% of the time the brakes are applied, so

$$n_b = \frac{.767(.0074)2000(15)22.67}{16.48} = (10,084)$$

$$= 2.36\ (10^6) \text{ cycles}$$

For Condition C at $\Delta$ P = 4000 psi (27.58 $MN/m^2$),

$$n_c = 100 \text{ cycles}$$

Material design allowables: Physical properties throughout the analyses were taken from MIL-HDBK 5 (Ref. 17) and are listed by components in Table 13.

Thermal Analysis Summary.

The thermal analysis was considered for the conditions to be encountered during dynamometer testing in order to evaluate the maximum fluid temperature that will be generated during the SOW test cycle (Appendix A) and to indicate the fluid power system cooling capacity required.

The major assumption was that heat would be generated through an adiabatic change from work accomplished, i.e., all the heat would be carried away by the system fluid. For the test, this was considered to be a conservative approach. For flight testing, a more comprehensive heat transfer analysis will be required to evaluate the effect of structural heating that may occur from the brakes during landing.

A summary of the anaysis results is presented in Table 14. A complete presentation of the conditions and calculations is contained in Appendix E.

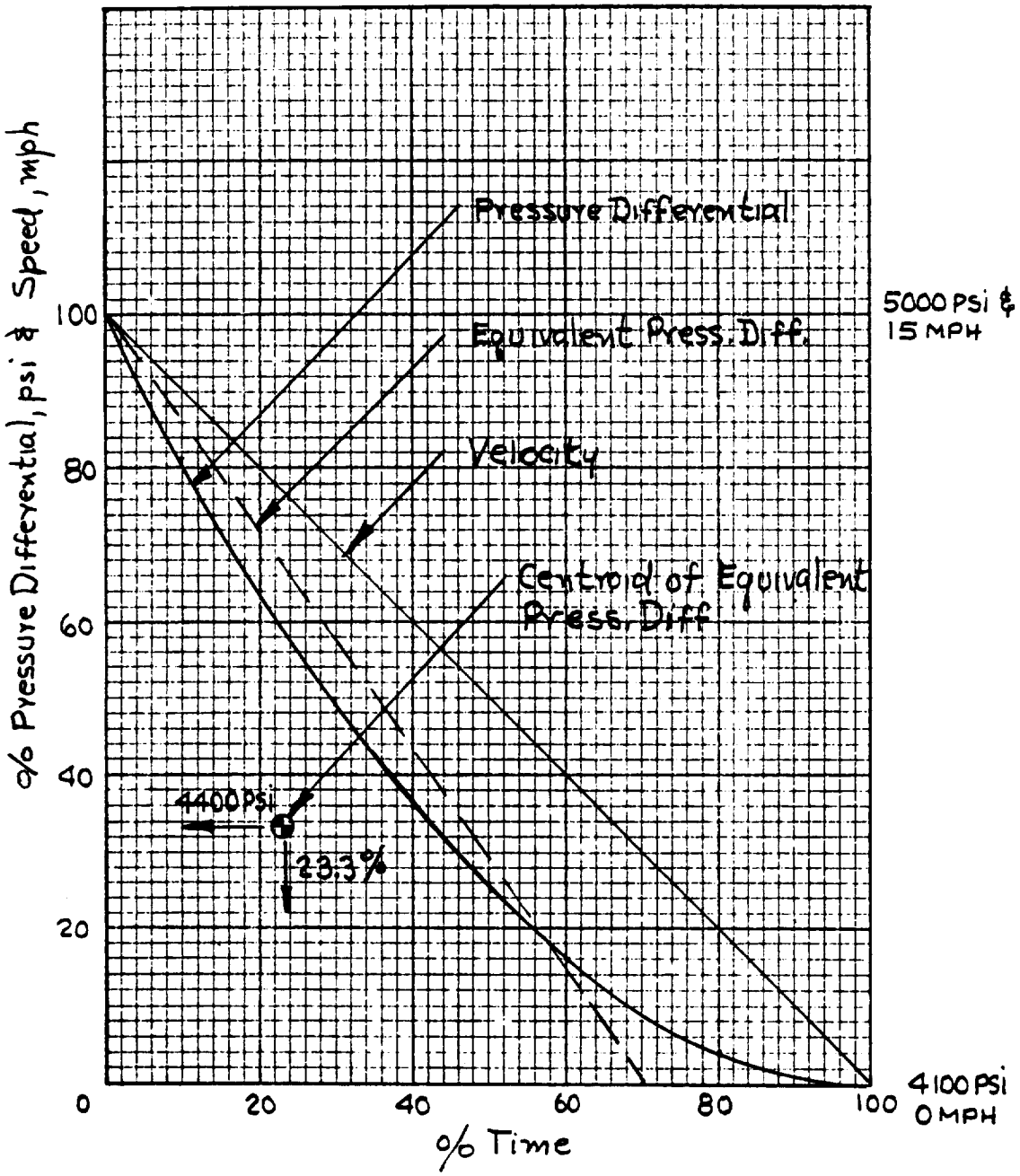


Figure 16. Equivalent Curves for Velocity & Pressure Differential at SOW Condition 2 (Braking)

TABLE 13. MARGINS OF SAFETY - SUMMARY

| Component | Part No. | Material | Ultimate Tensile Strength | Margins of Safety |
|---|---|---|---|---|
| Orbiter/Gear (Excluding tooth bending) | 3311970 & 3311974 | 4330 Mod. Vacuum Melt Low Ally Steel IAW AMS 6411 or MIL-S-8699 | 170,000 - 200,000 PSI (1172 - 1379 $MN/m^2$) | Ultimate +0.29 Yield +0.71 |
| Inboard Housing Annular Barrier | 3311945 | ↓ | 160,000 - 180,000 PSI (1103 $MN/m^2$-1241 $MN/m^2$) | @ Burst +0.16 @ Proof +0.69 |
| Outboard Housing: Entire Cavity Pressurized (All Cyl. Pressures Equal | 3311940 | ↓ | ↓ | @ Burst +0.53 @ Proof +1.03 |
| 1000 PSID (6.90 $MN/m^2$) Operation (Series mode with 0 psig back pressure) | | ↓ | ↓ | * |
| Sleeve Spacer (Contact Stress) | 3311972 | ↓ | 170,000 - 200,000 PSI (1172 - 1379 $MN/m^2$) | Maximum Rated +0.44 |
| Vane (Contact Stress) | 3311966 | ↓ | 220,000 - 240,000 PSI (1517 - 1655 $MN/m^2$) | +0.65 |
| Orbiter/Gear Spline (Contract Stress) | 3311970 & 3311974 | ↓ | 170,000 - 200,000 PSI (1172 - 1379 $MN/m^2$) | +20.0 |
| Drive Plate Spline (Contact Stress) | 3311969 | Alum. Alloy (7075 T73) IAW QQ-A-225/9 | 68,000 PSI Min. (469 $MN/m^2$) | +0.80 |
| Stud: Entire Cavity Pressurized | 3311973 | Steel Bar IAW AMS6487 or 6488 (Ref. H-11) | 220,000 - 240,000 PSI (1517 - 1655 $MN/m^2$) | @ Burst +0.14 @ Proof +0.47 |
| 1000 PSID Operation | | | | Ultimate +0.35 Yield +0.73 |
| Static Operation in Shear | | | | @ Burst +0.14 @ Proof +0.62 |
| In Shear | | | | Ultimate +0.012 |

*Max. stress level for this condition approx. 23% of that with entire cavity pressurized.

## Weight Summary.

The estimated weight impact of the two-wheel drive motors and modified wheels (excluding system power supply, plumbing and valving) on the 737-100 type aircraft is 213.5 lbs (96.9 kg). This weight is composed of an estimated weight of 168.57 lbs (76.45 kg) for each of the two-wheel drive motors, 175.16 lbs (79.45 kg) for each modified wheel/brake and a weight savings of 61.84 lbs (28.05 kg) for each wheel by removal of 60 percent of the brakes in each wheel. A detail breakdown of component estimated weights is presented in Tables 15 and 16.

The actual weight of the prototype assembly is 131.5 lbs (59.7 kg) not including the clutch plates (items 42, 43, and 50 of Table 15). Including the clutch plates the estimated weight of each unit is revised to 152.3 lb (69.1 kg). Based on this the revised stimated system weight impact is reduced 32.6 lbs (14.8 kg) to 180.9 (82.1 kg).

TABLE 14

SUMMARY OF THERMAL ANALYSIS SHOWING HEAT INPUT AND FLUID TEMPERATURE FOR SOW CONDITIONS

| Cond. No. | | Rolling Resistance % | Oper. Mode | Heat Input Btu/min (MJ/Min) | | Fluid Temp. Rise, °F(°C) | |
|---|---|---|---|---|---|---|---|
| 1 | Braking, 15-0 mph (24-0 km/h) | 2 | Series | 3012 | (3.18) | 80 | (44.4) |
| 2 | Accel., 0-7.5 mph (0-12 km/h) | 2 | Parallel | 1544 | (1.63) | 2.5 | (1.4) |
| 3 | Accel., 7.5-15 mph (12-24 km/h) | 2 | Series | 1520 | (1.60) | 2.5 | (1.4) |
| 4 | Constant 15 mph (24 km/h) with Pump Saturation | 2 | Series | 1955 | (2.07) | 12.25 | (5.8) |
| 5 | Reverse, 3 mph (4.8 km/h) with Pump Saturation | 2 | Parallel | 112 | (0.12) | 1.8 | (1.0) |
| 1 | Braking, 15-0 mph (24-0 km/h) | 4 | Series | 3012 | (3.18) | 69 | (38.3) |
| 2 | Accel., 0-7.5 mph (0-12 km/h) | 4 | Parallel | 1520 | (1.60) | 2.5 | (1.4) |
| 3 | Accel., 7.5-15 mph (12-24 km/h) | 4 | Series | 728 | (0.79) | 9.7 | (5.4) |
| * | Braking, 15-0 mph (24-0 km/h) | 4 Aiding | Series | 2673 | (2.81) | 131 | (72.8) |
| * | Constant 15 mph (24 km/h) without Pump Saturation | 2 | Series | 3005 | (3.17) | 18.8 | (10.4) |
| * | Constant 15 mph (24 km/h) | 0 | Series | 4458 | (4.70) | 27.9 | (15.5) |

*Condition not required by SOW.

TABLE 15

ESTIMATED WHEEL DRIVE ASSEMBLY WEIGHT (INCLUDING CLUTCH)

| Figure 5 Item No. | Component | Qty. Used | Weight, Each Pounds | Extended Weight, Lbs. (kg) | |
|---|---|---|---|---|---|
| 1 | Orbiter Match Assem. comprised of: | 1 | - | - | |
| | Ring Orbiter | 1 | 5.22 | 5.22 | (2.37) |
| | Vane | 12 | 0.06 | 0.77 | (0.35) |
| | Sleeve Spacer | 12 | 0.03 | 0.37 | (0.17) |
| | Spacer | 1 | 16.07 | 16.07 | (7.29) |
| | Inboard Housing | 1 | 48.98 | 48.98 | (22.22) |
| | Outboard Housing | 1 | 28.68 | 28.68 | (13.01) |
| 2 | Output Shaft | 1 | 8.10 | 8.10 | (3.67) |
| 3 | INA NK 95/26 Bearing | 1 | 0.80 | 0.80 | (0.36) |
| 4 | INA NK 105/26 Bearing | 1 | 1.11 | 1.11 | (0.50) |
| 9 | Orbiter Gear | 1 | 4.27 | 4.27 | (1.94) |
| 16 | Stud | 12 | 9.23 | 2.73 | (1.24) |
| 18 | Drive Plate Assembly | 1 | 7.60 | 7.60 | (3.45) |
| 21 | Thrust Bearing Assembly (Less Inner Rotor) | 1 | 3.90 | 3.90 | (1.77) |
| | Inner Rotor | 1 | 5.66 | 5.66 | (2.57) |
| 22 | Inner Race | 1 | 6.22 | 6.22 | (2.82) |
| 23 | Clutch Piston | 6 | 0.15 | 0.90 | (0.41) |
| 24 | Piston Housing | 6 | 0.11 | 0.69 | (0.31) |
| 29 | Spring Housing | 6 | 0.18 | 1.10 | (0.50) |
| 42 | Stator | 2 | 5.57 | 11.14 | (5.05) |
| 43 | Rotor | 1 | 5.66 | 5.66 | (2.57) |
| 50 | Backing Plate | 1 | 4.07 | 4.07 | 91.85) |
| - | Misc. Bolts, Washers, Seal, etc. | - | - | 4.50 | (2.04) |
| | TOTAL ESTIMATED WEIGHT . . . . . | | | 168.57* | (76.45) |

*131.5 lbs (59.7 kg) based on actual weights of items 1 through 29 assembled

TABLE 16

ESTIMATED WEIGHT OF THE MODIFIED
WHEEL/BRAKE AND THE WEIGHT IMPACT

| Component | Weight, Pounds (kg) | |
|---|---|---|
| Inboard Half | 50.46 | (22.89) |
| Outboard Half | 20.08 | ( 9.11) |
| Bearings | 6.19 | ( 2.81) |
| Rotor Drive Keys | 0.79 | ( 0.36) |
| Heat Shield | 0.56 | ( 0.25) |
| Tie Bolts, Nuts, Washers | 6.82 | ( 3.09) |
| Miscellaneous Parts | 0.50 | ( 0.23) |
| TOTAL MODIFIED WHEEL WEIGHT | 85.40 | (38.74) |
| Carrier (2601044) | 9.90 | ( 4.49) |
| Piston Assembly | 3.49 | ( 1.58) |
| Adjuster Parts | 2.15 | ( 0.98) |
| Pressure Plate (2602920) | 10.62 | ( 4.82) |
| Rotors (2602087) | 25.12 | (11.39) |
| Stators (2601104) | 12.79 | ( 5.80) |
| Torque Tube, Bearing Support | 19.93 | ( 9.04) |
| Backing Plate Linings (357242) | 4.26 | ( 1.93) |
| Miscellaneous | 1.5 | ( 0.68) |
| TOTAL MODIFIED BRAKES WEIGHT | 89.76 | (40.71) |
| TOTAL MODIFIED WHEEL WEIGHT | 175.16 | (79.45) |
| MINUS TOTAL 737 WHEEL/BRAKE INSTALL. WT. | -237.00 | (107.5 ) |
| MODIFIED WHEEL/BRAKE WEIGHT IMPACT | -61.84 | (-28.05) |

## RESULTS

The results of the program include fabrication of one complete powered wheel drive, as previously described, and the modification of the test unit to replace the 32 $in^{-1}$ (12.60 $cm^{-1}$) pitch gears to 24 $in^{-1}$ (9.45 $cm^{-1}$) pitch. The change required fabricating a new Orbiter Gear P/N 3311974 change B and a new Output Shaft P/N 3311968 change B. The change also required flame plating the sleeve spacers, P/N 3311972, to increase the outside diameters 0.0104 in (0.2647 mm), because of the decrease in the orbit eccentricity from 0.09575 to 0.0833 in (2.38125 to 2.11658 mm). The hardware produced is shown in Figures 17 through 25. For clarity the test results are presented in two sections based on the gear pitch. The test arrangements are shown in Figures 26 through 29.

### 32 Pitch Gear Configuration

This configuration of the powered wheel drive represents the original design as presented in the preceding sections of this report. Before the test program was interrupted by the occurrence of the gear mesh disengagement, some performance data was obtained and presented in the following paragraphs.

Intercircuit Leakage - Because of problems encountered during the copper brazing of the five plates comprising the Inboard Housing, P/N 3311945, a sub-assembly test was conducted to evaluate the leakage between the four hydraulic circuits. Leakages measured at 20, 50, and 100 psid (0.14, 0.35, and 0.69 $MN/m^2$) are shown in Figure 30. No measurable leakage occurred for the other combinations of the four circuits.

Differential Pressure Versus Flow - Because of the intercircuit leakage, it was decided to attempt to evaluate the individual motors separately this was accomplished in the arrangement as shown in Figure 31. In this arrangement the bypassed motor functions as a pump. During the test it was noted that the pressure generated at the outlet of the bypassed motor was approximately equal to the inlet pressure of the working motor. Since the differential pressure developed in

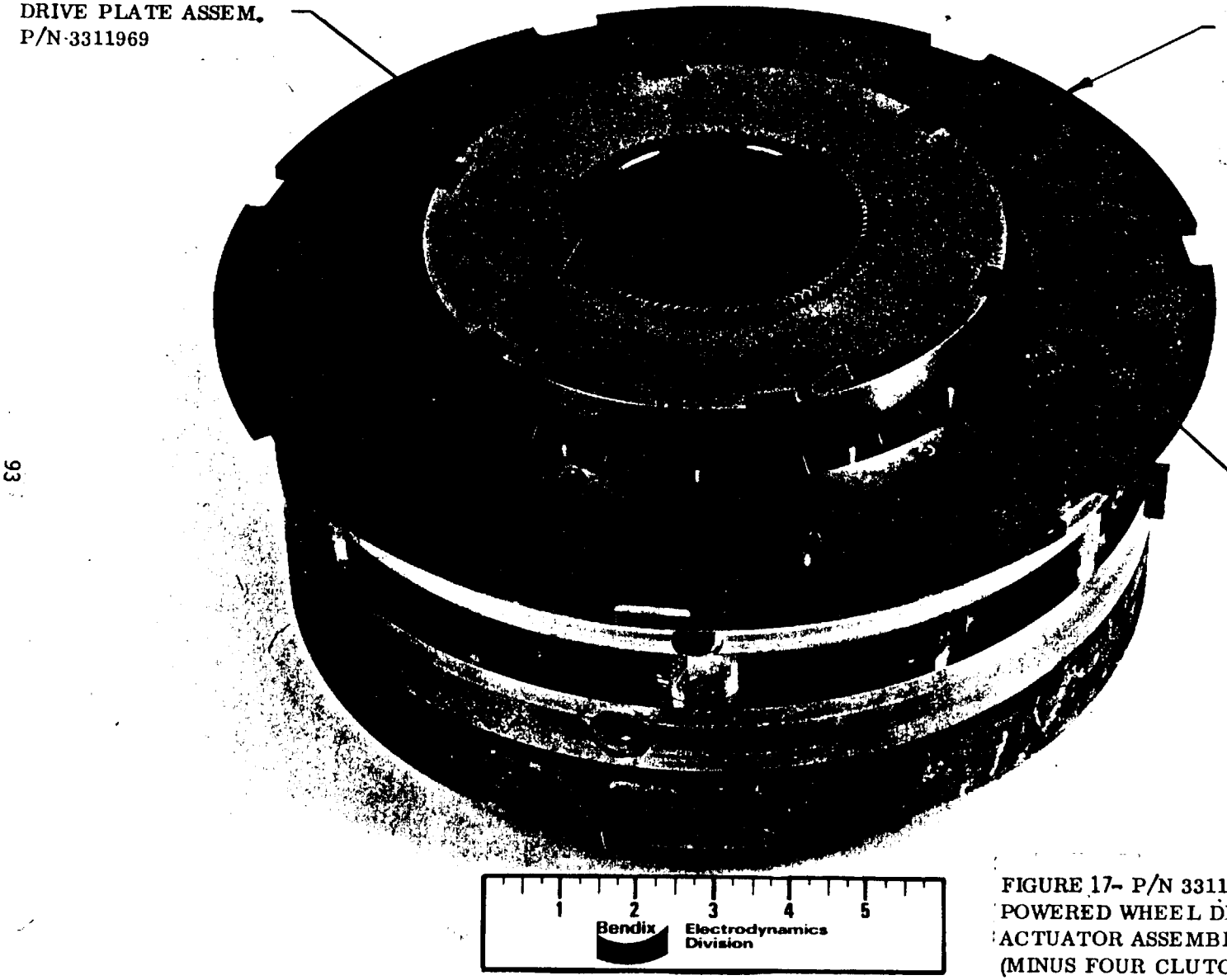


FIGURE 17- P/N 3311870
POWERED WHEEL DRIVE
ACTUATOR ASSEMBLY
(MINUS FOUR CLUTCH PLATES)

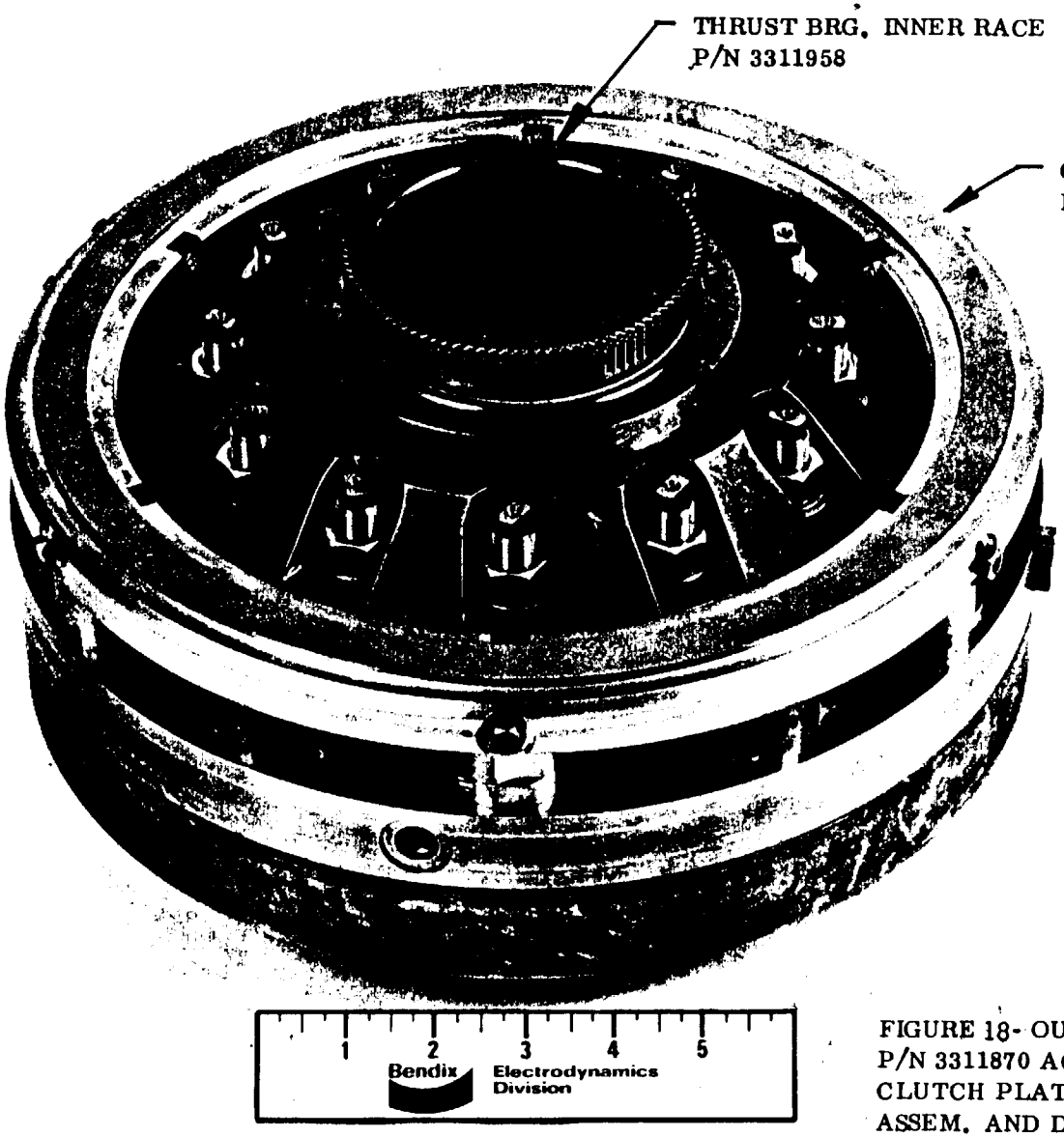


FIGURE 18- OUTBOARD VIEW OF P/N 3311870 ACTUATOR WITHOUT CLUTCH PLATES, THRUST BEARING ASSEM. AND DRIVE PLATE ASSEM.

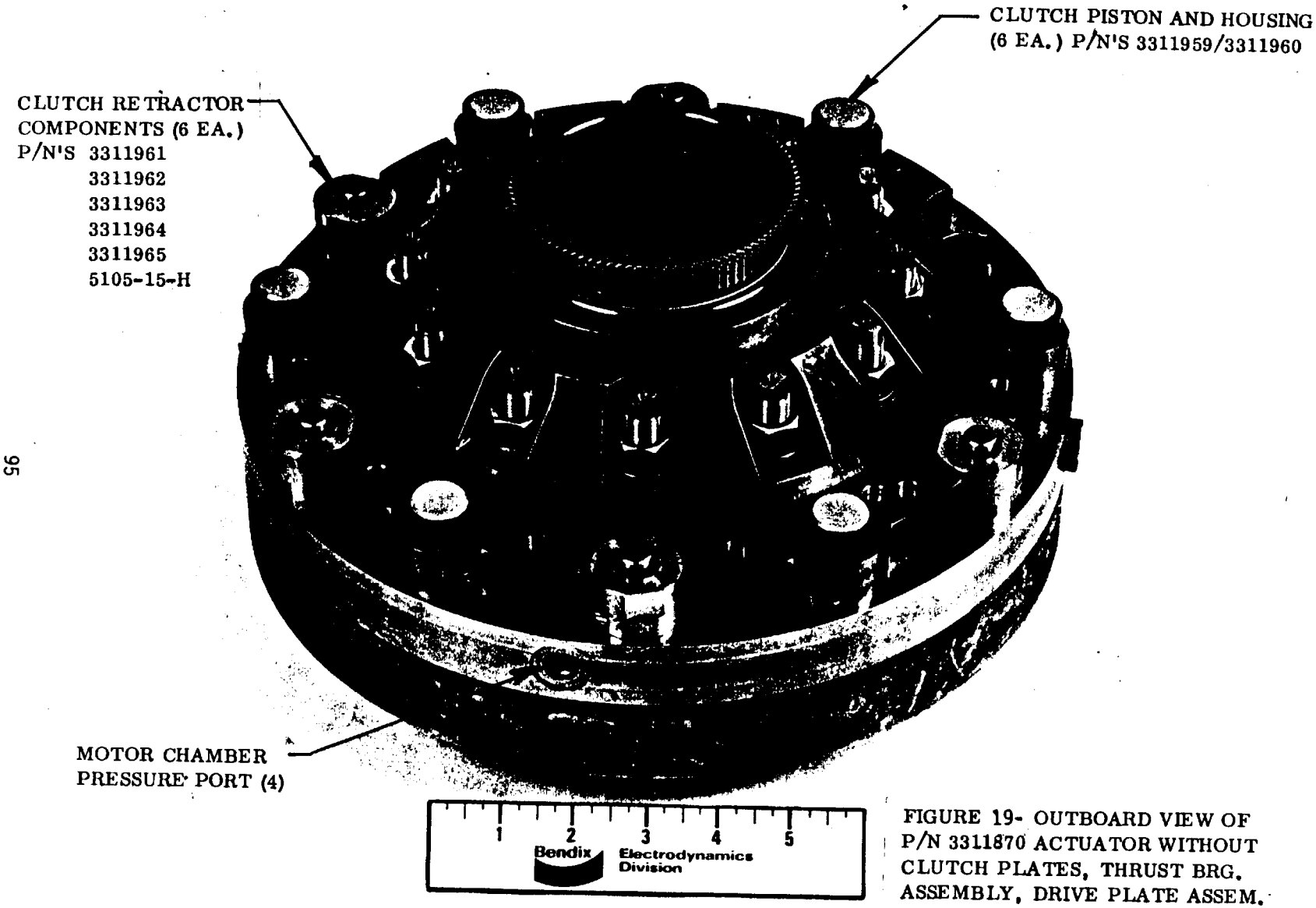


FIGURE 19- OUTBOARD VIEW OF P/N 3311870 ACTUATOR WITHOUT CLUTCH PLATES, THRUST BRG. ASSEMBLY, DRIVE PLATE ASSEM. AND INNER RACE

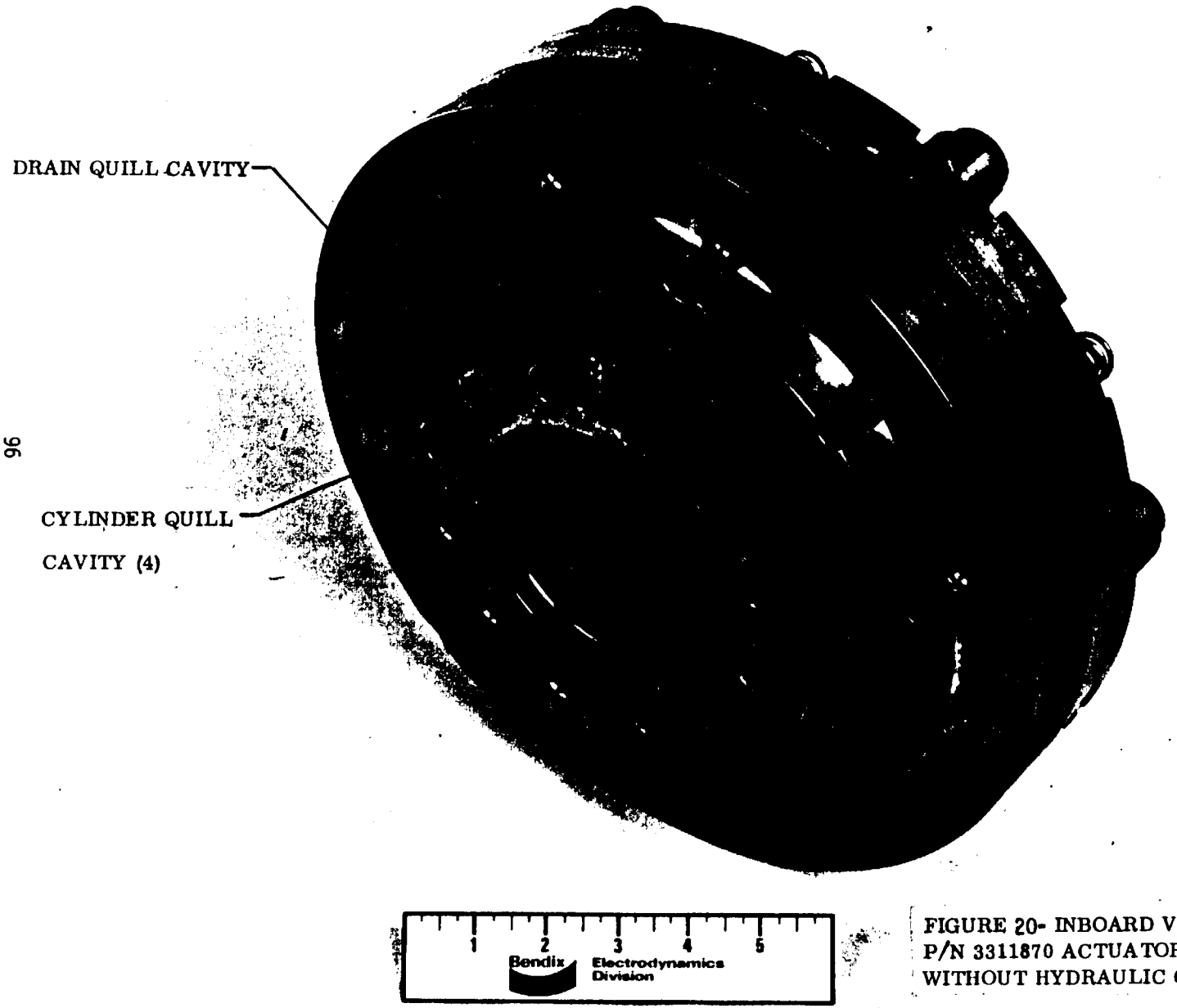


FIGURE 20- INBOARD VIEW OF P/N 3311870 ACTUATOR WITHOUT HYDRAULIC QUILLS

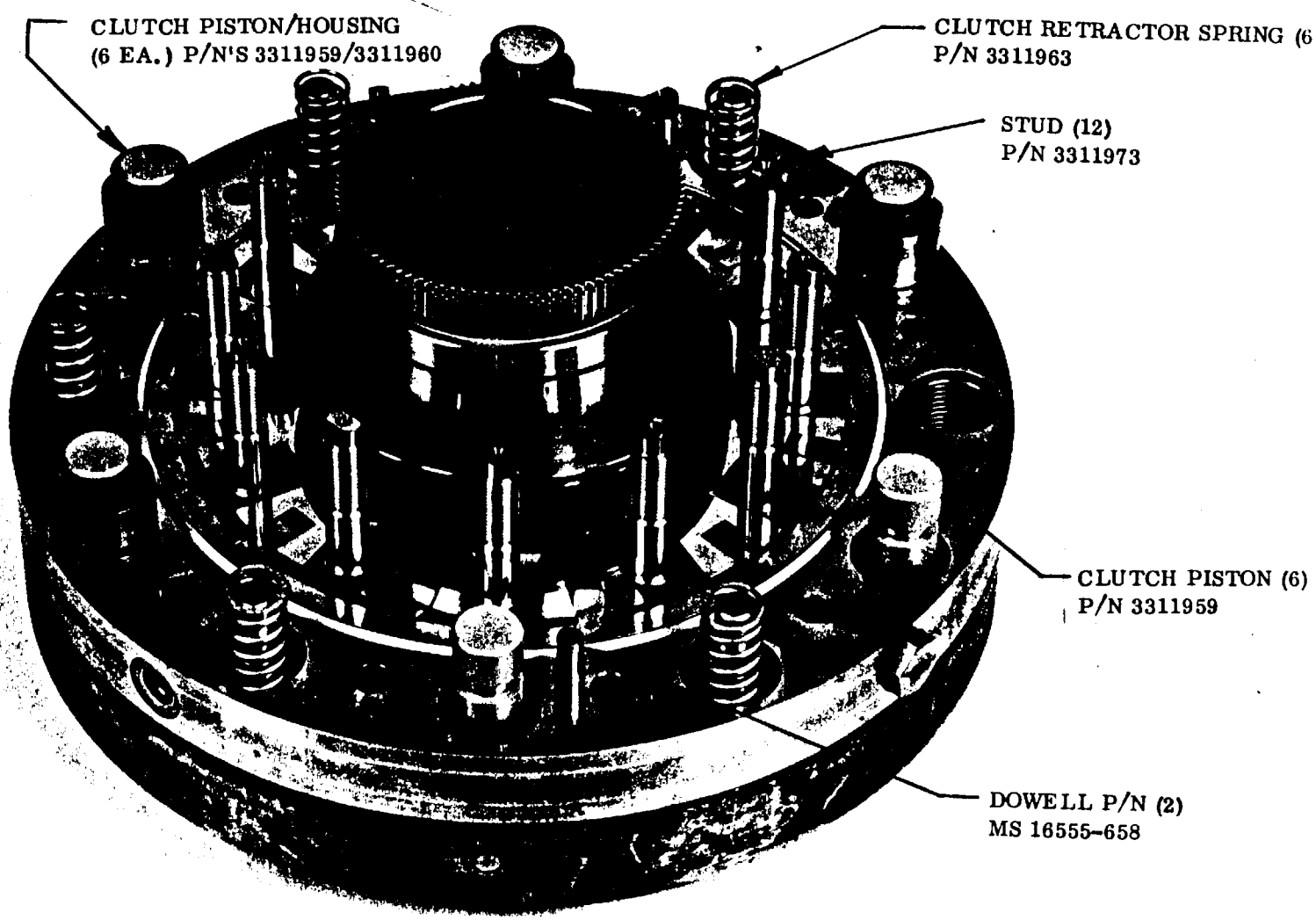


FIGURE 21- VIEW OF P/N 3311870 ACTUATOR WITHOUT OUTBOARD HOUSING

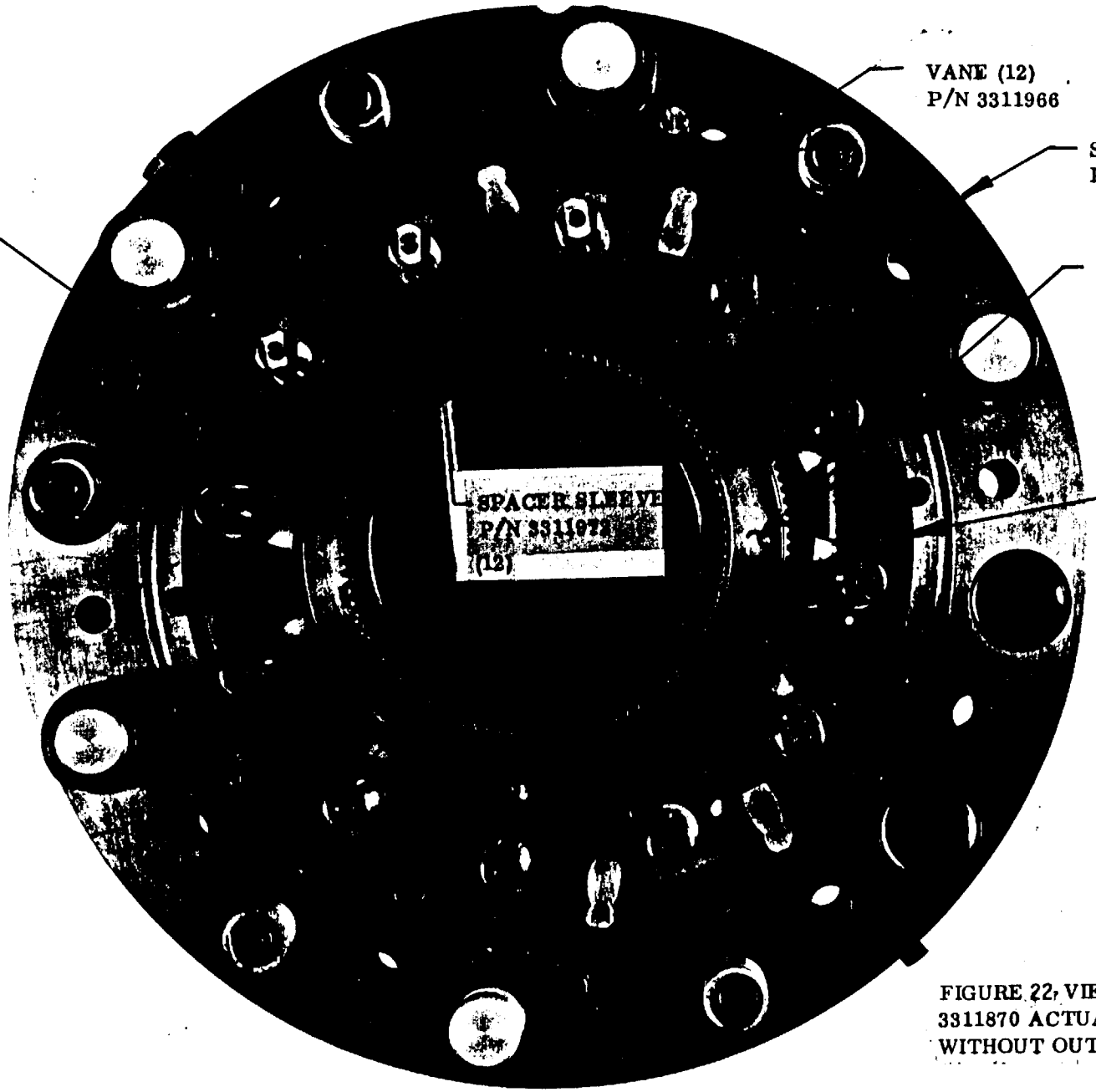


FIGURE 22, VIEW OF P/N 3311870 ACTUATOR WITHOUT OUTBOARD HOUSING

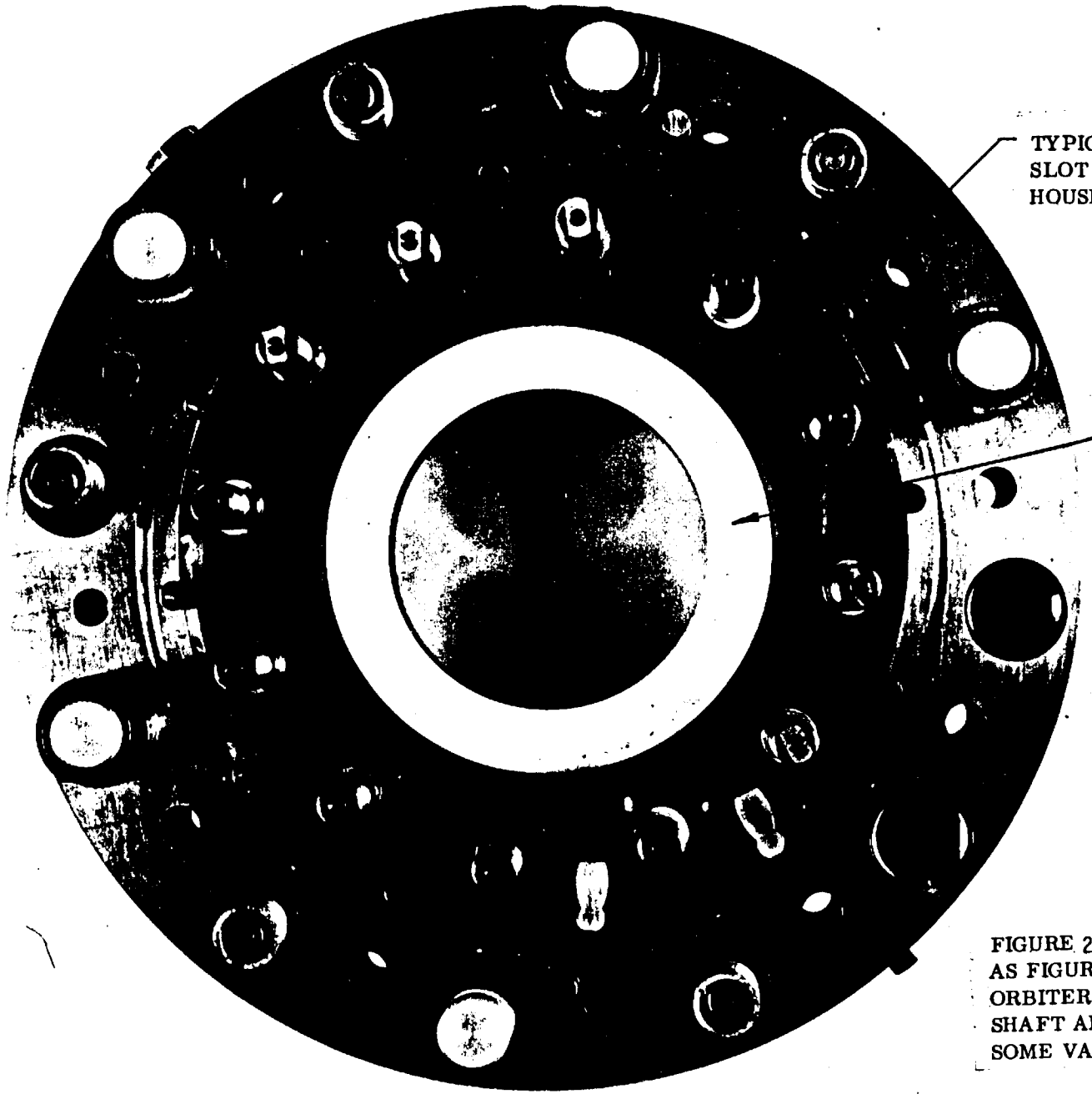


FIGURE 23. SAME VIEW AS FIGURE 22 WITHOUT ORBITER RING, OUTPUT SHAFT AND WITHOUT SOME VANES

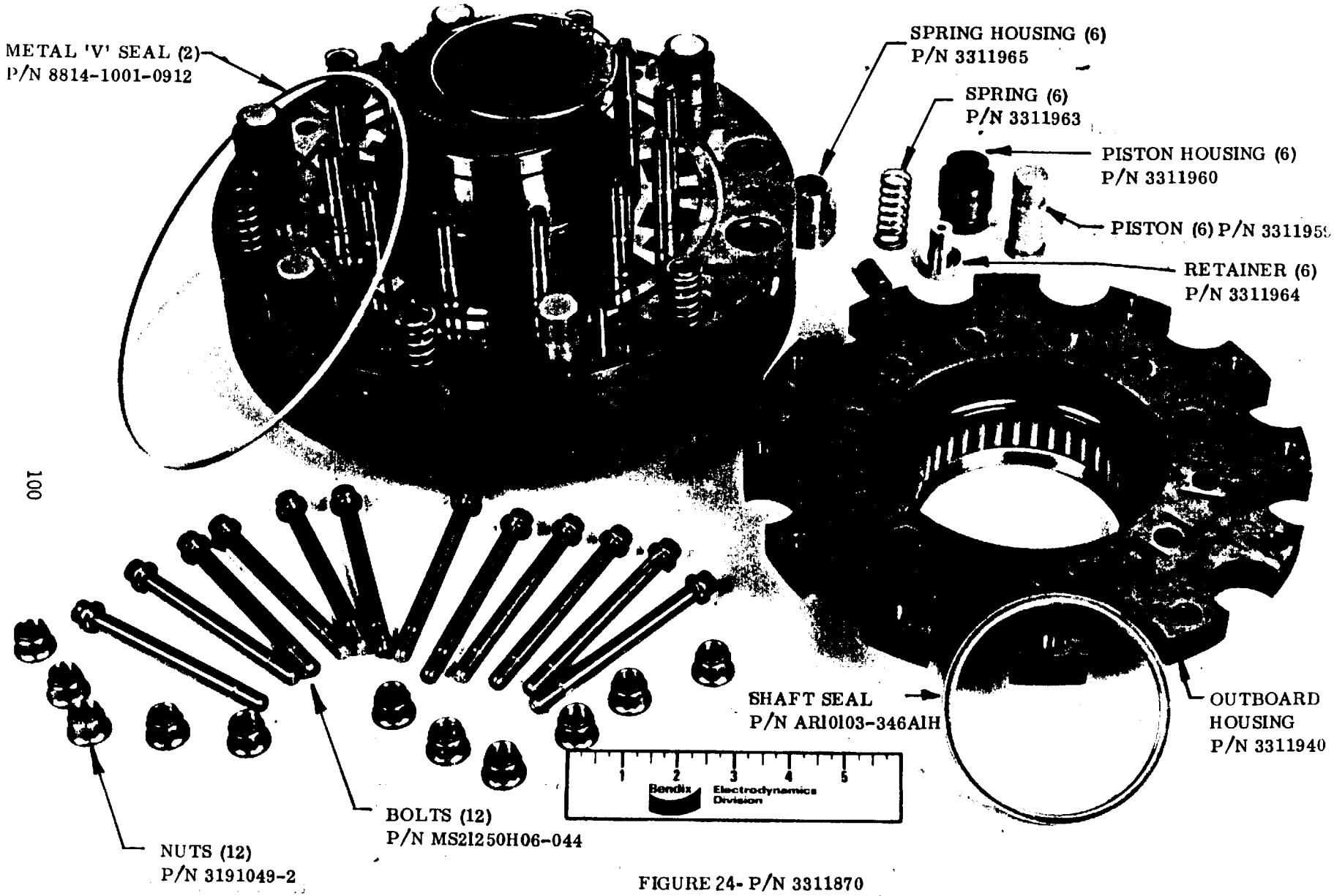


FIGURE 24- P/N 3311870
ACTUATOR SUBASSEMBLIES AND COMPONENTS

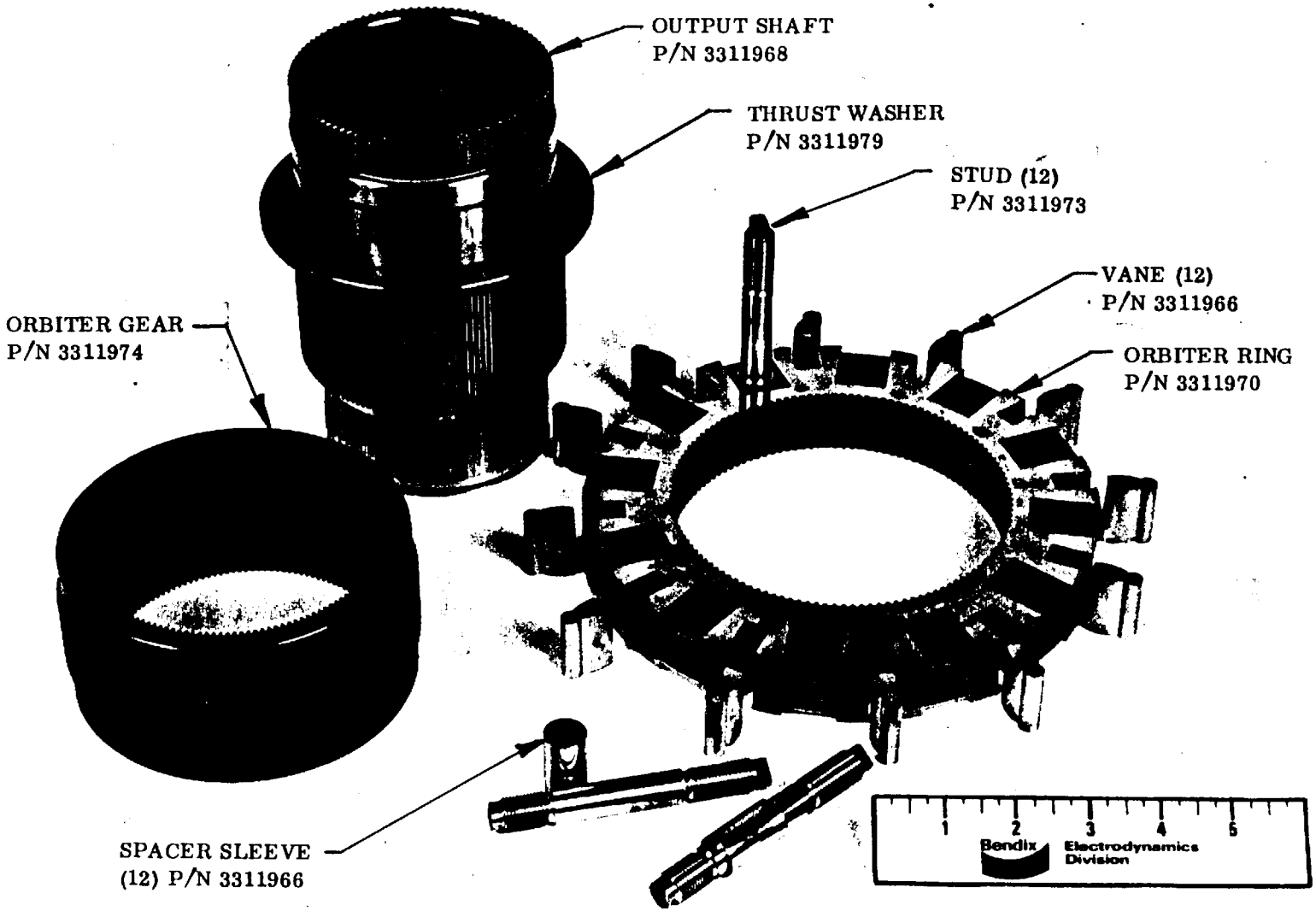


FIGURE 25- PART OF
P/N 3311870 ACTUATOR
COMPONENTS

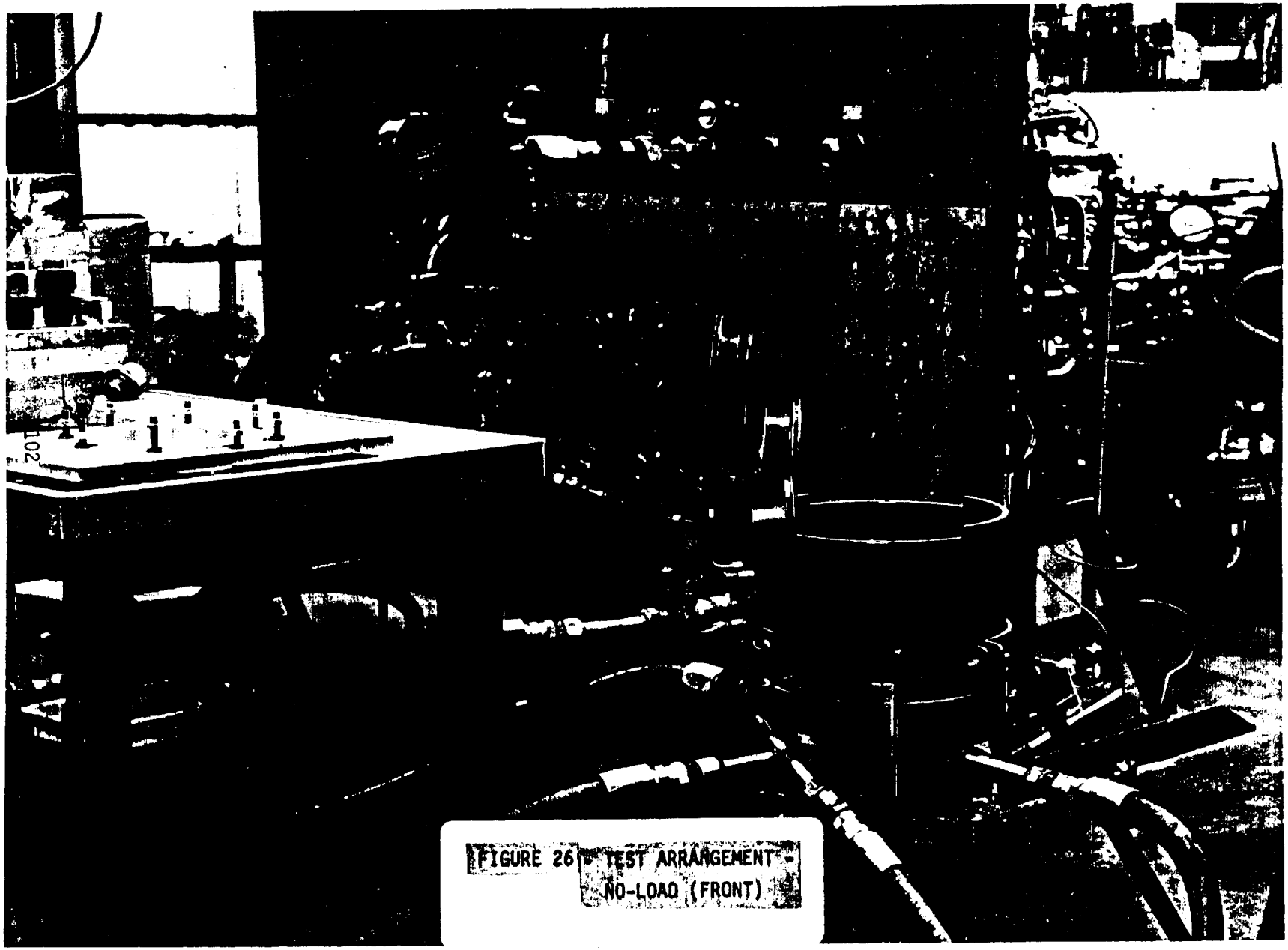

FIGURE 26 - TEST ARRANGEMENT - NO-LOAD (FRONT)

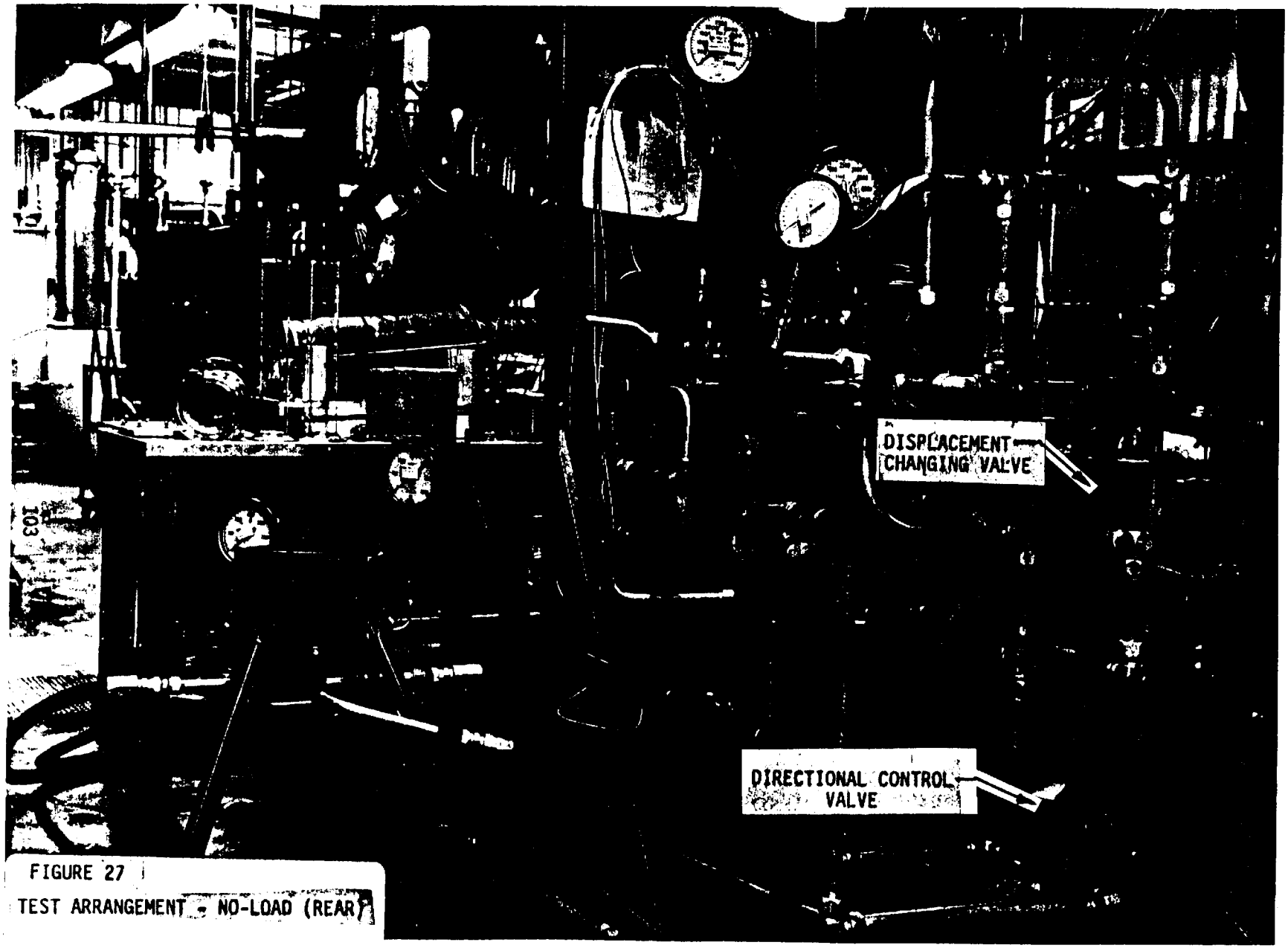


FIGURE 27
TEST ARRANGEMENT - NO-LOAD (REAR)

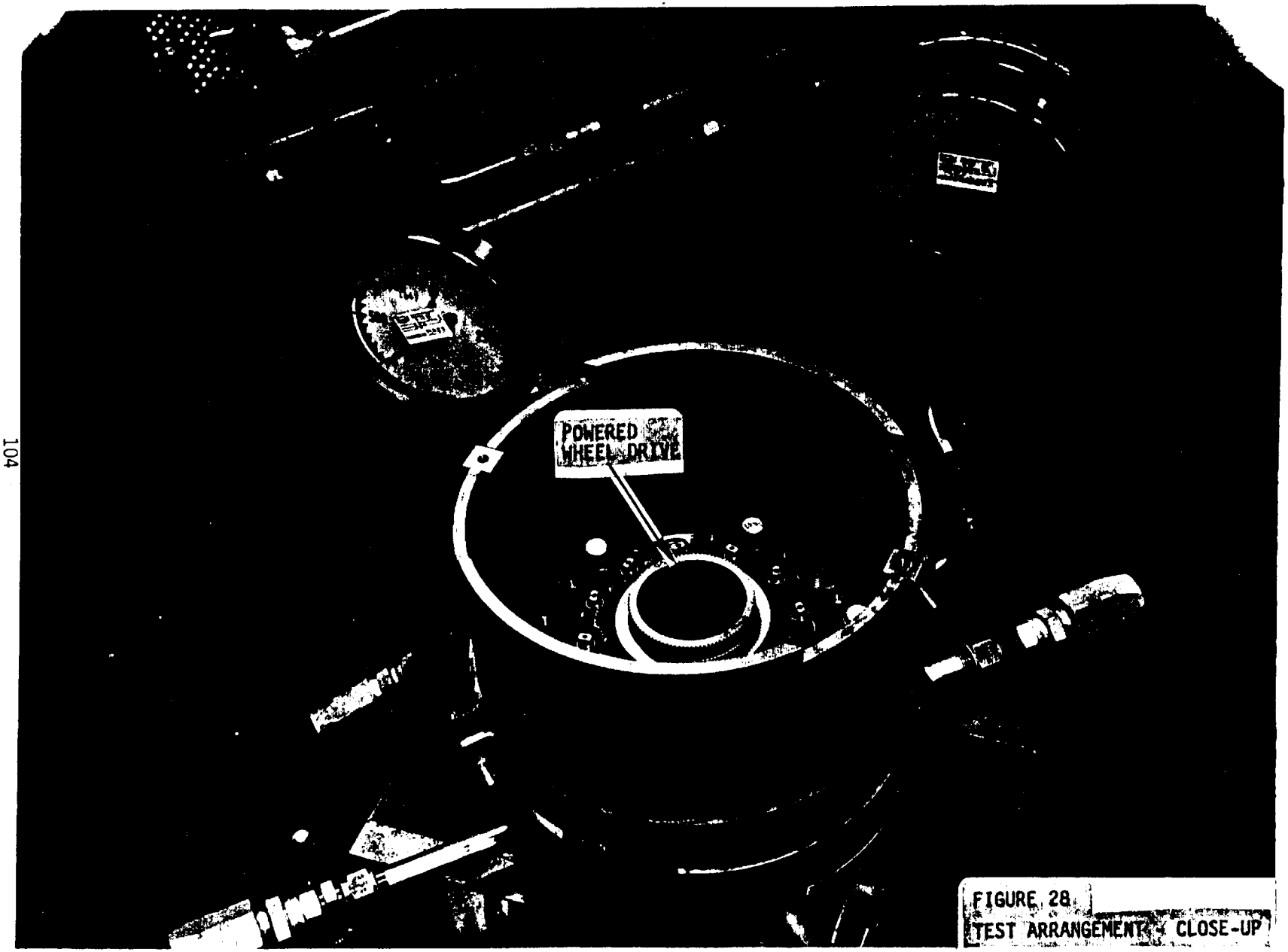


FIGURE 28
TEST ARRANGEMENT - CLOSE-UP

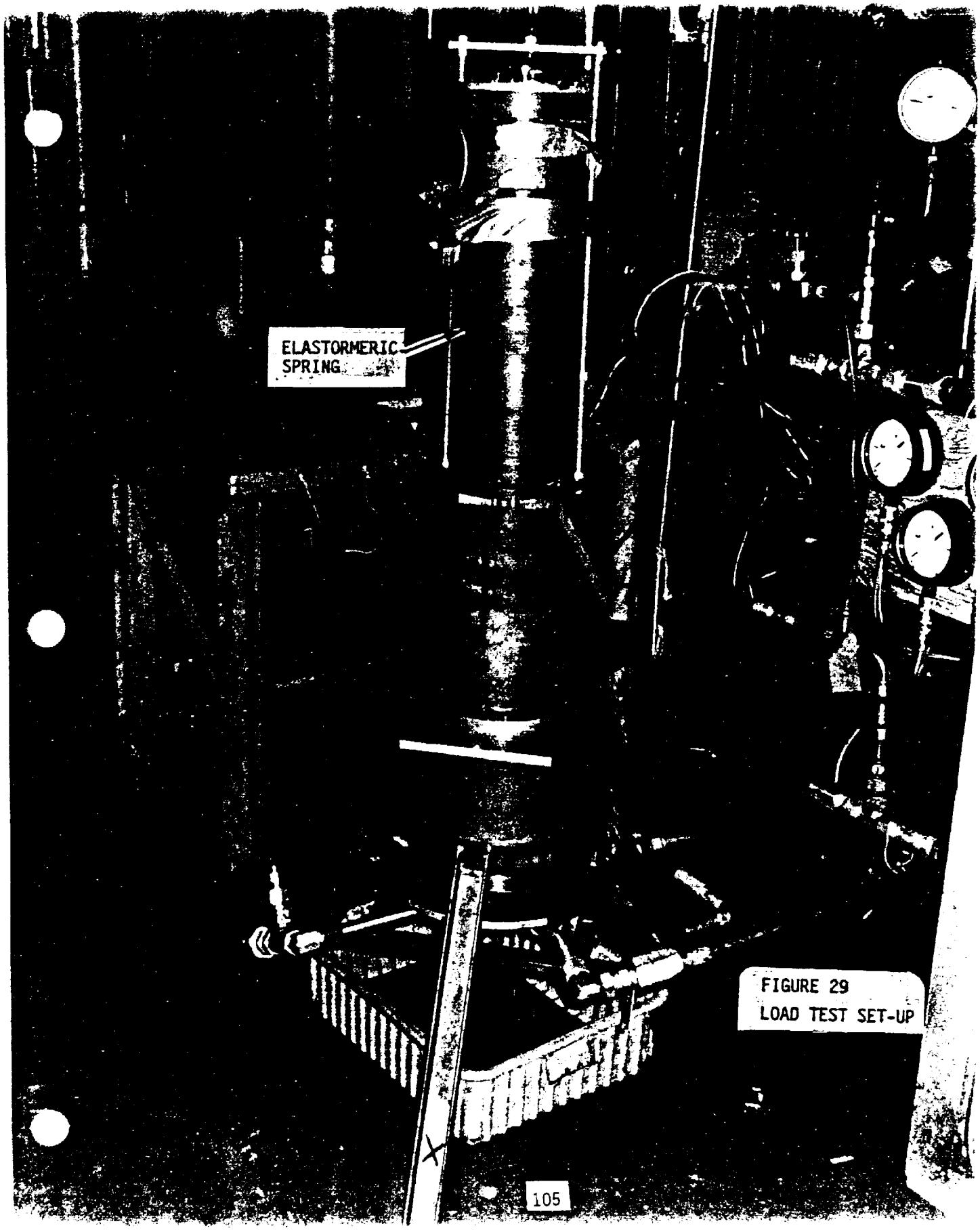


FIGURE 29
LOAD TEST SET-UP

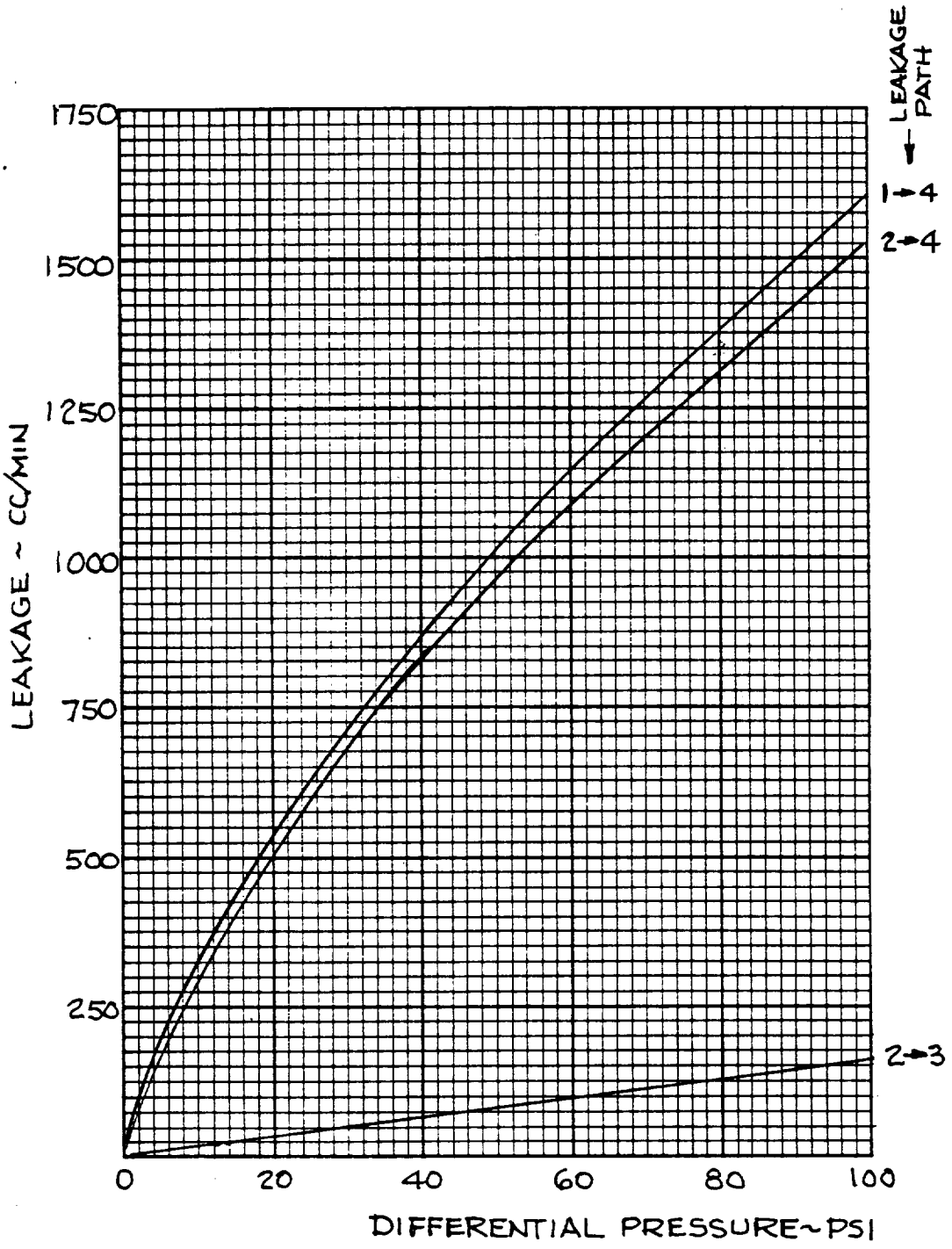


Figure 30. Inboard Housing Intercircuit Leakage Vs Differential Pressure

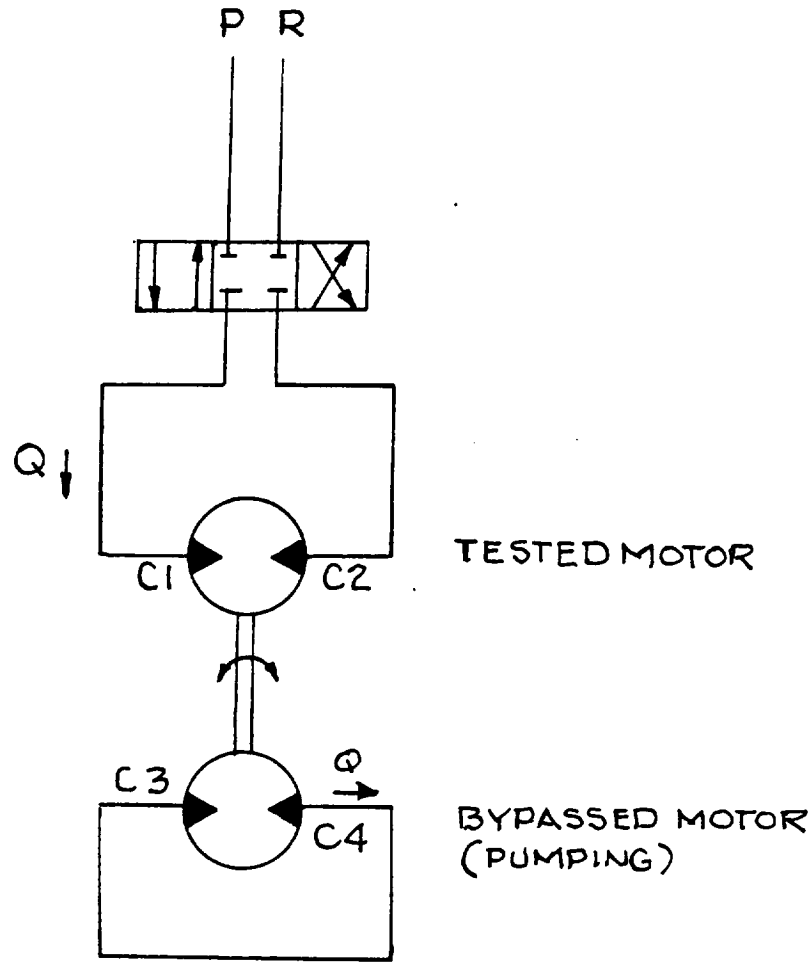


NOTE: MOTORS ARE INTEGRATED HAVING ALTERNATE CHAMBERS AND NOT SEPARATE AS SHOWN.

Figure 31. Individual Motor Test Arrangement

the pumping motor is required to overcome flow losses, then it was assumed that the summation of the pressure losses for both motors is equivalent to series mode operation, but with a difference. This difference is that in normal series mode operation, assuming ccw rotation, the individual cylinder pressure relative amplitudes are C1> C2, C2≈C3, and C3> C4, whereas for this test, C1> C3, C4≈C1, and C4> C3. Consequently with C4 approximately equal to C1, this leakage path is essentially eliminated, leaving only the C4 to C2 path affecting the results shown in Figure 32.

Line Loss Versus Flow - Figure 33 illustrates the line loss for the test system high pressure hoses. Line losses were measured with the test unit removed and line No. 1 coupled to No. 2 and line No. 3 coupled to No. 4. The hoses were normally connected to the test unit as shown in the test arrangement of Figure 34.

To measure the pressure loss of each hydraulic circuit in the inboard housing a test was conducted with the outboard housing disassembled. During the testing, the orbiter ring was clamped against the inboard housing metering surface after locating the orbiter ring to attain first, the minimum pressure loss of each individual circuit, then, the maximum loss. The losses were measured for flows of 10, 20, 30, and 40 gpm (37.86, 75.72, 113.58, and 151.44 lit/min). The results obtained are shown in Figure 35. The average pressure loss is plotted for all four circuits based on the maximum and minimum values also shown in the figure in tabular form.

Volumetric Efficiency Versus Pressure Level - Figure 36 shows the calculated volumetric efficiency as a function of the return pressure for two different constant differential pressure levels, 300 and 600 psi (2.07 and 4.14 $MN/m^2$) for each motor in each direction. One motor at a time was driven while the other was bypassed as shown in Figure 31.

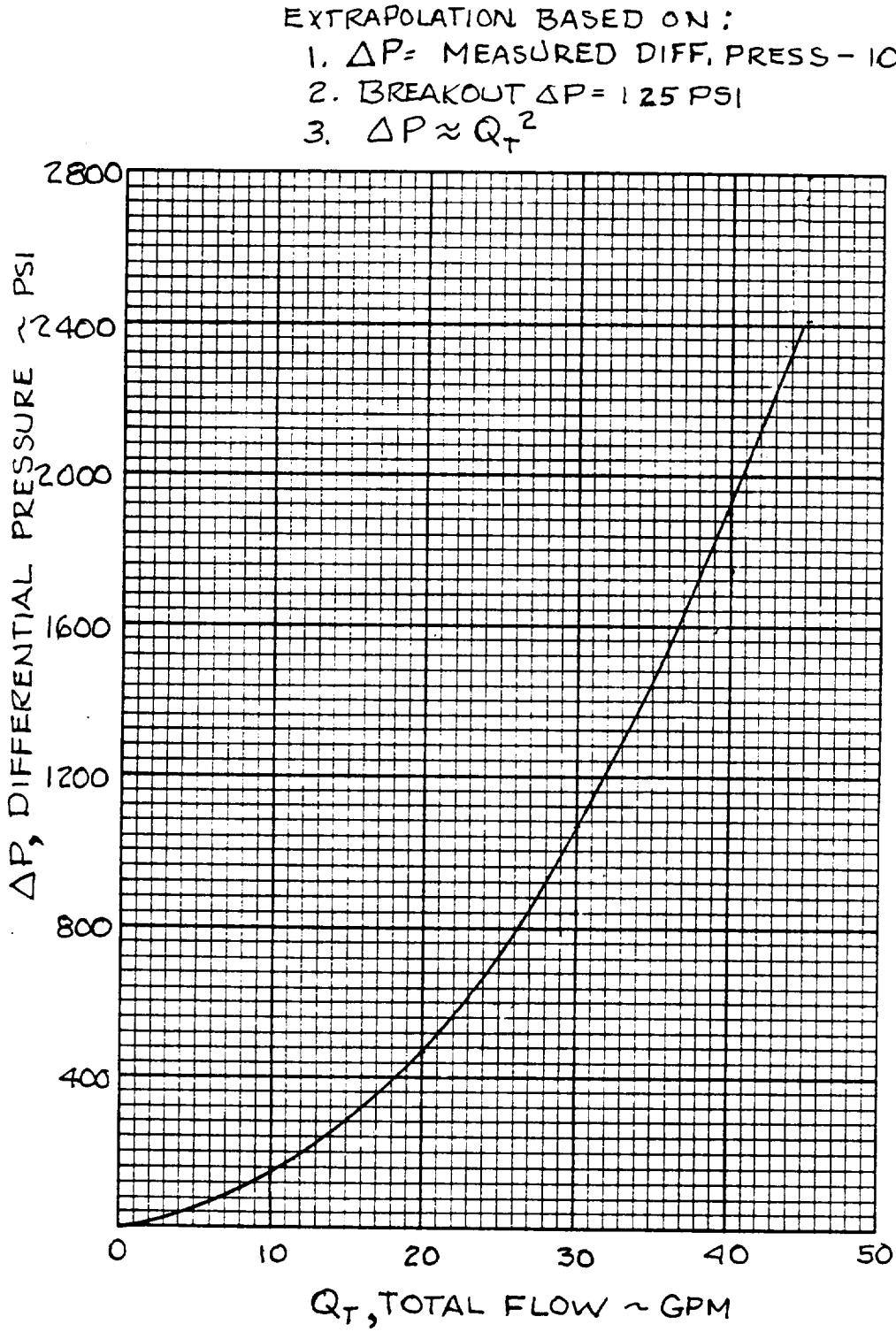


Figure 32. Series Mode Flow Vs Pressure Loss With One Idle Motor

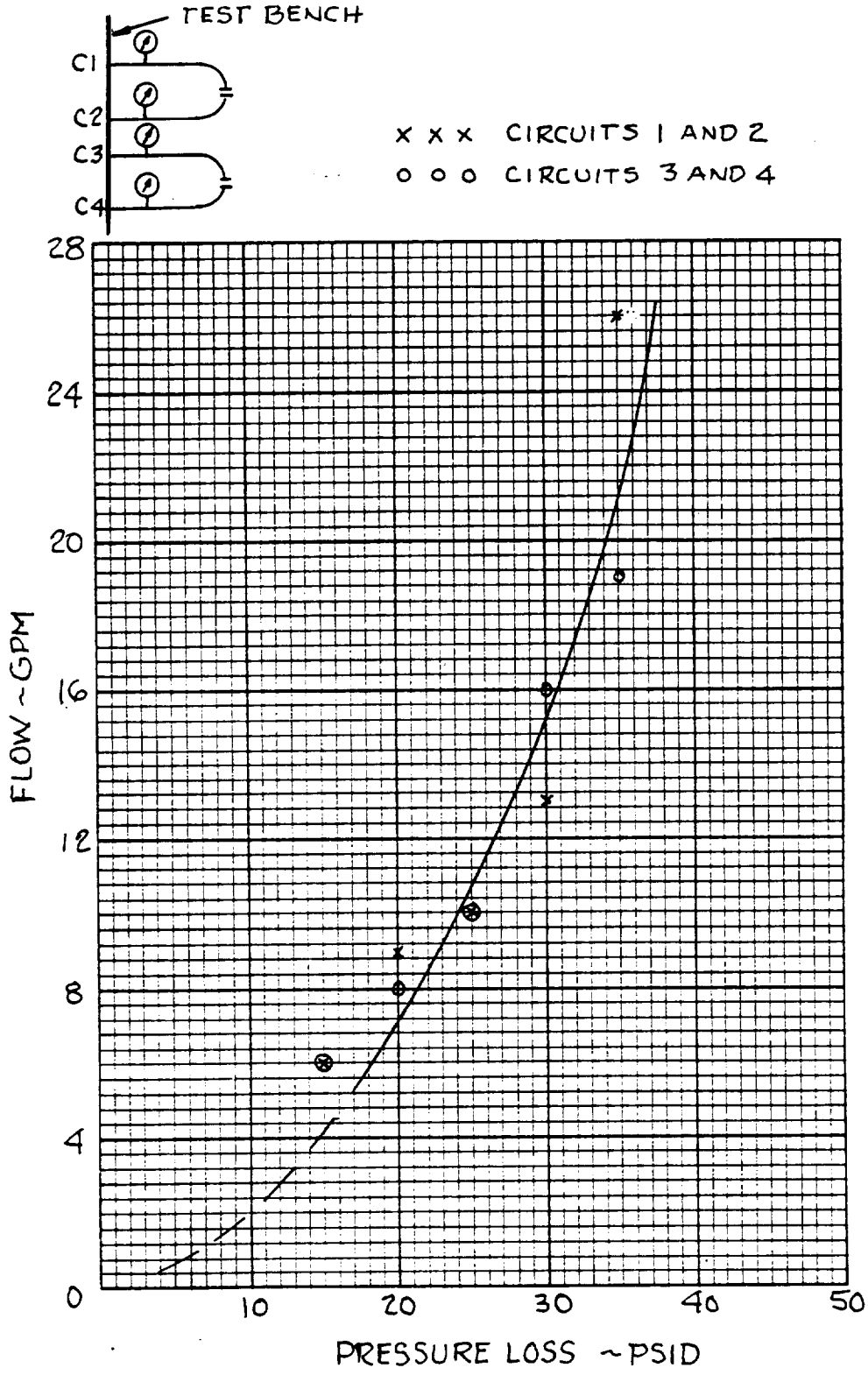


Figure 33. Test Arrangement Line Loss Vs Flow

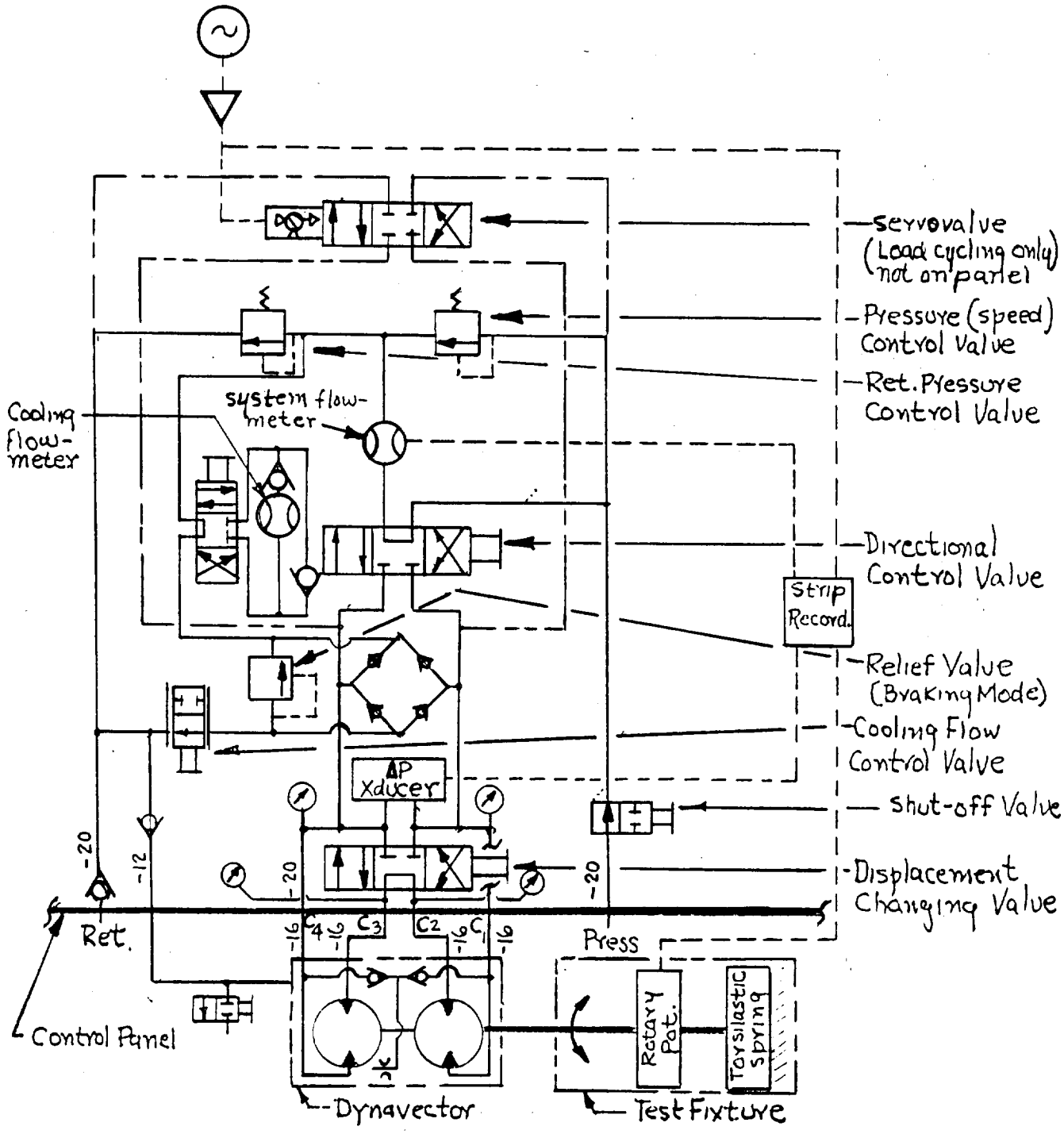


Figure 34. Cycling and Static Test Arrangement

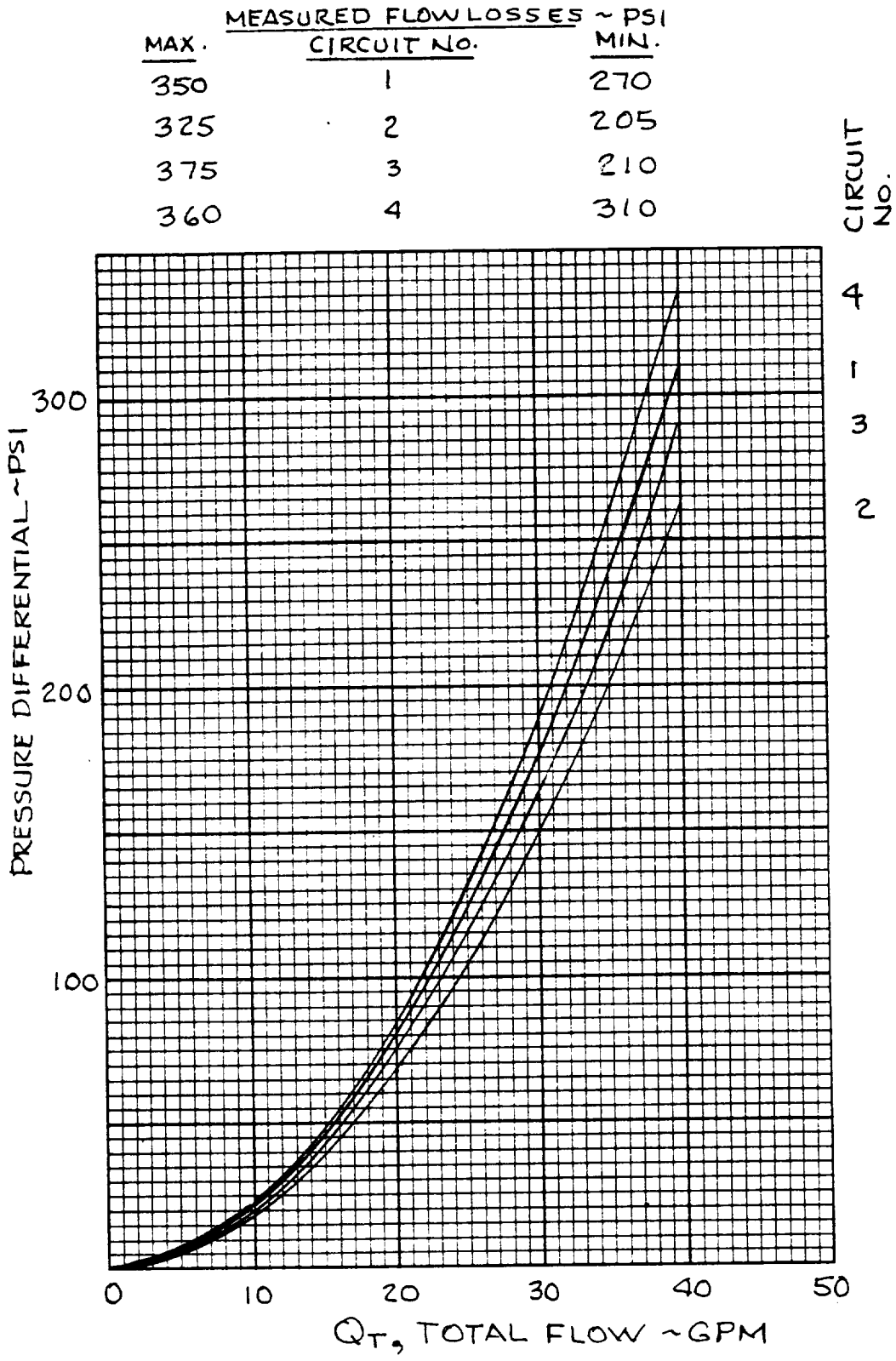


Figure 35. Individual Hydraulic Circuit Flow Vs Average Pressure Loss

$$\eta_v = \frac{das\, N_\omega}{(Qds + Q_\ell)231} = \frac{57.75\, N_\omega}{Q_T\, 231} = \frac{N_\omega}{4\, Q_T}$$

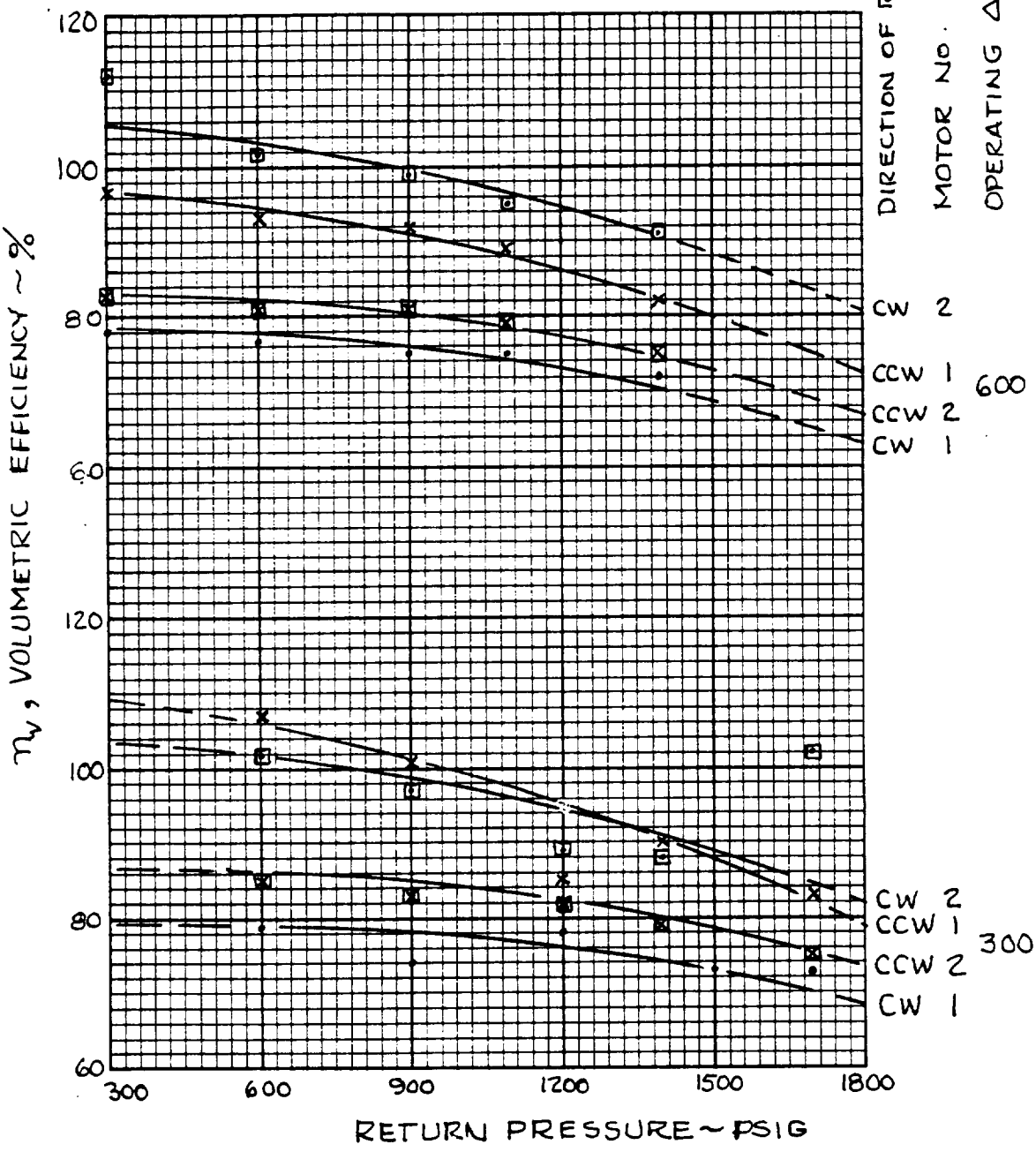


Figure 36. Pressure Level Effect on Volumetric Efficiency

Total Chamber Flow Versus Speed - A plot of total chamber flow versus speed is shown in Figure 37. Total chamber flow is defined as the total flow supplied to the test unit minus case drain leakage. The slope of the solid black line on the figure is the theoretical displacement of the test unit in the series mode. Only motor number 2 running in the cw direction has a lesser slope, indicating a smaller displacement.

Total Chamber Flow and Case Drain Leakage Versus Supply Pressure - The flow plots versus pressure of Figure 38 indicate the relative magnitudes of the total chamber flows and the case drain leakages. Because of the closeness of the leakages recorded for each condition, only a band is shown.

Gear Mesh Disengagement - During no-load testing the test unit inadvertently stopped running. The unit was disassembled and visually inspected to assess gear teeth damage. However, no damage was found on the teeth or any other feature of any component. Consequently the gears were reassembled and the unit retested at no load. After approximately two hours operation, inadvertent disengagement occurred. Again, visual observation following disassembly failed to reveal anything unusual, or any damage, or wear.

A dimensional inspection of the Orbiter Gear, P/N 3311974, and the Output Shaft (gear), P/N 3311968 failed to reveal any significant discrepancy. The assembled gears backlash was measured and found to be near the upper limit of the allowed 0.002 - 0.0035 in (0.0508 - 0.0889 mm), however, some concern was expressed that this might be excessive. So a spare shaft with a slightly larger gear pitch diameter was assembled with the ring gear which reduced the backlash about 50 percent to 0.0015 in. (0.0381 mm).

Testing with the second output shaft was undertaken with similar results as shown in Table 17, which is a compilation of the conditions existing just prior to, or at, the time of failure. The four failures occurring with the second shaft along with the two with the original shaft occurred at no-load and with no resultant gear damage.

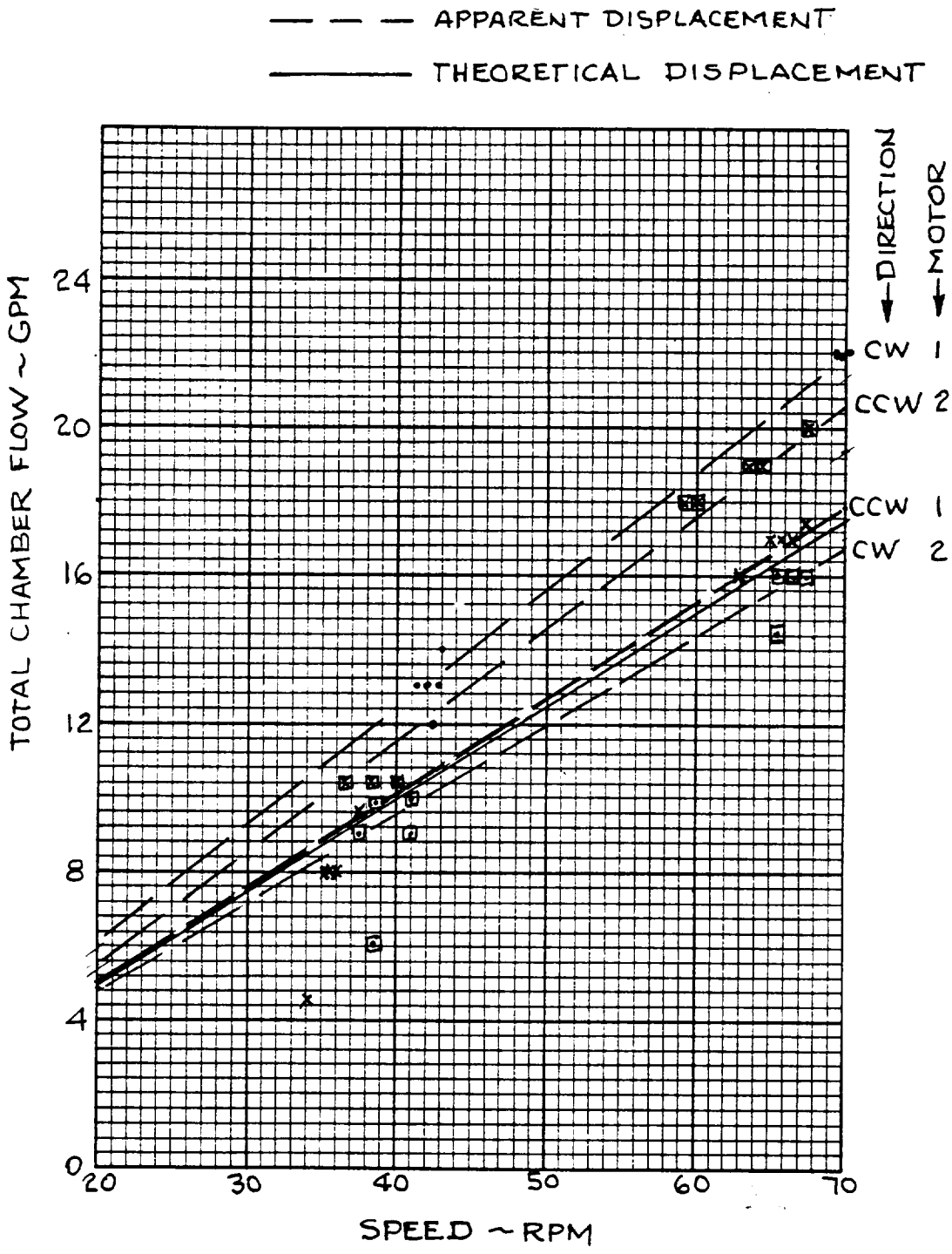


Figure 37. Total Chamber Flow Versus Speed

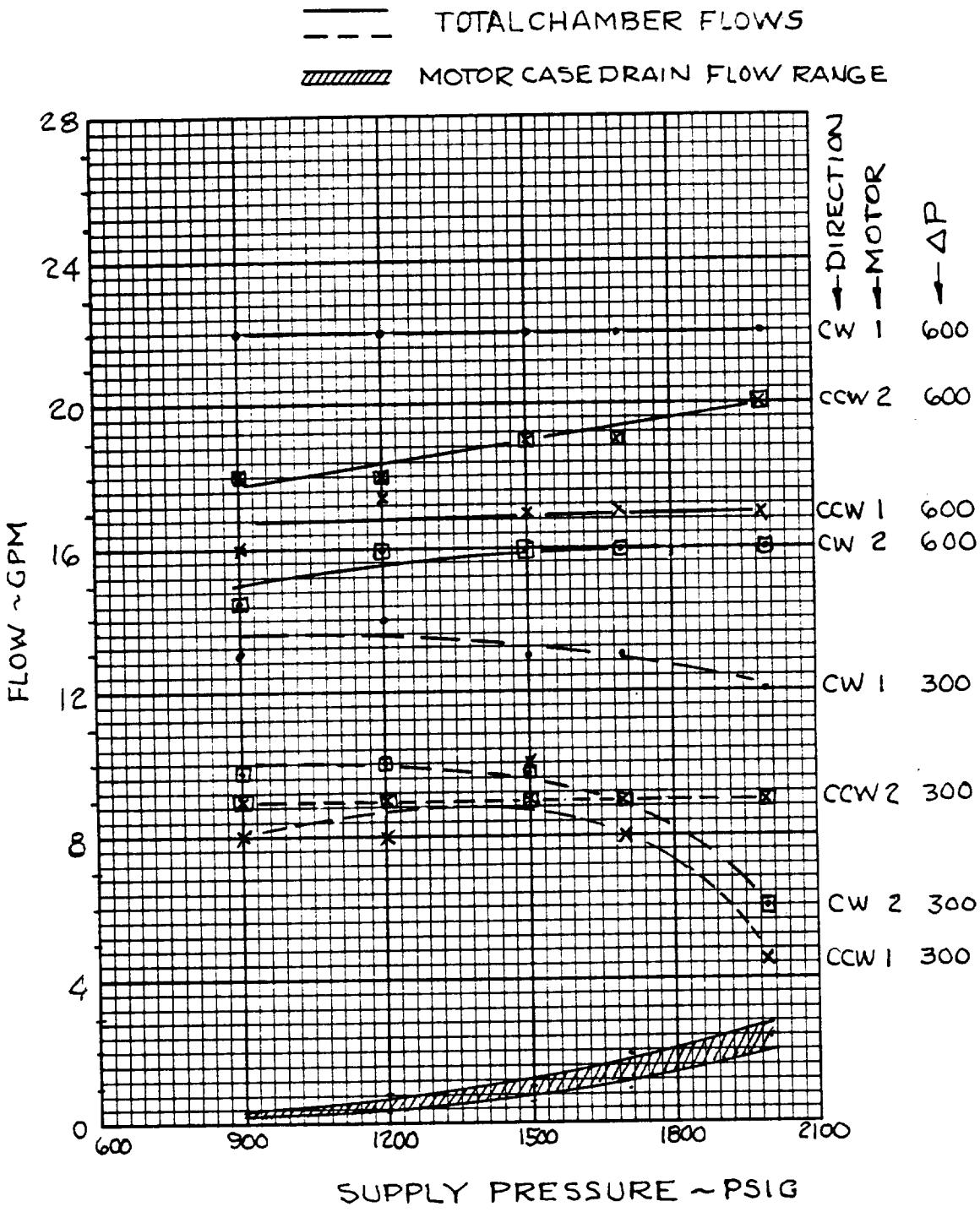


Figure 38. Total Chamber Flow and Case Drain Leakage Versus Supply Pressure

TABLE 17. POWERED WHEEL DRIVE GEAR DISENGAGEMENT DATA

| Failure No. (1) | Operating Mode | | | Rotation | | Flow | Pressure-psi | | Torque-lb-ft. | | | Prior Operating Condition | | | | | Accum. Oper. Time Hours | Remarks |
|---|---|---|---|---|---|---|---|---|---|---|---|---|---|---|---|---|---|---|
| | Series | Parallel | Recirc (2) | CW | CCW | gpm | Supply | Back (3) | Nut (6) | Back (7) | Fail (4) | Mode (5) | Speed rpm | Flow gpm | Press-psi Supply | Press-psi Back | | |
| 1 | - | - | X | X | - | 10 | 1900 | 1600 | 75 | (215) | 6 | #1 recirc | 42CW | 10 | 1800 | 1500 | 3 | No visual gear damage after disassembly. |
| 2 | - | - | X | X | - | - | 900 | 600 | 50 | - | - | #2 recirc | 70CW | 22 | 2000 | 1400 | 5 | No visual gear damage after disassembly. |
| 3N | - | - | - | - | - | - | - | - | <50 | - | 6 | - | - | - | - | - | 0 | 2nd shaft reduced backlash from .003 to .0015. Disengagement occurred while attempting to apply nut torque for smooth break-out. No visual gear damage. |
| 4 | - | X | - | X | - | - | ≈700 | - | 60 | 190 | 6 | - | - | - | - | - | 6.75 | Gears disengage on start-up after having vented line for back driving. No visual gear damage. |
| 5 | X | - | - | - | X | - | - | - | 50 | 200 (250) | - | parall | >50 CCW | - | 1000 | 200 | 7.25 | Some indication blueing off tops of teeth, but surface damage not evident. |
| 6N | - | X | - | - | X | - | - | - | 60 | 300 | 6-8 | series | >80 CCW | - | 800-900 | 300 | 1.0 | No gear damage. Some blueing off top of I.D. gear but not O.D. gear. |

NOTES:
1) "N" signifies use of the second shaft.
2) One motor #1 or #2) had inlet-discharge lines interconnected.
3) Refers to downstream pressure of driving motor(s).
4) Back driving torque after gear disengagement.
5) Refers to series, parallel or recirculating.
6) Refers to 12 stud nuts.
7) Refers to backdriving effort; parentheses indicate break-out pressure.

During testing with the second shaft, a total composite error (TCE) check was conducted for the first shaft. The results are shown in Figure 39.

The interpretation from the plots (a), (c), and (d) in Figure 39 is that the plus (+) deviation of 0.0020 to 0.0026 in (0.0508 to 0.0660 mm) indicates a TCE toward an undersize condition. Plot (b) in the figure displays an obvious drift to the right from bottom to top which exaggerates the magnitude of the error. Only one TCE plot, Figure 40, was attained for the ring gear because of interference of the holding fixture and the Fellows Gear Shaper test equipment. However, on the basis of the one plot, the internal gear is interpreted to have a TCE toward the oversize condition of about 0.0015 in (0.0381 mm).

## 24 Pitch Gear Configuration

Based on considerations made concerning the inadvertant disengagement of the gear mesh experienced during the testing of the 32 $in^{-1}$ (12.6 $cm^{-1}$) pitch gears it was decided to change to 24 $in^{-1}$ (9.4 $cm^{-1}$) pitch gearing. This necessitated resizing and remaking three components. These components with the before and after sizing and the resultant changes in the assembly parameters are listed in Table 18. Results of testing with the new gear mesh are presented in the following paragraphs.

Output Shaft Speed Versus Flow - Figure 41 shows the output shaft speed as a function of flow for the test unit operating no-load. The apparent displacement for series and parallel operation as determined by the reciprocal of each slope, in the range up to about 30 gpm flow, is 66 and 115.5 $in^3$/rev (1081 and 1893 cc/rev), respectively. Based on the design displacements of 57.75 and 115.5 $in^3$/rev, respectively the results indicate an apparent volumetric efficiency of 87.5 and 100 percent, respectively, as determined by

$$N_{va} = \frac{(N/Q)}{a} \qquad (104)$$

Where: $N_{va}$ = apparent volumetric efficiency
$(N/Q)$ = Figure 41 curve slope
$a$ = 4 for the series configuration and 2 for the parallel

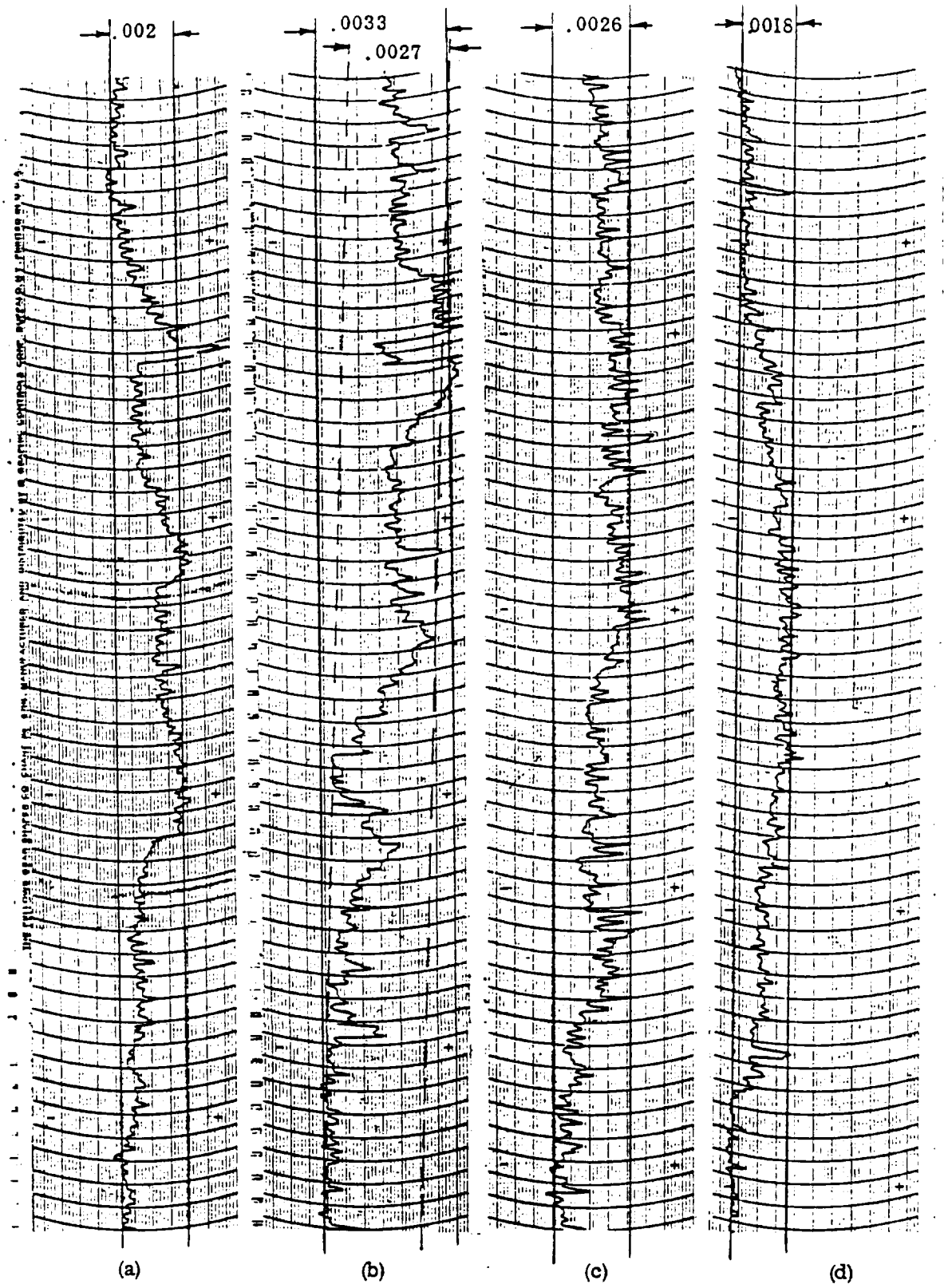


Figure 39. Output Shaft, Part No. 3311968 - Total Composite Error at Four Axial Locations

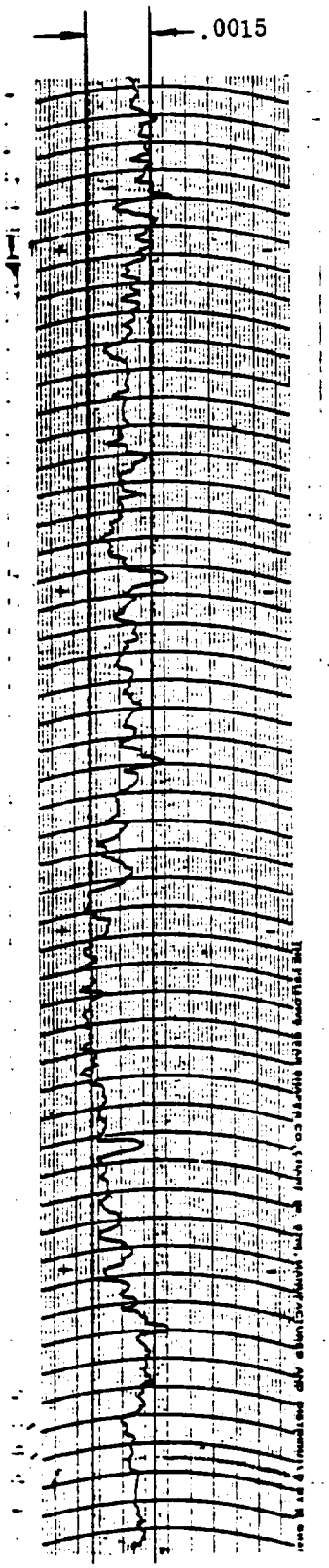


Figure 40. Orbiter Gear, Part No. 3311974 - Total Composite Error at Outboard Axial Location

TABLE 18. COMPONENT SIZE AND ASSEMBLY PERFORMANCE PARAMETER CHANGES

| | Before | | After | |
|---|---|---|---|---|
| Component or Parameter | Chg. Ltr. | Major Feature(s) | Chg. Ltr. | Major Feature(s) |
| Output Shaft P/N 3311968 | A | 32 Pitch<br>136 Teeth<br>4.250 Pitch Dia. | B | 24 Pitch<br>102 Teeth<br>4.250 Pitch Dia. |
| Orbiter Gear P/N 331974 | A | 32 Pitch<br>142 Teeth<br>4.4375 Pitch Dia. | B | 24 Pitch<br>106 Teeth<br>4.4167 Pitch Dia. |
| Sleeve Spacer P/N 3311972 | A | 0.6240<br>0.6237 in. O.D. | B | 0.6448<br>0.6445 in. O.D. |
| Gear Ratio ($R_t$) | - | 22.67 | - | 25.5 |
| Eccentricity (e) | - | 0.09375 in. | - | 0.08333 in. |
| Actuator Displacement<br>-Series (das)<br>-Parallel (dap) | - | <br>57.75 $in^3$/rev<br>115.50 $in^3$/rev | - | <br>57.75 $in^3$/rev<br>115.50 $in^3$/rev |

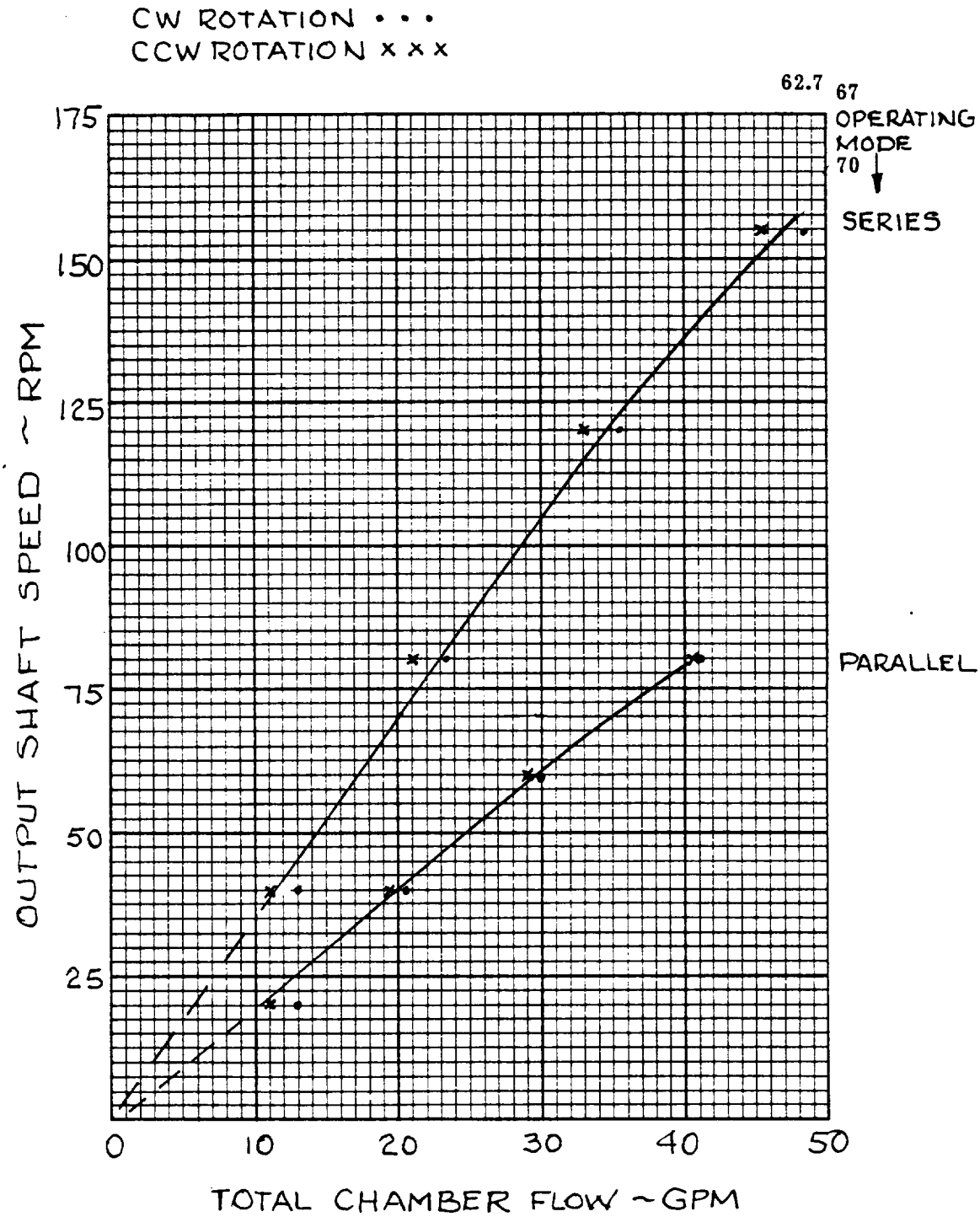


Figure 41. Powered Wheel Drive Output Shaft Speed Versus Flow

Pressure Loss Versus Flow - During the same runs made to develop the data in Figure 41, pressure loss across the test unit was recorded for the no-load operation. The results plotted against flow are shown in Figure 42, for both directions of rotation.

Gear Mesh Disengagement - Following a disassembly and assembly operation during which the bolts and studs active lengths were measured (for control of elongation, loading and running clearances), the test unit performance was very bad. Sustained rotation could not be achieved even up to 1500 psi (10.34 $MN/m^2$) pressure differential in the parallel mode. After a complete lack of response, the test unit was again disassembled, after which it was observed that the gear mesh had disengaged. Also, severe local surface damage had been inflicted on the metering surface of the inboard housing and the adjacent orbiter ring surface as shown in Figures 43 through 46.

Following repair of the damaged areas to remove the rough spots, repeated attempts to cause gear separation under no load conditions at up to 67 percent rated speeds in both modes of operation were without success. However a second advertent disengagement occurred. The occurrance followed a disassembly-modification-assembly event during which the Sleeve Spacers, P/N 3311972 were shortened by 0.0015 in (0.0381 mm), in an attempt to reduce internal leakage. On reinitiation of testing, the unit did not function smoothly, so the outboard housing was removed for visual inspection. Two abnormalities were observed. First, localized damage had occurred on the seal surface of the orbiter ring and on the mating surface of the outboard housing. As can be seen in Figures 47 through 50, the damage was about the same as shown in Figures 43 through 46 and at about the same angular location from the locating dowel pins. The second abnormality noted was that the gear mesh was partially disengaged and the gears jammed. It was also observed that the mid-point of the gear mesh appeared to be drametrically opposite the damaged surface area. In trying to reassemble the outboard housing so that pressure might be applied to help clear the jammed gears, the gears slipped back into mesh with no damage sustained.

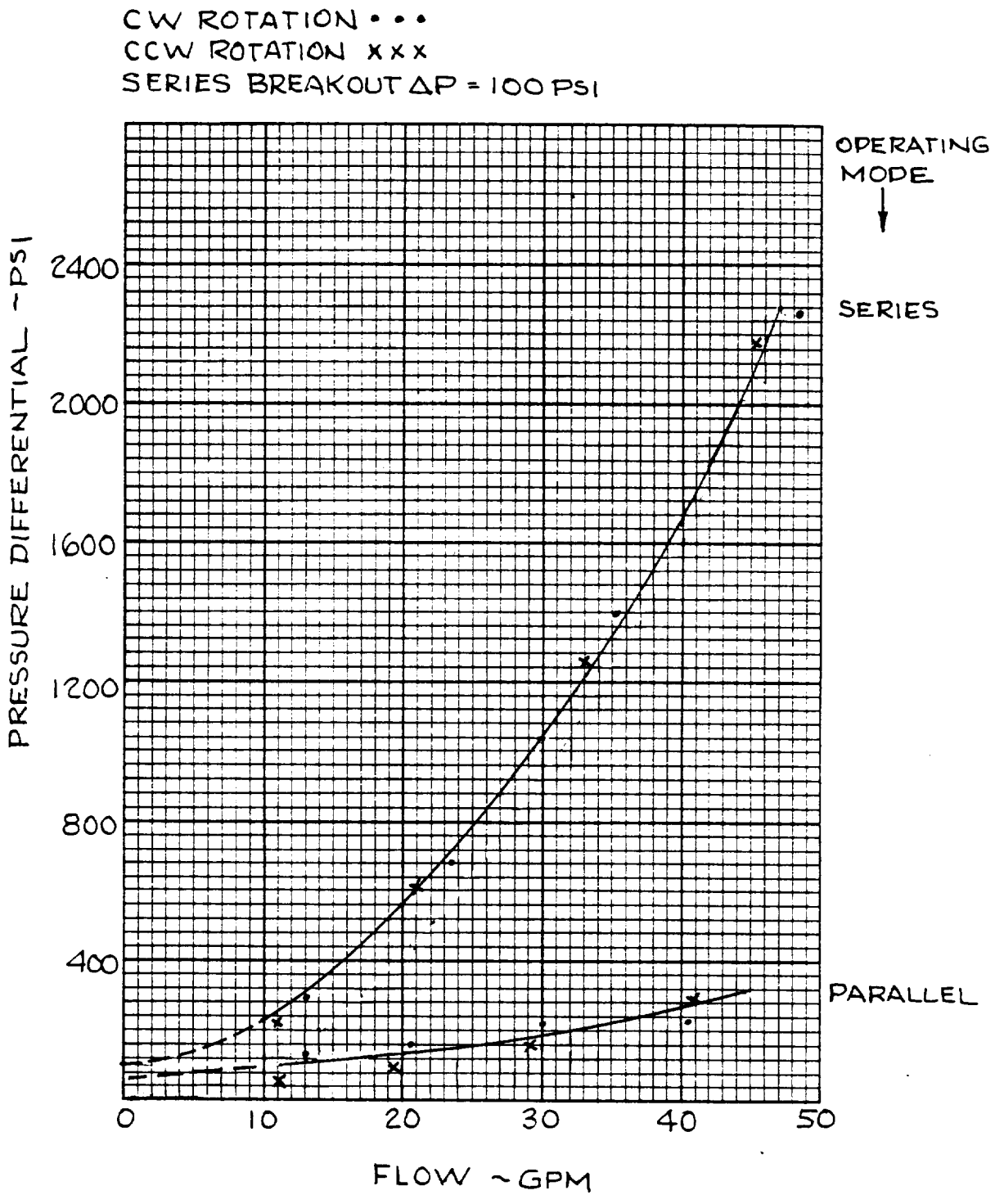


Figure 42. Powered Wheel Drive Pressure Loss Versus Flow

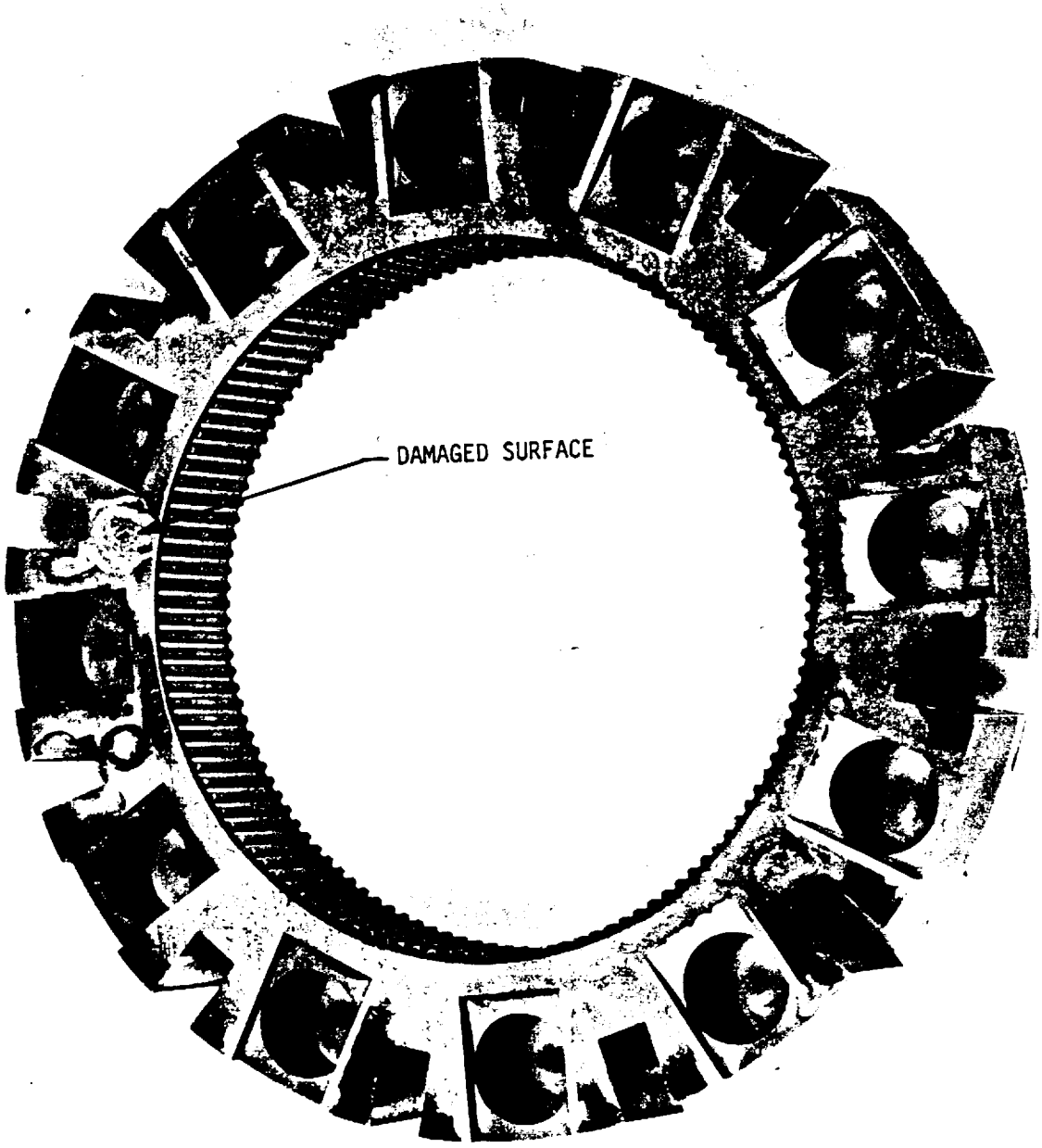


FIGURE 43. ORBITER RING P/N 3311970, SHOWING SURFACE DAMAGE

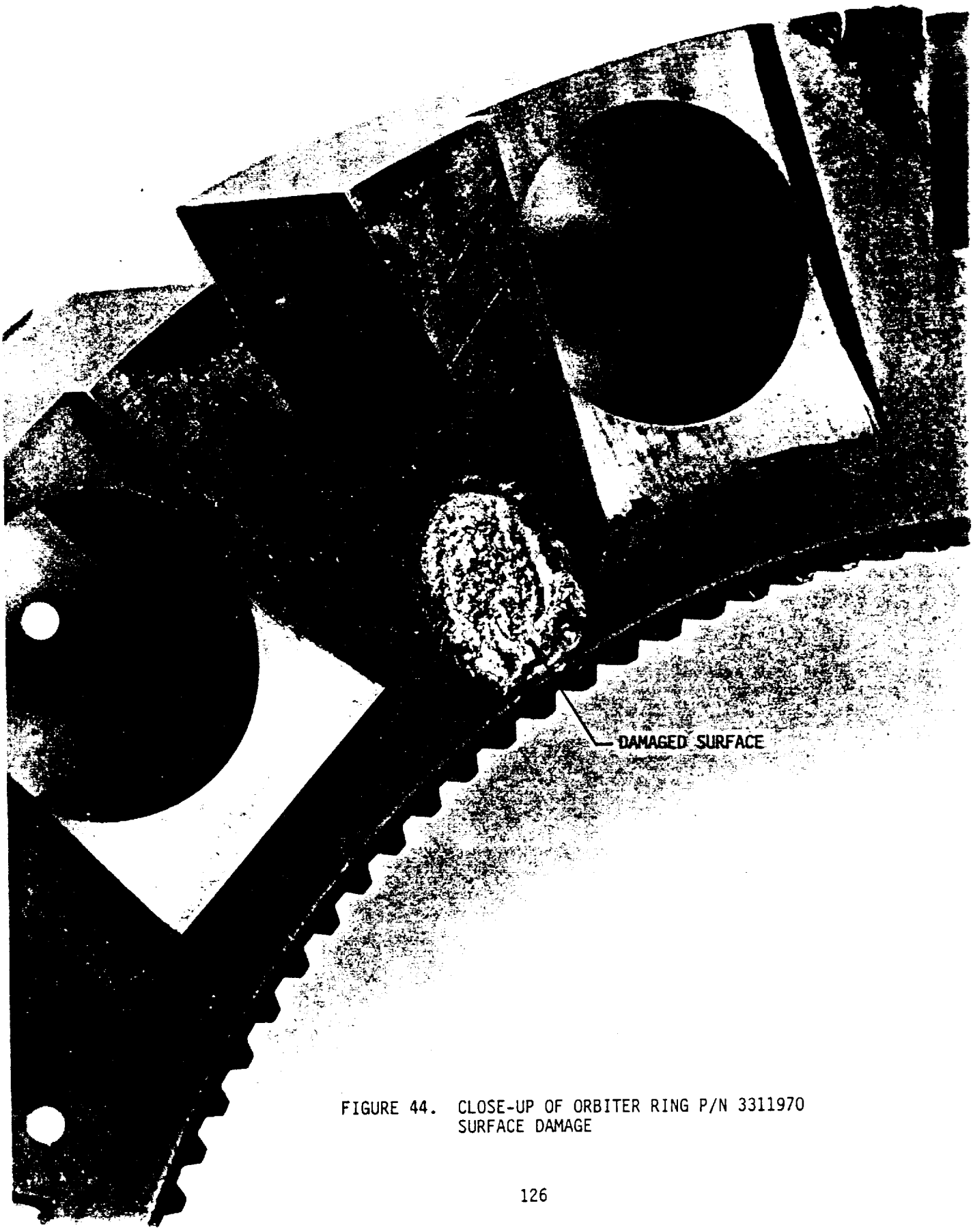


FIGURE 44. CLOSE-UP OF ORBITER RING P/N 3311970 SURFACE DAMAGE

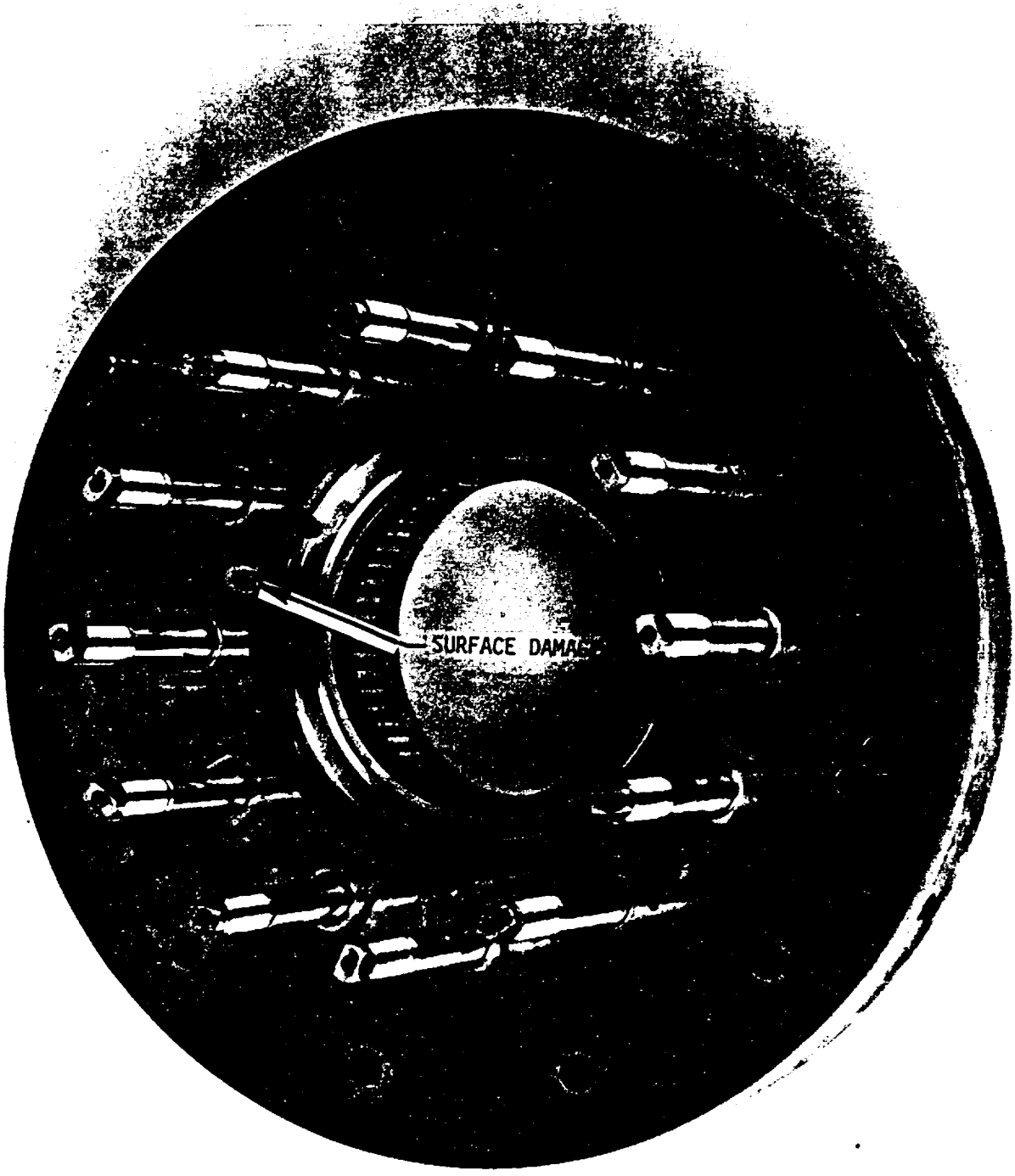


Figure 45. Inboard Housing, P/N 3311945, Showing Surface Damage

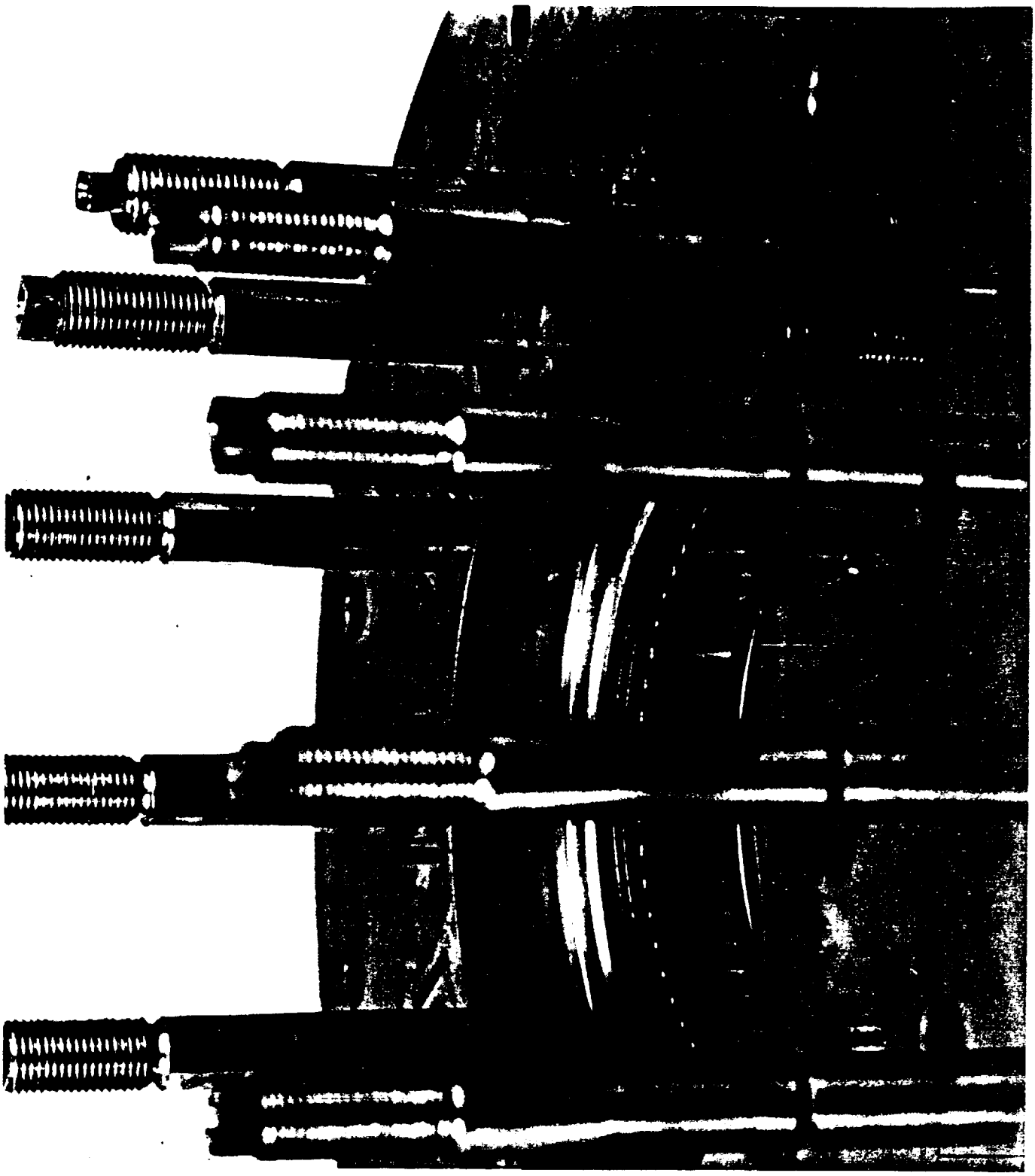

Figure 46. Close-up of Inboard Housing, P/N 3311945 Surface Damage

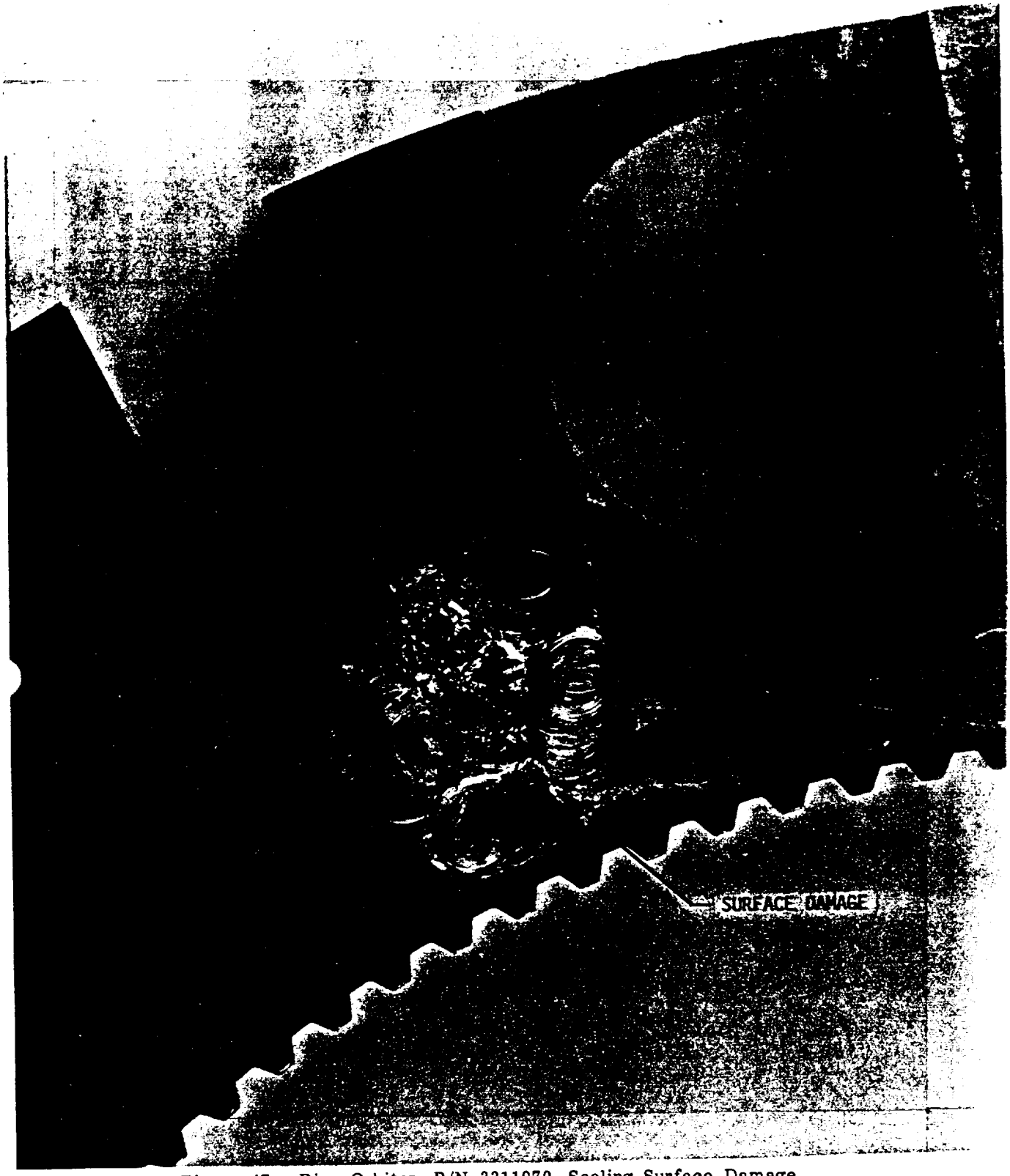


Figure 47. Ring Orbiter, P/N 3311970, Sealing Surface Damage

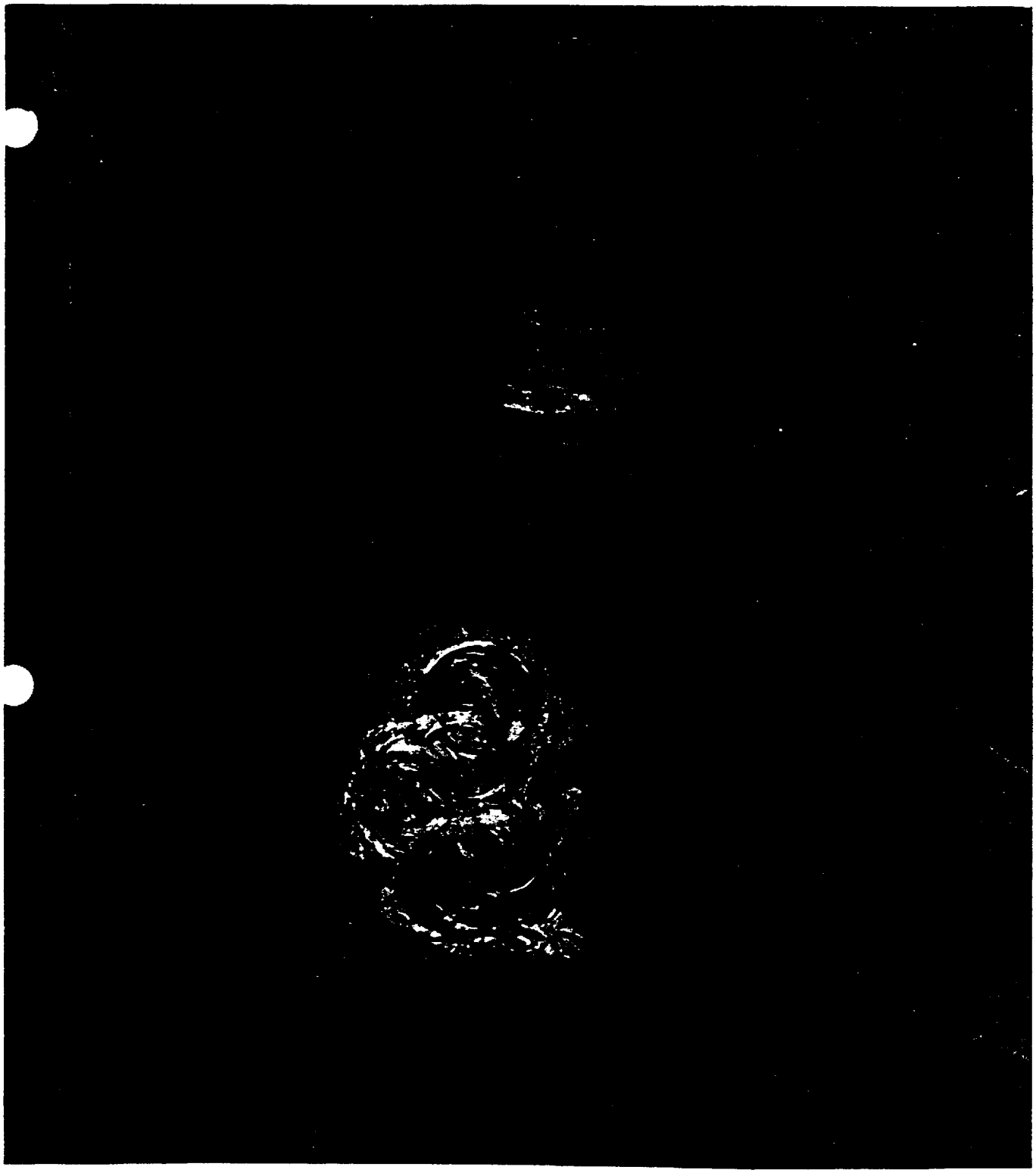

Figure 48. Outboard Housing, P/N 3311940, Metering Surface Damage



Reproduced from best available copy.

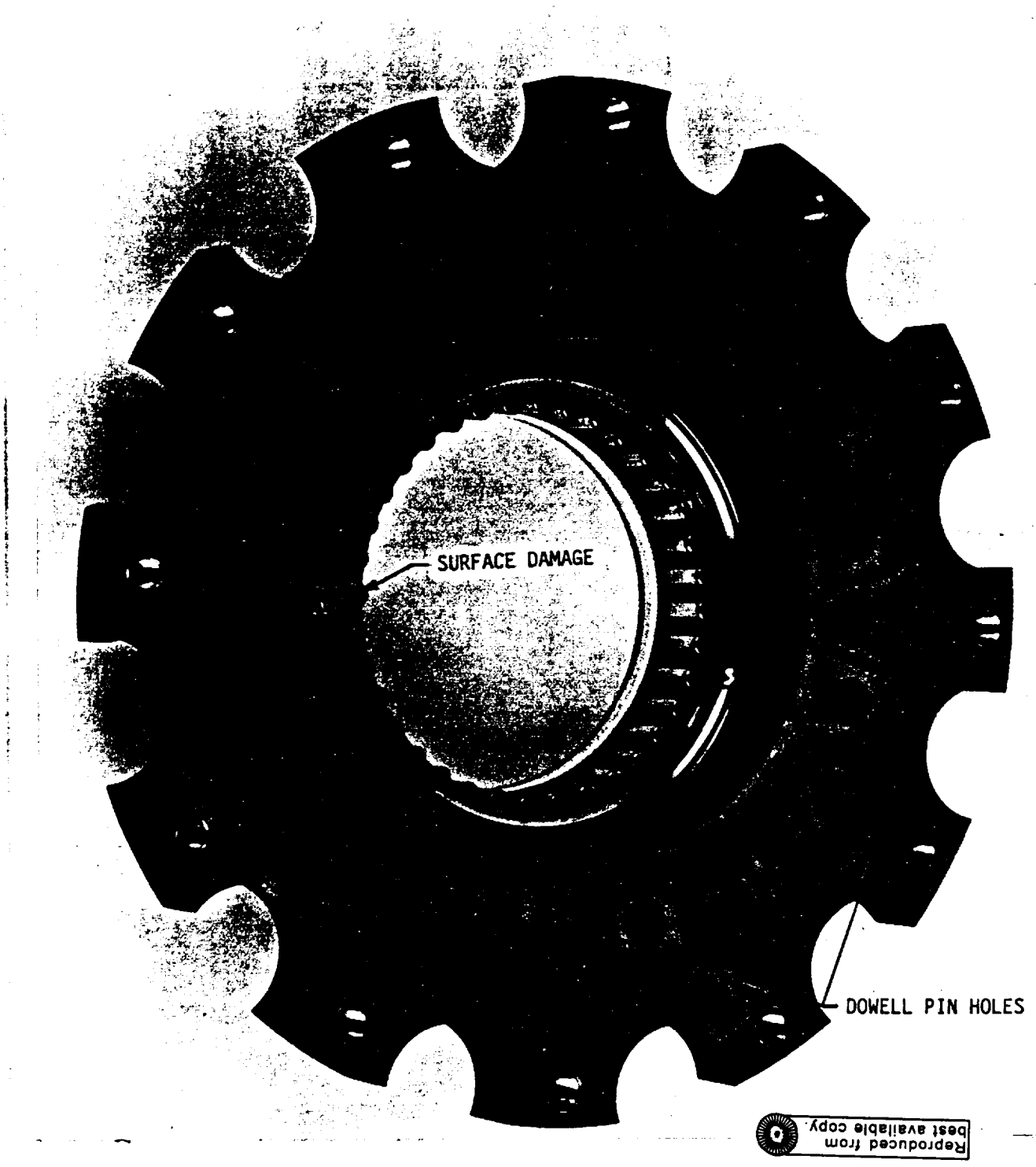


Reproduced from best available copy.

Figure 49. Outboard Housing, P/N 3311940, Metering Surface Damage

Figure 50. Ring Orbiter Sealing Pattern (Top side as Tested)

In an attempt to find out why the coarser pitch gears also disengaged in no load operation, a static load test, using a mechanically imposed load on the orbiter ring, was conducted. the first attempted load arrangement (configuration 1) is shown in Figure 51 in which the unit was completely assembled, except for the Spacer, P/N 3311952. Omission of the spacer allowed insertion of the test fixture plunger. Figure 52 shows a view of the setup with the outboard housing omitted for clarification. This load test was unsuccessful, because of displacement of the orbiter ring in a normal manner until the load was supported by the studs that limit orbiter ring displacement. Consequently, it was decided to support the orbiter ring directly on the Vee shaped fixture (configuration 2) while being loaded as in the previous arrangement and with the output shaft gear in mesh. Photographs of this arrangement are Figures 53 through 55. Results of the load test in the form of strain versus load for the assembled orbiter ring, ring gear and output shaft are shown in Figure 56. During this test with the application of 15,000 lbs (6820 kg), partial gear separation occurred as shown in Figure 54 for the arrangement of Figure 57. Figure 58 shows the strain versus load test results for another test (configuration 3) using only the ring gear. This test was conducted as a check because of the faily predictable results expected. the test arrangement was similar to that in Figure 57.

Metering Lap Leakage - Because of the inability to generate even 20 percent of the required torque a test was conducted to evaluate the leakage occurring when two chambers (180 degrees opposed) reach a position, once in each motor orbit, as shown in Figure 59. At this position the two edges of the metering slot in the orbiter ring are nominally line-to-line with the inside edge of each of the two metering ports in the housings. In this position, the two chamber metering conditions are nominally the same as for the neutral position of a zero overlap spool and sleeve type valve and should exhibit very low leakage. In conducting

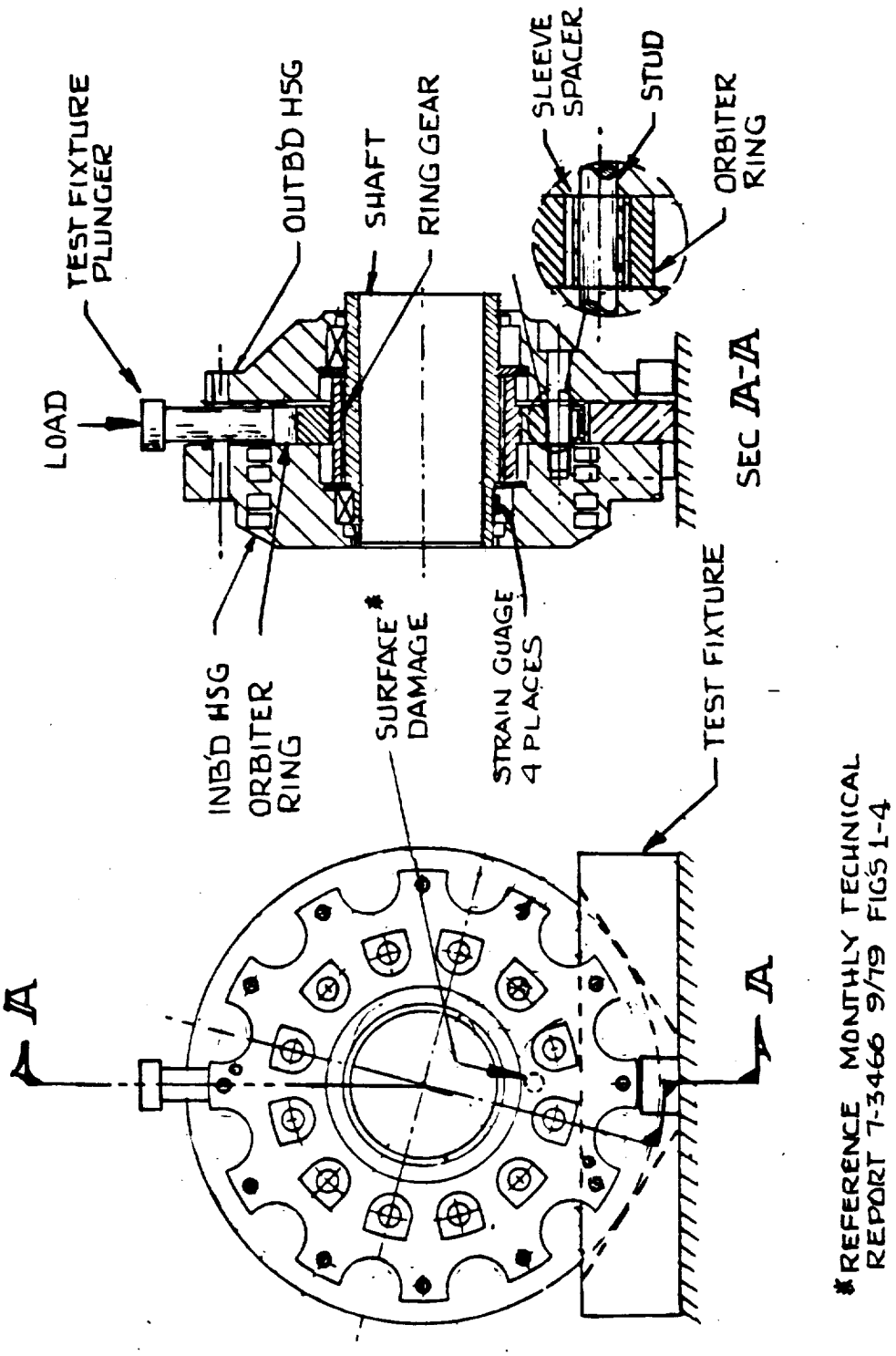


Figure 51. Configuration 1 Mechanical Load Test Arrangement

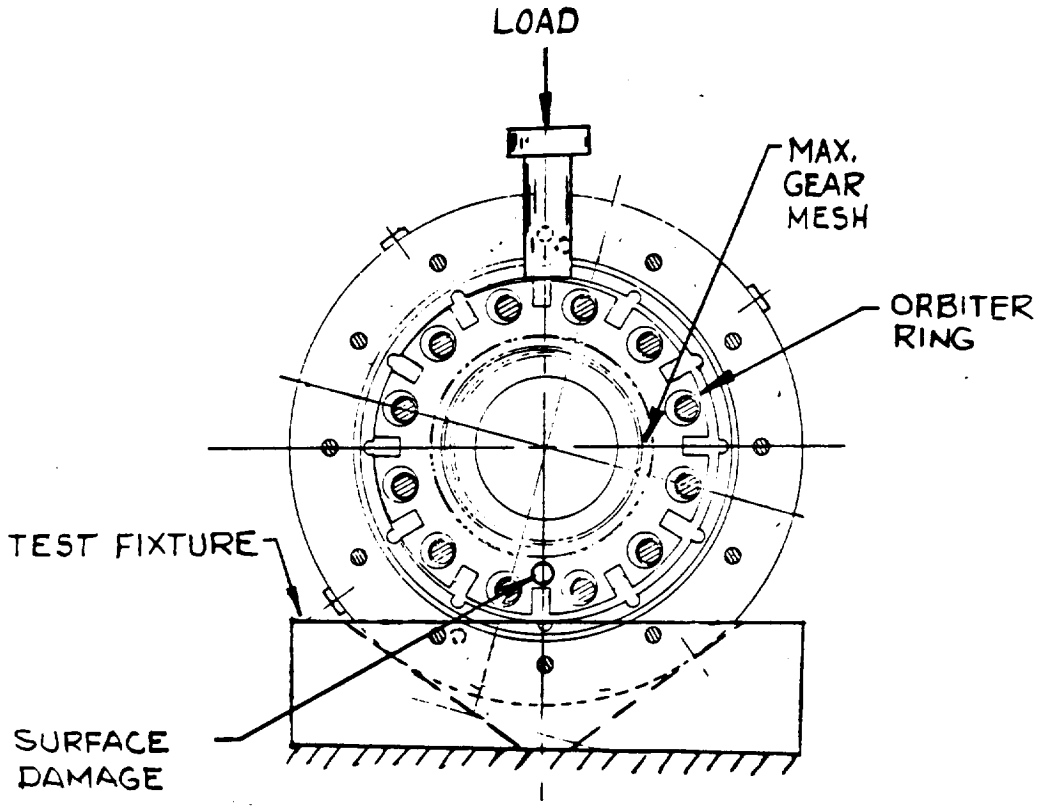


Figure 52. Configuration 1 - Mechanical Load Test Arrangement (Outboard Housing Removed for Clarity)

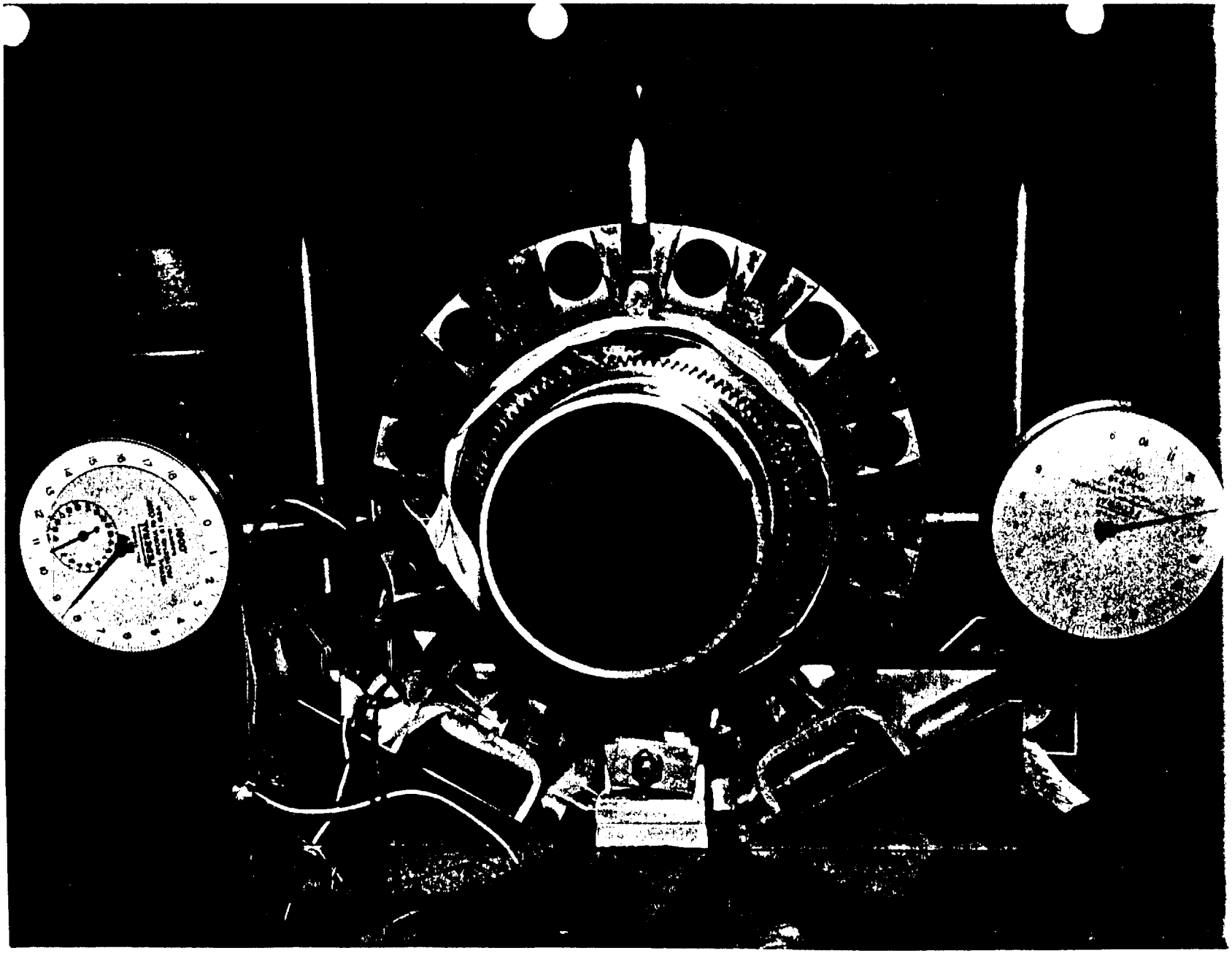

Figure 53. Orbiter Mechanical Load Test

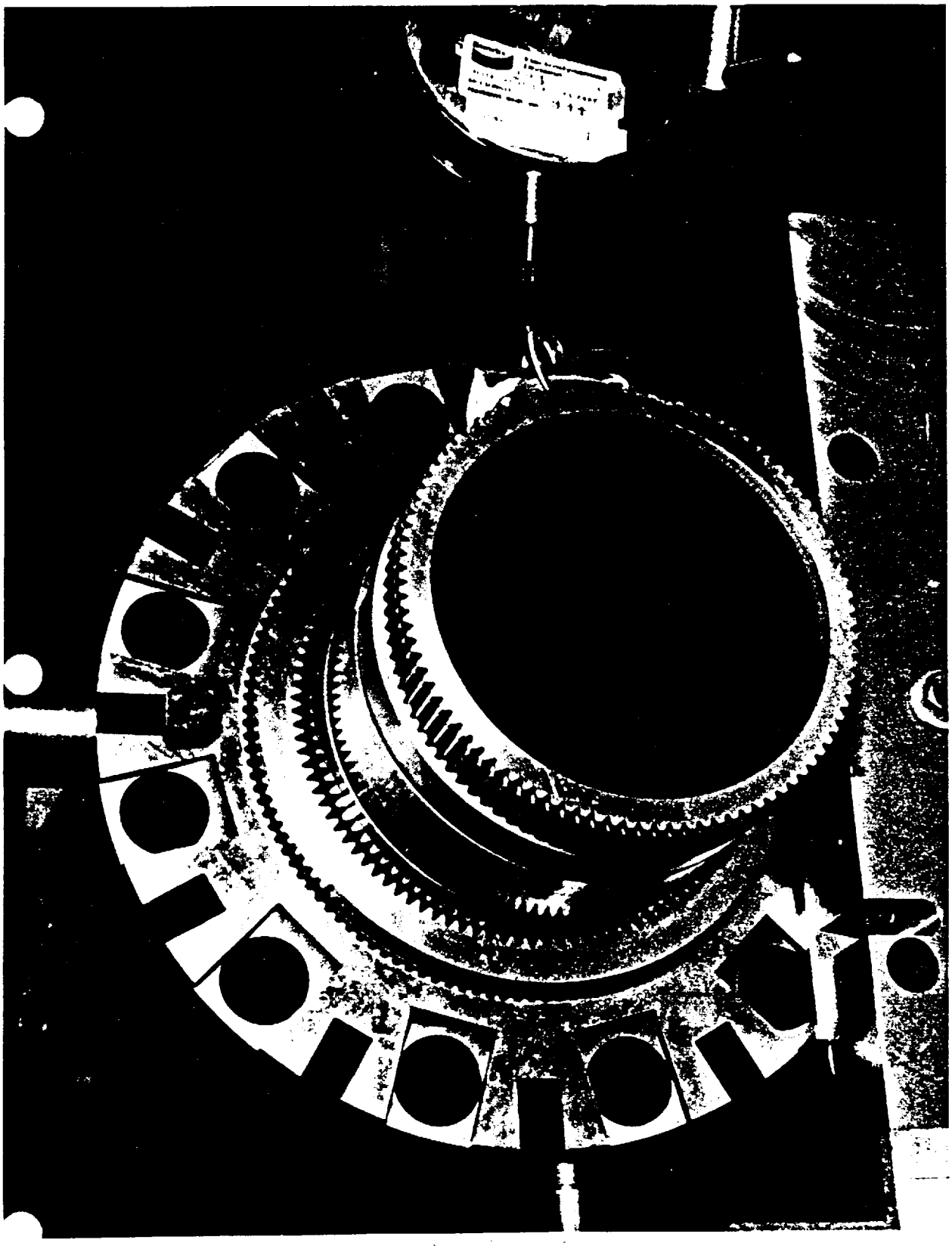

Figure 54. Orbiter Mechanical Load Test

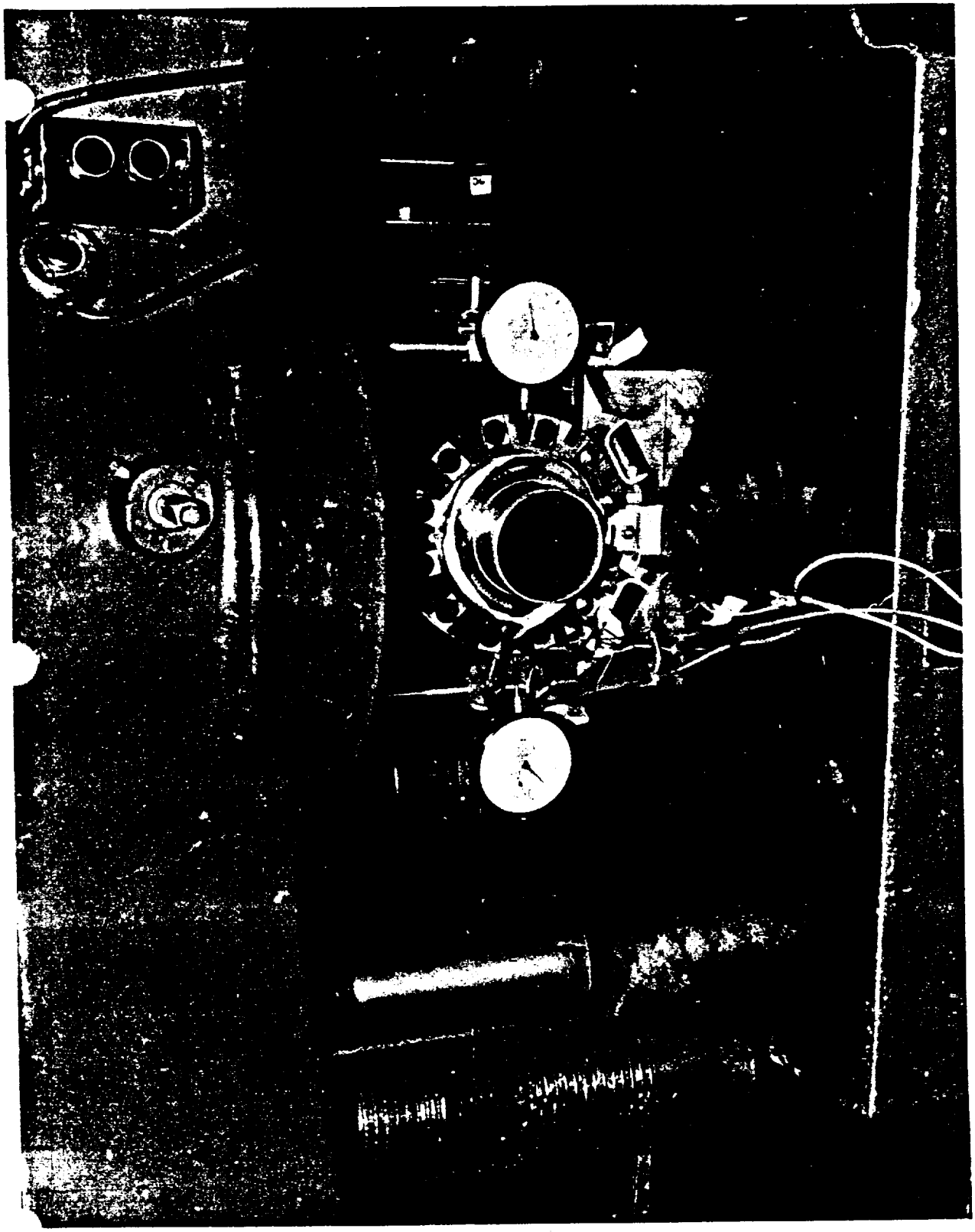

Figure 55. Orbiter Mechanical Load Test

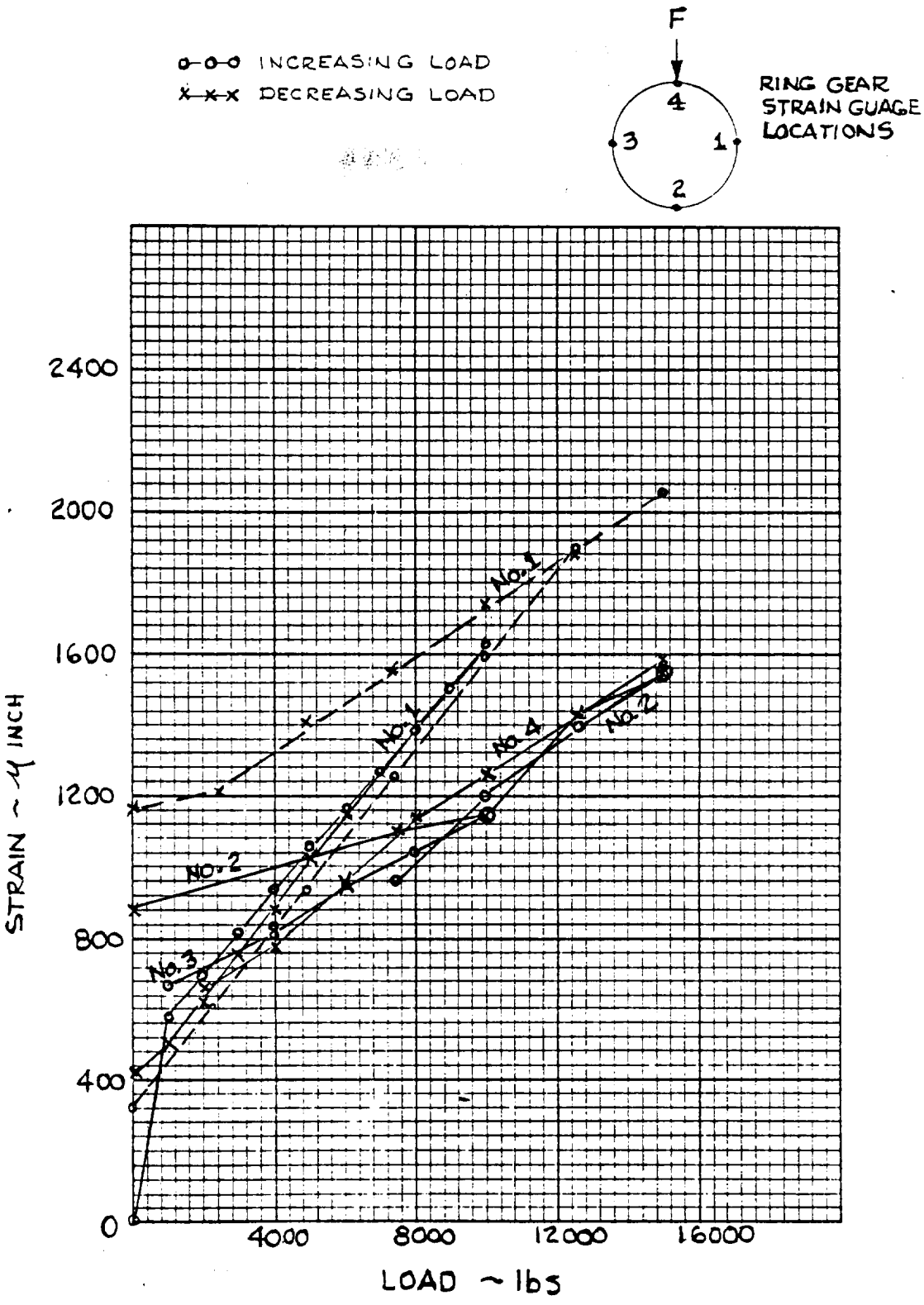


Figure 56. Orbiter Ring/Ring Gear/Output Shaft Assembly (Configuration 2) Load Test Results

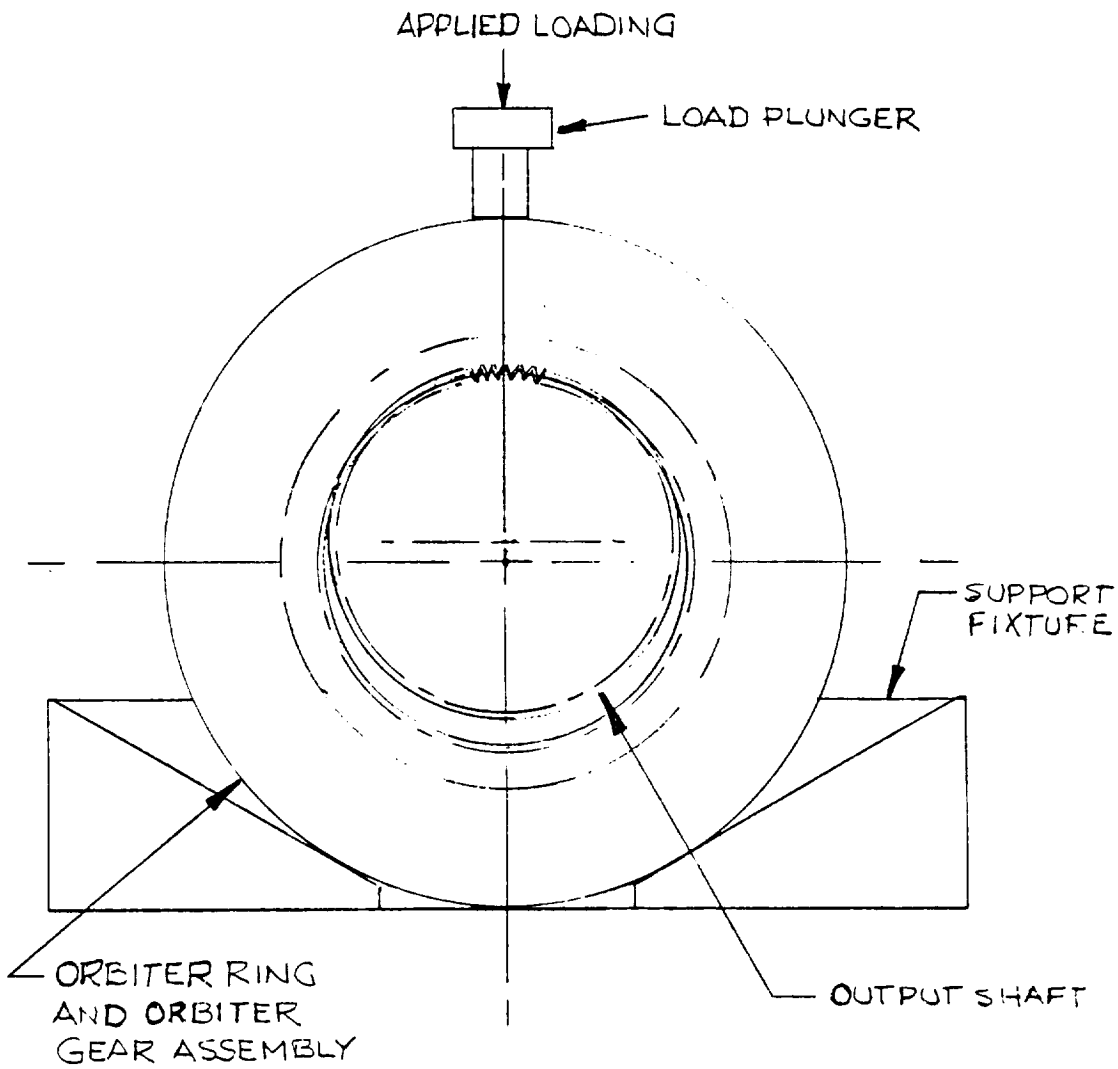


Figure 57. Orbiter Ring Mechanical Load Test Arrangement

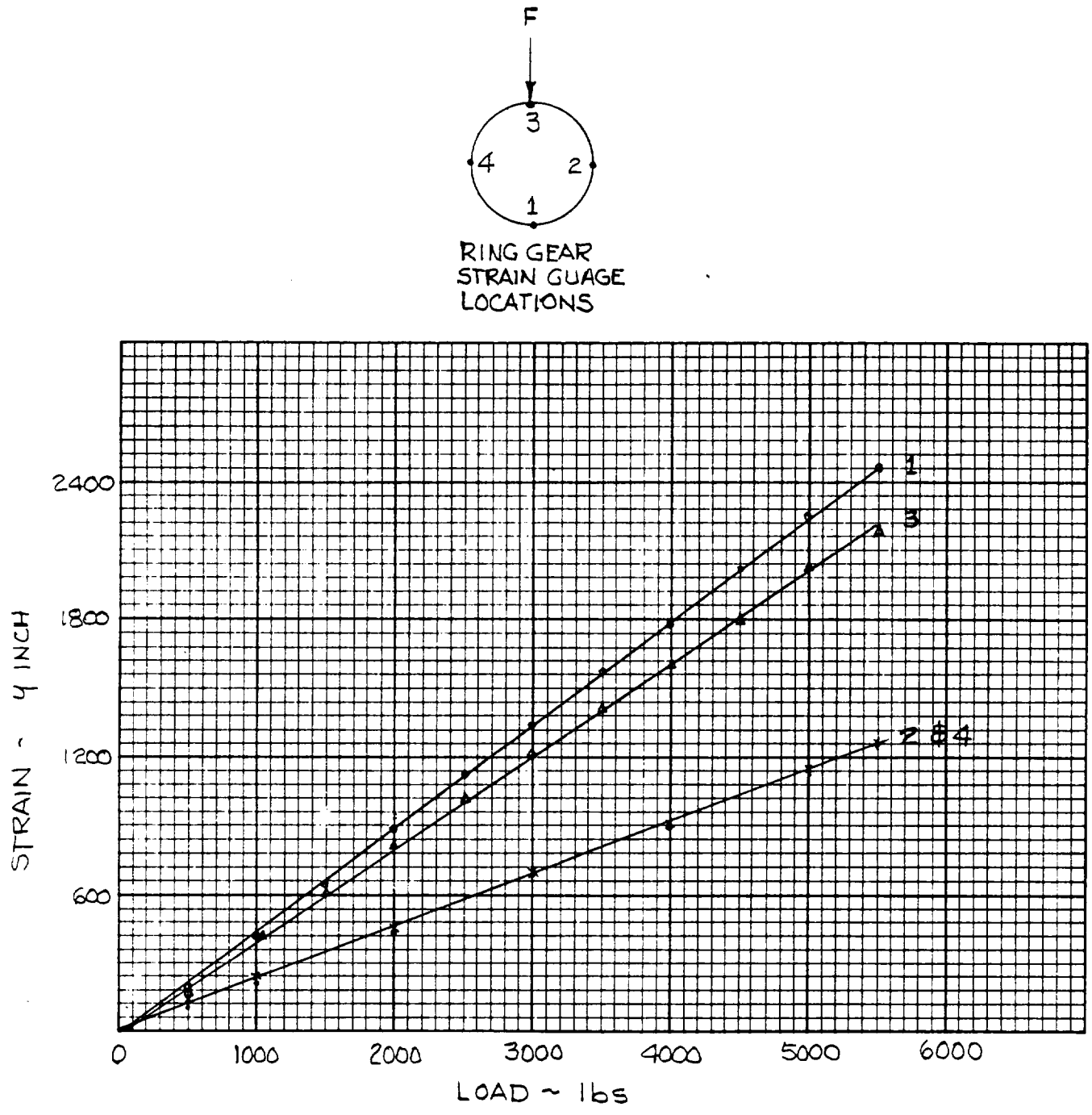


Figure 58. Ring Gear Load Test Results

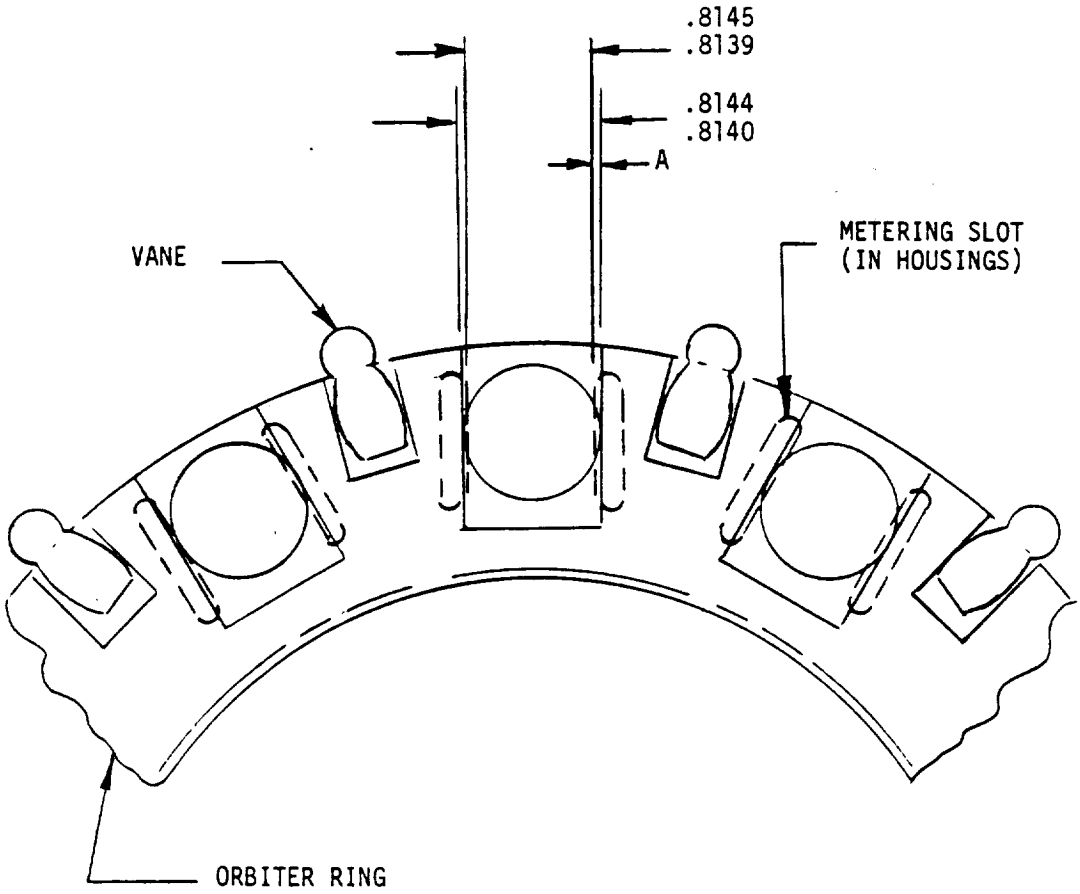


DESIGN OVERLAP DIMENSION, A=.0000 ± .0005

Figure 59. Metering Slot/Orbiter Ring Overlap

this test in the arrangement shown in Figure 60, the outboard housing was removed from the assembly and the orbiter ring/ring gear assembly was disengaged from the output shaft gear and centered, in respect to the metering plate. Then by trial and error, the rotational position of the orbiter ring was adjusted to obtain simultaneously the best average total leakage. With the orbiter ring clamped to the metering surface of the inboard housing in this position, individual and combined circuit leakages were determined as recorded in Table 19.

Because of the excessive leakage that occurred, it was decided to attempt plating the sides of the slots of the orbiter ring to reduce the .8140 - .8144 in. dimension in Figure 59 of the metering edges of the housing slots (reference discussion in CONCLUSIONS for this same subject). After a brief investigation it was concluded that the quickest and most economical plating with a fair chance of success was copper. Although, it was a concern that the copper, being very soft, would erode quickly, it was decided to try it. Consequently, the copper was applied to a thickness of 0.006 - 0.007 in. (0.152 - 0.179 mm) to reduce the slot width to about 0.801 in. the metering lap leakage results with the copper plating on the orbiter ring slots are shown in Table 20.

Another source of internal leakage besides the metering lap leakage is that occurring around the vanes. Although, indications of good surface contact between the individual vanes and their respective orbiter ring slots was provided by the removal of toolmakers blueing which had been applied to each vane, it was decided to measure this leakage. While this leakage could not be measured under operating conditions it was decided to perform a test in the arrangement of Figure 60. by pressurizing C1 and C2 with C3 and C4 connected to return, or open to atmosphere and measuring the C1 and C2 combined flow, the leakage past all the vanes is found. Since in this manner all the chambers in motor number 1 are pressurized simultaneously the leakage could be as much as twice that occurring in normal operation. The test results are given in Table 21. For the vane leakage tests, the unit was completely assembled.

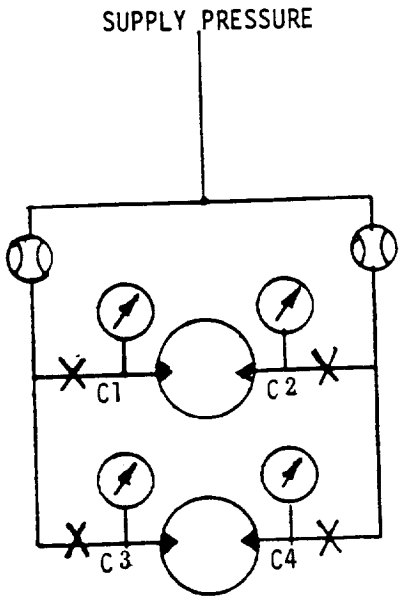


NOTE: TEST CONDUCTED WITH OUTBOARD HOUSING REMOVED AND THE ORBITER RING CENTERED (GEARS DISENGAGED)

Figure 60. Port Leakage Test Arrangement

TABLE 19. PORT LEAKAGE TEST RESULTS

| TEST NO. | DIFFERENTIAL PRESSURE-PSID | | | | CIRCUIT FLOW-GPM | | | | | |
|---|---|---|---|---|---|---|---|---|---|---|
| | C1 | C2 | C3 | C4 | C1 | C2 | C3 | C4 | C1/C3 | C2/C4 |
| 1 | 25 | | | | 5.0 | | | | | |
| 2 | | | 50 | | | | 4.2 | | | |
| 3 | | 50 | | | | 4.8 | | | | |
| 4 | | | | 30 | | | | 5.0 | | |
| 5 | 11.0 | 12.6 | 12.0 | 12.4 | | | | | 4.5 | 5.0 |

TABLE 20. PORT LEAKAGE TEST RESULTS AFTER PLATING ORBITER RING SLOTS

| TEST NO. | DIFFERENTIAL PRESSURE-PSID | | | | CIRCUIT FLOW-GPM | | | | | |
|---|---|---|---|---|---|---|---|---|---|---|
| | C1 | C2 | C3 | C4 | C1 | C2 | C3 | C4 | C1/C3 | C2/C4 |
| 1* | 280 | 285 | 300 | 288 | | | | | 5.0 | 4.0 |
| 2* | 290 | 295 | 310 | 285 | | | | | 4.2 | 5.0 |
| 3 | 200 | | | | 5.2 | | | | | |
| 4 | | 200 | | | | 0.8 | | | | |
| 5 | | | 200 | | | | 1.0 | | | |
| 6 | | | | 200 | | | | 5.5 | | |

*The neutral position where the two combined circuit flows would be equal lies in between these two minutely different positions but it could not be attained for lack of control.

TABLE 21. VANE LEAKAGE

| TEST NO. | DIFFERENTIAL PRESSURE-PSID | | | | CIRCUIT FLOW-GPM | | | |
|---|---|---|---|---|---|---|---|---|
| | C1 | C2 | C3 | C4 | C1 | C2 | C3 | C4 |
| 1* | 286 | 310 | ≈50 | ≈50 | — | — | 4.0 | 0.8 |
| 2* | 205 | 220 | ≈50 | ≈50 | — | — | 3.2 | 0.6 |
| 3* | 100 | 100 | ≈50 | ≈50 | — | — | 1.9 | 0.1 |
| 4** | 95 | 100 | ≈50 | ≈50 | — | — | 1.8 | 0.1 |
| 5** | 186 | 200 | ≈50 | ≈50 | — | — | 3.0 | 0.5 |
| 6** | 288 | 310 | ≈50 | ≈50 | — | — | 4.0 | 0.8 |
| 7** | ≈50 | ≈50 | 108 | 100 | 0.1 | 2.0 | — | — |
| 8** | ≈50 | ≈50 | 200 | 190 | 0.6 | 3.0 | — | — |
| 9** | ≈50 | ≈50 | 308 | 294 | 0.7 | 3.8 | — | — |
| 10⊛ | ≈50 | ≈50 | 112 | 100 | 0.1 | 2.1 | — | — |
| 11⊛ | ≈50 | ≈50 | 212 | 200 | 0.6 | 3.1 | — | — |
| 12⊛ | ≈50 | ≈50 | 305 | 292 | 0.9 | 4.0 | — | — |

| | TORQUE TO TURN SHAFT-LB-FT | STUD TORQUE-LB-FT |
|---|---|---|
| * | 80-90 | 50 |
| ** | 150+ | 60 |
| ⊛ | 40-50 | 30 |

## CONCLUSIONS

The conclusions based on the test results are also divided into two topics corresponding to the same divisions in the TEST RESULTS section.

### 32 Pitch Gear Configuration

Intercircuit Leakage - The intercircuit leakages are believed to stem from the problems encountered in brazing of the inboard and outboard housings as discussed in references 19 through 27. This conclusion is based on heat treat cracks sustained during recovery operations from the brazing failure Figures 61 through 63. The cracks which appeared in the metering plate (plate 4) of the inboard housing were repaired by TIG welding, Figure 64, but a subsequent observation revealed that separation between plates 4 and 5 existed. The separation was partially repaired by welding, as shown in Figure 65, to improve structural integrity, but leaving leakage paths between some individual circuits.

Based on the leakage as shown in Figure 30, the magnitude of the C2 to C3 leakage is considered inconsequential as it appears to be of a laminar nature based on the linear relationship shown. During parallel mode operation C2 and C3 pressures may differ by 200 psi (1.38 $MN/m^2$) so the estimated maximum C2-C3 leakage will only be 0.08 gpm (0.32 lit/min). The C1 to C4 and C2 to C4 leakages are more substantial, although during parallel mode operation C2 and C4 pressures will be nearly equal so little leakage will occur in this mode. Based on the shape of the curves in Figure 30, these two leakages appear to be a mixture of laminar and orifice, type flows with flow varying as the 0.6 to 0.8 power of the differential pressure as pressure increases. Assuming at a maximum differential pressure of 4000 psi (27.58 $NM/m^2$) that the laminar flow is more dominant, the estimated maximum leakage from C1 to C4 will be (based on the 0.8 power) 8.0 gpm (30.3 lit/min). Assuming that the displacement of both motors are equal and since

Figure 61. Braze Assembly P/N 3311946 Heat Treat Cracks

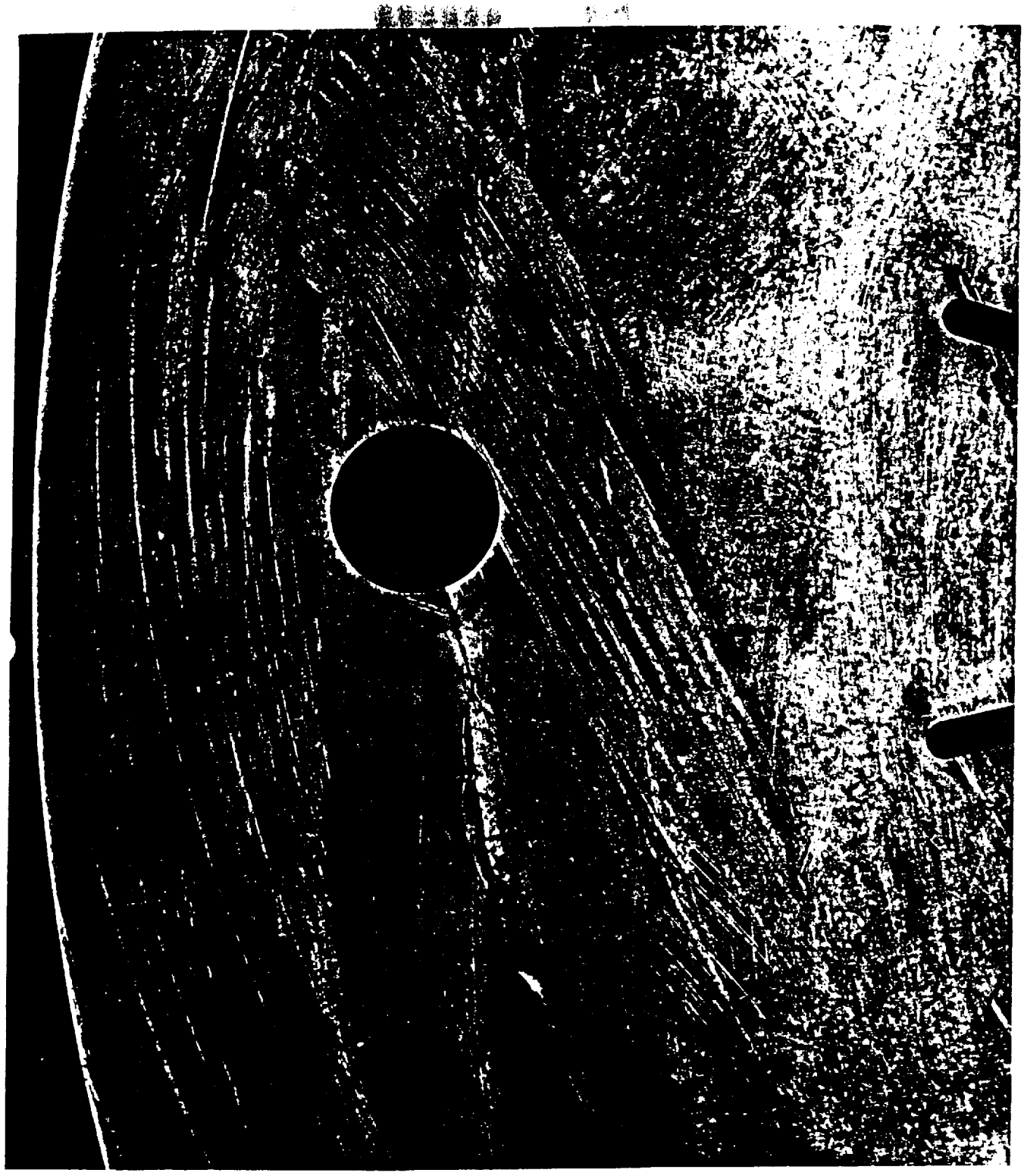

Figure 62. Braze Assembly P/N 3311946 Heat Treat Cracks

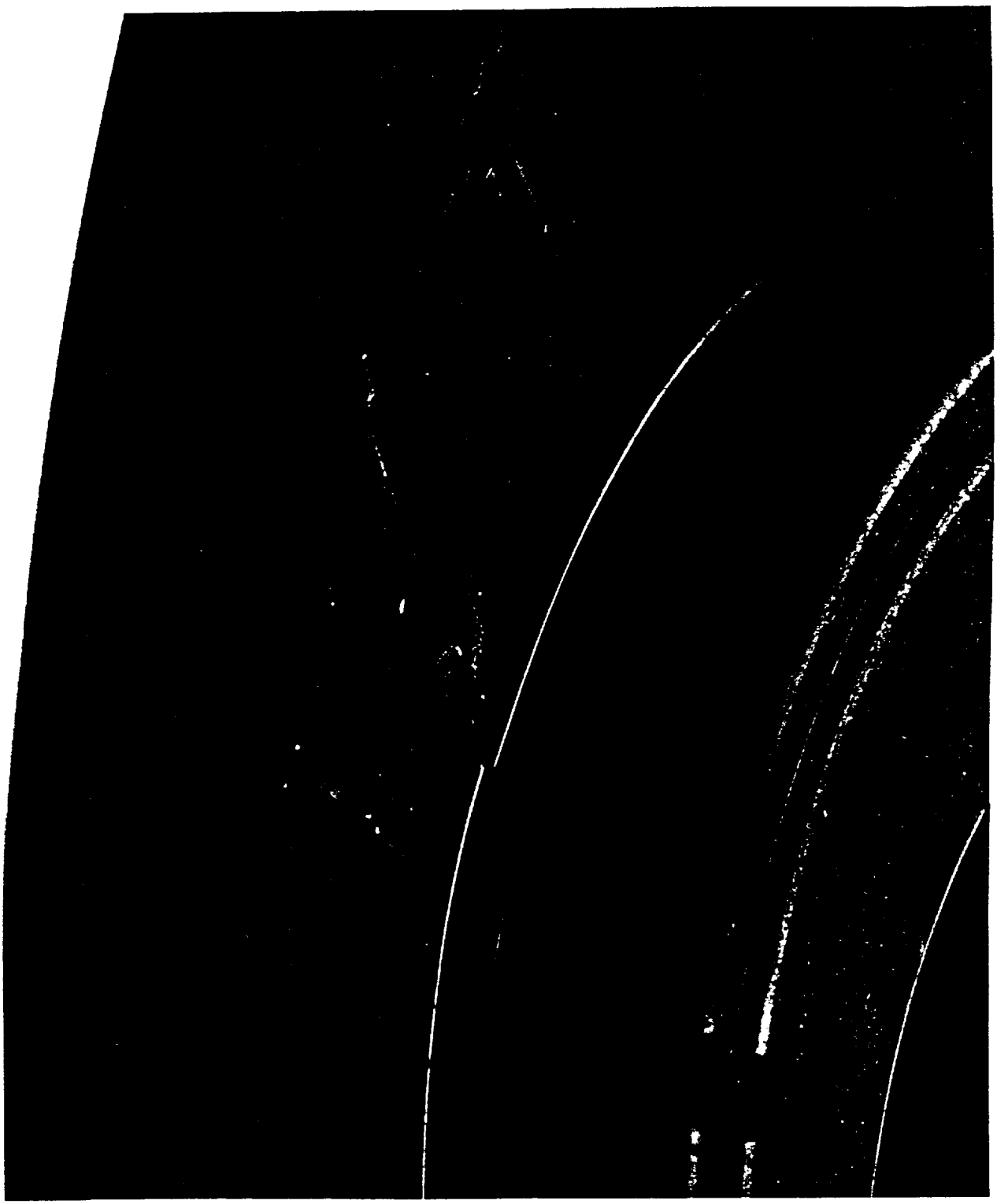

Figure 63. Braze Assembly P/N 3311946 - Plates 4 and 5 Separation

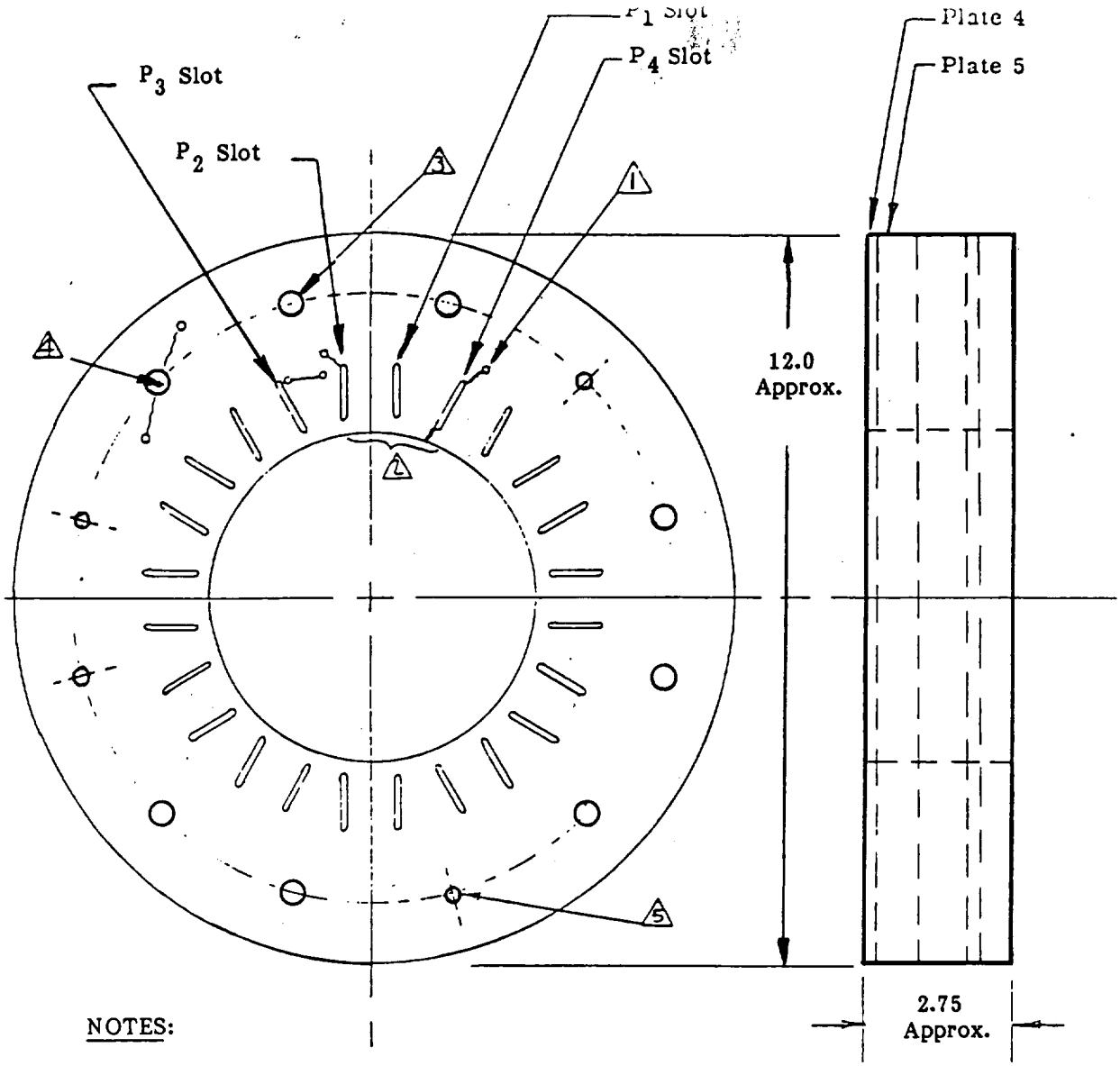


NOTES:

1. All cracks (6) are noted by termination in circles except where they intercept bolt holes, metering slots, or the part I.D.
2. Plates 4 and 5 are separated in the area noted so that the portion containing the noted $P_1$ slot has sprung outward approximately .060 inch.
3. The eight bolt holes shown exist in only the salvaged plates (4 and 5) from machining accomplished (3311945) on the first braze assembly.
4. A slight plate separation is evident in the hole I.D.
5. The four smaller holes shown are fixturing holes.

Figure 64. Braze Assembly P/N 3311946 - Sketch Showing Heat Treat Cracks

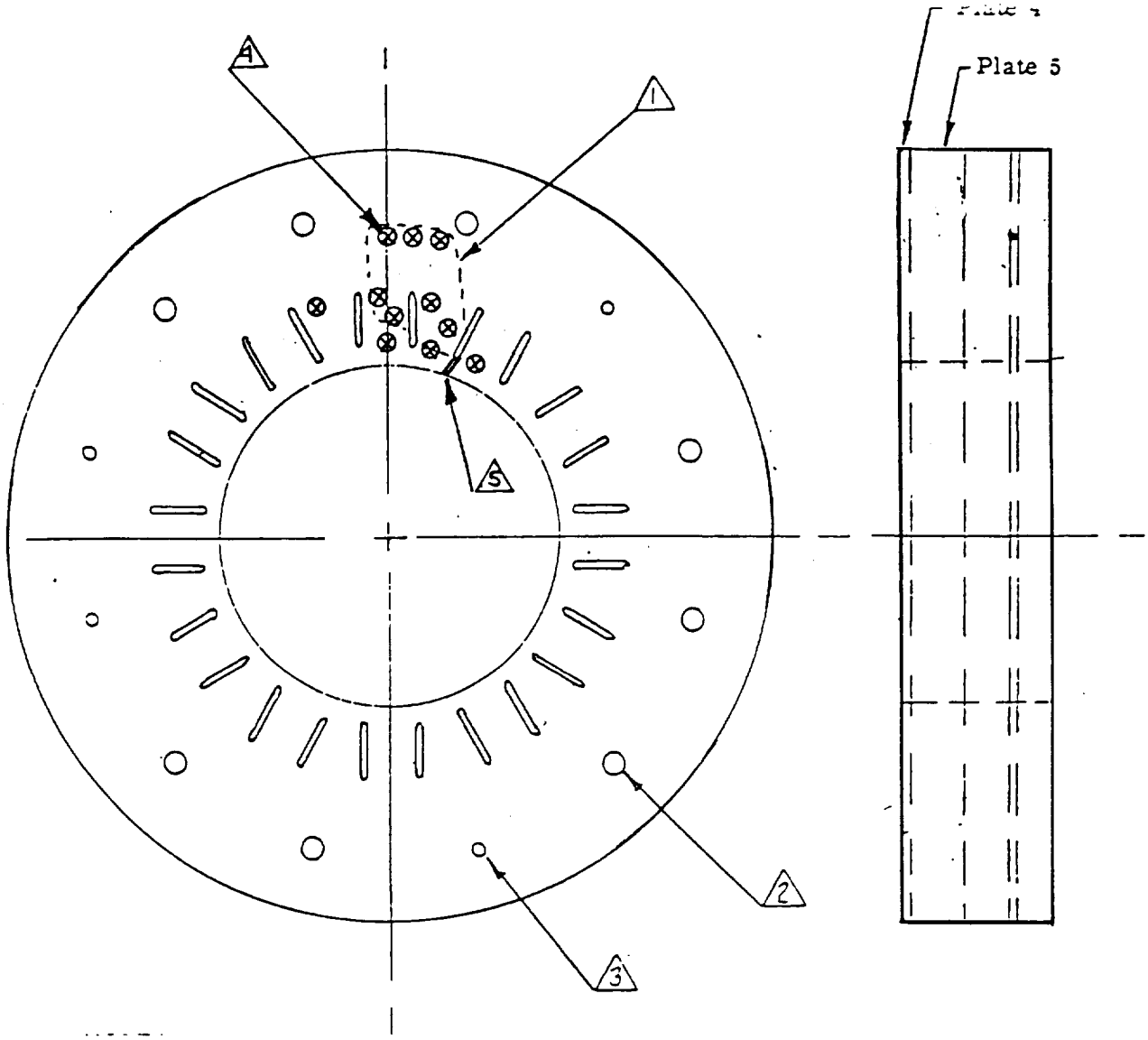


NOTES:

1. Dash lines indicate approximate location and size of unbrazed area between plates 4 and 5.
2. The eight bolt holes shown exist in only salvaged plates (4 and 5) from machining accomplished (3311945) on the first braze assembly.
3. The four smaller holes shown are fixturing holes.
4. Eleven plug welds made in 0.302 dia. x 60 deg. c'sink holes through plate 4.
5. One 0.080 deep x 90 deg. groove weld as shown in plate 4.

Figure 65. Braze Assembly, P/N 3311946, Showing Unbrazed Portion of Plates 4 and 5 and corresponding Repair Welding

their speeds have to be identical then the fluid passing through each must be equal. This means that the number 2 motor must drive the number 1 motor as a pump to make up for the 8.0 gpm bypassing motor number 1. This is accomplished at the expense of torque since the $\Delta P$ across motor 2 must be sufficient to do the pumping. Based on Figure 42 for parallel operation, it can be seen that to increase the flow from about 37 to 45 gpm (140.06 to 170.34 lit/min), a $\Delta P$ of 80 psi (.55 $NM/m^2$) is required. With an assumed torque efficiency of 85 percent the $\Delta P$ that is lost to the motor 2 is 94 psi (.65 $NM/m^2$). In addition, the 80 psi required to increase the flow through motor 1 reduces its torque output. Consequently the total $\Delta P$ loss because of leakage in the parallel mode is 174 psi (1.20 $NM/m^2$). Since this loss appears like an increase in return pressure to effectively reduce the system $\Delta P$ producing torque, the magnitude can be determined from equation 31 by multiplying the lost $\Delta P$ by 15.62. This indicates a lower torque at 76.5 rpm (maximum in parallel) of 2718 lb-in (0.31 kN-m). From the predicted performance shown in Figure 10, this does not appear to jeopardize performance.

In the case of series operation, where the leakage from C1 to C4 bypasses both motors, the effect would diminish speed proportionately, or reduce maximum speed from 153 to 122 rpm. In addition, the leakage from C2 to C4 which bypasses only motor 2, will necessitate pumping of this motor by the number 1 motor, thereby reducing torque also. The torque reduction can be estimated by looking for the $\Delta P$ required to increase the motor 2 flow from the series mode curve in Figure 42. Assuming a maximum $\Delta P$ across motor 2 of 1000 psi (6.9 $NM/m^2$), the C2-C4 leakage, based on Figure 30, would be 2.6 gpm (9.8 lit/min). The required $\Delta P$ for increasing motor 2 flow up to 35.9 gpm (equivalent to 122 rpm) from 33.3 gpm would be about 120 psi. With the 0.85 torque efficiency the $\Delta P$ lost to motor 1 would be 141 psi. This total lost $\Delta P$ of 261 psi converts to a lost torque of 2040 lb-in (0.23 kN-m) by equation 23.

Although this value is only 75 percent of the lost torque for the parallel mode, it is more consequential. This is because the torque output in series mode is theoretically half of the parallel mode output.

Additional sources of intercircuit leakage not accounted for in Figure 30 are metering lap leakage and leakage past the vanes which are discussed separately.

Differential Pressure Versus Flow - The testing of one motor at a time with the second motor recirculating the pumped fluid in the arrangement of Figure 31 approximated series operation for the pressure differential versus flow relationship fairly well as can be noted by comparing Figure 32 and 42. However, the result of the average nonoperational pressure loss measurements shown in Figure 35 is only 79 percent of the Figure 42 maximum loss. Perhaps, the opening and closing of the parts by the orbiting member creates additional pressure losses, that are not existing for the Figure 35 test conditions. As later discussed, evidence exists that indicates cavitation occurs in operation and this is a flow loss which may not have occurred in the nonoperational test.

Volumetric Efficiency Versus Pressure Level - As shown in Figure 36 the volumetric efficiency of each motor varied nonlinearly with level of the supply pressure. By replotting the efficiency as a function of supply pressure rather than return pressure as shown in Figure 66, it is obvious the results for the two conditions are much the same. However, as might be expected the efficiency at the higher differential pressure is lower, except for motor number 2 in the cw direction. The reason being that as the pressure differential is increased more intercircuit and more case drain leakage is expected. Although the case drain leakage for both pressure differentials did not vary substantially in relation to the total chamber flows as indicated in Figure 38, the addition of the intercircuit leakage previously addressed should result in lower efficiencies at high differential pressure.

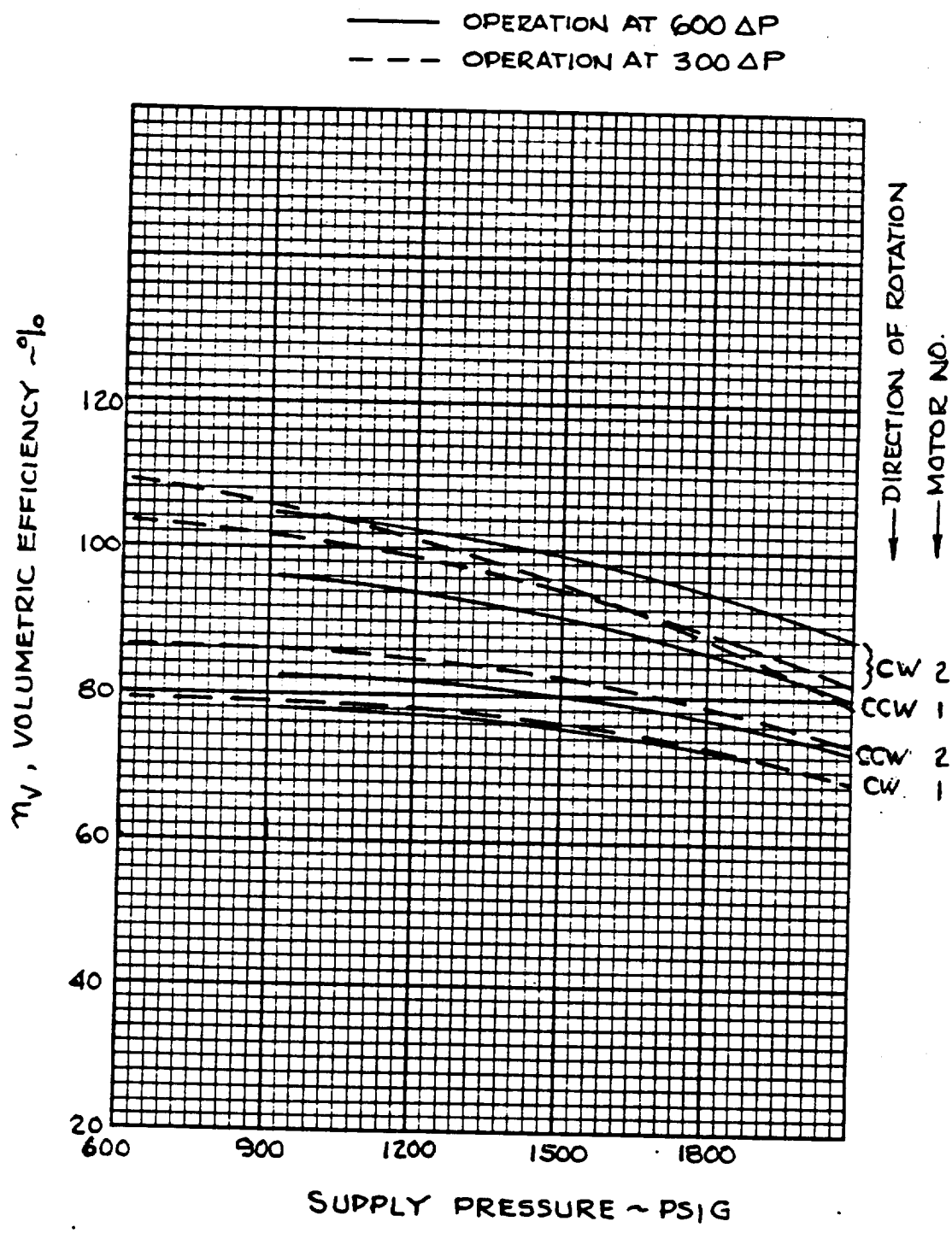


Figure 66. Supply Pressure Effect on Volumetric Efficiency

The decrease of the efficiency as a function of the supply pressure is probably the result of compliance of the assembly structure which increases the running clearance through which leakage occurs.

Total Chamber Flow Versus Speed - The total chamber flow as a function of speed as shown in Figure 37 indicates a variation from the theoretical as indicated. Since the motors were tested with one of the motors plumbed so that the inlet and outlet were directly connected, the slope of the lines plotted should be 0.25 gal/rev or 57.75 $in^3$/rev (946 cc/rev). In the cw direction, the motor number 1 apparent displacement is 27 percent greater, while that of motor number 2 is 4 percent lower than theoretical. In the ccw direction the motor number 1 apparent displacement is only 2 percent higher, while motor number 2 is 20 percent higher than theoretical. Since the apparent displacement neglects case drain leakage, it should check the design, or theoretical, value. The fact that both motors in one direction (but opposite directions) exceed the theoretical indicates leakage other than case drain occurs. This suggests leakage by a vane, or vanes and/or housing internal leakage.

Total Chamber Flow and Leakage Versus Supply Pressure - The total chamber flow and supply pressure are essentially independent of each in most cases, as indicated in Figure 38. This is a result of operating no-load and at constant differential pressure. Since total chamber flow is the flow in the return line and with a constant differential pressure across the test unit, it seems that the flow should have remained constant with increasing pressure. This is assuming that the only pressure loss was from flow and that mechanical friction was constant.

Case drain leakage on the other hand is dependent on supply pressure as indicated in Figure 38 and was approximately the same for all eight tests as indicated by the cross-hatched band. Using average flow from the band, the flow increases by the power of the pressure ratio from about 1.8 at 1200 psig to 2.6 at 2000 psig. This is believed to be the effect of higher internal pressure opening

the capillary leakage paths from chambers to case drain. Assuming little or no increase of the pressure ratio power from 2000 psig (13.79 $MN/m^2$) to the stall pressure of 4000 psig (27.58 $MN/m^2$), the case drain leakage could be 15 gpm (63.9 lit/min). Based on 45 gpm (170.34 lit/min), the volumetric efficiency could be only about 67 percent rather the design expectation of 85 percent. Naturally, at loads less than the maximum, requiring full system pressure, the efficiency will increase to where at one quarter load it would have about 90 percent efficiency. This is based on an assumption of no other leakage losses, 85 percent torque efficiency and 2000 psi (13.79 $NM/m^2$) pressure loss.

Gear Mesh Disengagement - The gear mesh disengagement experienced with the 32 pitch gears was most likely a combination of not enough wrap-around overlap of the gear teeth and compliance of the ring orbiter and ring gear assembly. With the 32 pitch gears the difference in number of teeth between the gears was six and was greater than most previous application. The effect of this greater difference was to reduce the maximum overlap of the teeth. It is this overlap of gear teeth that reacts the separating loads imposed on the gears as shown in Figure 67 and 68. As shown in Figure 67, the load on the output shaft gear, $F_r$, applied tangentially at the pressure angle, $\phi$, is made up of a torque required horizontal vector force, $F_x$ and a vertical vector force, $F_y$, that tries to separate the gears. This vertical force is reacted by the equal and opposite force, $F_h$, that is the hold-in force provided by the overlapped teeth in the gear mesh as shown in Figure 68. This latter figure shows only two teeth of the approximately 52, that are in mesh at any time, with 26 of these on either side of the zero tooth, Figure 68 (a). The other tooth shown is the 21st which has the maximum overlap as shown. As noted the maximum overlap is 0.008 in (0.203 mm) occuring at the 21st tooth. Consequently, it was finally concluded after considerable study, testing, and dimensional investigation that the total-composite-error (TCE) recorded for the gears in Figures 39 and 40 was too great for the amount of overlap.

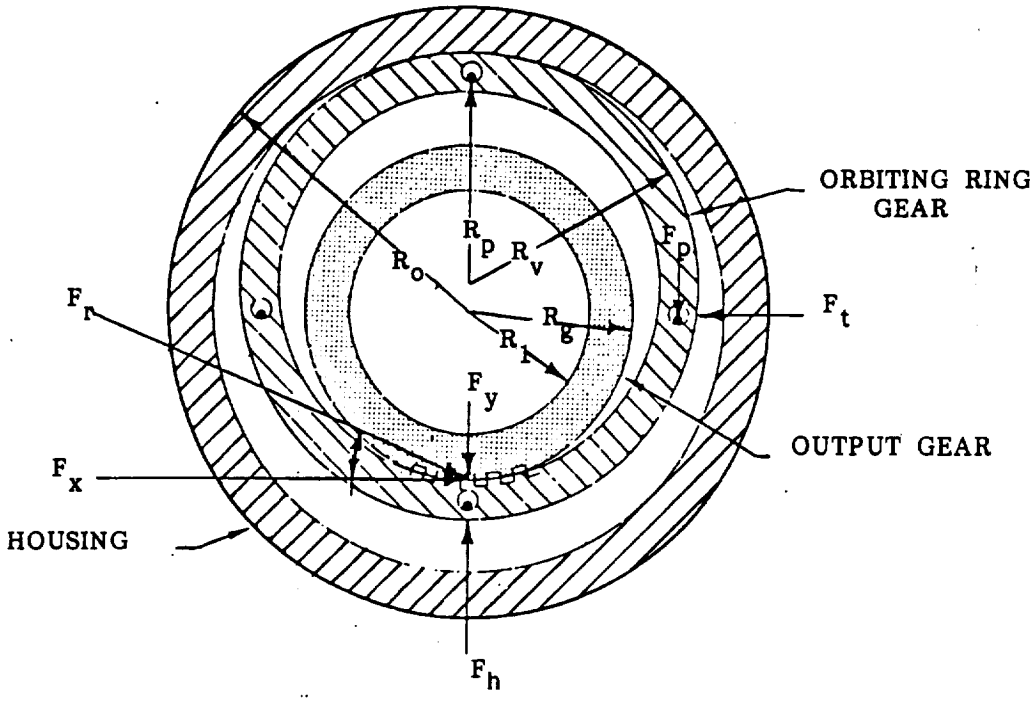


Figure 67. Orbiter Ring Forces Diagram

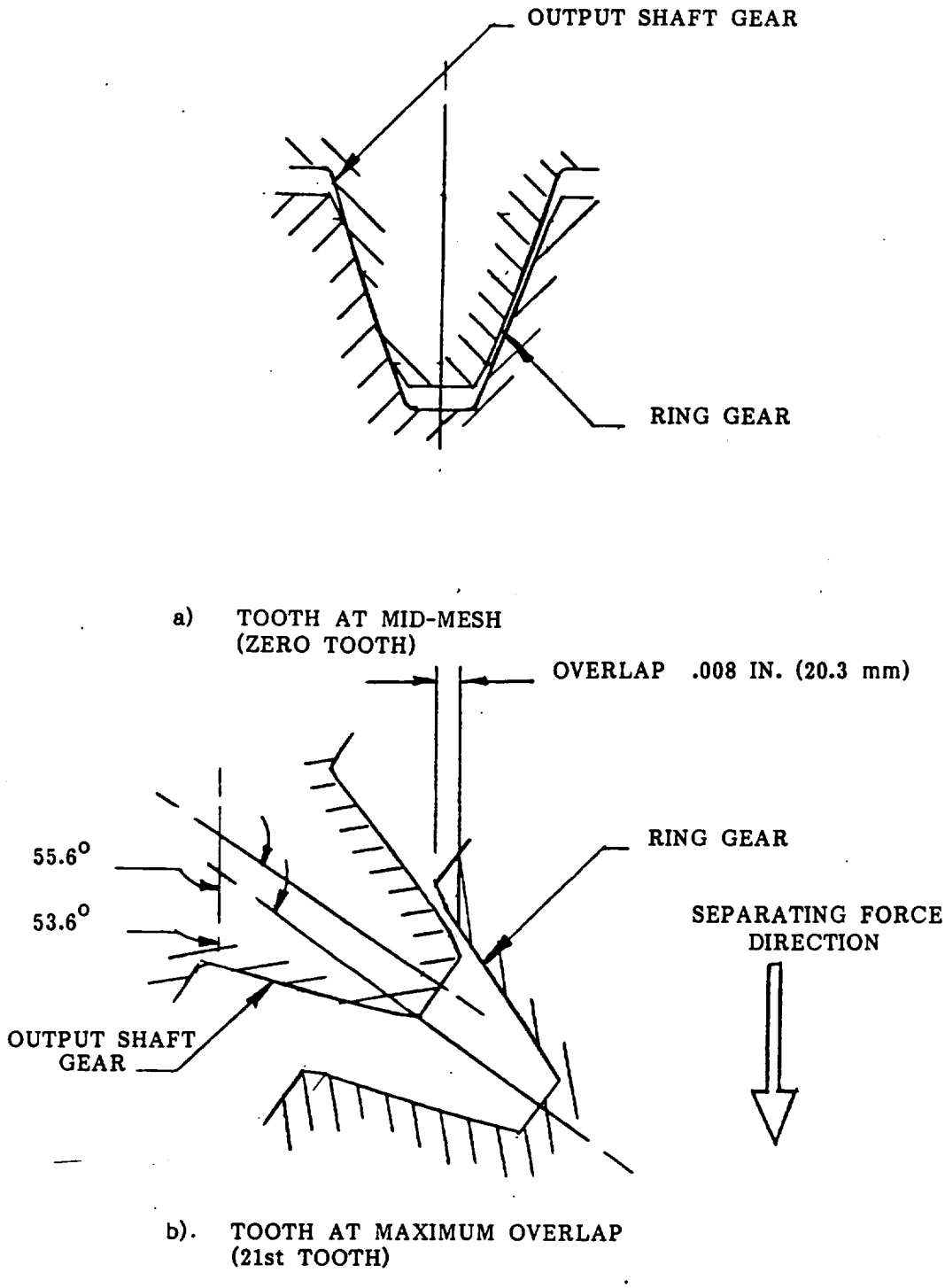


Figure 68. 32 Pitch Gears Maximum Overlap

The (a), (c), and (d) plots in Figure 39 for the output shaft indicate an undersize condition of 0.0020 to 0.0026 in. (0.0508 to 0.0660 mm). While this discrepancy magnitude is not too bad in itself, it was considered unacceptable combined with the TCE for the orbiter (ring) gear which was 0.0015 in. (0.0381 mm) towards the oversize condition. At the right time and conditions, a combined maximum TCE for the mesh of about 0.004 in (0.1016 mm) appeared to be too much. However, since the machining accuracy was considered reasonable, it was decided to modify the design to increase the overlap. This explains the origin of the 24 pitch gear design which increased the overlap from 0.008 to 0.018 in. (0.203 to 0.457 mm). The results with the lower pitch gears is discussed in the following section.

## 24 Pitch Gear Configuration

Output Shaft Speed Versus Flow - As can be seen by comparing Figures 37 and 41, the assumption made in the testing with one motor driving and one pumping as shown in Figure 31 seems justified, because the results are similar to regular series operation. This is based on the fact that the average of the four slopes in Figure 37 is within 4 percent of the slope in Figure 41. The reason for the difference in the apparent volumetric efficiencies for series operation (87.5 percent) and parallel (100 percent) is probably the combined effect of a couple of factors.

The first has to do with the impact of vane leakage on the two modes of operation. Since the chambers of motor number 1 are separated by the number 2 motor chambers, there is more opportunity for vane leakage in series than in parallel. This is because in series the relative pressure levels are $C1 > C2 \approx C3 > C4$, or $C4 > C3 \approx C2 > C1$, whereas for parallel $C1 = C3$ and $C2 = C4$ with $C1 > 4$ or $C4 > C1$, depending on direction of rotation. The vane leakage recorded in Table 21 however, indicates except for one, or more, vanes separating C2 and C3, that this source of leakage is not excessive and is about 3 percent of maximum flow. The second

factor is the intercircuit leakage which is significant only between circuits 1 and 4 and 2 and 4. In series, since both C1 and C2 are at different pressure levels than C4, the leakages will occur in both paths and be additive. In parallel, since C2 and C4 are always nearly equal, this source of leakage is eliminated, so the efficiency should be higher in parallel.

The volumetric displacements indicated in Figures 37 and 41 are defined as apparent displacements because the case drain leakage was not included in the measured flow. The case drain leakage was ignored because it was dependent on the torque applied to the stud nuts, the return pressure, the load, and pressure losses in the unit.

Differential Pressure Versus Flow - As can be seen by observing Figure 42 the pressure loss at no-load and 45 gpm (170.34 lit/min) is 2080 psi (14.34 $MN/m^2$) in the series mode and 320 psi (2.21 $MN/m^2$) in parallel. By subtracting the breakout differential pressure of 100 psi (0.69 $MN/m^2$) and an extrapolated line loss of 70 psi (0.24 $MN/m^2$) from Figure 33 for series operation, the test unit flow loss is reduced to 1910 psi (13.42 $MN/m^2$), which is 109 percent greater than estimated by equation 18 for two motors in series (916 psi). Subtracting a breakout of 60 psi (0.41 $MN/m^2$) from the parallel mode loss leaves 220 psi (1.52 $MN/m^2$) flow loss, or 92 percent larger than estimated by equation 18 for one motor at half maximum flow. The ratio of the two losses of 8.7 to 1 is 8.8 percent greater than theoretical and is due to errors in accurate pressure measurement with a fluctuating guage needle, especially at the lower values.

Gear Mesh Disengagement - The disengagement of the gears, twice, after increasing the wrap-around overlap of the teeth from 0.008 in (0.2032 mm) to 0.018 in (0.4572 mm) as explained previously and shown in Figures 68 and 69, necessitated additional investigation to try to pin point the problem. While it was known that the orbiter ring and orbiter gear assembly compliance could effect

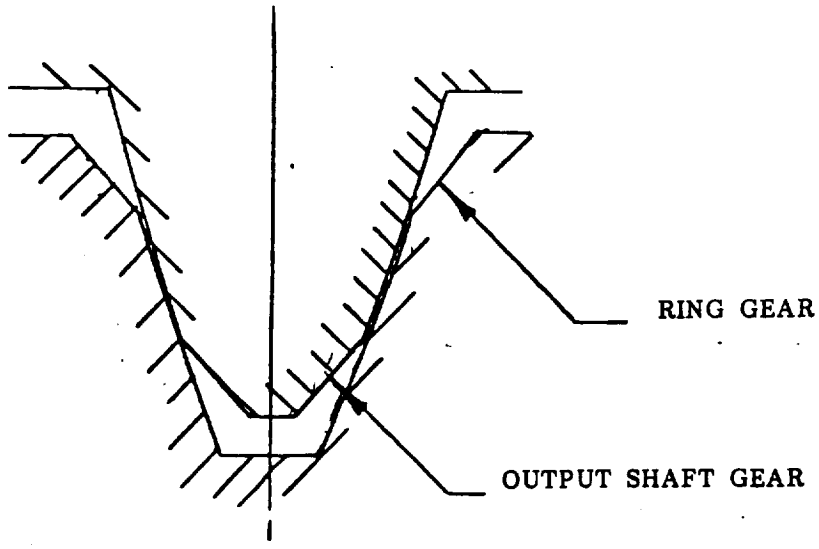


a) TOOTH AT MID-MESH
(ZERO TOOTH)

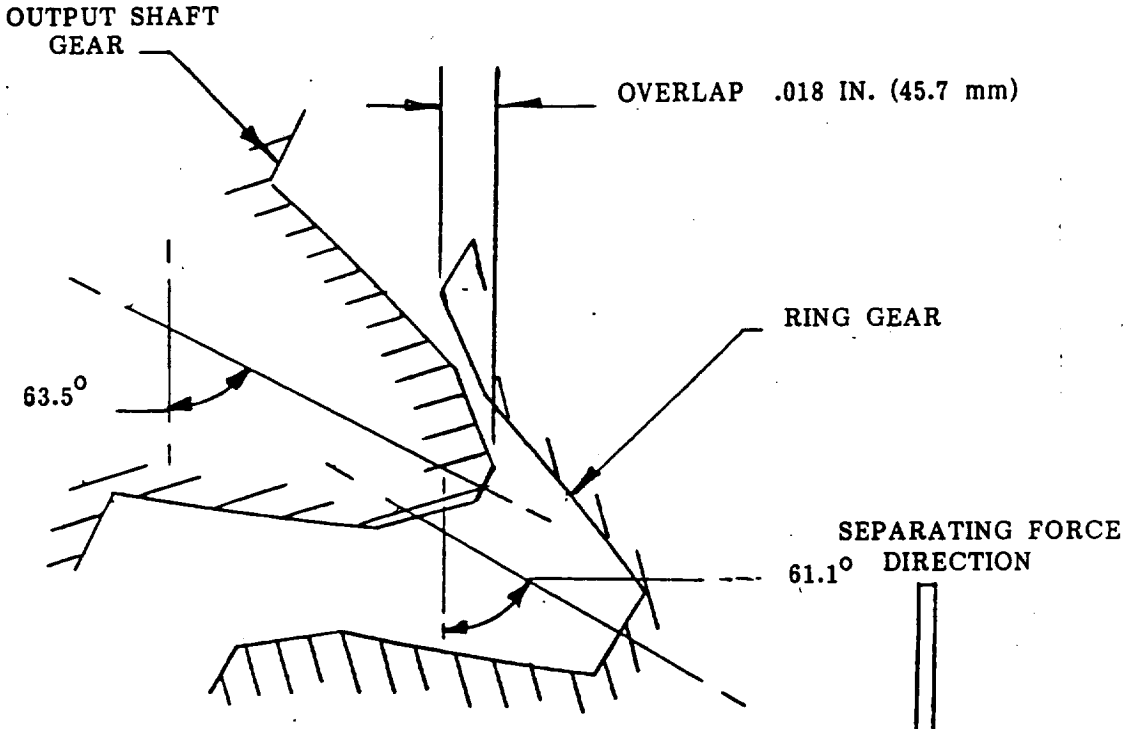


b) TOOTH AT MAXIMUM OVERLAP
(18TH TOOTH)

Figure 69. 24 Pitch Gears Maximum Overlap

the mesh, through distortion, it was believed that distortion was not of sufficient magnitude and form to prevent disengagement. This belief was based on a computer aided analysis that was conducted in the design phase and reported in reference 18. Figure 70 from this reference shows the form and predicted magnitude of the orbiter ring and orbiter gear distortion. However, since some simplying assumptions were made in the analysis it was believed that doing the static load tests on the actual hardware as described in the section TEST RESULTS might be more edifying than trying to refine the analysis.

Although the mechanics of gear mesh failure could not be understood, it became apparent that the orbiter ring/gear and housing surfaces damage sustained with both failures of the 24 pitch gear set might be a factor. In reviewing possibilities of how the damage might influence the gears, it became apparent that during no-load operation, during which the failures occurred, the friction force might require greater or unusual reaction forces then required for the normal loading. In Figure 71(a) the Orbiter Ring/Gear assembly is shown meshed with the output (shaft) gear. The friction force ($F_f$) is considered as acting in the center of the damaged area at a distance X from pitch diameter, $D_s$, as shown. Summing forces and torques for Figure 71(a):

$$\Sigma F_x = 0 \qquad F_R = F_G = F_{G1} + F_f\left(1 + \frac{2x}{D_o}\right) \tag{105}$$

$$\Sigma F_y = 0 \qquad F_p = F_H \tag{106}$$

$$\Sigma T = 0 \qquad F_R\left(\frac{D_o}{2}\right) = F_p R_p \tag{107}$$

Where: $F_f$ = friction force

$F_{G1}$ = $2\,T_L/D_o$ = output force

$F_H$ = tau $\emptyset$ $(F_{G1} + F_f)$

$F_P$ = reaction pin force

$T_L$ = output torque

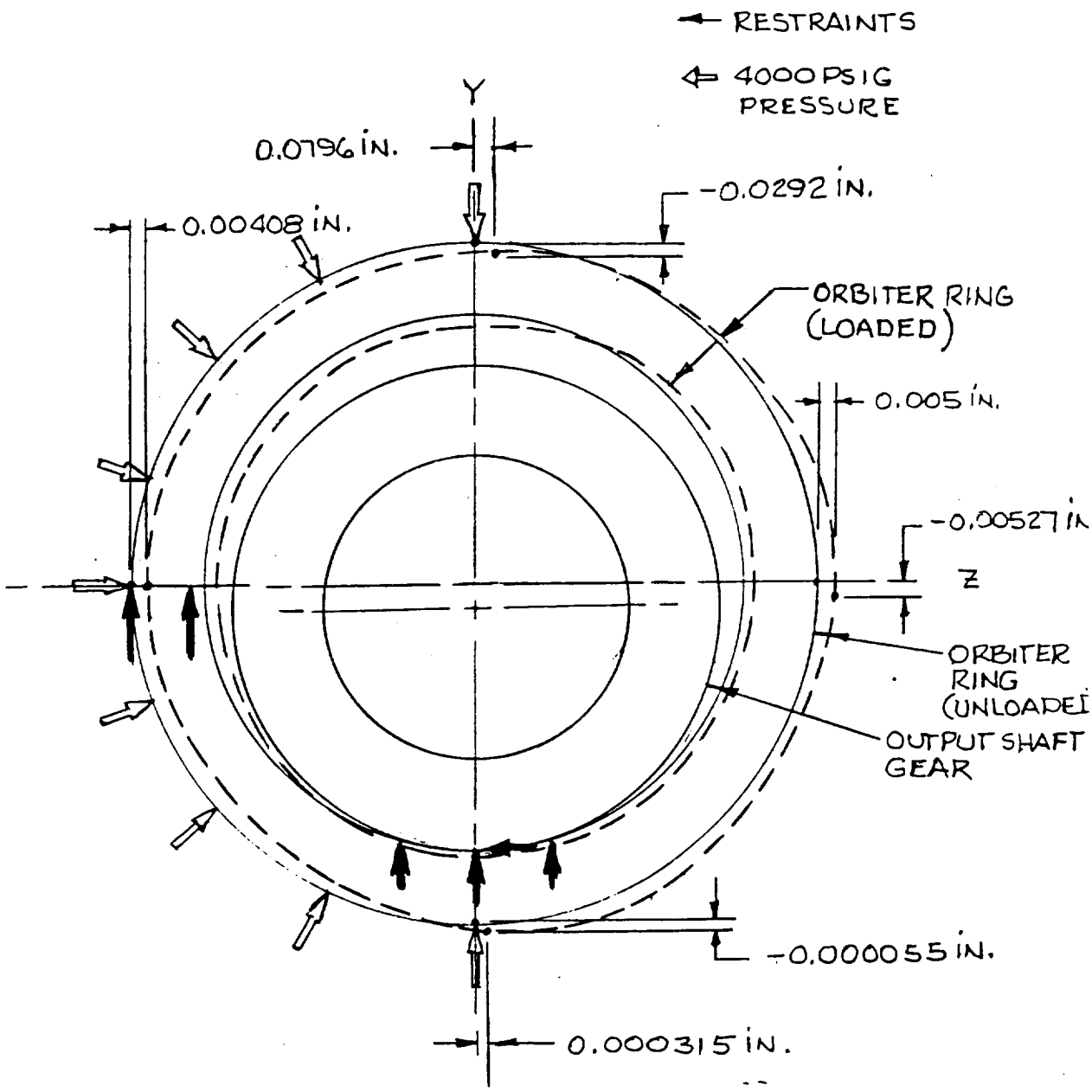


Figure 70. Computer Program Generated Load Deflected Form of Oribiter Ring

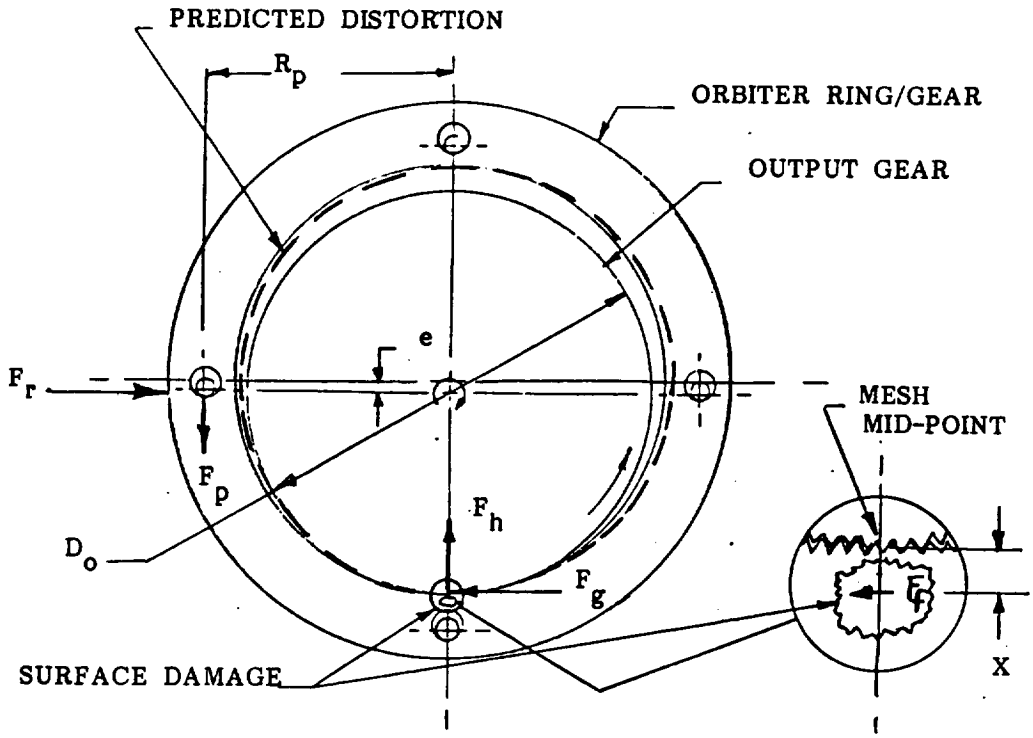


a) COMPUTER PROGRAM ORBITER RING DISTORTION PREDICTION

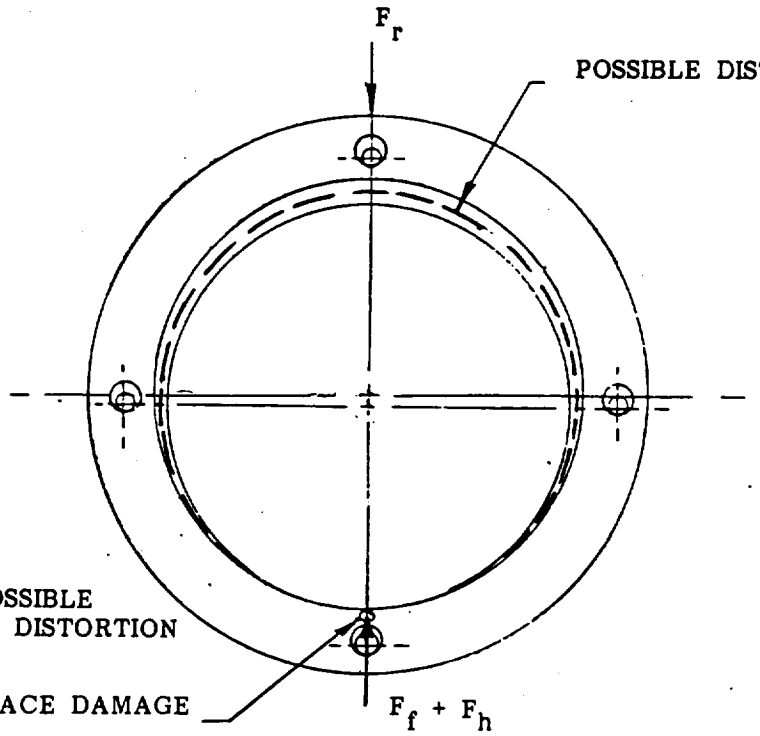


b) THEORIZED POSSIBLE ORBITER RING DISTORTION

Figure 71. Concentrated Frictional Orbiter Ring Loading

$D_o$ = output gear pitch dia

$R_p$ = reaction pin lever arm length

X = damage area locating dimension

$\phi$ = gear teeth pressure angle

Except for redefinition of $F_G$ in equation 105, the equations are the same as for the case where $F_f = 0$ in the normal case. However in the case where the gear mesh separated, the force $F_{G1} = 0$. Now based on the observed P of 1500 psi (10.34 $MN/m^2$) at failure, the output torque should have been, pursuant with equation (11):

$$T = \Delta P \eta_t \, dap/2\pi \qquad (108)$$

$$= 1500\ (.85)\ 115.5/2\pi$$

$$= 23{,}437.6 \text{ lb-in } (2.65 \text{ kN-m})$$

Since this potential torque output was absorbed by the internal friction, the friction force can be determined from the following relationships based on eq. 105 and 107:

$$T = F_R \frac{D_o}{2} = F_f \left(1 + \frac{2x}{D_o}\right) \frac{D_o}{2} = F_f \left(\frac{D_o}{2} + X\right) \qquad (109)$$

$$F_f = T/\left(\frac{D_o}{2} + X\right) \qquad (110)$$

@ X = 0.63 in (16.00 mm)

$$F_f = 23{,}437.6/\left(\frac{4.25}{2} + .63\right)$$

$$= 8507.3 \text{ lb } (3862.3 \text{ kg})$$

Then

$$F_H = \tan \phi \, F_f \qquad (111)$$

$$= \tan 20^\circ \ 8507.3 = 3096.4 \text{ lbs } (1405.7 \text{ kg})$$

Since this hold-in force is slightly less than one third of that developed at the rated torque, for which the gears were designed, it was not the magnitude of the friction force that was directly responsible for the separation. However, suppose that the predicted distortion in Figure 71(a) was large enough that the commutation porting controlled by the orbiter ring, advanced the hydraulic force $F_R$, in the clockwise (Figure 71(a)) direction, which it would tend to do. Now suppose the friction force stalled the orbiter ring and the pressure increased because of the lack of flow, or the pressure was increased manually to attempt to force movement, the additional distortion would tend to rotate $F_R$ even more. Carried to an extreme $F_R$ might be rotated out of phase 90 degrees as shown in Figure 71(b). In this case because of the ellipical shape of the distortion, centered on $F_R$, the mesh would tend to be opened and the hold-in force would tend to disappear, leaving $F_R = F_f$. this is less than $F_R$ had to be for equilibrium in equation (105), so the orbiter/gear assembly could possibly be moved to separate the gears.

In an attempt to determine if separation could occur if the foregoing suppositions actually happened, the mechanical load tests were performed as reported in TEST RESULTS. The loading of the orbiter/gear assembly with a concentrated load equivalent to the distributed pressure would undoubtedly accentuate the distortion somewhat, but it was the only practical way to accomplish the evaluation .

The reason for the erratic and nonlinear results of Figure 56 was not understood until sometime after the test when it was noted that the output shaft gear had partially disengaged from the orbiter gear. This condition was recorded in the photographs in Figures 53 and 54. Figure 53 shows the mesh apparently engaged from the side which was being observed during the test. Figure 54 shows the mesh partially disengaged from the side not being observed during test. It was this condition of a partially disengaged mesh that was the cause of the erratic and nonlinear strain measurements, since the partial disengagement created teeth interference and prevented the parts returning to a zero strain condition upon load removal.

For purposes of establishing a good strain gauge data base, the ring gear (configuration 3) alone was load tested as shown in Figure 57. So from the strain versus load results shown in Figure 58, based on the No. 2 and 4 gauge readings at 5500 lbs load:

$$\text{Stress} = \text{Strain X Young's Modulus} \qquad (112)$$

$$1260\ (10^{-6})\ 29\ (10^{6})$$

$$36{,}540 \text{ psi } (251.9 \text{ MN/m}^2)$$

To determine if the stress is typical of a relatively thin, uniform cross section, circular ring, the Case 1 moment equation from reference 28 is used as follows:

$$M_{MAX} = -0.1817\ WR \text{ @ } 90 \text{ deg from the load} \qquad (113)$$

Letting, $W = 5500$ lbs (2497 kg)

$R = 2.39$ in (60.71 mm)

Then, $M_{MAX} = -2388.4$ lb-in (0.27 kN-m)

Since stress,

$$S = M_{MAX}\, c/I \qquad (114)$$

and letting,

$c = d/2 = 0.2065$ in (5.25 mm)

$I = bd^3/12 = 2.5\ (.413)^3/12 = 0.01468 \text{ in}^4\ (0.6110 \text{ cm}^4)$

then

$S = -33606.8$ psi (231.72 MN/m$^2$)

Since this agrees within 8 percent of the value determined from the strain gauge measurement, it seems reasonable to use the reference 28 equation for horizontal growth of the perpendicular ring diameter under load, which is:

$$D_x = .137\ \frac{WR^2}{EI} \qquad (115)$$

$$= .010 \text{ in}$$

Therefore, at the 15,000 lbs (6810 kg) applied load the diameter increase would be:

$$D_x = .010 \text{ in } \frac{15{,}000}{5500} = .028 \text{ in } (0.71 \text{ mm}) \qquad (116)$$

With the 24 pitch gear set, the maximum hold-in overlap of any tooth on the ring gear with any tooth on the output shaft gear being only .018 in, it is conceivable, actually evident from actual experience, that the compliance of the orbiter ring/output gear assembly combined with the loading created by excessive internal friction is sufficient to cause disengagement.

Although the configuration 2 test results were unexpectedly complicated by the partial gear mesh separation that occurred, which left the teeth jammed and under stress with the load removed, the initial load application data is useful. Using the data from the first two load tests in Configuration No. 2, before gear separation had occurred, the average slope is 1.16 ($10^{-7}$) microinches per pound inch. This is 51 percent of the slope recorded in Figure 57.

Since, $$\delta = S/E \qquad (117)$$

$$= \frac{Mc}{EI}$$

and for a rectangular cross section

$$\frac{C}{I} = \frac{d/2}{bd^3/12} = \frac{6}{bd^2} \qquad (118)$$

So, $$\delta = \frac{M\ 6}{E\ bd^2} \qquad (119)$$

Since the two components are made of the same material, 4330M steel, the strain ratios should be about the same as their parameters, $6M/bd^2$, or stress. From eq 114, for the orbiter gear stress,

$$S = \frac{6M}{bd^2} = \frac{6\ (-2388.4)}{2.5\ (.413)^2} = -33606 \text{ psi } (231.7 \text{ MN/m}^2) \qquad (120)$$

For the orbiter ring, $$S = \frac{6M}{bd^2} = \frac{6\ (-.1817)\ WR}{1.088\ (.713)^2} \qquad (121)$$

At the same load, W = 5500 lbs and using the mean radius, R = 3.36 inches.

$$S = \frac{6(-.1817)\ 5500\ (3.36)}{1.088\ (.713)^2} = -36425 \text{ psi } (251.1 \text{ MN/m}^2)$$

This indicates that the two components are indeed proportioned so that the load is about equally carried so that the strain recorded on the orbiter gear by itself is about double that recorded when it is loaded through the orbiter.

So, based on the calculated stresses the strain ratio is,

$$\delta_R = \frac{-33606}{-36\ 425 + (-33608)} (100) = 48\% \qquad (122)$$

This agrees well with the ratio of slopes of 51 percent from Figures 56 and 58.

While the test results indicate that if the supposition of orbiter ring/gear assembly distortion arising from the friction did cause the hydraulic force to get out of phase with the mesh point of the gears, sufficient distortion could nullify the wrap-around overlap of the teeth and permit disengagement. However, two facts keep this supposition from being completely feasible. First, the concentrated load used in the static load tests would produce more ring distortion than the actual distributed pressure loading. Second, even the more exaggerated distortion which caused gear separation in the load test of configuration 2 does not seem sufficient to achieve the necessary change in porting required. For instance, the decrease in the vertical diameter of the orbiter/gear assembly that would occur with the expansion of the horizontal diameter of 0.028 (0.71 mm), determined by equation (116), is determined from reference 28 as:

$$D_y = -0.149 \frac{WR^2}{EI} \qquad (123)$$

Therefore on the basis of just the difference in the constant coefficients and signs of equations (115) and (123), at 15,000 lbs load:

$$D_y = .028 \frac{(-.149)}{.137} = .030 \text{ in } (0.762 \text{ mm})$$

Thus it would seem that the horizontal centerline of the orbiter ring/gear assembly would just be lowered by half the deflection, or only 0.015 in (0.381 mm). Since in the unloaded state in assembly the horizontal centerline is a distance e above the output shaft centerline, as shown in Figure 71(a). Since e is 0.083 in. (2.108 mm) the 0.015 in. (0.381 mm) decrease does not appear sufficient. This can be illustrated as shown in Figure 72. For the hydraulic force vector to be in the Figure 71(b) position would require the low pressure ports (in the upper right hand quadrant) to be closed and the high pressure ports (in the upper right hand quadrant) to be opened. As can be visualized this would require a minimum distortion downward of the orbiter near the horizontal centerline an amount equal to e. Therefore, a reasonable evaluation of the facts based on the static load testing does not seem to support the supposition of how the separating force was generated, but does suggest the type and magnitude of orbiter ring/gear assembly distortion that could allow gear mesh disengagement without damaging teeth.

Metering Lap Leakage - Lap leakage occurring as a direct short circuit through the metering ports in each motor pressure chamber as indicated by the results in Table 19 are excessive, the average underlap for the metering slots can be determined based on the orificial type flow equation,

$$A = 3.85\, Q/k \sqrt{\Delta P} \quad \text{in}^2 \ (\text{cm}^2) \qquad (124)$$

where:

$k$ = 103 $\text{in}^2$/ lb sec (31.2 $\text{cm}^2/\sqrt{\text{gm sec}}$) for MIL-H-5606 fluid

$Q$ = gpm (lit/min)

$\Delta P$ = Total pressure differential across both slots, $\text{lb/in}^2$ ($\text{gm/cm}^2$)

3.85 = $\text{in}^3$/sec/gpm (16.4 cc/sec/lit/min)

Therefore the average underlap areas for each circuit individually, based on the Table 19 values are:

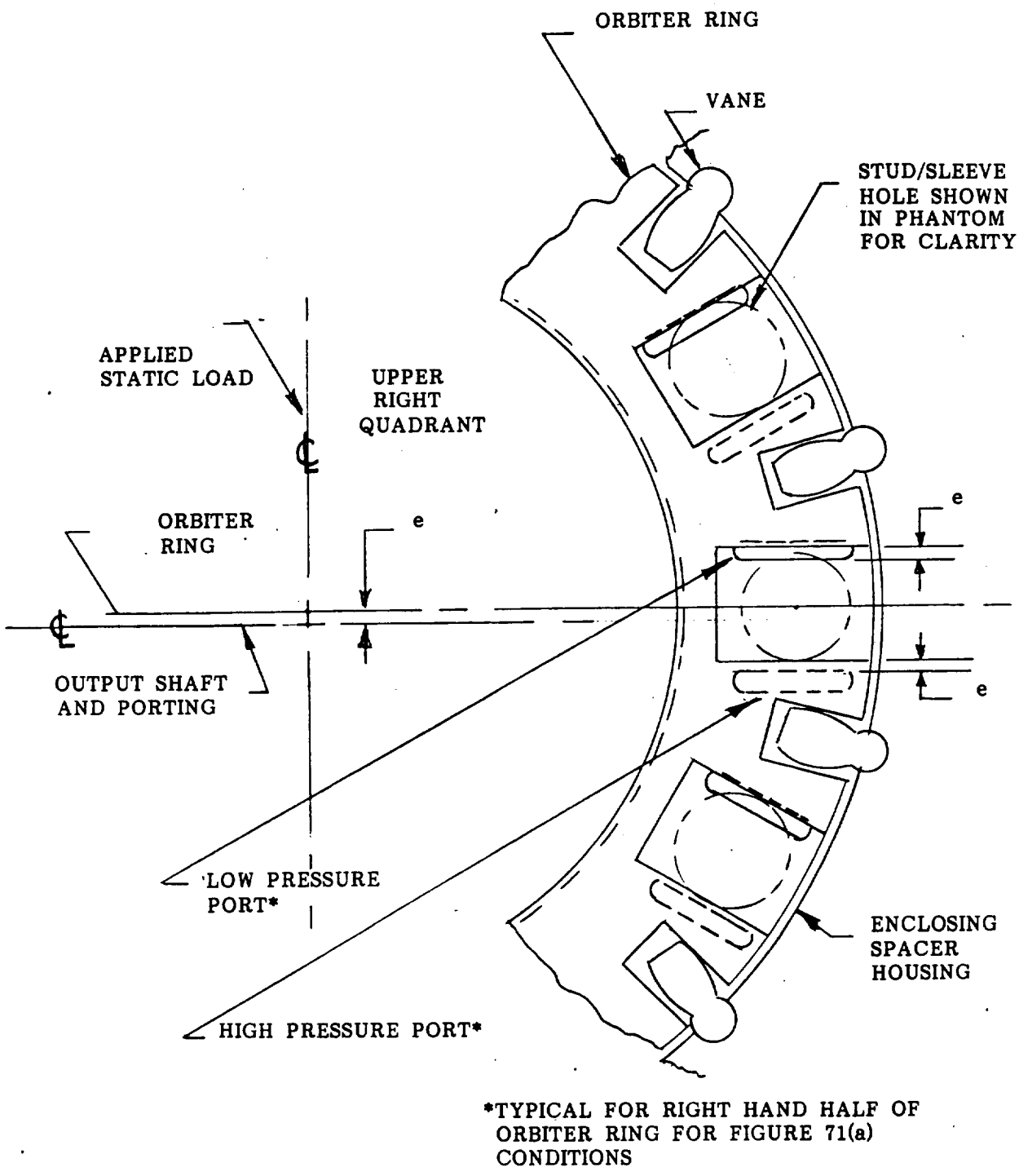


Figure 72. Normal Porting Conditions Corresponding to Figure 71(a) Orientation

For the C1 circuit,

$$A_1 = 3.85\ (5)/103\sqrt{25} = .037\ in^2\ (0.239\ cm^2)$$

Then based on six slots per circuit with a nominal length of 0.810 in (2.06 cm),

C1 average underlaps = .037/6(.810) = .0076 in. (0.019 cm)

For the C2 circuit,

$$A_2 = 385\ (412)/103\sqrt{50} = .022\ in^2\ (0.142\ cm^2)$$

and

C2 average underlaps = .022/6(.810) = .0046 in (0.0116 cm)

For the C3 circuit,

$$A_3 = 3.85\ (4.8)/103\sqrt{50} = .025\ in^2\ (0.161\ cm^2)$$

and

C3 average underlaps = .025/6(.810) = .0052 in (0.0133 cm)

For the C4 circuit,

$$A_4 = 3.85\ (5)/103\sqrt{30} = .034\ in^2\ (0.219\ cm^2)$$

and

C4 average underlaps = .034/6(.810) = .0070 in (0.0178 cm)

Since the design provided for an overlap condition of 0.0000 $\pm$0.0005 in (0.0000 $\pm$0.0127 mm) for each slot, the slots in the metering plates and in the orbiter ring were not fabricated accurately and/or erosion and/or cavitation have occurred. Since lap leakage was not measured when the parts were new, it is only indirectly possible to assess the fabrication accuracy. Some things that are known that suggest that in general the accuracy of fabrication was good, except for the damage occurring from the weld repair discussed in Intercircuit Leakage. are (1) the distance between the still sharp edges of the orbiter ring slots agree with the design requirement and (2) ignoring the edge damage, the same is true for the housing slots. As can be seen in Figure 65, extensive welding was done around several slots, which necessitated having to mill the slots to clear weld interference.

One of these slots in the inboard housing is shown in Figure 73. The most severe irregularity in the straight right side of the slot is not important since it is only the left side that mates with the metering slot in the orbiter ring. However, even on this side, moderate damage occurred in the repair operation necessary to overcome the poor brazing of the inboard housing. This same general discrepancy existed on one other slot, as shown in Figure 74, at roughly the 12 o'clock position. The slot at the left of the stud of the 12 o'clock position is recognizable as the one in Figure 73, while the slot to right of the stud is the other badly damaged slot. The interesting facts about Figures 73 and 74 are that 74 was taken before the unit was ever operated, while 73 was taken just prior to termination of the program. Visual observation of Figure 74 with a magnifying lens of moderate power reveals very little difference in the slot edges shown in Figure 73. Also observation indicates fairly good sharp edges on most slots in Figure 74. Now, looking at Figures 75 through 78, taken near the termination time in testing, the metering edges (nearest the stud) of each slot show the effects of erosion. Also Figures 77 and 78 indicate that chunks of flame plate have been dislodged. Also, note that in each case the edge not involved in metering (away from the stud) is sharp and shows what is believed representative of the fabrication quality. These photographs present a strong case that the cause of the underlap condition and high internal leakage is the result of erosion and/or cavitation.

Looking at Figures 79 through 82, which are the metering slots of the outboard housing, also photographed at the same time as Figures 75 through 78, it is obvious that the erosion is not as severe. This is concluded to be the fact that the flow through the outboard housing is much less than in the inboard housing, because the outboard housing slots are provided only to create pressure balance on the orbiter ring and primarily only case drain leakage flow occurs.

Figure 73 Inboard Housing Metering Slot



Reproduced from best available copy.

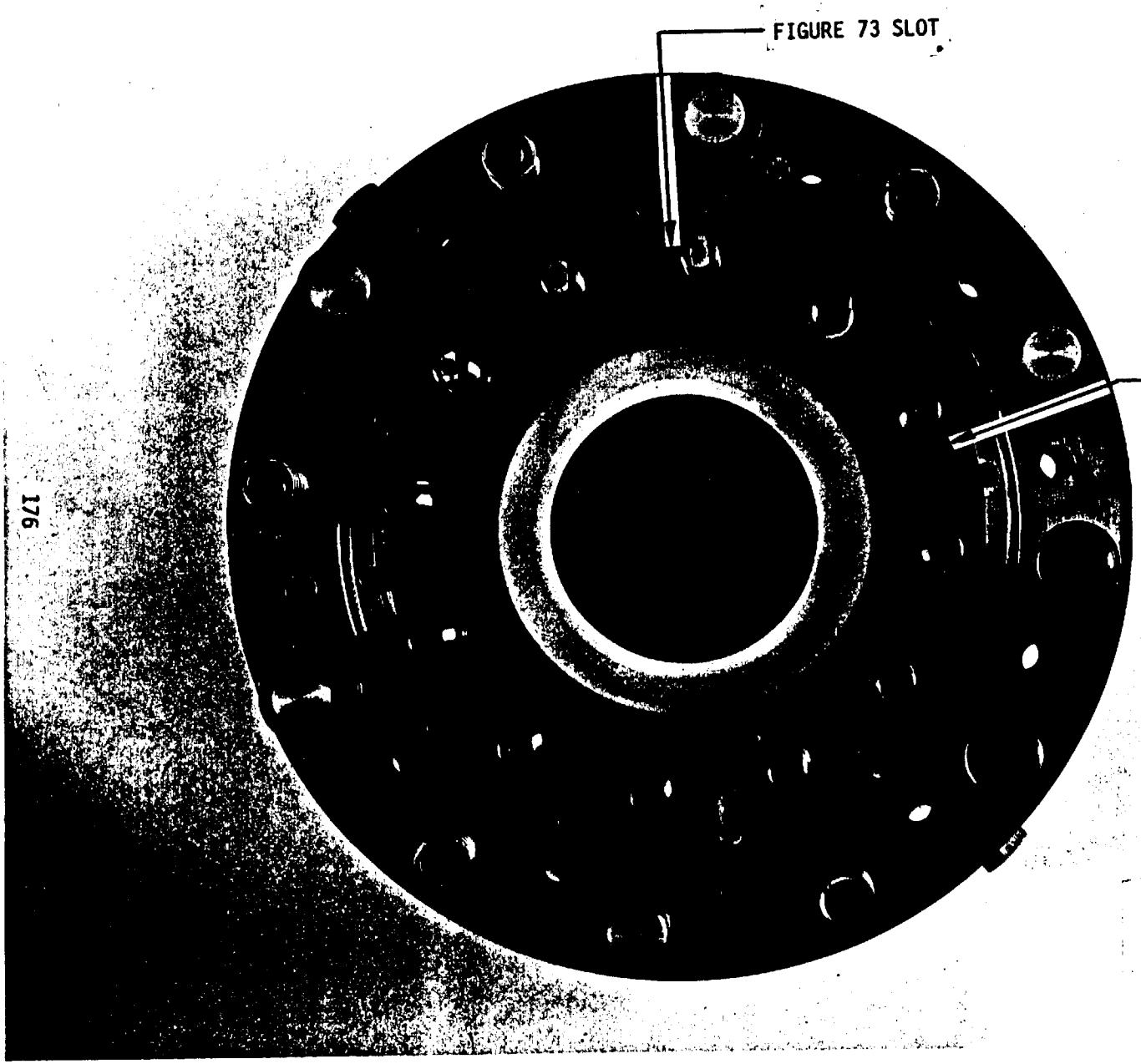


FIGURE 74 - SAME VIEW AS FIGURE 22 WITHOUT ORBITER RING, OUTPUT SHAFT AND WITHOUT SOME VANES

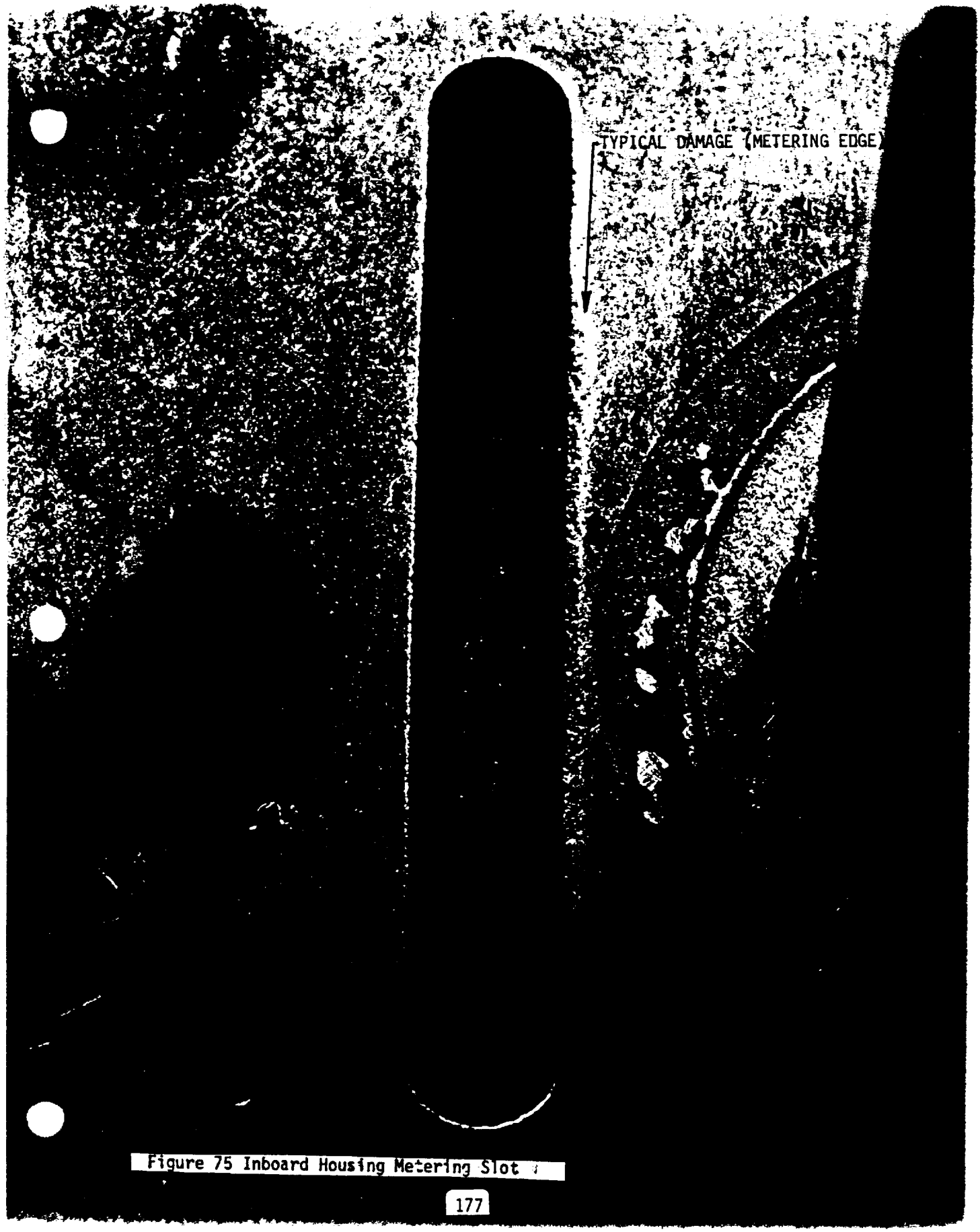


Figure 75 Inboard Housing Metering Slot

Figure 76 Inboard Housing Metering Slot

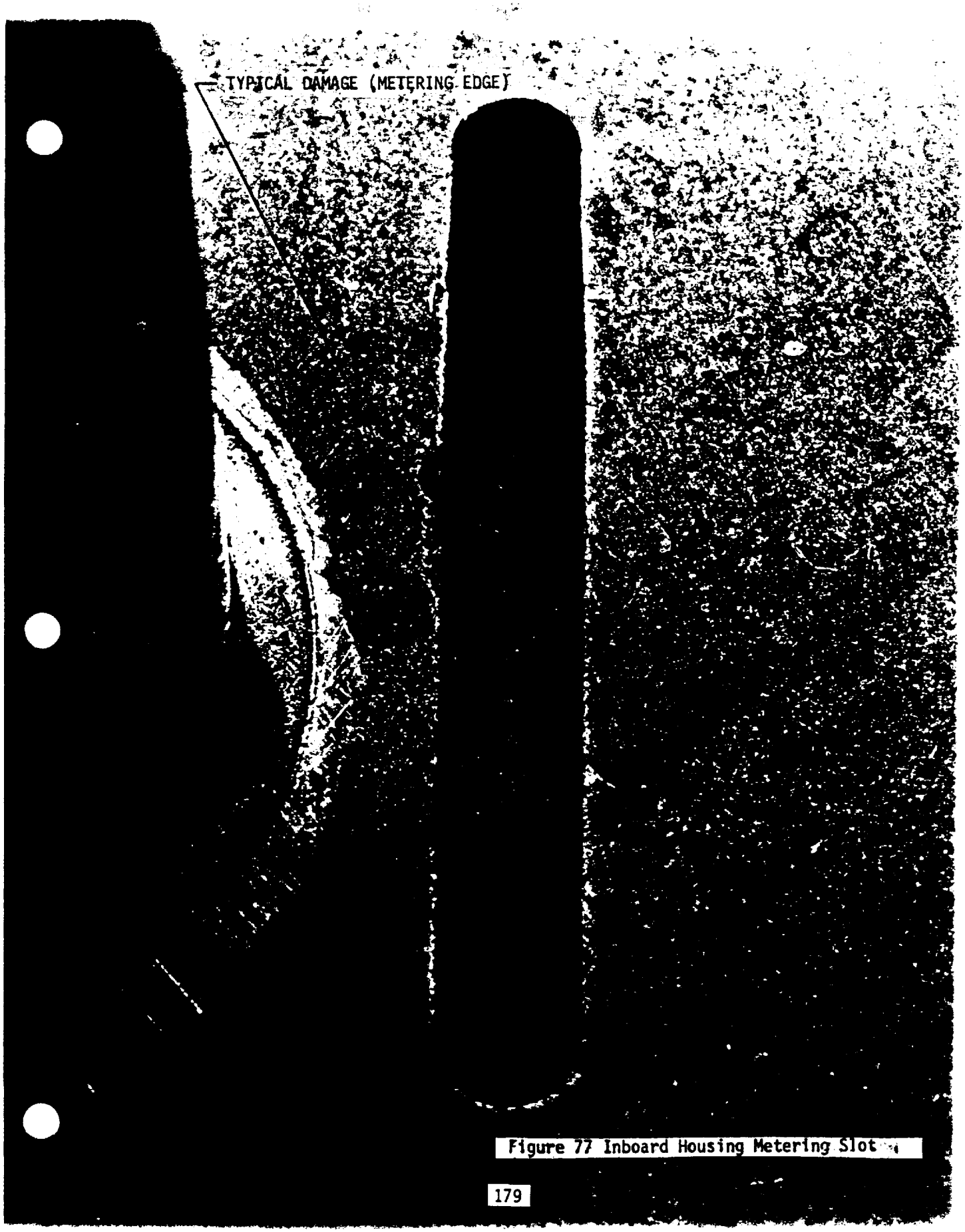


Figure 77 Inboard Housing Metering Slot

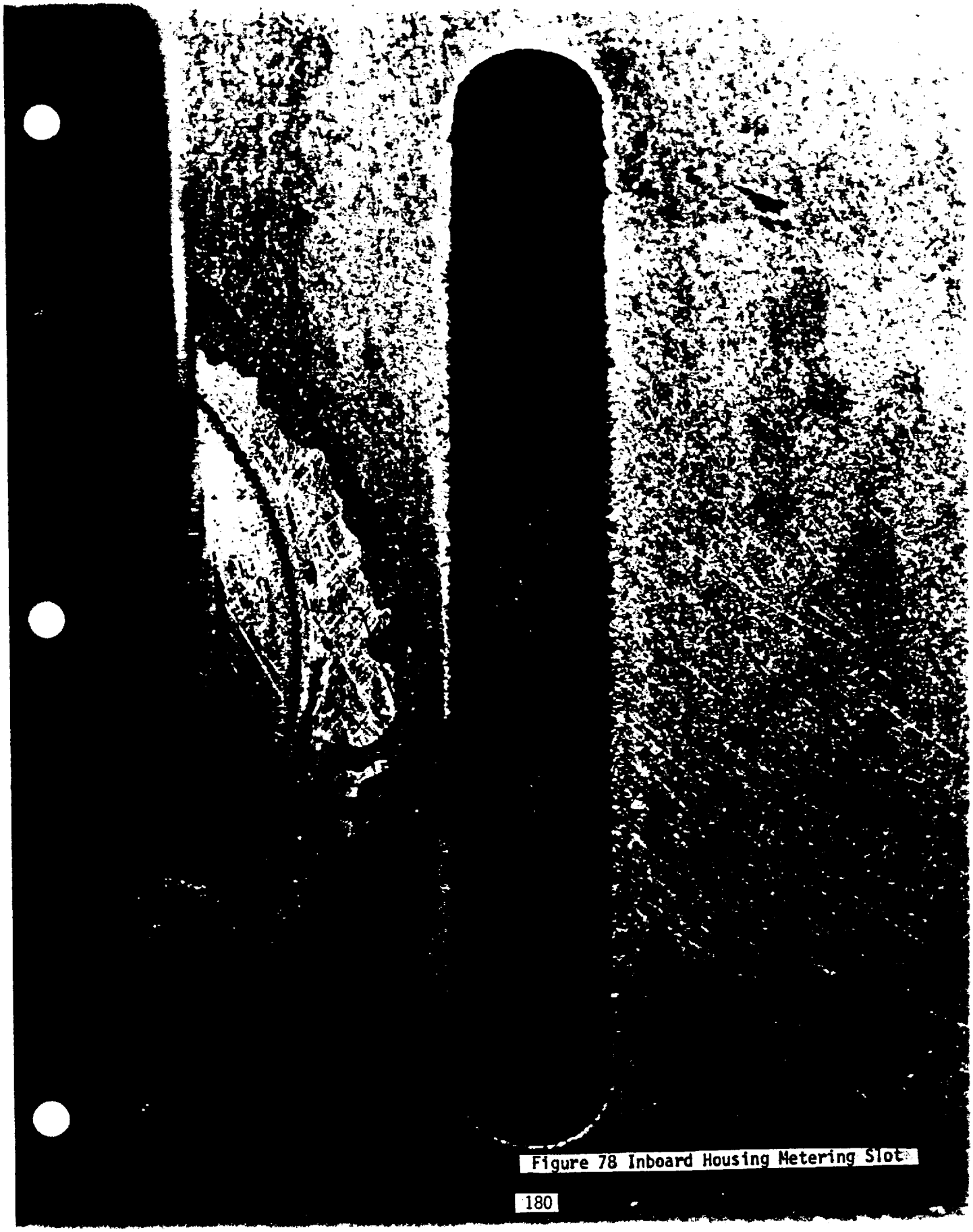

Figure 78 Inboard Housing Metering Slot

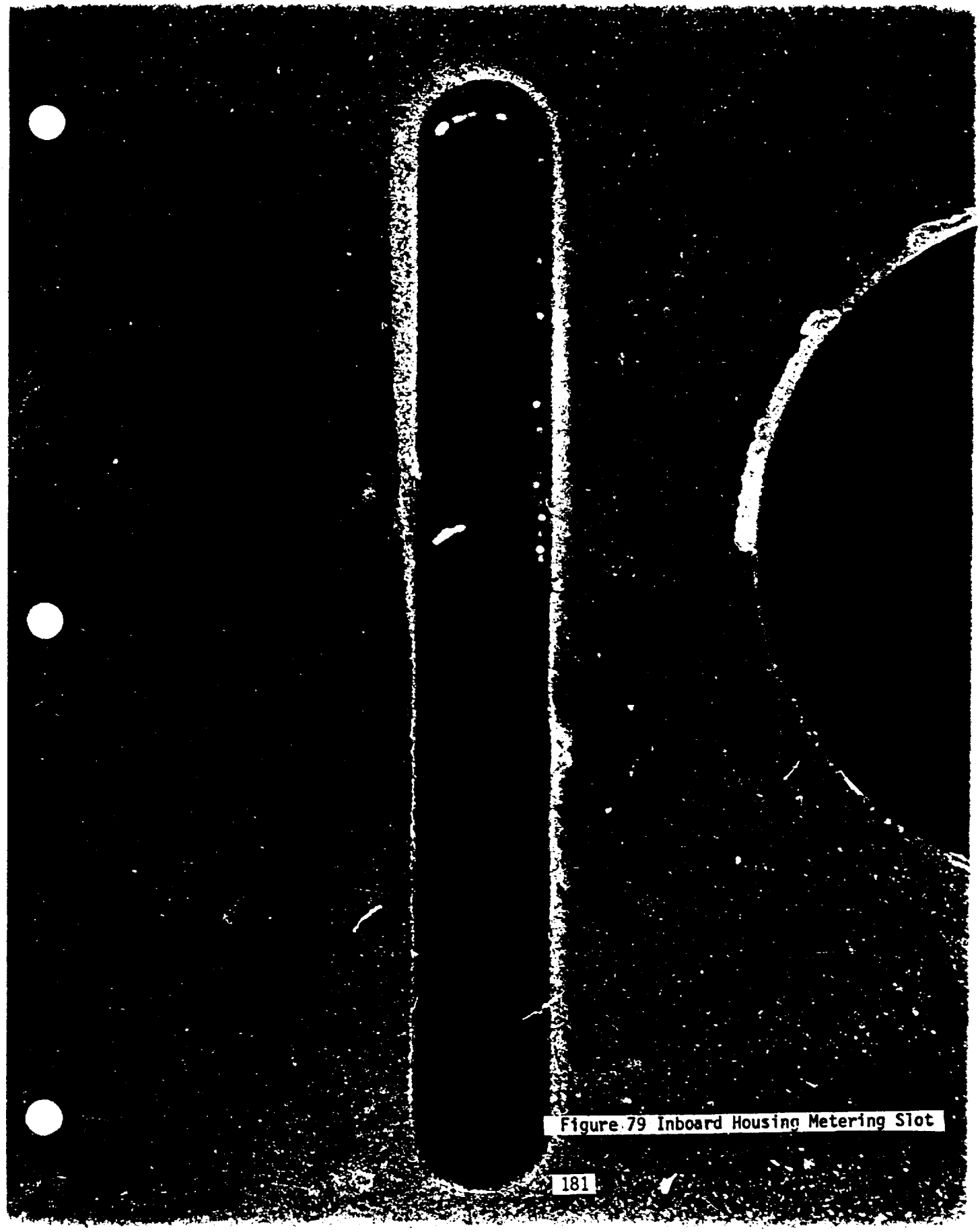

Figure 79 Inboard Housing Metering Slot

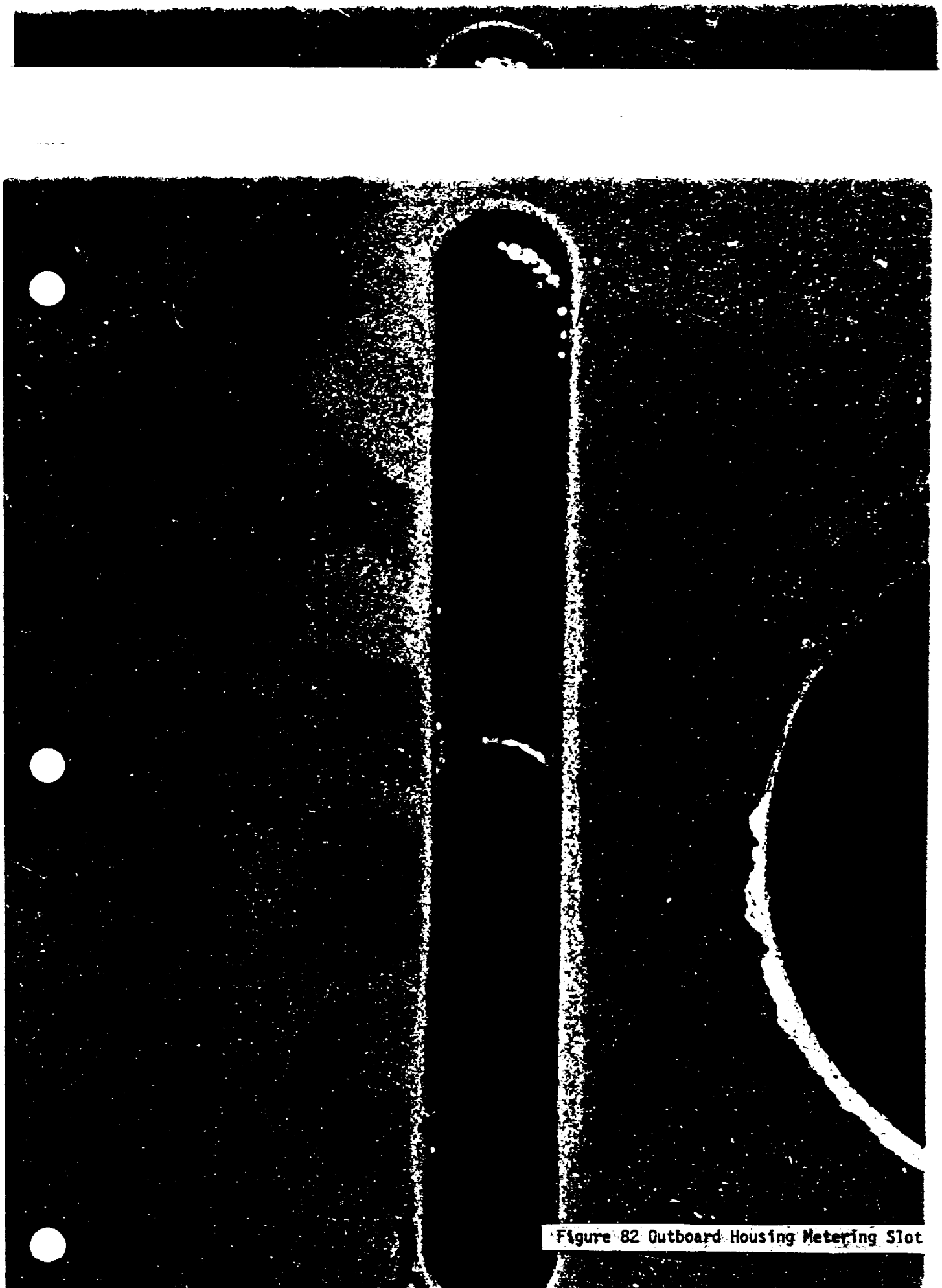

Figure 82 Outboard Housing Metering Slot

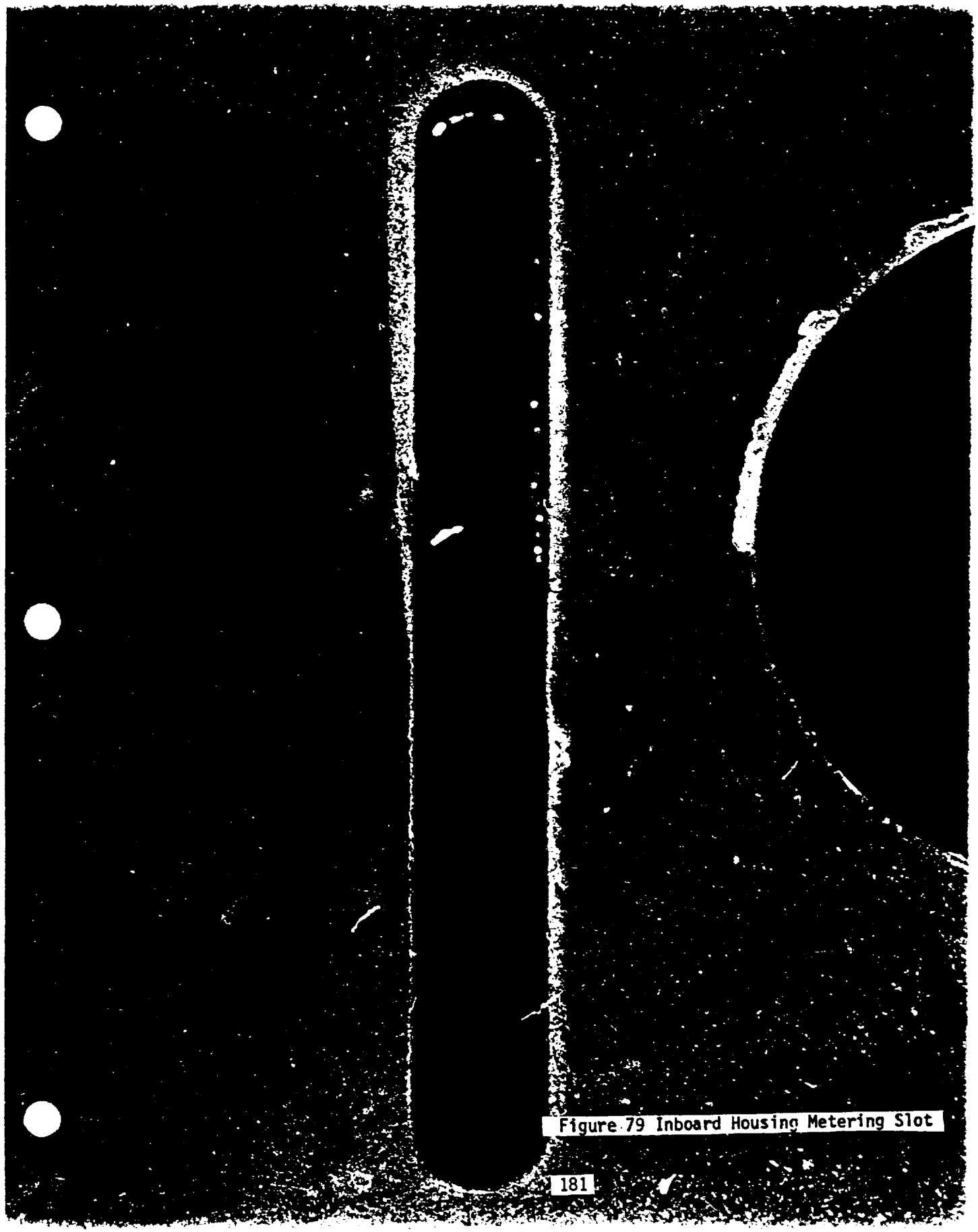

Figure 79 Inboard Housing Metering Slot

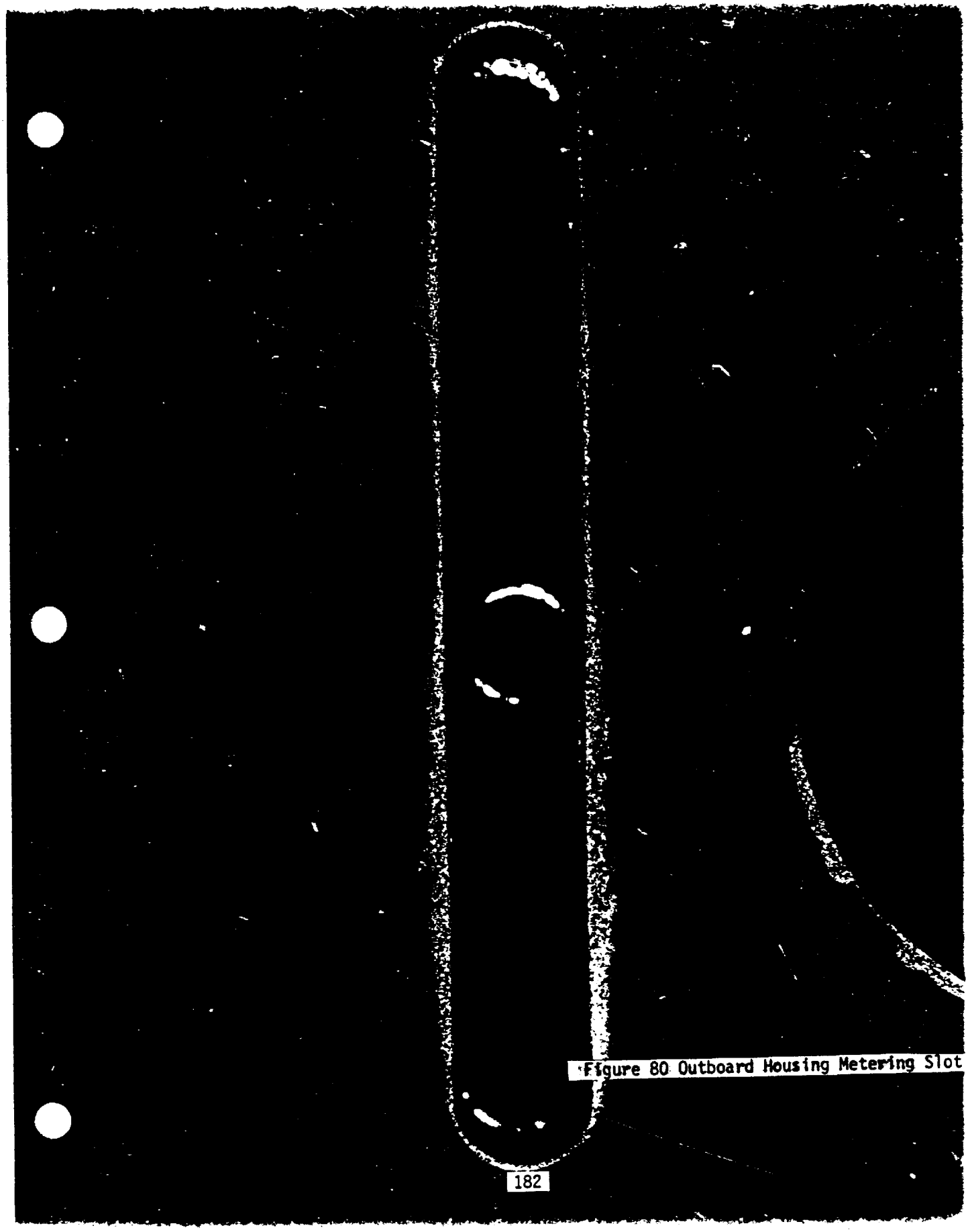

Figure 80 Outboard Housing Metering Slot

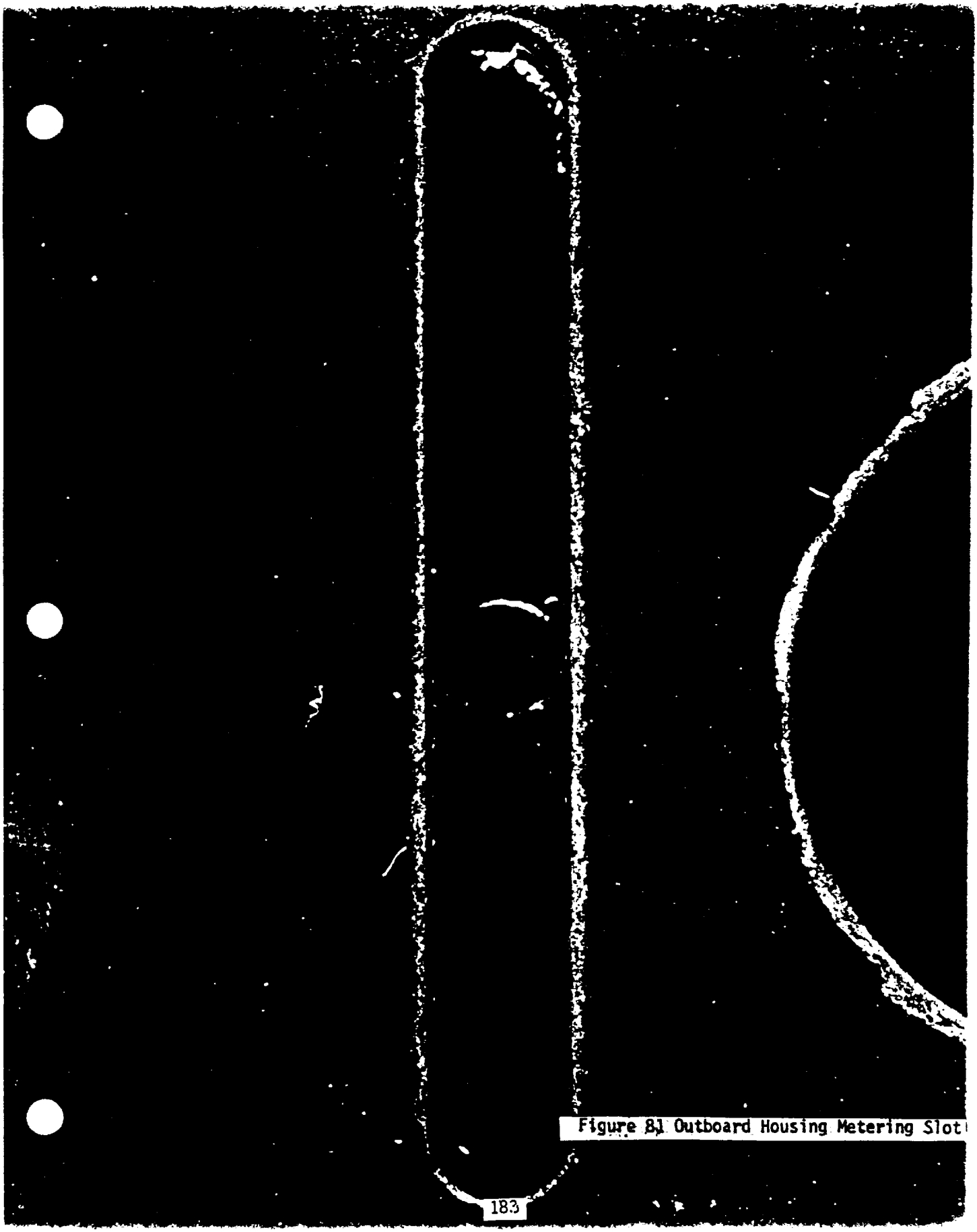

Figure 81 Outboard Housing Metering Slot

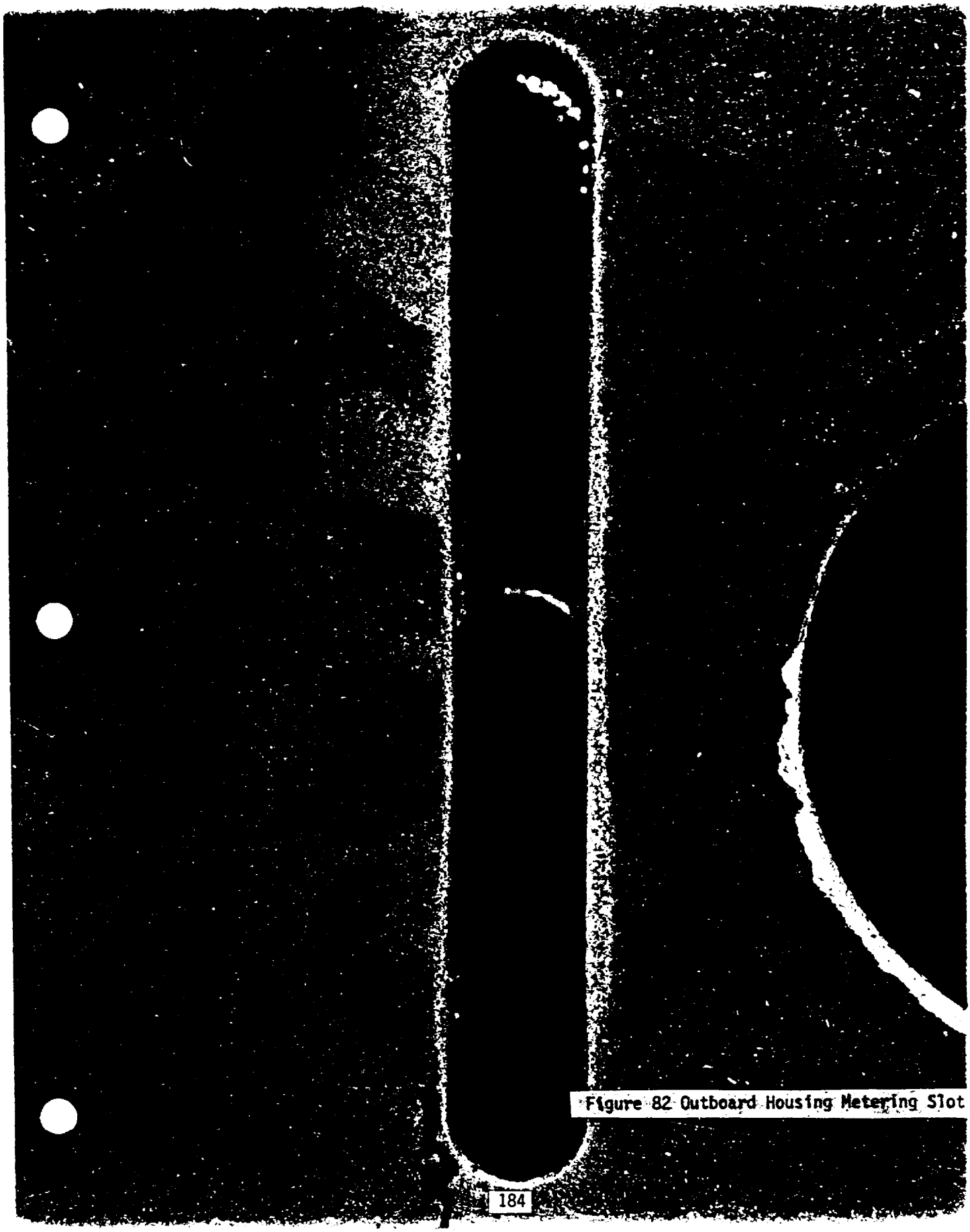

Figure 82 Outboard Housing Metering Slot

Another interesting condition visible in Figures 79 through 82 is that the slight erosion that did occur tended to affect the entire slot circumference. This is different than experienced in the inboard housing slots, because in testing, the test unit was oriented with the shaft vertical and the inboard housing down. this caused the orbiter ring to rest against the inboard metering plate surface with the running clearance occurring between the orbiter ring and the outboard metering surface. Consequently, at times before the stud nuts were tightened to reduce the clearance, excessive leakage probably occurred, emanating all around the slots causing the appearance shown.

Also another interesting conditon, visible in the Figures 79 through 82 is the chipped condition of the edge of the stud holes. It is believed that this was caused in assembly of the outboard housing over the studs and may well having precipitated damage that occurred at least between the orbiter ring and the outboard housing metering surface reported in the Gear Mesh Disengagement discussion for the 24 Pitch Gear Configuration. The dislodgement of pieces of the hard titanium carbide particles in the flame plate can also explain the appearance of circular scratches (same diameter as the orbiter ring orbit, i.e. dia=2e) evident whenever the parts were observed after operation.

After copper plating the slots of the orbiter ring to compensate for the erosion/cavitation damage to the housing slots, the leakage was greatly reduced as indicated by the values in Table 20 compared to Table 19. The leakage in the individual circuits, each consisting of six slots, was reduced by a factor of from 2.4 to 12.0. On the basis of this greatly improved leakage it was decided to re-evaluate the torque capability of the unit. However, it was determined that the internal leakage was just as bad as before the plating, and several tests did not reveal the source. So a disassembly was undertaken, and it was observed that over one third of the plating had separated in integral strips, and most of the rest

was adhering poorly and could be easily removed manually. This is the reason for excessive internal leakage and the inability to produce much torque. It is also the reason, possibly, for the excessive vane leakage from C2 to C3 indicated by the results in Table 21.

From Table 21 it can be seen that with C1 and C2 pressurized simultaneously, that leakage from C3 is much higher than C4. Then with C3 and C4 pressurized simultaneously, the higher leakage is from C2. These two tests indicate that the vane leakage was much greater from C2 to C3 and vice versa than for C1 to C4. The results indicate that the leakage varies with the .41 to .55 power of differential pressure from which it is concluded that the leakage is essentially orifice type flow. Also, this leakage did not vary much from a change in the torque on the stud nuts, which did affect back driving torque on the output shaft. The reason that it was previously stated that the loss of copper plating may have caused excessive vane leakage is because one, or more, of the loose copper strips may have interferred with vane displacement after the strip was dislodged.

As previously stated, it is believed that slot metering edge damage is the result of erosion and/or cavitation. Since, in general, test system contamination is controlled through the use of 5 micron absolute filters to maintain a class II hydraulic system pursuant with Bendix Specification BEPS 1,008, (equivalent to NAS1638, classes 5 to 6) erosion energy should have been low. As shown below, both flow phenomenons are a function of the differential pressure, so it may be mostly an academic matter to know which caused the damage. However, since materials exhibit greater resistance to one phenomenon than the other (reference 32), it would be useful to know which caused the damage.

It is known (reference 32) that the volume of material lost in erosion,

$$V_e = E_e/R_e \qquad (125)$$

where, $E_e$ = erosion input energy, lb-in

$R_e$ = material apparent erosion resistance, $lb/in^2$

Since,

$$E_e = .5\ MV^2 \tag{126}$$

where, M = mass of matter causing erosion, $lb\text{-}sec^2/in$

V = velocity of matter causing erosion, in/sec

and

$$V^2 = (2g/w)\Delta P \tag{127}$$

Therefore, from equations (125) through (127), the volume of material lost to erosion,

$$V_e = W\Delta P(R_e w) \tag{128}$$

where, W = total weight of matter causing erosion, lbs

$\Delta P$ = differential pressure, psi

w = specific weight of matter causing erosion, $lb/in^3$

Likewise, for the volume of material lost by cavitation,

$$V_c = E_c/R_c \tag{129}$$

where, $E_c$ = cavitation input energy

$R_c$ = material apparent cavitation resistance, $lb/in^2$

Since,

$$E_c = Qt\Delta P \tag{130}$$

where, Q = flow rate, $in^3/sec$

t = total time, sec

$\Delta P$ = differential pressure, psi

and

$$Q = ka\sqrt{\Delta P} \tag{131}$$

where, k = proportionality constant

a = flow area, $in.^2$

then, from equations (129) through (131),

$$V_c = \text{kat } \Delta P^{1.5}/R_c \qquad (132)$$

Consequently, from equations (128) and (132) it is seen that the volume of material lost to erosion and/or cavitation is a function of the $\Delta P$ and $\Delta P^{1.5}$, respectively. It is not the purpose of this discussion to quantitize the damage that can occur from erosion or cavitation, especially cavitation, because of limited knowledge of the phenomenon and the exact test conditions in regards to the fluid properties and pressure profile. It is, perhaps, more accurate to say that the energy input is a function of $\Delta P$ and $\Delta P^{1.5}$ for the two phenomenons, respectively. This is because scientific investigators have found cavitation damage varied from the first power of velocity (the square root of $\Delta P$) to a high as the sixth power of velocity (the cube of $\Delta P$) depending on many variables occurring in test conditions. In fact, cavitation may not occur at all, since incipient cavitation is generally defined as the ratio of the differential pressure causing flow to the difference of the upstream pressure and fluid vapor pressure. In other words, the downstream static pressure of the flow differential has to be lower than the fluid vapor pressure to form the damaging bubbles which will occur for ratios of about one, or greater, depending on the presence of entrained air, or other inducing nuclei. However, it seems any reduction of the $\Delta P$ across the metering edges should reduce the damage. Since the $\Delta P$ is fixed based on the torque requirements, it can not be reduced directly. Indirectly, though, or in a way impacting only what is imposed on the metering edges, the $\Delta P$ can be reduced. This can be accomplished as shown exaggerated in Figure 83. The addition of the venting slot to the metering slot effectively reduces the $\Delta P$ imposed across the major portion of the metering edge. The damage that may still occur on the edge of the venting slot will result in only a small increase in leakage with little change in performance of the assembly. It is known from experience in valve design that the venting slot concept will work.

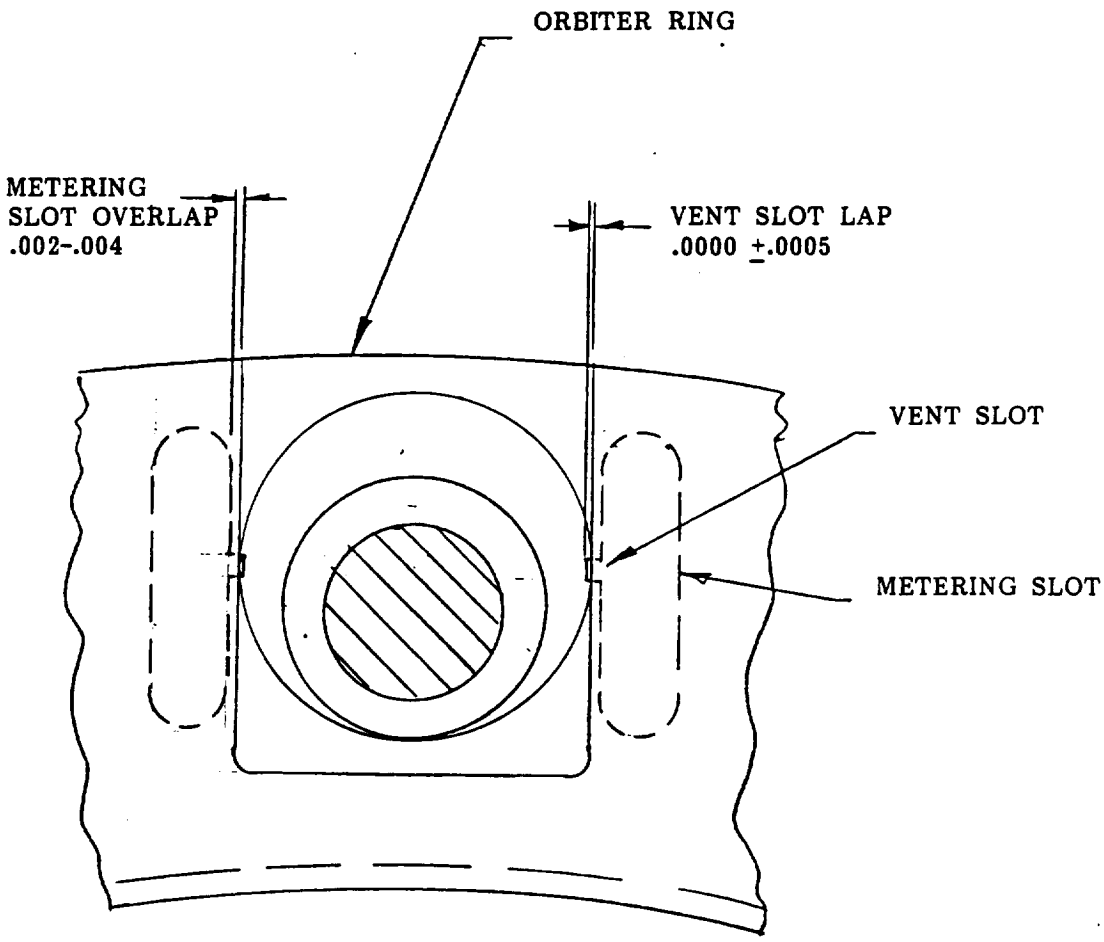


Figure 83. Additional Vent Slots to Eliminate Erosion/Cavitation Damage to Metering Slot Edges

Also, it is believed that the lack of damage to the slot in Figure 73, is the result of the inadvertently imposed vent in the form of the semicircular breakout damage inflicted on the metering edge.

Although the question of whether it is erosion, or cavitation, that primarily provides the damaging mechanism has not been answered, it is believed that cavitation is the most likely source. This belief is based on the fact (reference 32) that the alloy of tungsten carbide (94%) and cobalt (6%) is over four times more resistant to erosion than cavitation. Since the flame plating used consisted of 87% tungsten carbide and 13% cobalt, the ratio of resistances may even be greater. This opinion is based on a belief that the harder carbide particles are uprooted from the relative soft cobalt binder by cavitation induced forces.

## RECOMMENDATIONS

Although the Test Results and Conclusions were each broken into two main topics 32 Pitch Gear Configuration and 24 Pitch Gear Configuration, the recommendations will not be treated in this way for obvious reasons. The recommendations will be presented in such a way as to reflect the more important ones first, in the program area, then in the design area and, last, for the test area.

### Program

Recommendation No. 1 - Because of the design deficiencies encountered with the one test unit as produced that prevent realization of a reasonable performance, the remainder of the test program, mainly dynamic testing in simulated taxi tests on a dynomometer, should be abandoned. It is recommended that consideration be given to a new program based on design recommendations that are presented later. It is believed that the basic DYNAVECTOR concept on which the Powered Wheel Drive is based has been sufficiently proven in other programs (References 6, 29 and 30) and that need for substituting a more energy savings way of taxing aircraft, than using the main engines, is so evident (reference 1) that additional development is justified.

Recommendation No. 2 - It is also recommended that if the program recovery costs are so prohibitive that a new test unit with the recommended design improvements cannot be afforded, then consideration should be given to the refabrication of a key component, Orbiter Ring, P/N 3311970, with a slight modification and to the making of four to six cams to prevent gear mesh disengagement as recommended in reference 31.

The necessary orbiter ring modification consists of reducing the width of the twelve metering slots, as shown in Figure 59, from 0.8139 - 0.8145 in. (20.673 - 20.688 mm) to compensate for the change in the Inboard Housing P/N 3311945, metering slots caused by erosion. The exact decrease of the slots

would be determined at a later time, but an approximate nominal width would be 0.7902 in. (20.071 mm). This nominal dimension represents a decrease of about 0.0120 in. (0.3048 mm) to just compensate for the erosion and another 0.012 to provide overlap to compensate for future erosion until the testing is completed. as can be noted in Figure 59 the stud hole diameter 0.8125 - 0.8126 is nominally the same as that for the slot width. Since this hole diameter is necessary for assembly (and for the cams discussed later) it is noticed that a slight conflict arises as shown in Figure 84. This elimination of a portion of the edge of the orbiter ring slots by the hole results in a leakage area shown by the cross hatched areas, equivalent to 0.0011 $in^2$ (0.720 $mm^2$) for each slot. This is equivalent to having two slots of 0.111 x 0.010 in. dimensions creating an underlap condition as shown in Figure 84 (b). This is not altogether an adverse condition although lap leakage results, since the limited underlap obviates pressure surging that would occur if no leakage occurred at all. This is the way the slots between the inboard housing and orbiter ring should have interfaced rather than trying to achieve an essentially line-to-line condition with the original design. It is estimated that the internal leakage that will occur as a result of the Figure 84 (a) condition will be, based on two equal orifice areas in series with 4000 psig (27.5 $NM/m^2$) differential pressure, 2.6 gpm (10.0 lit/min). This is an acceptable value. Also the leakage created by the small slot effect is believed beneficial in preventing erosion since it dissipates the high velocity over a limited slot width. This is substantiated by actual results, as well as theory, as can be seen in Figure 73. The inadvertent damage inflicted in weld repair and evident from the notch effect in the center of the left side (metering side) is considered to be the reason the edge does not indicate the magnitude of erosion evident in Figures 75 through 78.

This substitution of four, or six, cams to replace the equivalent number of Sleeve Spacers, P/N 3311972, is considered necessary to prevent orbiter ring/output

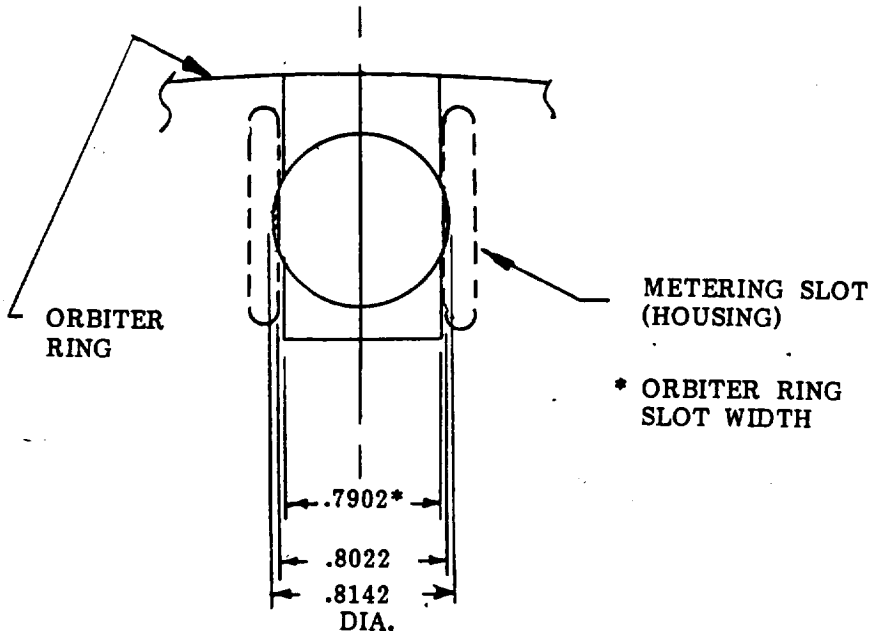


(a) RECOMMENDED ORBITER RING SLOT WIDTH

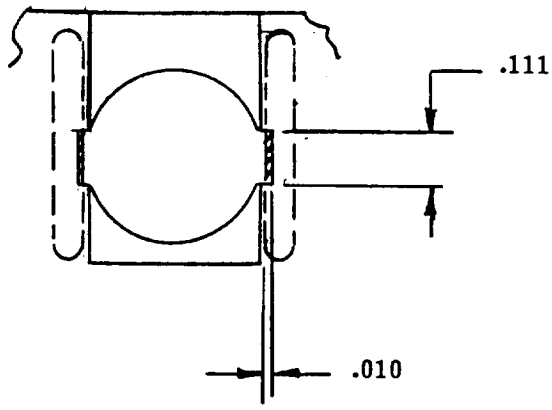


(b) EFFECTIVE SIZE OF VENTING SLOTS

FIGURE 84. RECOMMENDED ORBITER RING SLOT WIDTH CHANGE TO CREATE EFFECTIVE VENTING SLOTS

gear assembly distortion and the resultant gear mesh disengagement. Figure 85 shows the addition of the cams for every other stud of the twelve studs. With the cams the orbiter/gear distortion loads would be transmitted to the studs to reduce distortion. Even at stall load and only one stud carrying the load in double shear, the shear stress would only be 88,000 psi (607 $MN/m^2$). This is well below two thirds of the minimum ultimate tensile strength of 220,000 psi (1.52 $GN/m^2$). Also, with a tensile stress of 4000 psi of 159,875 psi (1.10 $GN/m^2$) the maximum combined stress would be only 182,494 (1.26 $GN/m^2$). For the cam bearing stress with a diametrical clearance that would be held for the cam and the orbiter ring hole (0.002 in. max), the cam Hertz stress would be a reasonable 105,000 psi (0.724 $GN/m^2$) using a bearing bronze. However, at a maximum orbiting velocity of 3900 rpm the PV value for the cam would far exceed the capability of any plain bearing material, even assuming equal load sharing by the six cams. Assuming an allowable PV value of 50,000 psi - ft/min (105 $MN/m^2 - \frac{m}{min}$) with three of the six cams sharing the load and 25% of stall torque in the parallel mode, the maximum allowable shaft speed would be restricted to 15 rpm. This restriction would permit a bearing life of many hundreds of hours, so obviously, by increasing load or speed, the cam bearing life would be decreased. While this limitation is probably unacceptable for dynamic testing on a dynamometer, it could increase confidence in the capability of the test unit to generate the required torque and evaluate the performance of the metering modification for possible future use of the flame plated metering surface.

With these two modest modifications, it is believed that sufficient information and experience would exist that would reduce the risks in any future development. The largest remaining effort for future design that would still have to be undertaken would be a trade study to determine which means of increasing orbiter/ring gear assembly stiffness (to eliminate gear mesh disengagement) would have the least

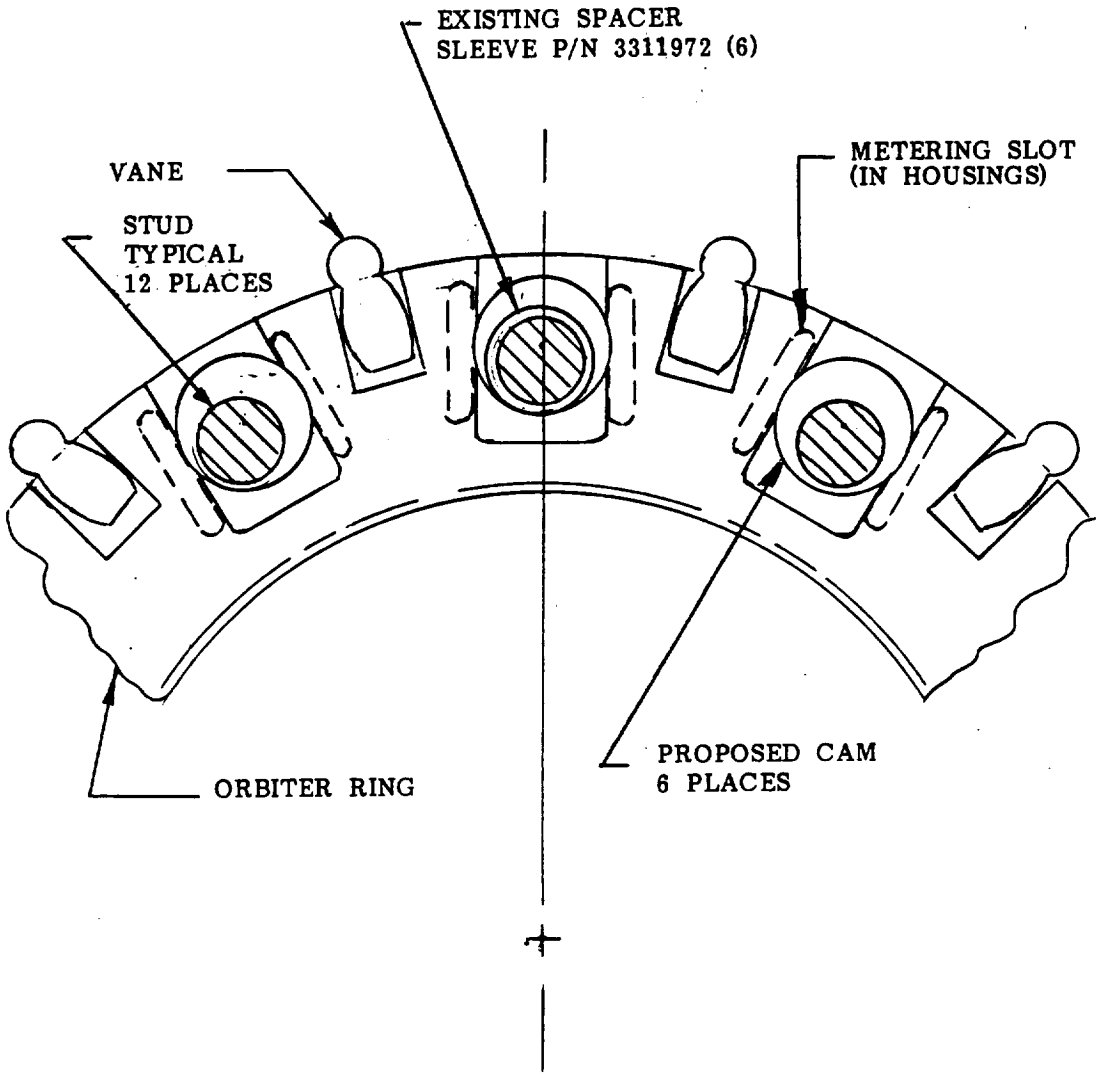


FIGURE 85. PROPOSED CAMS TO PREVENT GEAR DISENGAGEMENT

package size impact, the increase of the combined moment of inertia of the assembly, or the use of cams with anti-friction roller bearings (reference Appendix H).

Design

Recommendation No. 3 - Modify the existing design to stiffen the orbiter ring/ring gear assembly to prevent gear mesh disengagement. As mentioned in the previous recommendation, this can be achieved in two ways. The first way, increasing the movement of inertia of the orbiter ring/ring gear combination is the least complex, but perhaps the most space consuming. This opinion is based on the fact that assuming a constant orbiter ring thickness and a constant ring gear pitch diameter, the increase in the combined inertia will be approximately proportional to the increase in the orbiter ring diameter. This in itself does not appear promising, but combined with a change to optimize the orbiter ring shape to reduce the vane slot effect, it might suffice. A possible change in installing the vane to improve the orbiter ring moment of interia is suggested in Figure 86. The vanes are actually inverted to retain them in the orbiter ring and transpose the sealing slots into the Spacer, P/N 3311952, at an expense to the package diameter of about 0.75 in. (1.91 cm). Looking at Figure 1 of the installation in the 737 wheel, the increase seems reasonable.

In addition, an increase in stiffness can be obtained proportional to an increase in the Young's Modulus of the orbiter ring material. Naturally, this requires a change in material from the existing 4330 modified alloy steel. A possible material selection for consideration might be the tungsten alloy, Kennertium, produced by Kennametal, Inc. This material in Grade W-2 has a modulus of elasticity of 50 ($10^6$) psi ($.34TN/m^2$) or almost double that of the steel used. A more thorough consideration of the other characteristics of Grade W-2 would be necessary before a substitution is definitely recommended, but preliminary considerations seem promising.

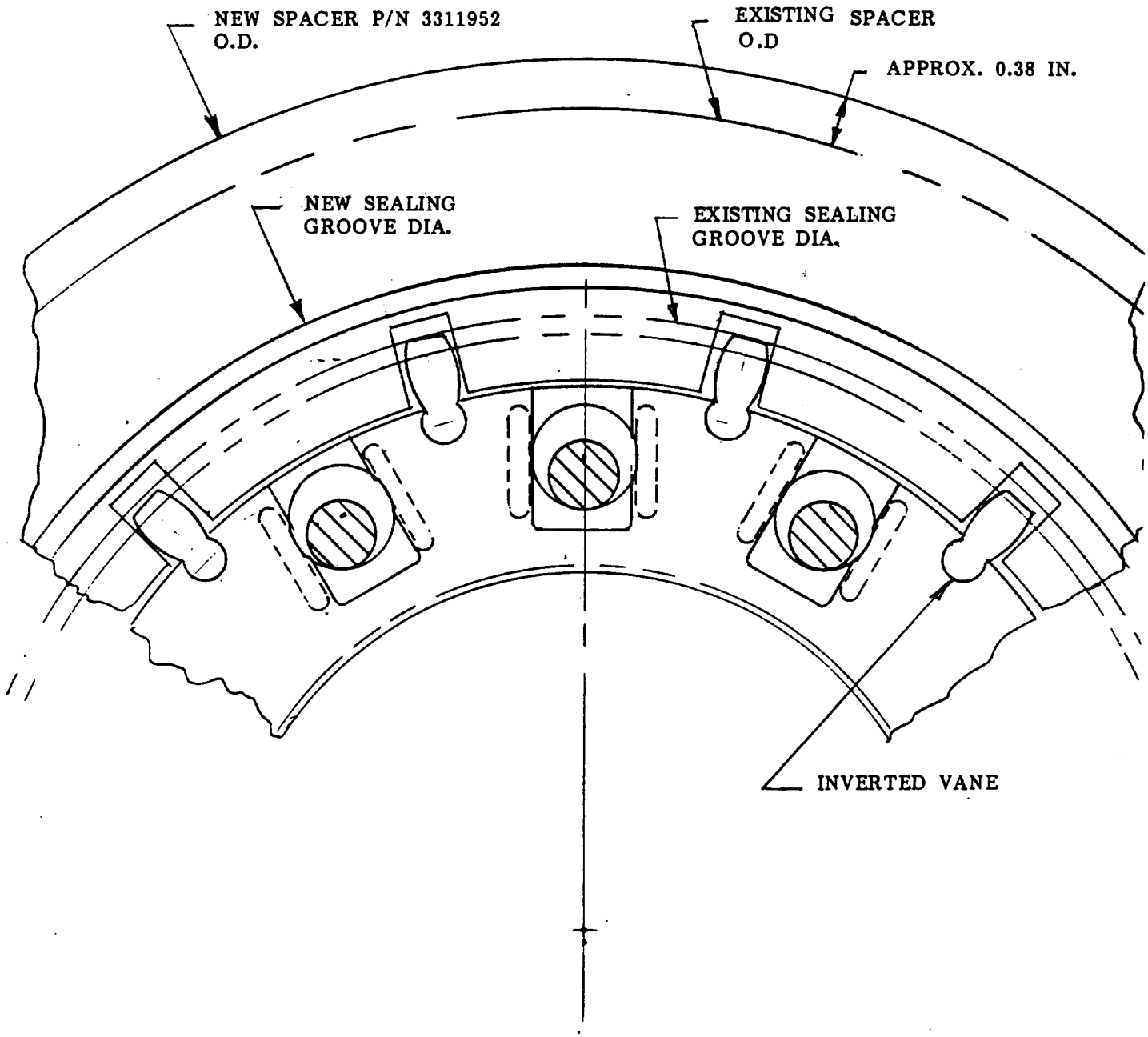


FIGURE 86. INVERTED VANE MODIFICATION OF ORBITER RING P/N 3311952

Tungsten alloys are available from several suppliers and find many uses in the aerospace field. They are produced by powdered metal techniques and could offer economical fabrication of the finished part.

Recommendation No. 4 - Consideration of other flame spray materials, or other wear coatings or treatments should be made for any new design. While the existing tungsten carbide coating has exhibited good wear characteristics, it has, on the other hand, shown poor erosion resistance. The plating used was Union Carbide LW-1N30 (87% WC and 13% Co) with a finish thickness of 0.003 - 005 in. (0.076 -0.127 mm). Actually with the pressure balanced orbiter ring design, operating with the axis horizontal, wear resistance may be secondary to erosion resistance. If so, thin-dense chrome plating may be a better selection than the tungsten carbide flame plating. A proprietary synergistic coating (NEDOX) of hard chromenickel alloy infused with one of the flurocarbons provided by General Magnaplate Corporation may offer advantages with a maximum surface hardness of Rockwell C-65, along with a low coefficient of friction, and an applied thickness of 0.0004 -0.0008 in (0.0102 - 0.0203 mm).

There are many proprietary coatings on the market which are used in many rough applications. A survey to find the best coating to match the requirements of the metering plate environment is recommended for the follow-on development.

Recommendation No. 5 - To eliminate the possibility of damage to any coating applied to the metering surface of the Outboard Housing, P/N 3311940, the coating should be stopped short of the through-holes for the inboard housing studs. This precaution is necessary to prevent impacting the coating during assembly of the outboard housing with the risk of causing chips that could damage the sliding surfaces.

Recommendation No. 6 - Because of flow pressure loss about double that predicted, it is necessary that any redesign include means of reducing this loss.

Most of the loss must be eliminated by increasing flow areas, since the tortuous flow paths are more difficult to change. Since many of the passages require a calculated flow velocity of 35 ft/sec, and greater, it is desirable to reduce this to 25 ft/sec to reduce the loss to half of that experienced.

Recommendation No. 7 - A desirable design change that would make the powered wheel drive assembly much easier to assemble and perhaps give much less case drain leakage would allow the metering plates of both housings to float on circumferential seals so that each plate could be maintained in intimate contact with the Orbiter Ring by pressure in the Housings. In order to effect this change it probably would be necessary to eliminate the metering slots of the metering plates and accomplish the metering by valves on each of the twelve studs. These valves would function like the cams suggested in Recommendation No. 2. As the valves rotate, once each Orbiter Ring orbit, they would port to inlet pressure half of the rotation and to outlet pressure the other half rotation. The valves would provide the convenience of being replaceable if erosion occurred. To minimize bearing wear of the valves and friction it would be necessary to carefully select the material and wear coating, if necessary, plus provide sufficient Orbiter Ring/Ring Gear assembly stiffness so that not much hydraulic loading is transmitted to the valving.

# APPENDIX A

## STATEMENT OF WORK

DESIGN, MANUFACTURE AND

TEST OF A PROTOTYPE

POWERED WHEEL FOR AIRCRAFT

LANGLEY RESEARCH CENTER
HAMPTON, VA
23665

INDEX

SUMMARY

1.0 Introduction

2.0 Contract Objectives

3.0 Technical Requirements - Guidelines and Constraints

- 3.1 Operational Considerations
- 3.2 Design Requirements
  - 3.2.1 Weight and Inertia Limitations
  - 3.2.2 Environmental Conditions
  - 3.2.3 Design Factors
- 3.3 Systems Requirements
  - 3.3.1 Pressure Medium
  - 3.3.2 Torque Requirements
  - 3.3.3 Velocity
  - 3.3.4 Braking
  - 3.3.5 Power Transfer
  - 3.3.6 Geometrical Restrictions
- 3.4 Component Test Requirements
- 3.5 Powered Wheel Test Requirements
  - 3.5.1 Test Equipment
  - 3.5.2 Test Envelope
  - 3.5.3 Data Acquisition

4.0 Contractor Tasks

- 4.1 Analyses
  - 4.1.1 Stress Analyses
  - 4.1.2 Thermal Analyses
  - 4.1.3 Dynamic Analyses

INDEX (Continued)

4.2 Design

4.2.1 Drawings

4.2.2 Specifications

4.3 Fabrication

4.4 Test Program

4.5 Reliability and Quality Assurance Program

4.5.1 Design Review

4.6 Safety Program

## 1.0 INTRODUCTION

Over the years there has been much discussion of the benefits that could be realized if aircraft were not required to use their main engines for ground operations. These include less noise around the terminal, less atmospheric pollution, and less congestion on the airport ramp by elimination of towing vehicles. Safety is enhanced by better communications among the ground crews. Fuel is conserved by using efficient high speed auxiliary power units rather than the main propulsion engines at idling speeds. There are also some advantages for military use. The development of one or more methods for driving the wheels is, therefore desirable. The NASA intends to use the results of this contract to establish the feasibility and set the design requirements for a flying installation on a 737-100 type aircraft. The purpose of the flight system, which is not a part of this contract, would be to demonstrate feasibility and evaluate handling qualities.

## 2.0 CONTRACT OBJECTIVES

The objective of this contract is the analysis, design, fabrication, dynamometer tests, and report of a full scale prototype powered wheel suitable for use on a 737-100 type aircraft. The power unit shall fit within the hub with minimum modification to the existing wheel design and shall be capable of moving the aircraft during all normal ground operations. The dynamometer tests shall demonstrate the wheel unit over the entire operational range including noninterference at take-off and landing speeds.

The contract shall be phased as follows:

Phase A shall include the design effort, analyses, the design review, and compliance with the action items generated at the design review.

Phase B shall include the fabrication of the demonstration unit, the dynamometer testing, and the preparation of the final report.

## 3.0 TECHNICAL REQUIREMENTS - GUIDELINES AND CONSTRAINTS

### 3.1 Operational Considerations

The powered wheel unit to be designed must be compatible with a Boeing 737-100 type aircraft. The outboard wheel on each main truck will be powered. The brake assembly on the powered wheel may be modified by removing 3 of the 5 plates. Other wheels and brake assemblies shall not be altered nor their operation constrained by the modifications. Ground checkout, removal, and replacement for tires, anti-skid systems, and brakes shall be essentially the same as those of the unmodified wheels.

### 3.2 Design Requirements

#### 3.2.1 Weight and Inertial Limitations

Minimum weight and inertia shall be a design goal.

#### 3.2.2 Environmental Conditions

All system components and the materials selected shall function satisfactorily under flight conditions in atmospheric ambient temperatures from $-65^{\circ}$ to $+120^{\circ}F$.

All system components shall be protected from damage by foreign matter thrown by the tires. This protection and/or the system components must be designed so that the component will operate when there is an accumulation of dirt, mud, ice, or any other material.

#### 3.2.3 Design Factors

Material strength properties shall be based on the "A" values as listed in the latest edition and/or change notice of MIL-HDBK-5 "Metallic Materials and Elements for Flight Vehicle Structures". Components are to be designed to have positive margins of safety. The margin of safety is to be computed by the following equation.

$$MS = \frac{\text{Allowable Yield Stress}}{\text{Design Yield Stress}} - 1$$

$$MS = \frac{\text{Allowable Ultimate Stress}}{\text{Design Ultimate Stress}} - 1$$

The Allowable Yield Stress is the yield stress of the material being considered as specified in the appropriate standard with reductions to account for the expected thermal environment. The Allowable Ultimate Stress is the breaking or rupture stress for the material being considered as specified in the appropriate standard with reductions to account for the expected thermal environment and for fatigue.

The Design Yield Stress is the Design Limit Stress multiplied by the Yield Factor of Safety. The Design Ultimate Stress is the Design Limit Stress multiplied by the Ultimate Factor of Safety. The Design Limit Stress is the maximum stress that will be imposed on the material under the worst possible combination of loads including those due to thermal environments, linear and angular accelerations, structural loads, and aerodynamic loads, if applicable.

The Ultimate Factor of Safety for storage tanks, actuators, motors, and similar pressure vessels is not to be less than 2.5. The Yield Factor of Safety for such vessels is not to be less than 1.65.

The Ultimate Factor of Safety for tubing, piping, fittings, valves, and similar components is not to be less than 4.0. The Yield Factor of Safety for these items is not to be less than 2.65.

3.3 Systems Requirements

3.3.1 Pressure Medium

The pressure medium shall be Skydrol 500 or other standard hydraulic fluid having similar characteristics so that a flight system could use Skydrol 500 without changing the basic design.

3.3.1.1 Fluid Pressure

The design pressure shall be 4000 psi.

3.3.1.2 Fluid Flow

The maximum flow rate shall be not more than 45 gal/min for each powered wheel.

3.3.1.3 Case drain design press shall be 150 psig

3.3.2 Velocity

The powered wheel shall have the capability of driving the aircraft to a velocity of 15 mph ground speed which is 153 rpm of the 737 wheel. Higher velocities are desirable and should be considered as an ultimate design goal.

3.3.4 Braking

The unit shall have limited braking capabilities when being driven as a pump by the aircraft. Torques developed during braking shall not exceed the stall torque and fluid pressure shall not exceed the design pressure.

3.3.5 Power Transfer

The power unit shall utilize a device for power transfer to the wheel that can be engaged or disengaged at any point throughout its operating range of 0-15 mph. The engaging mechanism shall have an inherent or designed capability of momentary "slippage" to prevent impact loading of any part. The power unit shall be capable of driving the aircraft in a forward or reverse direction. The power transfer mechanism operation shall respond directly to system pressure in that the wheel is engaged by the drive unit when hydraulic pressure is applied to the actuator and disengaged when the pressure is removed.

3.3.6 Geometrical Restrictions

The drive unit must fit within the wheel hub. No belts, chains, or shafts from the wing will be permitted. Only hydraulic lines and electrical wires will be allowed across the gear hinge points and shock strut region. A feasibility study at Langley Research Center has developed a concept that will meet the requirements of this paragrpah and those of the preceding paragraphs.

3.4 Component Test Requirement

The power unit case shall undergo a proof pressure cost of 6750 psi for 5 minutes. No permanent yielding shall occur in any components.

3.5 Powered Wheel Test Requirement

3.5.1 Test Equipment

The tests do demonstrate the operational capabilities of the wheel unit shall be performed on a dynamometer. The dynamometer shall be capable of simulating the landing, taxi, and take-off velocities of a Boeing 737-100. The inertia of the 737-100 aircraft shall be simulated by the dynamometer wheel.

3.5.2 Test Envelope

The tests shall demonstrate a typical use cycle including reverse for 100 yards, taxi two and one-half miles at 15 mph, disengage power unit, accelerate wheel to 180 mph, stop, pause and cool for an interval to simulate a short flight, accelerate very rapidly to 180 mph, slow to 15 mph, engage power unit, taxi two and one-half miles at 15 mph, stop. During the test program the goal shall be to successfully perform 100 cycles. If a failure occurs in the test unit prior to reaching the goal that will not be economical to repair, the Contractor and the Contracting Officer will reach a mutual agreement on the proper course of action to pursue thereafter. Time may be allowed between cycles to simulate loading and unloading operations, however, a sufficient number of use cycles at close intervals should be performed to establish the thermal capabilities of the unit during such operations. The braking capabilities shall be demonstrated by throttling the flow from the unit to stop the inertia wheel of the dynamometer.

3.5.3 Data Acquisition

The data acquisition system shall record a continuous time history during all tests showing the fluid inlet pressure, outlet pressure, inlet temperature, outlet temperature, flow rate, wheel velocity, and wheel torque output.

## 4.0 CONTRACTOR TASKS

### 4.1 Analyses

#### 4.1.1 Stress Analyses

The Contractor shall carry out analytic studies of the stresses in all component sufficient to establish that the requirements of Paragraph 3.2.3 have been met.

#### 4.1.2 Thermal Analyses

The Contractor shall analyze the thermal conditions in the power unit under all operating conditions to establish the material requirements and define the operational limitations of the system.

#### 4.1.3 Dynamic Analyses

The Contractor shall analyze the motions and accelerations of components to establish design loads and operational limits. He shall analyze the fluid flows to establish the theoretical torsional output at all velocities and the calculated efficiency of the system under all conditions.

### 4.2 Design

The Contractor shall design the powered wheel unit to meet all requirements of Section 3.0 of this Statement of Work.

#### 4.2.1 Drawings

The Contractor shall prepare shop drawings in accordance with his own standards. Such drawings shall conform to generally accepted good practice in the aerospace industry. The Contractor shall furnish four prints of each drawing to the Contracting Officer after the design review. The Contractor shall furnish one high quality reproducible (on Mylar or equal) of each drawing to the Contracting Officer with the final report. each original drawing shall include an LRC drawing number. This number is to be fixed beneath the Contractor's number and will have the form Lx-xxxxxxx. The first "x" represents the drawing size (same as

the Contractor's designation). This is followed by a dash and a 6-number LRC designation (to be furnished by LRC. The last "x" represents the drawing revision (contractor's designation).

4.2.2 Specifications

The Contractor shall prepare specifications for parts and components when appropriate. The specifications shall describe the functional and physical requirements for the article. The Contractor shall submit four copies of each specification to the Contracting Officer when the document is released to the Contractor's organization.

4.3 Manufacturing

The Contractor shall fabricate or procure all parts and components required to complete one assembly including power unit, power transfer mechanism, and other hardware required to mount the unit to the dynamometer.

4.4 Test Program

The Contractor shall carry out the test program described in Section 3.4 of this Statement of Work. He shall furnish a dynamometer, auxiliary power sources, data acquisition instrumentation, and other test equipment required to complete the tests. The Contractor shall prepare a test plan that outlines the complete sequence of tests. He shall also prepare test procedures and specifications as required. Four copies of each document shall be submitted to the Contracting Officer not less than two weeks before beginning the tests.

4.5 Reliability and Quality Assurance Program

The Contractor shall carry out a Reliability and Quality Assurance Program based on his established in-house procedures and capabilities to ensure that the project will be completed with a reasonable degree of certainty and that the test results are not unduly affected by manufacturing tolerances, poor assembly methods, or poor testing techniques.

4.5.1 Design Review

The Contractor shall conduct three (3) design reviews after he has completed the analyses and design, but before he begins fabrication. The Contractor shall notify the Contracting Officer and the two shall agree upon dates. The first two (2) reviews will be held at the Contractor's plant with the Government's review committee in attendance by telephone. The final review will be held at Langley Research Center. The first review will cover the following items as a minimum:

A. Schematics

B. Orientation with assembly drawings

C. Results of the engineering analyses

D. Detailed Test Plan

E. Schedule

F. Problem Areas Encountered and Anticipated.

The Contractor shall prepare the minutes of the design reviews and submit four (4) copies to the Contracting Officer. The disposition of all action items generated at the reviews shall be attached to the minutes.

4.6 Safety Program

The Contractor shall carry out a system safety program that extends from the design phase through the completion of the test program. The objective of the program shall be to eliminate hazards to personnel and to minimize the probability of damage to equipment that could jeopardize the schedule and funding of the project. it is anticipated that the Contractor's existing safety manuals or regulations will largely meet this requirement.

# APPENDIX B

## PRESSURE LOSS ANALYSES

## APPENDIX B

## PRESSURE LOSS ANALYSIS

### 1. INTRODUCTION

Since the Wheel Drive Actuator consists of two hydraulic motors connected in series or parallel, as illustrated by the schematic, Figure B1, there are four hydraulic connections (not counting the case drain) to the two motors, or two connections to each motor. In this analysis, the pressure loss will be evaluated from the displacement changing valve (DCV) to the motors and back to the DCV. The flow capacity of the DCV is such that the pressure loss it causes will be negligible.

It is assumed that 10 feet of 0.75 Dia. X 0.070 tubing is used from the DCV to the actuator quill for each connection, terminating in a 90-degree MS fitting. From each quill, the fluid is conducted through a series of rectangular cross-section pasages, including a 360-degree annulus, to the rectangular metering slots in the commutation plate assembly. The calculation of the pressure loss throughout is straightforward; however, it is necessary to estimate the flow distribution around the flow annuli to the metering slots, which follows, first.

### 2. FLOW DISTRIBUTION IN THE ANNULI

Each annular flow path must handle the rated motor flow, but since at any given time each of the four annuli feeds only three chambers, the flow distribution can vary dependent on the location of the flow entry point to the annulus in respect to the three slots. Referring to Figures B2 and B3, it will be shown that two extremes for the distribution can exist.

Figure B2 assumes the flow entry point is located approximately 180 degrees from Port 1, which in turn is midway between Ports 2 and 3. As shown in the figure, Port 1 is wide open, but Ports 2 and 3 are only partially open and approximately equal. In this case, the lumped resistance representing the flow

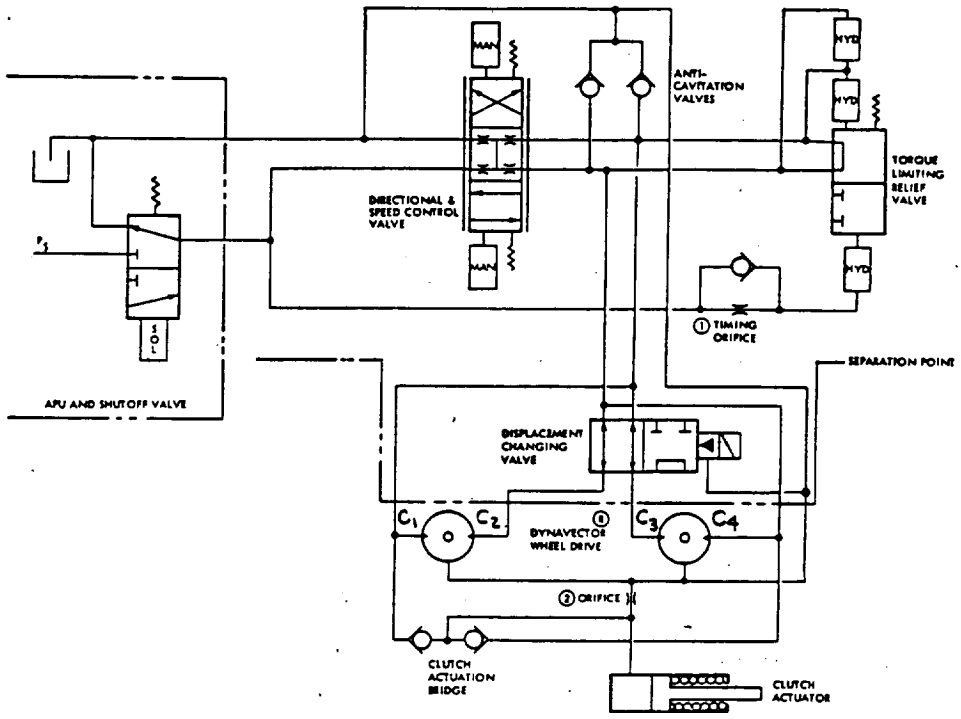


Figure B1. System Schematic

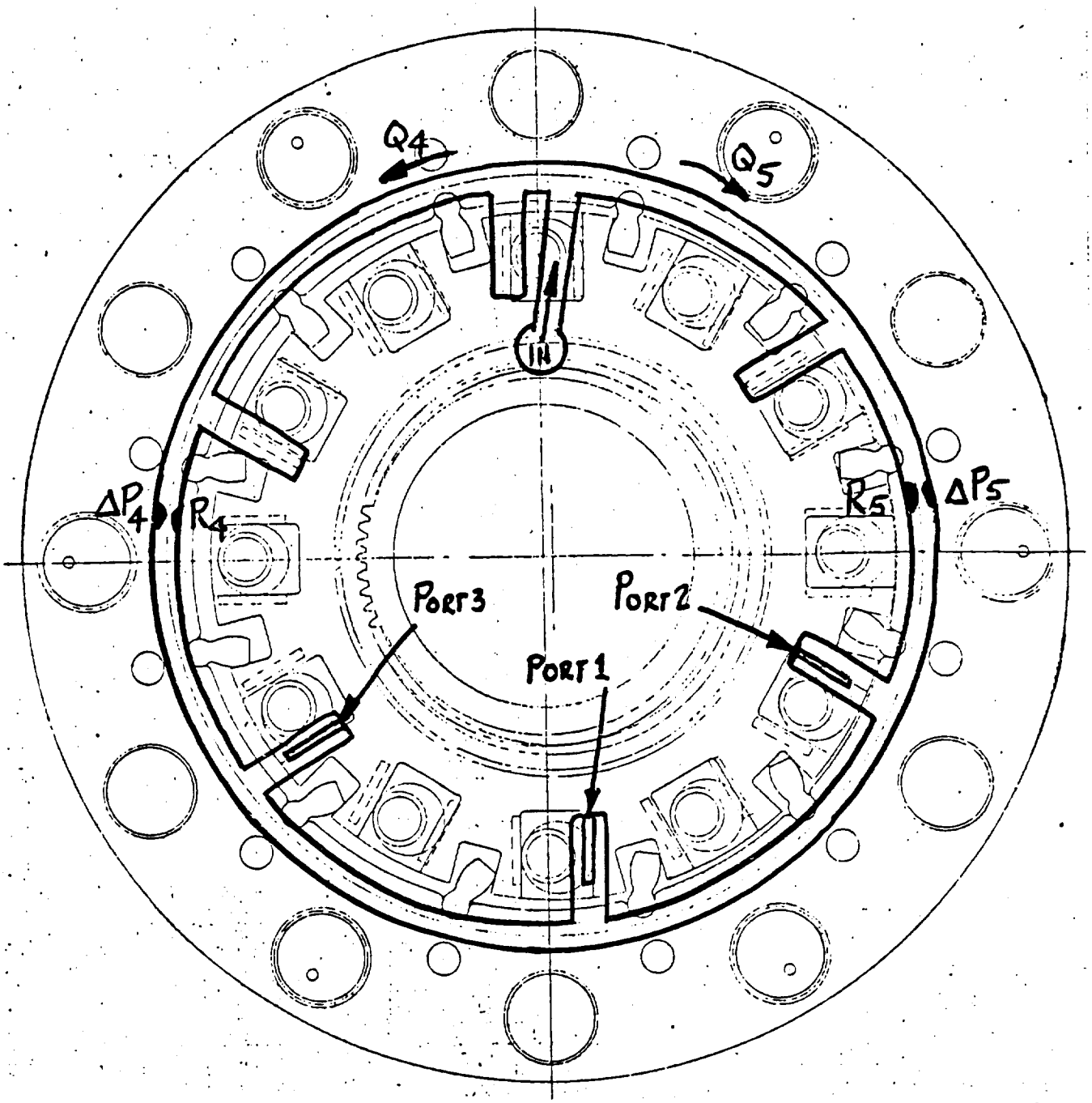


Figure B2

resistance each way from the entry point will obviously be equal so that the flow divides evenly for the most favorable pressure loss condition. However, a "worst case" condition must be considered.

Figure B3 assumes the flow entry point is very close (within 10 degrees) to Port 1. Now the flow distributes unevenly about the annulus. For this case, assume,

$$Q_{MAX} = Q_1 + Q_2 \quad (1)$$

$$Q_{MAX} = q_1 + q_2 + q_3 \quad (2)$$

Where:

$Q_{MAX}$ = Maximum Motor Flow

$Q_1$ = Maximum Annulus CW Flow

$Q_2$ = Maximum Annulus CCW Flow

$q_1$ = Maximum Port 1 Flow

$q_2$ = Maximum Port 2 Flow

$q_3$ = Maximum Port 3 Flow

Letting,

$$q_2 = q_3 \quad (3)$$

From (2)

$$q_1 = Q_{MAX} - 2\,q_2 \quad (4)$$

For a 12-chamber motor, the maximum chanber flow can be shown to be $.268\ Q_{MAX}$, which is equivalent to the two 6-chamber motors of this design. For the series mode motor configuration since the flow is doubled, the maximum chamber flow is doubled so that,

$$Q_1 = .536\ Q_{MAX} \quad (5)$$

Equating (4) and (5)

$$.536\ Q_{MAX} = Q_{MAX} - 2\,q_2 \quad (6)$$

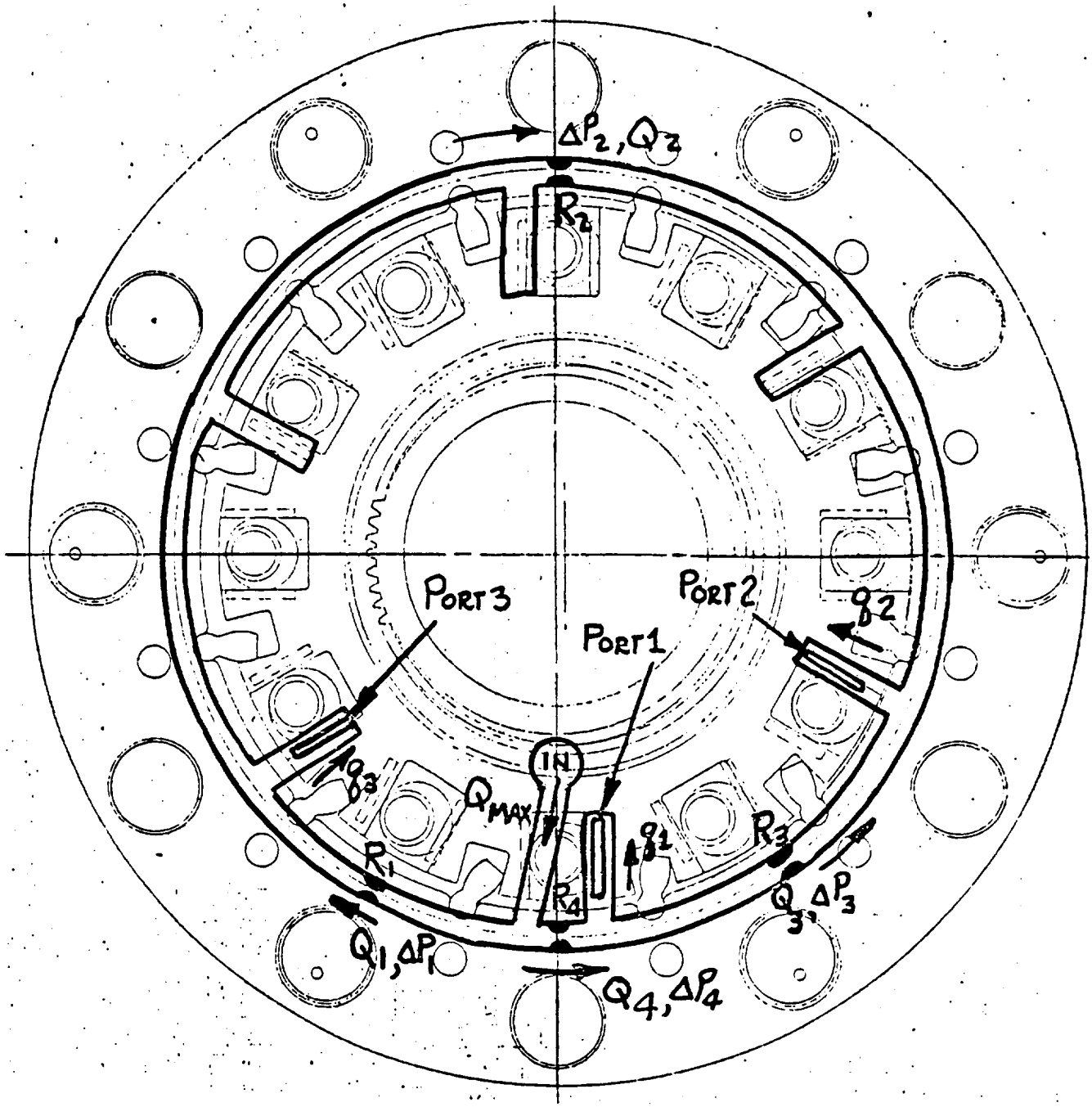
ΔP2, Q2
R2
PORT 3
PORT 2
PORT 1
Qb2
IN
Qb3
QMAX
Qb1
R1
R4
R3
Q3, ΔP3
Q1, ΔP1
Q4, ΔP4

Figure B3

from which

$$q_2 = .232\ Q_{MAX} \tag{7}$$

Normalizing $Q_{MAX}$ to 1,

$$q_1 = .536 \tag{8}$$

$$q_2 = .232 \tag{9}$$

$$q_3 = .232 \tag{10}$$

Since the summation of pressure losses around the annulus is zero,

$$P_1 + P_2 = P_3 + P_4 \tag{11}$$

and letting,

$$P = RQ^2$$

we can say,

$$P_1 = R_1 Q_1^2 \tag{12}$$

$$P_2 = R_2 Q_2^2 \tag{13}$$

$$P_3 = R_3 Q_3^2 \tag{14}$$

$$P_4 = R_4 Q_4^2 \tag{15}$$

From Figure B3, it is apparent that

$$Q_2 = Q_1 - q_3 = Q_1 - .232 \tag{16}$$

$$Q_3 = Q_4 - q_1 = Q_4 - .536 \tag{17}$$

Consequently, using (16) and (17) in (13) and (14) respectively,

$$\Delta P_2 = R_2 (Q_1 - .232)^2 \tag{18}$$

$$\Delta P_3 = R_3 (Q_4 - .536)^2 \tag{19}$$

Based on published data[1], the loss factor, K, for bends will be used for resistance values ($R_1$ through $R_4$) based on the assumed angle of flow change in the annulus, or

(1) Hydraulic and Pneumatic Power and Control, Franklin D. Yeaple

| Resistance | Angle | K Value |
|---|---|---|
| $R_1$ | $50^o$ | 0.40 |
| $R_2$ | $240^o$ | 2.79 |
| $R_3$ | $60^o$ | 0.55 |
| $R_4$ | $10^o$ | 0.04 |
| | $360^o$ | |

Using these values for R and substituting (12), (15), (18), and (19) in (11),

$$0.4\ Q_1^2 + 2.79\ (Q_1 - .232)^2 = 0.55\ (Q_4 - .536)^2 + 0.04\ Q_4^2 \qquad (20)$$

Expanding and collecting,

$$3.19\ Q_1^2 - 1.29\ Q_1 + .15 = .59\ Q_4^2 - .59\ Q_4 + .16 \qquad (21)$$

Since, by inspection of Figure D3,

$$Q_{MAX} = Q_1 + Q_4 = 1 \qquad (22)$$

$$Q_1 = 1 - Q_4 \qquad (23)$$

Substituting (23) in (21),

$$3.19 - 6.38\ Q_4 + 3.19\ Q_4^2 - 1.29 + 1.29\ Q_4 + .15 = .59 - 1.18\ Q_4 + .59\ Q_4^2 - .59\ Q_4 + .16$$

$$2.05 - 5.09\ Q_4 + 3.19\ Q_4^2 = .16 - .59\ Q_4 + .59\ Q_4^2$$

$$2.60\ Q_4^2 - 4.50\ Q_4 + 1.89 = 0$$

Solving for $Q_4$ by the quadratic equation,

$$Q_4 = .72$$

and from (23)

$$Q_1 = .28$$

Thus, the maximum annular flow is 72 percent of the maximum actuator flow, and the pressure loss will be determined accordingly.

3. PRESSURE LOSS EVALUATION

The pressure losses will be determined on the basis of the total resistance through one motor. Since the motor flow passages are essentially identical for both motors, this will facilitate determination of the pressure loss for both modes of operation, series and parallel. Figure B4 is a model representation of the flow passages through each motor.

Series Mode Operation

From Table B1, the summation of $\frac{K}{\left(\frac{A_{dn}\, Q_t}{Q}\right)^2}$ is 380.1 $in^{-4}$

Since this has been developed on the basis of one motor, it is then doubled for the series configuration since the flow passages are nearly identical. Therefore, for the total pressure loss,

$$\frac{K}{\left(\frac{A_{dn}\, Q_t}{Q}\right)^2} = 2\ (380.1) = 760.2 \qquad (24)$$

Since,

$$\Delta P_S = \frac{K\ Q_t^{\,2}\ \rho}{\left(\frac{A_{dn}\, Q_t}{Q}\right)^2\ 2g} \qquad (25)$$

Where:

$Q_t$ = 45 GPM (3.85) = 173.25 $IN^3/SEC.$

$\rho$ = MIL-H-5606 SPEC. WEIGHT = .031 $LB/IN^3$

$g$ = 386 $IN/SEC^2$

$$\Delta P_S = \frac{760.2\ (173.25)^2\ .031}{2\ (386)} = 916.3\ PSI$$

To this $\Delta P$ must be added the line loss for 4 lengths of tubing (10 ft. long each) between the DCV and the actuator. This loss was not considered in Table B1 since the resistances were considered as a series of equivalent orifices.

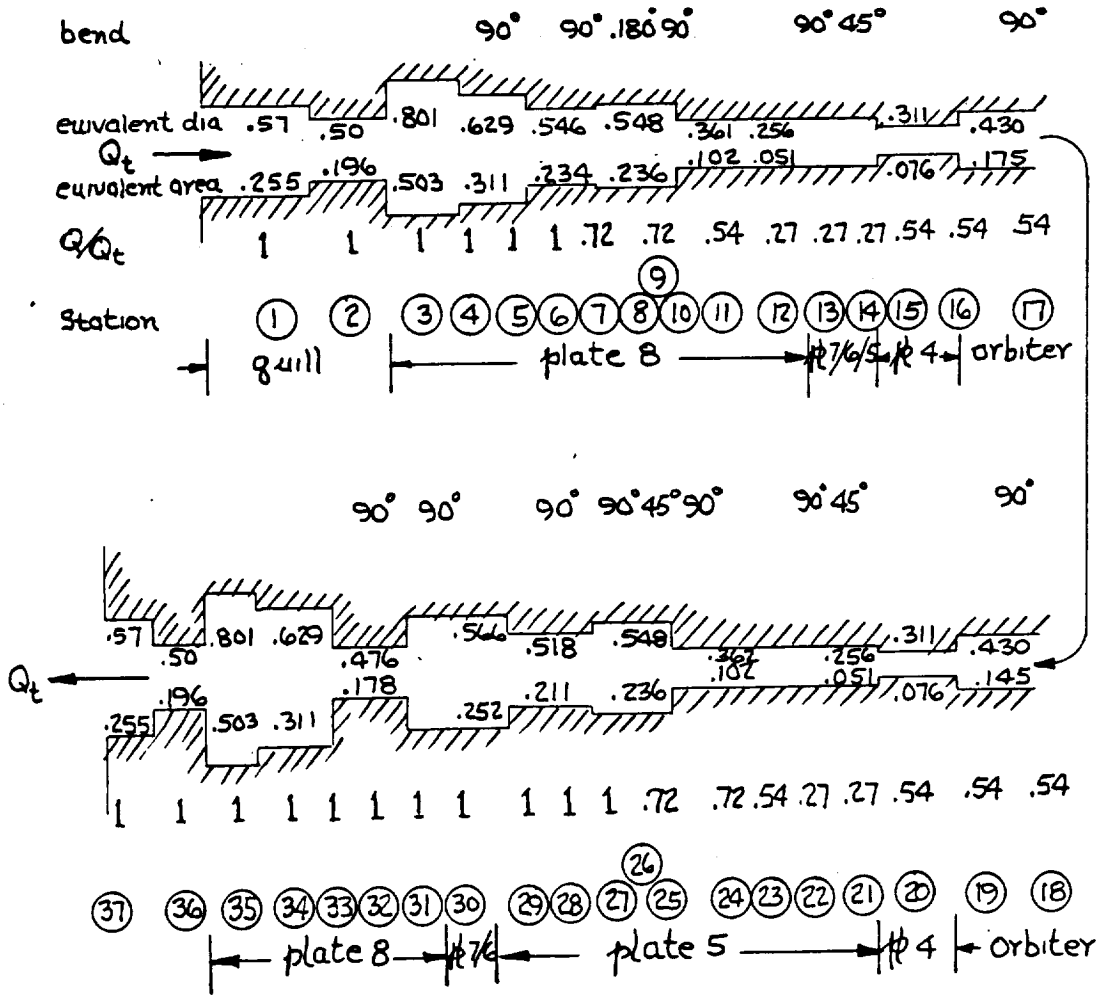


Figure B4. Flow Channel Model Through One Motor ($C_2/C_1$ Circuit Shown)

TABLE 3 $\left(\frac{\Sigma K}{\frac{A_{dn} Q_t}{Q}}\right)^2$ DETERMINATION FOR FLOW THROUGH ONE MOTOR ($C_2/C_1$ FLOW)

| Sta. No. | Resistance Type | Flow Ratio $Q/Q_t$ | (1) Area Ratio $A_{dn}/A$ up | Press. Loss Factor K | Downstream Velocity Ft/Sec | Area $A_{dn}$, $IN^2$ | $\left(\frac{A_{dn} Q_t}{Q}\right)^2$ | $\left(\frac{\Sigma K}{\frac{A_{dn} Q_t}{Q}}\right)^2$ |
|---|---|---|---|---|---|---|---|---|
| 1 | Contract. | 1 | 0 | .44 | 28.3 | .255 | .065 | 6.767 |
| 2 | Contract. | 1 | .769 | .07 | 36.8 | .196 | .038 | 1.822 |
| 3 | Expansion | 1 | .390 (1) | .40 | 28.7 | .503 | .253 | 1.581 |
| 4 | Contract. | 1 | .618 | .18 | 46.4 | .311 | .097 | 1.861 |
| 5 | 90° Bend | 1 | - | 1.2 | 61.7 | .311 | .055 | 21.818 |
| 6 | Contract. | 1 | .752 | .08 | 61.7 | .234 | .055 | 1.455 |
| 7 | 90° Bend | .72 | - | 1.1 | 61.2 | .234 | .107 | 10.238 |
| 8 | Expansion | .72 | .992 (1) | 0 | 61.2 | .236 | .107 | 0 |
| 9 | 180° Bend | .72 | - | .2 | 61.2 | .236 | .107 | 1.869 |
| 10 | 90° Bend | .54 | - | 1.2 | 82.9 | .177 | .030 | 39.602 |
| 11 | Contract. | .54 | .576 | .21 | 76.4 | .102 | .036 | 5.88 |
| 12 | Flow Divide | .27 | 1 | .26 | 76.4 | .051 | .036 | 0 |
| 13 | 90° Bend | .27 | - | 1.2 | 76.4 | .051 | .036 | 33.33 |
| 14 | 45° Bend | .27 | .745 | .50 | 101.8 | .051 | .020 | 25.00 |
| 15 | Contract. | .536 | .745 | .08 | 101.8 | .076 | .020 | 3.979 |
| 16 | Expansion | .536 | .524 (1) | .25 | 53.4 | .145 | .073 | 3.416 |
| 17 | 90° Bend | .536 | - | 1.2 | 53.4 | .145 | .073 | 16.438 |
| 18 | 90° Bend | .536 | - | 1.2 | 53.4 | .145 | .073 | 16.438 |
| 19 | Contract. | .54 | .524 | .25 | 102.5 | .076 | .020 | 12.621 |
| 20 | Expansion | .27 | .745 (1) | .08 | 76.4 | .051 | .036 | 2.22 |
| 21 | 45° Bend | .27 | 1.342 | .5 | 76.4 | .051 | .036 | 13.88 |

NOTE: (1) For expansions, the area ratio is $\frac{A \text{ up}}{A_{dn}}$

TABLE 3 $\left(\frac{\Sigma K}{\frac{A_{dn} Q_t}{Q}}\right)^2$ DETERMINATION FOR FLOW THROUGH ONE MOTOR ($C_2/C_1$ FLOW) (Continued)

| Sta. No. | Resistance Type | Flow Ratio $Q/Q_t$ | (1) Area Ratio $A_{dn}/Aup$ | Press. Loss Factor K | Downstream Velocity Ft/Sec | Downstream Area $A_{dn}$, $IN^2$ | $\left(\frac{A_{dn} Q_t}{Q}\right)^2$ | $\frac{\Sigma K}{\left(\frac{A_{dn} Q_t}{Q}\right)^2}$ |
|---|---|---|---|---|---|---|---|---|
| 22 | 90° Bend | .54 | 1.00 | 1.2 | 76.4 | .102 | .036 | 33.63 |
| 23 | 90° Bend | .72 | 1.74 | 1.2 | 44.0 | .236 | .107 | 11.169 |
| 24 | Expansion | .72 | .576 (1) | .21 | 44.0 | .235 | .107 | 1.963 |
| 25 | 45° Bend | .72 | - | .35 | 44.0 | .236 | .107 | 3.271 |
| .26 | 90° Bend | 1 | - | 1.2 | 68.4 | .211 | .045 | 26.954 |
| 27 | Contract. | 1 | .645 | .15 | 68.4 | .211 | .045 | 3.369 |
| 28 | 90° Bend | 1 | - | 1.2 | 57.3 | .252 | .064 | 18.896 |
| 29 | Expansion | 1 | .837 (1) | .03 | 57.3 | .252 | .064 | 0.472 |
| 30 | 90° Bend | 1 | - | 1.2 | 81.1 | .178 | .032 | 37.87 |
| 31 | Contract. | 1 | .706 | .10 | 81.1 | .178 | .032 | 3.16 |
| 32 | 90° Bend | 1 | - | 1.2 | 46.4 | .311 | .097 | 12.407 |
| 33 | Expansion | 1 | .572 (1) | .22 | 46.4 | .311 | .097 | 2.268 |
| 34 | Expansion | 1 | .618 (1) | .18 | 28.7 | .503 | .253 | 0.711 |
| 35 | Contract. | 1 | .390 | .31 | 73.7 | .196 | .038 | 1.628 |
| 36 | Expansion | 1 | .769 (1) | .07 | 56.6 | .255 | .065 | 1.077 |
| 37 | Expansion | 1 | .419 (1) | .37 | 23.7 | .609 | .371 | 0.998 |

$\Sigma$ = 380.1 $IN^{-4}$

(9.13 $cm^{-4}$)

For tubing loss,

$$\Delta P_{ls} = f \frac{L_s \rho V_s^2}{D\ 2\ g} \qquad (26)$$

Where:

$f$ = Surface Roughness Factor = .03

$L_s$ = Total Line Length = 40(12) = 480 IN

$V_s$ = Fluid Velocity

$= \frac{Q_t}{A} = \frac{45(3.85)}{} = 594.75$ IN/SEC.

$D$ = Tubing I.D. = 609 IN

$$\Delta P_{ls} = \frac{.03\ (480)\ .031\ (594.75)^2}{.609\ (2)\ 386} = 335.86 \text{ PSI}$$

The total pressure loss in the series mode is,

$$\Delta P_{ts} = \Delta P_s + \Delta P_{ls} = 1252 \text{ PSI} \qquad (27)$$

Parallel Mode Operation

For the parallel mode of motor operation, the summation of $\left(\frac{K}{\frac{A_{dn}\ Q_t}{Q}}\right)^2$

From Table B3 is 380.1 so

$$\Delta P_p = \frac{K\ \rho\ Q_p^2}{\left(\frac{A_{dn}\ Q_t}{Q}\right)^2\ 2\ g} \qquad (28)$$

Where:

$Q$ = 22.5 GPM (3.85) = 86.63 $IN^3$/SEC.

$$\Delta P_p = \frac{380.1\ (86.63)^2\ .031}{2\ (386)} = 114.5 \text{ PSI, or 1/8 the series mode P.}$$

The line loss through the tubing is now based on one-half the length of the series configuration, or for 20 feet, so

$$\Delta P_{lp} = f \frac{L_p \rho V_p^2}{D\ 2\ g} \qquad (29)$$

Where:

$L_p$ = Total Line Length = 20 (12) = 240 IN.

$V_p$ = Fluid Velocity

$$= \frac{Q_p}{A} = \frac{22.5\ (3.85)}{.2913} = 297.37 \text{ IN/SEC.}$$

$$\Delta P_{lp} = \frac{.03\ (240)\ .031\ (297.37)^2}{} = 41.98 \text{ PSI, or 1/8 the series } \Delta P.$$

Total parallel mode pressure loss,

$$\Delta P_{tp} = \Delta P_p + \Delta P_{lp} = 114.5 + 41.98 = 156.5 \text{ PSI}$$

Summarizing

In the series mode operation, total pressure loss at 45 GPM pump flow,

$$\Delta P_{ts} = k\, Q^2_{MAX} \qquad (30)$$

$$= .618\ (45)^2 = 1252 \text{ PSI}$$

and for parallel operation at 45 GPM pump flow,

$$\Delta P_{tp} = .077\ (45)^2 = 156.5 \text{ PSI}$$

# APPENDIX C

## DYNAMIC PERFORMANCE

## APPENDIX C

## DYNAMIC PERFORMANCE

### GENERAL

The dynamic performance of the motor consists of the static torque-speed curves applied to the aircraft in conjunction with the actuator inertia, oil volume under compression and the control valving. A full analysis of the Powered Wheel/Aircraft System shown in Figures C-1 and C-2 would require the use of a computer and considerable effort but it does not appear that this would be economically justified at this time. However, without the use of a computer, various natural frequencies can be determined and compared with known aircraft landing gear frequencies and some parameters evaluated, such as actuator spin-up time after clutch actuation, etc. The lowest order response can be found by elimination of all higher order dynamics and considering only the aircraft wheel inertia with the pilot's control valve in some steady state condition.

Therefore, the system block diagrams can be simplified greatly with the following assumptions:

$K_v = \infty$

$V_t = 0$

$J_t = 0$

$J_w = 0$

$K_L = \infty$

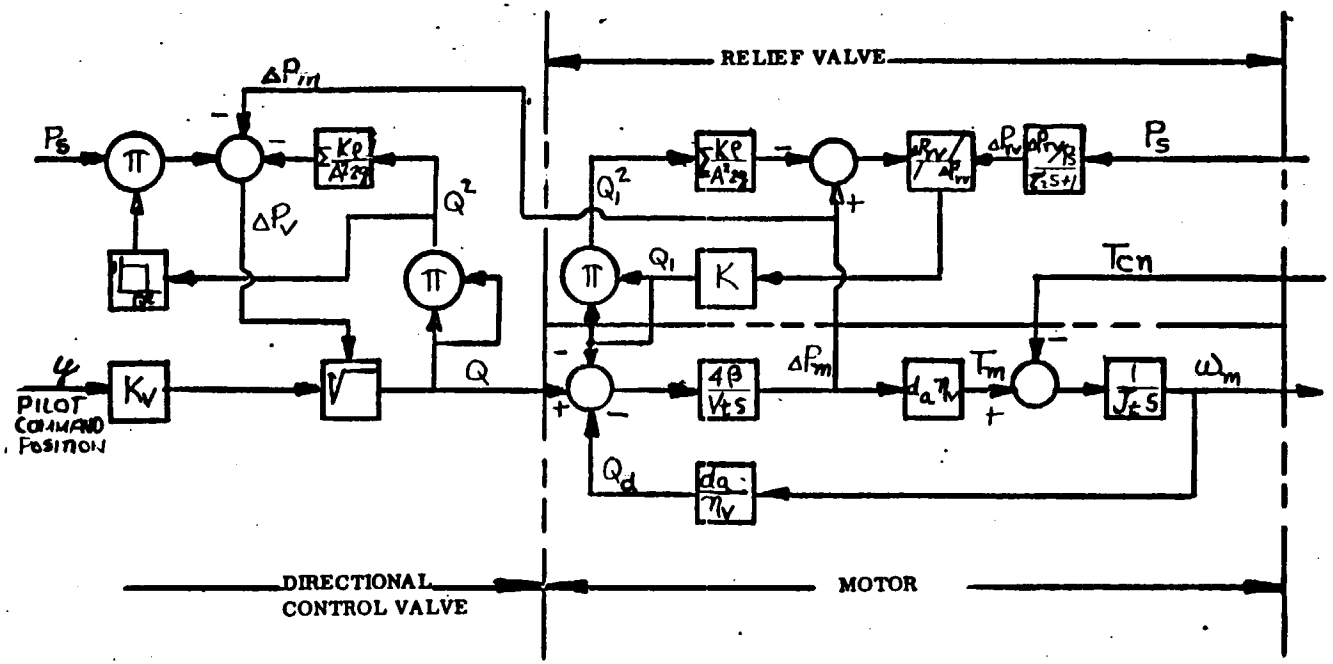


Figure C-1. Block Diagram - Directional Control Valve and Motor

(Ref.: Table C-1 for Symbology)

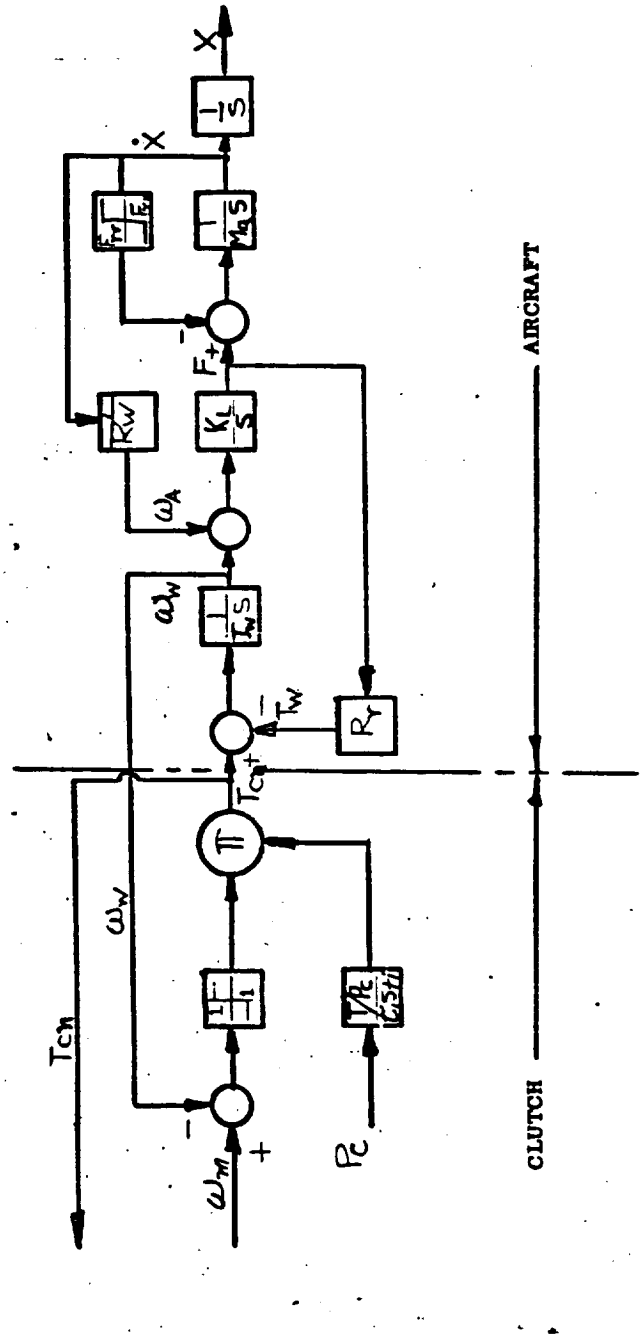


Figure C-2. Block Diagram - Clutch and Aircraft (Ref.: Table C-1 for Symbology)

TABLE C-1. BLOCK DIAGRAM SYMBOLOGY

| PARAMETER | DESCRIPTION |
|---|---|
| $d_a$ | Actuator Displacement in parallel or series mode |
| $F_m$ | Force Developed by Actuator |
| $F_{rr}$ | Rolling Resistance |
| g | Acceleration of Gravity |
| $J_t$ | Actuator Inertia (moving parts) |
| $J_w$ | Wheel Inertia |
| $K_v$ | Directional Valve Flow Gain |
| $M_a$ | Aircraft Mass |
| $P_s$ | Supply Pressure |
| Q | System Supply Flow |
| Q1 | Relief Valve Flow |
| $Q_d$ | Actuator Motor Flow |
| $R_r$ | Wheel Rolling Radius |
| $R_t$ | Transmission Ratio |
| S | Laplace Operator |
| $T_{cm}$ | Clutch Torque |
| $T_m$ | Motor Torque |
| $T_w$ | Wheel Torque |
| $V_t$ | Fluid Volume Under Compression |
| X | Aircraft Displacement |
| $\dot{X}$ | Aircraft Speed |
| $\beta$ | Fluid Bulk Modulus |
| $\Delta P_c$ | Clutch Piston Actuating Pressure |
| $\Delta P_m$ | Actuator Motor Differential Pressure |

TABLE C-1. BLOCK DIAGRAM SYMBOLOGY (Continued)

| PARAMETER | DESCRIPTION |
|---|---|
| $\Delta P_{rv}$ | Relief Valve Differential Pressure |
| $\Delta P_t$ | Total Flow Pressure Loss |
| $\Delta P_v$ | Directional Control Valve Differential Pressure |
| $\eta_T$ | Torque Efficiency |
| $\eta_v$ | Volumetric Efficiency |
| $\omega_A$ | Aircraft Angular Velocity |
| $\omega_m$ | Actuator Angular Velocity |
| $\omega_w$ | Wheel Angular Velocity |
| $\pi$ | Multiplier |
| $\rho$ | Fluid Specific Weight |
| $\Sigma\ K/A^2$ | Associated Velocity Head Loss and Area Ratio |
| $T_1$ | Clutch Piston Pressure Rise Time Constant |
| $T_2$ | Relief Valve Timing Orifice Time Constant |

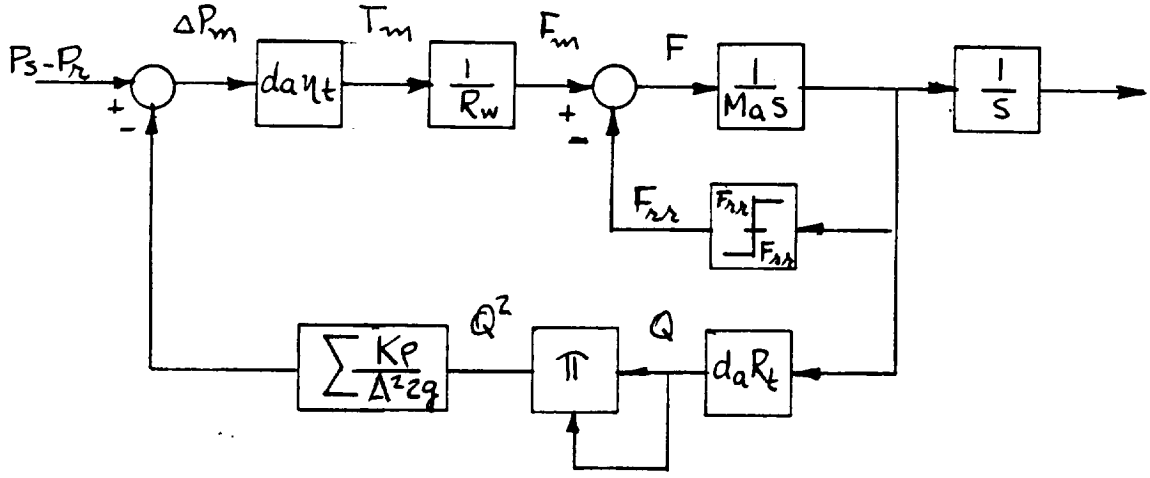


STATEMENT OF WORK TEST CONDITIONS

Before evaluating the accelerations associated with the five SOW test conditions (Appendix A), it is necessary to derive the acceleration equations for motoring and braking in both series and parallel modes of operation.

Since $F = Ma$ (1)

where from the block diagram above,

$F_m = (\Delta P_m \, d_a \, \eta_t / R_w) - F_{rr}$ Lbs. (2)

$\Delta P_m = P_s - \Delta P_t \; @ \; P_r = 0$ PSI (3)

$\Delta P_t = (\Sigma \, K\rho / A^2 \, 2 \, g) \, d_a \, R_t \, \dot{X})^2$ PSI (4)

$= (\Delta P_t)_{\dot{X}MAX} \, (\dot{X}/\dot{X} \text{ Max.})^2$ (5)

$\Delta P_t$ = Pressure Loss at $\dot{X}$ Max.

$\Delta P_{ts}$ = 1252 PSI at 22 Ft/Sec (Series

$\Delta P_{tp}$ = 156.5 PSI at 11 Ft/Sec (Parallel)

Ref. APPENDIX B

$M_a$ = One-half Aircraft Mass = 42,800/32.2 = 1,329.2 Lb-sec$^2$/ft

$F_{rr}$ = Resistance Force, Lb.

$a$ = Aircraft Acceleration = $dv/dt = \dot{X}\, d\dot{X}/dX$

$d_a \triangleq d_{as}/2\pi = 57.75/2\,\pi = 9.1912$ In$^3$/Rad. (Series)

$d_a \triangleq d_{ap}/2\pi = 115.2/2\,\pi = 18.3824$ (Parallel)

$\eta_t$ = .85 Torque Efficiency

$R_w$ = Wheel Radius = 16.48 In.

For the conditions of the actuator driving the wheel, the output force from equations (2) through (5) is for the series mode,

$$F_{ms} = \left[3900 - (1252/22^2)\,\dot{X}^2\right]\ 9.1912\ (.85)/16.48 - F_{rr} \qquad (6)$$

and from equations (1) and (6)

$$a_s = (1849 - 1.22\,\dot{X}^2 - F_{rr})/1329.2 \qquad (7)$$

For the parallel mode,

$$E_{mp} = (3900 - 156.5\dot{X}^2/11^2)18.3824(.85)/16.48 - F_{rr} \qquad (8)$$

$$a_p = (3698 - 1.22\,\dot{X}^2 - F_{rr})/1329.2 \qquad (9)$$

For the aircraft weight of 42,800 lbs.,

@ 2 percent Rolling Resistance

$F_{rr}$ = .02(42,800) = 856 Lbs.

@ 4 percent Rolling Resistance

$F_{rr}$ = .04(42,800) = 1712 Lbs.

Therefore, for the 4 motoring modes and resistance combinations derived from (7) and (9)

@ 2 percent Resistance

$$a_{s2} = .7471 - .000918\,\dot{X}^2 \qquad (10)$$

$$A_{p2} = 2.138 - .000918\,\dot{X}^2 \qquad (11)$$

@ 4 percent Resistance

$$a_{s4} = .1036 - .000918\,\dot{X}^2 \qquad (12)$$

$$a_{p4} = 1.4946 - .000918\,\dot{X}^2 \qquad (13)$$

For the conditions of the aircraft driving the actuator, or braking,

$$\Delta P_m = P_{rv} + \Delta P_t \quad (14)$$

where $P_{rv}$ = Relief Valve Setting = 4100 PSI

So for the series mode from (5) and (14)

$$\Delta P_m = 4100 + 1252/22^2 \dot{X}^2 \quad (15)$$

No consideration is given to the parallel mode during braking as it has been recommended in Appendix D, Section 3, that this condition be avoided to prevent overloading the shaft bearings.

The force developed,

$$F_{mb} = (\Delta P_m d_a/\eta_t R_w) + F \quad (16)$$

Consequently, from (15) and (16) at 2 percent resistance,

$$a_2 = 2.668 + .001277 \dot{X}^2 \quad (17)$$

At 4 percent resistance,

$$a_4 = 3.312 + .001277 \dot{X}^2 \quad (18)$$

So for,

Condition 1 - Brake to 0 mph from 15 mph (series mode and 2 percent resistance) from Eq. (17)

$$a_2 = d\dot{X}/d_t = 2.668 + .001277 \dot{X}^2 \quad (19)$$

Solving for $d_t$,

$$d_t = d\dot{X}/2.668 + .001277 \dot{X}^2 \quad (20)$$

Integrating,

$$\int dX/a + bX^2 = (1/\sqrt{ab}) \tan^{-1} X \sqrt{ab}/a \quad (21)$$

Substituting, (20) and (21)

$$t = \left[1/\sqrt{2.668\ (.001277)}\right] \tan^{-1} \dot{X} \sqrt{2.668(.001277)/2.668} \Big|_0^{22} \quad (22)$$

$$t = 7.68 \text{ Sec.}$$

From Eq. (17)

$$a_2 = \dot{X}\, d\dot{X}/dX = 2.668 + .001277 \dot{X}^2 \quad (23)$$

Solving for dX,

$$dX = \dot{dX}^2/2(2.668 + .001277\ \dot{X}^2) \quad (24)$$

Integrating,

$$\int dX/a + bX = 1/b\ \ln\ (a + bX\Big|_0^{22} \quad (25)$$

Substituting (24) into (25)

$$2X = 1/.001277\ \left|\ln\left[(2.668 + .001277(22)^2\right] - \ln\ 2.668\right| \quad (26)$$

$$X = 81.6\ \text{FT.}$$

Repeating condition 1 for 4 percent resistance, from Eq. (18)

$$a_4 = \dot{dX}/d_t = 3.312 + .001277\ \dot{X}^2 \quad (27)$$

Substituting a = 3.312 and b = .001277 and Eq. (27 into (21),

$$t = \left[1/\sqrt{3.312(.001277)}\right] \tan^{-1}\ \dot{X}\sqrt{3.312(.001277)/3.312}\Big|_0^{22} \quad (28)$$

$$t = 6.27\ \text{Sec.}$$

From Eq. (27)

$$\dot{dX}/d_t = \dot{X}\ \dot{dX}/dX = 3.312 + .001277\ \dot{X}^2 \quad (29)$$

Then substituting a = 3.312 and b = .001277 and Eq. (29) into (25),

$$X = 1/2(.001277)\ \left|\ \ln\ \left[3.312 + .001277\ (22)^2\right] - \ln\ 3.312\right| \quad (30)$$

$$X = 67.01\ \text{FT.}$$

For Condition 2 - Accelerate to 7.5 mph from 0 mph (Parallel mode and 2 percent Resistance)

From Eq. (11)

$$a_{p2} = \dot{dX}/d_t = 2.138 - .000918\ \dot{X}^2 \quad (31)$$

Solving for $d_t$,

$$d_t = \dot{dX}/2.138 - .000918\ \dot{X}^2 \quad (32)$$

Integrating,

$$\int dX/a + bX^2 = (1/2\sqrt{ab})\ \ln(a + X\sqrt{ab}\ /\ a - X\sqrt{a\ b}) \quad (33)$$

Substituting a = 2.138, b = .000918 and (32) and (33)

$$t = (1/2\sqrt{2.138(.000918)}\ \ln \frac{2.138 + \dot{X}\sqrt{2.138(.000918)}}{2.138 - \dot{X}\sqrt{2.138(.000918)}}\Bigg|_0^{11} \quad (34)$$

$t = 5.20$ Sec.

From Eq. (11),

$$a_{p2} = \dot{X}\, d\dot{X}/dX = 2.138 - .000918\ \dot{X}^2 \quad (35)$$

Solving for dX,

$$dX = d\dot{X}^2/s\ (2.138 - .000918\ \dot{X}^2) \quad (36)$$

Integrating and substituting a = 2.138, b = .000918 and Eq. (36)

$$X = \left[1/2\ (-.000918)\right] \ln (2.138 - .000918\ \dot{X}^2) - \ln 2.13\Big|_0^{11} \quad (37)$$

$X = 29.9$ FT.

Repeating Condition 2 for 4 percent resistance from Eq. (13)

$$a_{p4} = d\dot{X}/d_t = 1.4946 - .000918\ \dot{X}^2 \quad (38)$$

Solving for $d_t$,

$$d_t = dX/(1.4946 - .000918\ \dot{X}^2) \quad (39)$$

Integrating and substituting a = 1.4946, b = .000918 and Eq. (39)

$$t = \left[1/2\sqrt{1.4946(.000918)}\right] \ln \frac{1.4946 + \dot{X}\sqrt{1.4946(.000918)}}{1.4946 - \dot{X}\sqrt{1.4946(.000918)}}^{11}_{0} \quad (40)$$

$t = 7.55$ Sec.

From Eq. (13)

$$a_{p4} = \dot{X}\, d\dot{X}/dX = 1.4946 - .000918\ \dot{X}^2 \quad (41)$$

Solving for dX,

$$dX = d\dot{X}^2/2\ (1.4946 - .000918\ \dot{X}^2) \quad (42)$$

Integrating and substituting a = 1.4946, b = .000918 and Eq. (42)

$$X = \left[1/2\ (.000918)\right] \ln 1.4946 - \ln \left[1.4946 - .000918\ (11)^2\right]$$

$X = 42.09$ FT.

For Condition 3 - Accelerate to 15 mph from 7.5 mph (series mode and 2 percent resistance)

From EQ. (10)

$$a_{s2} = d\dot{X}/d_t = .7471 - .000918\ \dot{X}^2$$

Solving for $d_t$

$$d_t = d\dot{X}/(.7471 - .000918\ \dot{X}^2 \qquad (43)$$

Integrating and substituting a = .7471, b = .000918 and Eq. (43)

$$t = \frac{1}{2\sqrt{.7471(.000918)}}\left(\ln\frac{.7471 + 22\sqrt{.7471(.000918)}}{.7471 - 22\sqrt{.7471(.000918)}} - \ln\frac{.7471 + 11\sqrt{.7471(.000918)}}{.7471 - 11\sqrt{.7471(.000918)}}\right) \qquad (44)$$

$$t = 23.50 \text{ Sec.}$$

From Eq. (10)

$$a_{s2} = \dot{X}\, d\dot{X}/dX = 7471 - .000918\ \dot{X}^2 \qquad (45)$$

Solving dX

$$dX = d\dot{X}^2/2(.7471 - .000918\ \dot{X}^2) \qquad (46)$$

Integrating and substituting a = .7471, b = .000918 and Eq. (46)

$$X = 1/2(.000918)\left|\ \ln\left[.7471 - .000918\ (11)^2\right] - \ln\left[.7471 - .000918\ (22)^2\right]\right|$$

$$X = 404.2 \text{ FT.}$$

Repeating condition 3 for 4 percent resistance from Eq. (12)

Distance required to travel, assuming actuator torque saturation and maximum speed of 15 mph cannot be attained.

$$X = 2.5\ (5280) - 42.1 = 13\ 158 \text{ FT.}$$

From Eq. (12)

$$a_{s4} = \dot{X}\, d\dot{X}/dX = 1036 - .000918\ \dot{X}^2 \qquad (47)$$

Solving for dX

$$dX = d\dot{X}^2/2\ (.1036 - .000918\ \dot{X}^2) \qquad (48)$$

Integrating and substituting a = .1036, b = .000918

$$X = 13{,}158 \text{ and Eq. (48)}$$

$$X = \left[1/2(.000918)\right]\ \ln\left[.1036 - .000918\ (11^2)\right] - (.1036 - .000918\ X^2)$$

$$13{,}158(2)\ .000918 = \ln\left[.1036 - .000918\ (11^2)\right] - \ln\ (.1036 - .000918\ X^2)$$

$$24.1581 = \ln(-0.007478) - \ln(.1036 - .000918\ \dot{X}^2)$$

Since a logarithm of a minus number doesn't exist, the minus value of the first term of the right side of the equation indicates that 11 FT/SEC cannot be attained at 4 percent rolling resistance. So assuming torque saturation occurs after shifting to the series mode, wheel speed will fall below 11 FT/SEC.

Letting

$$a_{s4} = \frac{d\dot{X}}{d_t} = .1036 - .000918\ \dot{X}^2 = 0$$

$$\dot{X}^2 = \frac{.1036}{.000918}$$

$$\dot{X} = 10.62 \text{ FT/SEC}$$

The time to travel the remaining distance is then equal to,

$$t = \frac{13158}{10.62} = 1239 \text{ Sec.}$$

A summary of the times and distances to attain the various conditions are as shown below

| Cond. No. | Required | Rolling Resistance % | Operating Mode | Time Req'd. Sec. | Distance Req'd. Ft. |
|---|---|---|---|---|---|
| 1 | braking from 15 mph to 0 mph | 2 | series | 7.68 | 81.6 |
| 2 | accelerate to 7.5 mph from 0 mph | 2 | parallel | 5.20 | 29.9 |
| 3 | accelerate to 15 mph from 7.5 mph | 2 | series | 23.50 | 404.2 |
| 1 | braking from 15 mph to 0 mph | 4 | series | 6.27 | 67.0 |
| 2 | accelerate to 7.5 mph from 0 mph | 4 | parallel | 7.55 | 42.1 |
| 3 | accelerate to 15 mph from 0 mph | 4 | series | * | * |

* Condition cannot be met as torque saturation occurs which limits the speed to approximately 7.2 mph.

Motor Inertia and Clutch Spin-up Loads

The inertia of the DYNAVECTOR Motor is very small even though the orbiter mass is large because the orbiter does not rotate but orbits in a circle of very small radius, which is the eccentricity, e. Therefore,

$$J_{or} = (W_{or}/g)e^2 \text{ Lb.-In.-Sec.}^2 \quad (51)$$

where:

$W_{or}$ = Orbiter and Ring Gear Weight = 9.49 Lbs.

$g$ = 386 In/Sec$^2$

$e$ = .09375 In.

$$J_{or} = (9.49/386)(.09375)^2 = .0002161 \text{ Lb.-IN.-Sec.}^2$$

$J_{or}$ reflected to the output is multipled by the transmission ratio squared, or,

$$J_o = J_{or} R_t^2 \quad (52)$$

$$J_o = .0002161\ (22.67)^2 = .1111 \text{ Lb.-In.-Sec.}^2$$

The inertia of the output shaft,

$$J_s = (W_s/g)\ \bar{R}_s^2 \quad (53)$$

where: $W_s$ = Output Shaft Weight = 8.10 Lbs.

$\bar{R}_s$ = Average Shaft Radius = 1.9 In.

$$J_s = 8.10/386\ (1.9)^2 = 0.0758 \text{ Lb.-In.-Sec.}^2$$

The inertia of the clutch drive plate and two rotor discs,

$$J_c = (W_c/2g)\ R_c^2 + r_c^2 \quad (54)$$

where: $W_c$ = Combined weight of drive plate and 2 discs

= 7.60 + 3.5 (26,94) = 23.76 Lbs.

$R_c$ = Outer Radius of discs = 6.3 In.

$r_c$ = Inner Radius of Drive Plate = 2.0 In.

$$J_c = \left[23.76/2(386)\right] (6.3^2 + 2.0^2) = 1.3447 \text{ Lb.-In.-Sec.}^2$$

Therefore total motor inertia at the output,

$$J_t = J_o + J_s + J_c = .1111 + .0758 + 1.3447 = 1.5316 \text{ Lb-IN-Sec}^2 \quad (55)$$

The actuator spin-up acceleration with no pressure differential applied to the motor (bypass load limiting valve in the bypass mode and the directional control valve in neutral) is,

$$\alpha = T_{cn}/J_t \quad (56)$$

Where $T_{cn}$ = 44,744 Lb-In from Appendix D

$$\alpha = 44,744/1.5316 = 29,213.89 \text{ Rad/Sec}^2$$

The time to reach maximum speed of 15 mph,

$$t = \omega / \alpha \quad (57)$$

$$= 16.02 \text{ Rad/Sec}/29,213.89 \text{ Rad/Sec}^2 = .00055 \text{ Sec.}$$

This exceedingly small amount of time due to low inertia suggests that the full clutch torque will not be applied while slipping since it is highly unlikely that the clutch piston pressure can respond that quickly.

Assuming a time constant for the piston pressure rise of .050 second, clutch torque is,

$$T_c = T_{cn} (1 - e^{-t/T}) \quad (58)$$

$$= 44,744 (1 - e^{-t/.050})$$

$$= (T_c - T_m)/J_t = d\omega/dt$$

$$d\omega/dt = [44,744(1 - e^{-t/.050}) - 0] /1.5316 \quad (59)$$

$$d\omega/dt = 29213.89 - 29213.89 e^{-t/.050}$$

Solving for $d\omega$,

$$d\omega = (29213.89 - 29213.89 e^{-t/.05})dt$$

and

$$\omega = 29213.89 t - 29213.89 (.05) (1 - e^{-t/.05})$$

For $\omega$ = 16.02 Rad/Sec.

$$t = .00758 \text{ Sec.}$$

Therefore the maximum torque developed in time, t, = .00758 sec.,

$$T_c = 44{,}744\ (1 - e^{-.00758/.050}) = 6{,}294 \text{ Lb-In.}$$

Of this amount of torque, the amount that loads the output shaft bearings is in proportion to the ratio of the orbiter and ring gear inertia (at the output) to the total actuator inertia, or

$$T_{cb} = (J_o/J_t)\ T_c \qquad (60)$$

$$= (.1111/1.5316)\ (6294) = 457 \text{ Lb-In.}$$

Actuator Natural Frequency

The natural frequency of the actuator and wheel,

$$\omega_n = \sqrt{K_h\ K_s/(K_h + K_s)\ (J_w + J_t)} \qquad (61)$$

where: $K_h$ = Hydraulic Spring Rate, LB-IN/RAD

$K_s$ = Output Shaft Spring Rate, LB-IN/RAD

$J_t$ = Inertia of Wheel, Lb-In-Sec$^2$

Because of the very large oil volume associated with the displacement changing valve and fluid lines, $K_s$ will be very large with respect to $K_h$, so let $K_s = \infty$. Also because wheel inertia is so large in comparison to $J_t$, EQ. (61) becomes,

$$\omega_n = \sqrt{K_h/J_t} \qquad (62)$$

Since,

$$K_h = 4\beta\ d_m{}^2/V_t \qquad (63)$$

where: $\beta$ = Fluid Bulk Modulus = 100,000 PSI

$d_m$ = d'a/2 $\pi$ = 57.75/2 $\pi$ = 9.19 In$^3$/Rad

$V_t$ = 231 IN$^3$

$$K_h = 4(100{,}000)9.19^2/231 = 146{,}244 \text{ Lb-In/Rad.}$$

and letting $J_w$ = 84 Lb.-In.-Sec.$^2$

(Based on skid control experience with the 737 aircraft) from Eq. (62),

$\omega_n$ = 146,244/84 = 41.725 Rad/Sec

Or 6.64 Hz

This frequency is about the same as that normally attributed to aircraft landing gears based on Bendix's experience, so it seems that some coupling could occur with a resultant gear oscillation. However, since the torque generated is so small compared to the typical brake torque, oscillation would be small in magnitude. In addition, it is anticipated that for installation on the 737, the oil volume could be reduced to 40 percent of the 231 $In^3$ estimated for dynamometer testing by eliminating 20 feet of .75 diameter tubing and using a much smaller displacement changing valve. This smaller volume (92.4 $In^3$) would increase the natural frequency to 10.50 Hertz. This is still quite near the normal gear frequencies, so assuming that a further oil volume reduction to 30 $In^3$ can be achieved by packaging the displacement changing valve and relief valves together, the natural frequency would increase to 18.43 Hertz, which should be sufficiently high to preclude any noticeable coupling effects on the 737 landing gear.

In summary based on a simplified dynamic model of the Powered Wheel Actuator - Wheel - Aircraft System, the lowest order dynamics indicates that no significant coupling of the actuator dynamics (during braking) with landing gear dynamics should occur. The analysis does indicate that a reasonable effort should be made to reduce the volume of oil under compression in the plumbing to a minimum to separate actuator and landing gear natural frequencies.

# APPENDIX D

## CLUTCH TORQUE CAPABILITY

## APPENDIX D

## CLUTCH TORQUE CAPABILITY

### 1. CLUTCH TORQUE

The force exerted by the clutch actuating pistons,

$$F_c = n A_p \Delta P_c \quad (1)$$

Where: $A_p$ = Clutch Piston Area = .540 $IN^2$

$\Delta P_c$ = Clutch Actuation Pressure

(The highest of the two motor inlet absolute pressures minus atmospheric pressure or gage pressure), PSIG.

$n$ = Number of Clutch Pistons = 6

At no load, assuming equal pressure loss from supply pressure to the inlet cylinder pressure and return cylinder pressure to return pressure, the $\Delta P$ in equation (1) will be one-half of supply pressure so that,

$$F_c = 6\ (.504)\ 4000/2 = 6048 \text{ Lbs.}$$

With four clutch friction surfaces (3 Stator Discs and 2 Rotor Discs), the torque developed by the clutch,

$$T_c = F_c \bar{R} f n_s \quad (2)$$

Where: $\bar{R}$ = Clutch Average Radius, In.

$$= \sqrt{\frac{R_o^2 + R_i^2}{2}}$$

$f$ = Coefficient of Friction (Dry)

$n_s$ = Number of friction surfaces = 4

$$T_c = 6048 \sqrt{(6.3^2 + 4.02^2)/2} \quad .35\ (4) = 44744 \text{ LB-IN}$$

This is the torque exerted by the wheel to spin up the motor during braking.

The maximum clutch torque is produced during braking when the maximum load $\Delta P$ (series mode) is applied. This pressure differential is 5352 PSID (4100 relief valve setting and 1252 line loss) occurring at 15 mph braking. Therefore,

$$T_{cMAX} = T_c \ \Delta P_{cMAX} / \Delta P_c \qquad (3)$$

$$= 44{,}744\ (5252/2000) = 119736\ \text{LB-IN.}$$

At stall torque, the $\Delta P_c$ is 4000 PSID Max., and

$$T_{cs} = 44{,}744\ (4000/2000) = 89{,}488\ \text{LB-IN.}$$

This is a margin over the required 57,000 LB-IN of,

$$(1 - 89{,}488/57{,}000)\ 100 = 57\%$$

or, the coefficient can be less than the .35 assumed and still be all right. The lower value can be,

$$f = .35/1.57 = .22$$

2. CLUTCH DISC CONTACT PRESSURE

The maximum disc contact pressure, which will occur in braking at 15 mph is,

$$P_{cc} = F_c/A_c \qquad (4)$$

Where: $A_c$ = Clutch Contact Area

$$= \pi (R_o^2 - R_i^2)$$

$$P_{cc} = \frac{n\ A_p\ \Delta P_c}{\pi (R_o^2 - R_i^2)} = \frac{6\ (.504)\ 5352}{(6.3^2 - 4.02^2)}$$

$$= 219\ \text{PSI}$$

This is 55 percent of that recommended by the manufacturer as a maximum.

3. MAXIMUM CLUTCH TORQUE CAPABILITY IMPACT ON THE ACTUATOR BEARINGS

If the motors are connected in the parallel mode during landing, then at 15 mph braking, each of the two motors will produce 45 GPM for a total of 90 GPM. From equation (30), Appendix B, the line loss developed is,

$$\Delta P_p = .0773\ (90)^2 = 626\ \text{PSI}$$

To this, add the relief valve pressure of 4100 to attain the torque resisting $\Delta P$ of 4726 PSI. Then, as shown in the bearing analysis,

$$F_o = 8.62\ \Delta P = 8.62\ (4726) = 40{,}738 \text{ Lbs.}$$

Also from the same bearing analysis

$$F_{B1} = .526\ F_o = .526\ (40738) = 21{,}428 \text{ Lbs.}$$

With a static rating of 18,299 lbs. for INA BRG NK 105/26, the

$$\text{Static Ratio} = \frac{21{,}428}{18{,}299} = 1.1$$

or the bearing would be 17 percent overloaded. While this would not result in a catastrophic failure, it probably would shorten the bearing life. To prevent this condition from ever being realized, it is possible and desirable to prevent actuation of the wheel drive actuator during landing with the motors connected in parallel. During dynamometer testing, this can be accomplished by the operating procedure, and during flight test, it would have to be insured by pilot procedure, or automatic switch sequencing from the landing gear operation.

Similarly for the INA Bearing NK 95/26,

$$F_{B2} = .474\ F_o = 19{,}310 \text{ Lbs.}$$

Therefore, the Static Ratio = 19,310/16,315 = 1.18

4. MAXIMUM CLUTCH ACTUATING FORCE

The maximum peak force developed by the six pistons to actuate the clutch will occur in the braking mode in series operation (assuming parallel mode operation is not possible). The differential pressure developed is,

$$P_{cMAX} = P_{rv} + .90\Delta P_{ts}$$

where: $P_{rv}$ = Relief Valve Setting = 4100 PSIG

$\Delta P_{ts}$ = Series Mode Press. Loss; Eq. (27) Appendix B

= 1252 PSI

$$P_{cMAX} = 4100 + .90\ (1252) = 5{,}227$$

and from Eq. (1),

$$F_{cMAX} = 6(.504)\ 5227 = 15{,}806 \text{ Lbs.}$$

## 5. CLUTCH ELEMENT STRENGTH

Considering the case of the maximum stall torque developed, $T_{MAX}$, using an allowable bearing stress of 200,000 PSI for the AMS 4130 clutch plate material, the safety factor in bearing for the driving keys of the two DYNAVECTOR driven clutch plates is,

$$SF = \sigma_{ab}\ 2\ R_i\ N_k\ A_{b1}/T_{MAX}$$

where: $N_k$ = Number of driving keys in each plate = 6

$A_{b1}$ = Key bearing area = .25 X .25 = .0625 $IN^2$

$\sigma_{ab}$ = Allowable bearing stress = 200,000 PSI

$$SF = 200{,}000\ (2)\ 4.02\ (6)\ .0625/57{,}000 = 10.6$$

For the middle, wheel driven clutch plate which absorbs half of the torque,

$$SF = \sigma_{ab}\ 2\ R_r\ N_k\ A_{b2}/T_{MAX}$$

Where: $R_r$ = Radius of rim driving keys = 6.63 In.

$A_{b2}$ = Key bearing area = .1 X .25 = .025 $IN.^2$

$$SF = 200{,}000\ (2)\ 6.63\ (6)\ .025/57{,}000 = 7.0$$

Since the inboard and outboard clutch plates absorb only half the torque imposed on the middle plate, the safety factor is doubled to 14.0.

The 4-3/8 diameter bolts attaching the outboard clutch plate to the wheel are conservatively stressed in shear with a magnitude

$$\sigma_s = T/4\ R_b\ N_b\ A_s$$

where: $R_b$ = Radius of bolt location = 5.34 In.

$N_b$ = Number of bolts = 4

$A_s$ = 3/8 - 16 UNC3A bolt shear area

= .6190 $In^2$

$$\sigma_s = 57{,}000/4(5.34)\ 4(.6190) = 1078\ PSI$$

# APPENDIX E

# THERMAL ANALYSIS

## APPENDIX E

## THERMAL ANALYSIS

This analysis is concerned with the conditions to be encountered during dynamometer testing of the wheel drive actuator in order to evaluate the maximum fluid temperature that will be generated during the SOW test cycle (Ref. Appendix A) and to indicate the fluid power system cooling capacity required.

The major assumption is that heat is generated through an adiabatic change from work accomplished, i.e. that all heat is carried away from the Dynavector by the oil. For the test, this should be a conservative assumption. For flight testing, a more comprehensive heat transfer analysis will be required to evaluate the effect of structural heating that may occur from the aircraft brakes during landing.

In general, the heat generated by the system is given as,

$$q = \frac{(P_s Q - T\omega)}{155.5} \quad \text{Btu/min} \qquad (1)$$

where: $P_s$ = Supply Pressure, PSI

$Q$ = System Flow, $In^3/Sec$

$T$ = Motor Torque, Lb-In.

$\omega$ = Motor Output Speed, Rad/Sec.

For 2 Percent Rolling Resistance

Condition 1 - Brake to 0 mph from 15 mph (Series Mode)

The direction - speed control valve spool is centered by pilot command and it is assumed that,

Average Motor Torque = $d_a \Delta P_m / 2\pi \eta_t$ = 48,847 Lb-In.*

Average Motor Speed = 76.5 RPM

Average Supply Flow Mixed with Recirc. Flow = 5 GPM

*Based on $\Delta P_m$ equal to the relief valve setting (4100 psig) plus the average line loss ($\Delta P_{tsmax}/3$ = 417 PSI).

From EQ (1)

$$q = \frac{4000\ (5)\ 3.85 + 48847\ (76.5)\ 2\ \pi\ /60}{155.5} = 3012 \text{ Btu/min}$$

This condition pursuant to Appendix C lasts for 7.68 seconds, therefore the input heat,

$$H = qt = (3012)\ 7.68/60 = 385.5 \text{ Btu}$$

The differential equation for this condition (assuming adiabatic change), based on,

Heat In = Heat Out + Heat Stored is,

$$q_{in} = Q\gamma\ C\ \Delta T + V_t \gamma\ C\ d\ \Delta T/dt \qquad (2)$$

where: $Q$ = Supply Make-up Flow, GPM

$\gamma$ = Weight Density, Lb/Gal.

$C$ = Specific Heat, Btu/Lb/$^{o}$F

$V_t$ = Total Fluid Volume, Gal.

$\Delta T$ = Temp. Rise Above Inlet Temp., $^{o}$F

$t$ = Total Time at Specific Condition, Sec.

Separating variables, and solving for dt,

$$dt = V_t\ \gamma C\ \ d\Delta T/(q - Q\ \gamma C \Delta\ T) \qquad (3)$$

Integrating,

$$t = V_t\ \gamma C \left| - 1/Q\gamma C \left[1n\ (q - Q\ \gamma C\ \Delta T\right]\right|_0^T \qquad (4)$$

Substituting

$t$ = 7.68/60 = .128 Min.

$V_t$ = Motor Vol + Line and Valve Vol = 25 + 206 = 231 $in^3$ = 1 Gal

$\gamma$ = 7.09 Lb/Gal for MIL-H-5606B

$C$ = 0.5 Btu/Lb/$^{o}$F, MIL-H-5606B

$Q$ = 5 GPM

and solving for $\Delta T$,

$$.128 = 3.545 \left| - 1 / 17.73 \left[ 1n (3012 - 17.73\ \Delta T) \right] \right|_0^T$$

$$.128 = .2 \left[ 1_n\ 3012 - 1_n\ (3012 - 17.73\ \Delta T) \right]$$

$$.640 = 1n\ 3012 - 1n\ (3012 - 17.73\ \Delta T)$$

$$7.370 = 1n\ (3012 - 17.73\ \Delta T)$$

$$1588.20 = 3012 - 17.73\ \Delta T$$

$$\Delta T = 80.30^{\circ}F \text{ Rise Above Inlet Temperature}$$

Condition 2 - Accelerate to 7.5 mph from 0 mph (Parallel Mode)

From Equation (1) with average torque and pressure and flows and velocities as a function of time,

$$q = (4000\ Q - 57{,}000\ \omega) / 155.5 \qquad (5)$$

where: $Qt/t = 45\ GPM\ (3.85)\ t / 5.20\ Sec/60\ Sec/Min = 2010t$

$$\omega t/t = \frac{76.5\ RPM\ (2\pi\ Rad/Rev)t}{60\ Sec/Min\ (5.20\ Sec)/60\ Sec/Min} = 92.44\ t$$

$$q = \left[ 4000\ (2010\ t) - 57{,}000\ (92.44\ t) \right] / 155.5 = 17{,}819\ t$$

Substituting into Equation (2),

$$17{,}819\ t = 2010\ t \gamma C\ \Delta T + V \gamma C\ d\ \Delta T/d_t$$

Collecting terms,

$$17{,}819\ t - 2010 \gamma C\ \Delta T\ t = V \gamma C\ d\ \Delta T/d_t$$

and,

$$t\ dt = V_t \gamma C\ d\ \Delta T/(17{,}819 - 2010 \gamma C\ \Delta T)$$

Using the same values for $\gamma$, C and T as in condition 1, and integrating,

$$\int_0^t t\ d\ t = 3.545 \left| - 1/7125 \left[ 1n\ (16{,}237 - 7125\ \Delta T \right] \right|_0^T$$

$$t^{2}/2 = .0004975 \left[ 1n\ (17{,}819) - 1n\ (17{,}819 - 7125\ \Delta T) \right]$$

Substituting t = 5.20 Sec/60 Sec/Min = .867 Min.

$$.003758/ .0004975 = 9.7880 - 1n\ (17{,}819 - 7125\ \Delta T)$$

$$1n\ (16{,}237 - 6558\ \Delta T) = 9.7880 - 7.5538$$

$$17{,}819 - 7125\ \Delta T = 9.3390$$

$$\Delta T = 2.50^{\circ}F, \text{ which is insignificant.}$$

Condition 3 - Accelerate to 15 mph from 7.5 mph (Series Mode)

Substituting in Equation (1) similar to that just accomplished in Condition 2.

$$q = \frac{4000\,(86.63 + 221.2\,t) - (57{,}000/2)(8.011 + 20.45\,t)}{155.5} \qquad (6)$$

where: $Q = 22.5\ \text{GPM}\ (3.85 + \frac{22.5\ \text{GPM}\ (3.85)\ t}{23.50\ \text{Sec}/60\ \text{Sec/Min.}}$

$$= 86.63 + 221.2\,t$$

$$= \frac{76.5\ \text{RPM}(2\pi\ \text{Rad/Rev})}{60\ \text{Sec/Min.}} + \frac{76.5\ \text{RPM}(2\pi\ \text{Rad/Rev})}{60\ \text{Sec/min}(23.50\ \text{Sec})/60\text{Sec/Min.}}$$

$$= 8.011 + 20.45\,t$$

$$q = 25.72(86.63 + 221.2\,t) - 183.3(8.011 + 20.45\,t)$$

$$q = 760.2 + 1941\,t = 760.2(1 + 2.553\,t)$$

Substituting into EQ (2)

$$760.2\,(1 + 2.553\,t) = 86.63\,(1 + 2.553\,t)\,\gamma C\,\Delta T + V_t\,\gamma\,C\ \ d\,\Delta T/d_t$$

$$[760.2\,(1 + 2.553\,t) - 307.2\,(1 + 2.553)\,\Delta T \quad d_t = V_t\,\gamma C \quad d\,\Delta T$$

$$[2.475\,(1 + 2.553\,t) - 1 + 2.553\,t)\Delta T\,]\ d_t = .01154 \quad d\,\Delta T$$

$$[2.475(2.553)t - 2.553\,t\,\Delta T]\ \ d_t + 2.475 - \Delta T)]\,d_t = .01154\ d\Delta T$$

$$2.553\,(2.475 - \Delta T)\,t\,d\,t + (2.475 - \Delta T\ d_t = .01154\ d\,\Delta T$$

$$2.553\,t\,d\,t + d\,t = .01154\ d\,\Delta T/(2.475 - \Delta T)$$

Integrating

$$2.553\ t^2/2 + t = -.01154\ \ln(2.475 - \Delta T)\Big|_0^T$$

@ $t = 23.50\ \text{Sec}/60\ \text{Sec/Min} = .392\ \text{Min.}$

$$.5882 = -.01154\,[\ln(2.475 - \Delta T) - \ln 2.475]$$

$$50.97 = .9062 - \ln\,(2.475 - \Delta T)$$

$$-50.06 = \ln\,(2.475 - \Delta T)$$

$$2.475 - \Delta T = 1.809\ (10^{-22})$$

$\Delta T = 2.48^{\circ}\text{F}$. This is same as Cond. 2 and is a good check.

Condition 4 - Constant 15 mph for Remainder of 2.5 Mile Taxi

By substituting in Equation (1) the following,

$Q$ = 45 GPM (3.85 = 173.3 $In^3$/Sec.

$T_l$ = % Drag (W) $R_w$ = .02/42,800)16.48 = 14,107 Lb-In.

$\omega$ = 153 RPM 2 $\pi$ Rad/Rev/ 60 Sec/Min = 16.02 Rad/Sec.

$\Delta P$ = $\Delta P_m + \Delta P_s = 2\pi\ T/d_{as}\ \eta_t + \Delta P_S$ = $(2\pi 14107)/57.75(.85)+1252=3058$ psid

$q$ = 3058 (173.3) - 14,107 (16.02) /155.5 = 1955 Btu/min

$\Delta T$ = $q / Q \gamma C$ (7)

= $1955/\left[\frac{173.3}{3.85}\ (7.09)\ .5\right]$ = 12.25°F

Condition 5 - Reverse Direction for 100 Yards @ 3 mph (Parallel Mode)

Substituting as follows in Equation (1)

$Q$ = (3 mph / 15 mph) 45 GPM (2) = 18 GPM

$T_l$ = % Drag (W) $R_w$ = .02 (42,800) 16.48 = 14,107 Lb-In.

$\omega$ = (3 mph / 15 mph) 16.02 = 3.204 Rad/Sec.

$q$ = $\left[4000(18)3.85 - 14,107(3.204)\right] / 155.5$ = 1492 Btu/min

Substituting in Equation (7)

$\Delta T$ = $1492/\left[18(7.09).5\right]$ = 23.38°F

For 4 Percent Rolling Resistance

Condition 1 - Brake to 0 mph from 15 mph (Series Mode

Following the same procedure as for the 2 percent Rolling Resistance, Condition 1, the value of q = 3012 remains unchanged, but lasts t = 6.27 Sec. (Ref.: Appendix C, Pg. C-13).

Therefore,

$H$ = $\dot{q}t$ = 3012 (6.27 / 60) = 314.8 Btu

From Equation (3) using q and t just calculated and the various values as previously and integrating,

$$t = (1)\ 7.09\ (.5) \left| - 1/18(7.09).5\ [\ln 3012 - 18(7.09).5\,\Delta T] \right|_0^T$$

$$\text{or } 6.27/60 = 3.545 \left| -1/17.73\ [\ln 3012 - 17.73\ \Delta T] \right|_0^T$$

$$.105 = .20\ [\ln 3012 - \ln (3012 - 17.73\ \Delta T)]$$

$$.525 = \ln 3012 - \ln (3012 - 17.73\,\Delta T)$$

$$7.485 = \ln (3012 - 17.73\ \Delta T)$$

$$1781.8 = 3012 - 17.73\ \Delta T$$

$$17.73\,\Delta T = 12.30.2$$

$$\Delta T = 69.39^{\circ}F$$

Condition 2 - Accelerate to 7.5 mph from 0 mph (Parallel Mode)

In Equation (5), substitute

$$Q = 45\ GPM(3.85\ t\ /\ 7.55/60 = 1377\ t$$

$$\omega = 76.5\ (2\pi)\ t\ /\ 60\ (7.55)\ /\ 60 = 63.66\ t$$

So that,

$$q = [4000\ (1377\ t) - 57{,}000(63.66\ t)]\ /\ 155.5 = 12{,}086\ t$$

Substituting this value of q in Equation (2),

$$12{,}806\ t = 1377\ t\ \gamma C\,\Delta T + V\ \gamma C\ \ d\,\Delta T\ /\ dt$$

$$12{,}086\ t - 1377\ t\ \gamma C\ \Delta T = V\gamma\ C\ \ d\ \Delta T\ /\ dt$$

and

$$t\ d\ t = V\gamma\ C\ d\ \Delta T\ /\ (12{,}086 - 4881\ \Delta T)$$

Using the values of $\gamma$, C and $\Delta T$ and integrating,

$$\int_0^T t\ d\ t = 3.545 \left| - 1/4881\ [\ln (12{,}086 - 4881\,\Delta T] \right|_0^T$$

$$t^2/2 = .000726\ [\ln (12{,}086) - \ln (12{,}086 - 4881\,\Delta T)]$$

Substituting t = 7.55 / 60 = 0.126 Min.

$$.00792\ /\ .000726 = 9.3998 - \ln (12{,}086 - 4881\ \Delta T)$$

$$\ln (12{,}086 - 4881\ \Delta T) = -1.509$$

$$12{,}086 - 4881\ \Delta T = .860$$

$\Delta T = 2.4^{\circ}F$ still insignificant.

Condition 3 - Accelerate to 15 mph from 7.5 mph (Series Mode) *

From Appendix C for condition 3 @ 4 percent rolling resistance

$N_w$ = 73.85 RPM

$Q$ = (73.85/153) (45 GPM) 3.85 = 83.62 $In^3$/Sec.

$T$ = Percent Drag (W) $R_w$ = .04 (42,800) 16.48 = 28214 Lb-In.

$\omega$ = $2\pi N_w/60$ = 7.73 Rad/Sec

Substituting in Equation (1)

$q$ = $[4000 (83.62) - 28{,}214 (7.73)] /155.5$ = 748 Btu/min.

from $q = Q\gamma C\ \Delta T$, solving for $\Delta T$ and using value of $q$, $\gamma$, $C$ and $Q$,

$\Delta T$ = $748/7.09(.5)(83.62/3.85) = 9.71^{\circ}F$.

Worst Case Heating

Worst case heating will occur in stopping from 15 mph on a 4 percent aiding slope. Using the conditions of pressure loss calculated in Appendix B, the retarding force,

$F_R = T_m/16.48 - 1712$

where: $T_m = (da'/2\pi\ \eta_t)\ \Delta P = 57.75/2\pi\ (.85)\ \Delta P = 10.81\ \Delta P$

$\Delta P = 4100 + 1252\ (V/V_{MAX})^2$

$= 4100 + 1252V^2/22^2 = 4100 + 2.59V^2$

$F_R = [10.81\ (4100 + 2.59V^2)/16.48] - 1712$

$= 977.3 + 1.699V^2$

The deceleration,

$a = F_R\ g/\ W = (977.3 + 1.699V^2)\ (32.2)/42{,}800$

$a = .7353 + .001278V^2 = dv/dt$

*Condition cannot be met as shown in Appendix C because of torque saturation.

$$\int \frac{dv}{a+bV^2} = t = \frac{1}{\sqrt{ab}} \left(\tan^{-1} \frac{V\sqrt{ab}}{a}\right)$$

$$t = (1/.0307)\left[\tan^{-1} 22(.0307)/.7353\right] = 24.21 \text{ Sec.}$$

also,

$$a = vdv/dx = d(V^2)/2dx = .7353 + .001278V^2$$

Solving for dX and integrating between 0 and V

$$X = 1/.002556 \left| \ln \left[1.4706 + .002556(22^2)\right] - \ln 1.4706 \right|$$

$$X = 238.8 \text{ Ft.}$$

Average Speed = 238.8/24.21 = 9.86 Ft/Sec = 68.57 RPM = 7.18 Rad/Sec

Average Flow = (9.86/22) (173.3) = 77.67 $IN^3$/Sec.

Average Pump Flow = 5 GPM = 19.25 $IN^3$/Sec.

Average Motor Torque = 10.84 $\left[4100 + .0534(68.57)^2\right]$ = 47166 Lb-In.

From Equation (1)

$$q = \left[4000\ (19.25) + 47.166\ (7.18)\right] /155.5 = 2673 \text{ Btu/min.}$$

From Equation (4)

$$24.21/60 = .2\ \left[\ln 2673 - \ln (2673 - 17.73\ \Delta T)\right]$$

$$2.018 = \ln 2673 - \ln (2673 - 17.73\ \Delta T)$$

$$\ln (2673 - 17.73\ \Delta T) = 5.873$$

$$17.73\ \Delta T = 2317.70$$

$$\Delta T = 130.7^{\circ}F$$

Considering that this temperature increase does not consider heat transfer to the metal mass of Dynavector or wheel axle, it does not appear that heating will be a problem in dynamometer testing.

From this analysis, it is apparent that braking causes the highest heat input, but it lasts for such a short time that the heat load is low.

Consequently, the most severe heating can occur if pump saturation does not occur during high speed (15 mph) taxi conditions in the series mode.

Assuming,

$Q$ = 45 GPM (3.85) = 173.3 $In^3$/Sec.

$P_S$ = 4000 PSI

$T_l$ = 14,107 Lb-In.

$\omega$ = 16.02 Rad/Sec. (153 RPM)

From Equation (1)

$q$ = $[4000(173.3) - 14,107(16.02)]/155.5$ = 3005 Btu/min.

$\Delta T$ = $q/Q\gamma C$ = $3005/45(7.09).5$ = $18.83^{\circ}F$

The above are the anticipated heat input and temperature increase if the normal torque is developed; however, during dynamometer testing under no load or flight taxiing on a downgrade, the heat input will be,

$q$ = $4000(173.3)/155.5$ = 4458 Btu/min.

and the

$T_{MAX}$ = $4458/45(7.09).5$ = $27.94^{\circ}F$

Summary

On the basis of a thermal analysis for adiabatic conditions, the heat input and temperature increase of the fluid, assuming 5 GPM pump flow during braking, are for the following conditions as shown below:

| Cond. | Rolling Resist. | Action | Oper. Mode | Heat Input-Btu/min | Fluid Temp. Rise $^{\circ}F$ |
|---|---|---|---|---|---|
| 1 | 2% | Braking (15-0 mph) | Series | 3012 | 80 |
| 2 | 2% | Accel. (0-7.5 mph) | Parallel | 1544 | 2.5 |
| 3 | 2% | Accel. (7.5-15 mph) | Series | 1520 | 2.5 |
| 4 | (and with pump saturation) | Constant 15 mph | Series | 1955 | 12.25 |
| 5 | (and with pump saturation) | Reverse (3 mph) | Parallel | 1492 | 23.4 |
| 1 | 4% | Braking (15-0 mph) | Series | 3012 | 69 |
| 2 | 4% | Accel. (0-7.5 mph) | Parallel | 1520 | 2.5 |
| 3 | 4% | Accel. (7.5-15 mph) | Series | 748 | 9.7 |
| - | 4% Aiding | Braking (15 mph -0) | Series | 2673 | 131 * |
| - | 2% and no pump saturation | Constant 15 mph | Series | 3005 | 18.8 * |
| - | No Load | Constant 15 mph | Series | 4458 | 27.9 * |

*Conditions not required by SOW.

# APPENDIX F

## PARTS LIST

PARTS LIST

| | | | |
|---|---|---|---|
| | | The Bendix Corporation<br>Electrodynamics Division<br>North Hollywood, California | 77068 / 3311870 / B<br>CODE IDENT. NO. / SHEET 2 OF 5 / REV. |
| SPECIFICATION | TYPE - MODEL - SERIES | | ITEM ACTUATOR - POWERED WHEEL |
| GOVT. | | DATE | NEXT ASSY / USED ON |
| CONTR. | | APPR. | |
| BENDIX PRODUCT NO. | QUANTITIES SHOWN ARE NOT SUBJECT TO MULTIPLICATION WITHIN SCOPE OF THIS LIST. | | |

| ITEM NO. | SIZE | IDENTIFYING OR PART NO. | CHNG | DESCRIPTION OR PART NAME | QTY PER ASSY | LANGLEY RES. CENTER NO. | FOOT NOTE SYMBOL |
|---|---|---|---|---|---|---|---|
| | | 3311870 | | ACTUATOR POWERED WHEEL | | LE-815401A | |
| | | | | | | LE-815402A | |
| | | | | | | LE-815403A | |
| 1 | | 3311975 | | MATCH ASSY-ORBITER | 1 | LD-815404A | |
| | | 3311970 | | RING ORBITER | 1 | LE-815429B | |
| | | 3311966 | | VANE | 12 | LC-815430A | |
| | | 3311972 | | SPACER - SLEEVE | 12 | LC-815431A | |
| | | 3311967 | | HOUSING PIN ASSY | 1 | LE-815432A | |
| | | 3311952 | | SPACER | 1 | LE-815433A | |
| | | MS16555-658 | | PIN STRAIGHT | 2 | | |
| | | MS21250H06-056 | | BOLT | 12 | | |
| | | 3311945 | | HOUSING INBOARD | 1 | LE-815434D | |
| | | 3311946 | | PLATE-BRAKE ASSY | 1 | LD-815436A | |
| | | 3311944-2 | | PLATE #4 | 1 | LE-815438A | |
| | | 3311948 | | PLATE #5 | 1 | LE-815439A | |
| | | 3311949 | | PLATE #6 | 1 | LE-815440B | |
| | | 3311950 | | PLATE #7 | 1 | LE-815441A | |
| | | 3311951 | | PLATE #8 | 1 | LE-815442A | |
| | | 3311940 | | HOUSING OUTBOARD | 1 | LE-815435A | |
| | | 3311941 | | PLATE-BRAKE ASSY | 1 | LE-815437A | |
| | | 3311942 | | PLATE #1 | 1 | LE-815443A | |
| | | 3311943 | | PLATE #2 | 1 | LE-815444A | |
| | | 3311944-1 | | PLATE #3 | 1 | LE-815438A | |

SEE DWG NO. SHEET FOR ITEMS THRU

SEE DWG NO. SHEET FOR ITEMS THRU

THIS MATERIAL CONTAINS INFORMATION AFFECTING THE NATIONAL DEFENSE OF THE UNITED STATES WITHIN THE MEANING OF THE ESPIONAGE LAWS, TITLE 18, U.S.C. SECTION 793 AND 794, THE TRANSMISSION OR REVELATION OF WHICH IN ANY MANNER TO AN UNAUTHORIZED PERSON IS PROHIBITED BY LAW.

| PROJECT OR CONTR. NO. | | | |
|---|---|---|---|
| | ORIG. | K Young | 6-2-75 |
| | CHK. | Unreadable | 6-2-75 |
| | APPR. | Unreadable | 7-17-75 |

LB-815400B

CODE IDENT. NO. 77068

FORM 0130-515 1/73

F-2

PARTS LIST

| | | | | |
|---|---|---|---|---|
| | | The Bendix Corporation<br>Electrodynamics Division<br>North Hollywood, California | 77068 | 3311870 A |
| | SPECIFICATION | TYPE - MODEL - SERIES | CODE IDENT. NO. | SHEET 3 OF 5 REV. |
| GOVT. | | | ITEM ACTUATOR POWERED WHEEL | |
| CONTR. | | DATE | | |
| BENDIX PRODUCT NO. | | APPR. | NEXT ASSY | USED ON |
| | | QUANTITIES SHOWN ARE NOT SUBJECT TO MULTIPLICATION WITHIN SCOPE OF THIS LIST. | | |

| ITEM NO. | SIZE | IDENTIFYING OR PART NO. | CHNG | DESCRIPTION OR PART NAME | QTY PER ASSY | LANGLEY RES. CENTER Nº | | FOOT NOTE SYMBOL | LINE |
|---|---|---|---|---|---|---|---|---|---|
| 2 | | 3311968 | | SHAFT - OUTPUT | 1 | LE-815405A | | | 1 |
| 3 | | INA NK 95/26 | | BEARING | 1 | | | | 2 |
| 4 | | INA NK 105/26 | | BEARING | 1 | | | | 3 |
| 5 | | AR10103-396 AIH | | SEAL ASSEMBLY | 1 | | | | 4 |
| 6 | | AR10103-343 AIH | | SEAL ASSEMBLY | 1 | | | | 5 |
| 7 | | MS28775-012 | | PACKING | 6 | | | | 6 |
| 8 | | 8814-1001-0912 | | SEAL | 2 | PARKER SEAL | ALTERNATE: TVM4-2124-4 | | 7 |
| 9 | | 3311974 | | ORBITER GEAR | 1 | LD-815406A | (TETRAFLUOR INC.) | | 8 |
| 10 | | CKRA2.506005 | | CHECK VALVE | 2 | | | | 9 |
| 11 | | JETA1815900D | | ORIFICE | 1 | | | | 10 |
| 12 | | PLGA2501020 | | PLUG PIN | 1 | | | | 11 |
| 13 | | PLGA3431020 | | PLUG PIN | 2 | | | | 12 |
| 14 | | 7500-16 | | THREAD SEAL | 12 | PARKER SEAL | | | 13 |
| 15 | | MS20002C8 | | WASHER | 12 | | | | 14 |
| 16 | | 3311973 | | STUD | 12 | LD-815407A | | | 15 |
| 17 | | 3191049-2 | | NUT-SELF LOCKING | 12 | LD-815408B | | | 16 |
| 18 | | 3311969 | | PLATE DRIVE ASSY | 1 | LD-815409A | | | 17 |
| | | 3311967-1 | | PLATE MACHINE | 1 | LD-815409A | | | 18 |
| | | MS21209-F4-15 | | INSERT LOCKING | 6 | | | | 19 |
| 19 | | 3311971 | | KEY DRIVE | 6 | LD-815410A | | | 20 |
| 20 | | NAS 6514H8 | | SCREW CAP | 6 | | | | 21 |
| | | | | | | | | | 22 |
| | | | | | | | | | 23 |
| | | | | | | | | | 24 |
| | | | | | | | | | 25 |

SEE DWG NO. SHEET FOR ITEMS THRU

SEE DWG NO. SHEET FOR ITEMS THRU

THIS MATERIAL CONTAINS INFORMATION AFFECTING THE NATIONAL DEFENSE OF THE UNITED STATES, WITHIN THE MEANING OF THE ESPIONAGE LAWS, TITLE 18, U.S.C. SECTION 793 AND 794, THE TRANSMISSION OR REVELATION OF WHICH IN ANY MANNER TO AN UNAUTHORIZED PERSON IS PROHIBITED BY LAW.

PROJECT OR CONTR. NO.

| | | |
|---|---|---|
| ORIG. | R T Morey | 6-2-75 |
| CHK. | Unreadable | 9-1-75 |
| APPR. | Richard Rudd | 7-17-75 |

LB-815400A

CODE IDENT. NO. 77068

0130-515 1/73

F-3

PARTS LIST

| | | | | |
|---|---|---|---|---|
| | | The Bendix Corporation<br>Electrodynamics Division<br>North Hollywood, California | 77068 | 3311870 A |
| | | | CODE IDENT. NO. | SHEET 4 OF 5 REV. |
| SPECIFICATION | TYPE - MODEL - SERIES | | ITEM ACTUATOR POWERED WHEEL | |
| GOVT. | | DATE | NEXT ASSY | USED ON |
| CONTR. | | APPR. | | |
| BENDIX PRODUCT NO. | QUANTITIES SHOWN ARE NOT SUBJECT TO MULTIPLICATION WITHIN SCOPE OF THIS LIST. | | | |

| ITEM NO. | SIZE | IDENTIFYING OR PART NO. | CHNG | DESCRIPTION OR PART NAME | QTY PER ASSY | LANGLEY RES. CENTER NO | | FOOT NOTE SYMBOL |
|---|---|---|---|---|---|---|---|---|
| 21 | | 3311953 | | BEARING ASSY - THRUST | 1 | LO-815411A | | |
| | | 3311954 | | RACE - OUTER | 1 | LO-815445A | | |
| | | 3311955 | | RETAINER | 1 | LO-815446A | | |
| | | 3311956 | | HOUSING INNER | 1 | LO-815447A | | |
| | | 3311957 | | HOUSING OUTER | 1 | LO-815448A | | |
| | | Q-8254 | | ROLLER NEEDLE | 40 | TORRINGTON BEARING | | |
| | | MS 20427-4C10 | | RIVET | 8 | | | |
| | | ASO-28933 | | ROTOR - INNER | 1 | LO-815427A | BENDIX EC. | |
| | | MS 20427-4C12 | | RIVET | 8 | | | |
| 22 | | 3311958 | | RACE, INNER | 1 | LO-815412B | | |
| 23 | | 3311959 | | PISTON CLUTCH | 6 | LC-815413A | | |
| 24 | | 3311960 | | HOUSING PISTON | 6 | LC-815414A | | |
| 25 | | 3311961 | | RETAINER - PLUNGER | 6 | LC-815415A | | |
| 26 | | 3311962 | | PLUNGER | 6 | LC-815416A | | |
| 27 | | 3311963 | | SPRING | 6 | LC-815417A | | |
| 28 | | 3311964 | | RETAINER - SPRING | 6 | LC-815418A | | |
| 29 | | 3311965 | | HOUSING - SPRING | 6 | LC-815419A | | |
| 30 | | 5105-15-A | | WASHER - LOCK | 24 | WALDES KOHINOOR INC. | | |
| 31 | | MS28775-114 | | PACKING | 11 | | | |
| 32 | | MS28774-114 | | BACKUP | 16 | | | |
| 33 | | MS28778-12 | | GASKET | 6 | | | |
| 34 | | RS 4005 | | LOCK SPIRAL | 1 | RAMSEY (SPIROLOX) | | |

SEE DWG NO. SHEET FOR ITEMS THRU | SEE DWG NO. SHEET FOR ITEMS THRU

THIS MATERIAL CONTAINS INFORMATION AFFECTING THE NATIONAL DEFENSE OF THE UNITED STATES WITHIN THE MEANING OF THE ESPIONAGE LAWS, TITLE 18 U.S.C. SECTION 793 AND 794, THE TRANSMISSION OR REVELATION OF WHICH IN ANY MANNER TO AN UNAUTHORIZED PERSON IS PROHIBITED BY LAW.

| PROJECT OR CONTR. NO. | | | |
|---|---|---|---|
| ORIG. | R L Mong | 6-2-75 | LB-815400A |
| CHK. | [illegible] | 9-7-75 | |
| APPR. | R K [illegible] | 7-17-75 | CODE IDENT. NO. 77068 |

FORM 0130-515 1/73

F-4

PARTS LIST

| | | | |
|---|---|---|---|
| | | The Bendix Corporation<br>Electrodynamics Division<br>North Hollywood, California | 77068 3311870 |
| SPECIFICATION | TYPE - MODEL - SERIES | | CODE IDENT. NO. SHEET 5 OF 6 |
| GOVT. | | DATE | ITEM ACTUATOR POWERED WHEEL |
| CONTR. | | APPR. | NEXT ASSY USED ON |
| BENDIX PRODUCT NO. | QUANTITIES SHOWN ARE NOT SUBJECT TO MULTIPLICATION WITHIN SCOPE OF THIS LIST. | | |

| ITEM NO. | SIZE | IDENTIFYING OR PART NO. | CHNG | DESCRIPTION OR PART NAME | QTY PER ASSY | LANGLEY RES. CENTER NO | | FOOT NOTE SYMBOL |
|---|---|---|---|---|---|---|---|---|
| 35 | | | | QUILL - DRAIN | 1 | | | |
| 36 | | | | NUT | 1 | | | |
| 37 | | | | QUILL - CYL - UPPER | 4 | | | |
| 38 | | | | QUILL - CYL - LOWER | 4 | | | |
| 39 | | MS21250H09-012 | | BOLT | 4 | | | |
| 40 | | | | PIN - SHEAR | 3 | | | |
| 41 | | | | NUT - | 3 | | | |
| 42 | | AXO-28935 | | STATOR | 2 | LO-815420B | BENDIX EC | |
| | | AXO-28934 | | PLATE STATOR | 2 | LO-815421B | BENDIX EC | |
| 43 | | AXO-28936 | | ROTOR | 1 | LO-815428A | | |
| 44 | | MS20073-03-13 | | BOLT | 6 | | | |
| 45 | | MS17828-3F | | NUT | 6 | | | |
| 46 | | 3311977 | | RETAINER | 1 | LC-815423A | | |
| 47 | | 3311978 | | RETAINING RING | 1 | LC-815424A | | |
| 48 | | 3311976 | | WASHER | 1 | LC-815425A | | |
| 47 | | 3311979 | | WASHER ASSY-THRUST | 1 | LC-815426A | | |
| 50 | | AXO-28937 | | PLATE-BACKING | 1 | LO-815422A | BENDIX EC | |
| 51 | | MS24391C4 | | PLUG | 4 | | | |
| 52 | | MS28778-4 | | GASKET | 4 | | BENDIX EC | |
| 53 | | M9048-262 | | PIN-SLOTTED SPRING | 6 | | | |
| 54 | | MS16555-625 | | PIN | 1 | | | |

SEE DWG NO. SHEET FOR ITEMS THRU

SEE DWG NO. SHEET FOR ITEMS THRU

THIS MATERIAL CONTAINS INFORMATION AFFECTING THE NATIONAL DEFENSE OF THE UNITED STATES WITHIN THE MEANING OF THE ESPIONAGE LAWS, TITLE 18, U.S.C. SECTION 793 AND 794. THE TRANSMISSION OR REVELATION OF WHICH IN ANY MANNER TO AN UNAUTHORIZED PERSON IS PROHIBITED BY LAW.

| PROJECT OR CONTR. NO. | | | |
|---|---|---|---|
| ORIG. | [signature] | 6-2-75 | LB-815400E |
| CHK. | [signature] | 6-7-75 | |
| APPR. | [signature] | 7-17-75 | CODE IDENT. NO. 77068 |

FORM 0130-515 1773

F-5

# APPENDIX G

## REPORT 7-3266 RUN-IN, STATIC AND CYCLIC TEST PLAN

## REPORT 7-3267 DYNAMOMETER TEST PLAN

THIS DOCUMENT CONTAINS PROPRIETARY INFORMATION, AND SUCH INFORMATION MAY NOT BE DISCLOSED TO OTHERS FOR ANY PURPOSE NOR USED FOR MANUFACTURING PURPOSES WITHOUT WRITTEN PERMISSION FROM THE BENDIX CORPORATION.

APPLICATION

| NEXT ASSY | USED ON |
|---|---|
| | |

REVISIONS

| LTR | DESCRIPTION | DATE | APPROVED |
|---|---|---|---|
| A | Removed load torque as a recorded parameter under 5.2.1(b). Also, change load torque to $\Delta P$ under 5.2.2. Also deleted torque recording under 5.2.3, sheet 7.<br>Deleted output shaft torque under 6.1, sheet 8.<br>Deleted torque cell from output shaft in Fig. 1, Sheet 10.<br>Added drawing No. X98609 to para. 2.3(b), sheet 3 and to para. 5.2, sheet 6. | 5/3/76 | RKL |

| REV STATUS OF SHEETS | A | | A | | | A | A | A | | A | | | | | | | | | | | | | | | | | | |
|---|---|---|---|---|---|---|---|---|---|---|---|---|---|---|---|---|---|---|---|---|---|---|---|---|---|---|---|---|
| | 1 | 2 | 3 | 4 | 5 | 6 | 7 | 8 | 9 | 10 | 11 | 12 | 13 | 14 | 15 | 16 | 17 | 18 | 19 | 20 | 21 | 22 | 23 | 24 | 25 | 26 | 27 | 28 |

RELEASE STATUS
- ☐ UNLIMITED
- ☐ LIMITED
- ☐ DEVELOPMENTAL
- ☒ EXPERIMENTAL

MATERIAL

CONTRACT NO.

| | | |
|---|---|---|
| PREPARED | VAHAUSDAC | 5/19/75 |
| CHECKED | | |
| ENGINEER | RKLindell | 5/19/75 |
| APPROVED | [illegible] | 5/20/75 |
| APPROVED | | |

The Bendix Corporation
Electrodynamics Division
North Hollywood, California

# RUN-IN, STATIC AND CYCLIC TEST PLAN - POWERED WHEEL DRIVE ACTUATOR

| SIZE | CODE IDENT NO. | DWG NO. |
|---|---|---|
| A | 77068 | REPORT 7-3266 |

SCALE | WT | SHEET 1 OF 10

FORM 320A REV FEB. 1970

TABLE OF CONTENTS


| | | SHEET NO. |
|---|---|---|
| 1.0 | TEST PLAN PURPOSE | 3 |
| 2.0 | TEST LOG DOCUMENTATION | 3 |
| 3.0 | PERFORMANCE DISCREPANCY | 4 |
| 4.0 | ENVIRONMENTAL CONDITIONS | 4 |
| 5.0 | TEST REQUIREMENTS | 4 |
| 5.1 | Preliminary Tests | 4 |
| 5.2 | Static and Cyclic Tests | 6 |
| 6.0 | TEST FACILITY REQUIREMENTS | 8 |
| 6.1 | Instrumentation | 8 |
| 6.2 | Servovalve | 8 |
| 6.3 | Test System Characteristics | 8 |
| 6.4 | Filtration | 9 |
| 6.5 | Test Arrangement | 9 |
| FIGURE 1 - TEST ARRANGEMENT | | 10 |

## 1.0 TEST PLAN PURPOSE

This test plan defines the room temperature run-in, static and cyclic testing of the Wheel Drive DYNAVECTOR Assembly, P/N 3311870. The functional tests will be conducted at Bendix Electrodynamics Division prior to dynamometer testing of the unit at the Energy Controls Division pursuant to Dynamometer Test Plan - Powered Wheel Drive Actuator, Report 7-3267.

## 2.0 TEST LOG DOCUMENTATION

A log shall be compiled for the actuator test program containing the following..

### 2.1 Title Page

Static Test Log, Powered Wheel Drive Actuator

P/N 3311870, S/N _____

Job No. 05745040

### 2.2 Table of Contents

### 2.3 Section 1.0, Equipment

Specify the following as applicable documents:

a) Test Assembly, Actuator, Powered Wheel, Drawing 3311870.

b) Test Fixture Assembly, Drawing X98609

### 2.4 Section 2.0, Inspection Reports

All inspection reports relative to the assembly components are to be compiled in this section. These reports shall clearly define any discrepancies, dispositions, and subsequent acceptance.

### 2.5 Section 3.0, Calibration Data

List test equipment used and provide appropriate calibration data. Include a torque vs. displacement calibration for the torsilastic load spring.

2.6 Section 4.0, Performance Data

All data and observations pertaining to the run-in characteristics and static and cyclic performance of the test assembly and equipment shall be contained in this section.

3.0 PERFORMANCE DISCREPANCY

Failure of the test assembly to perform satisfactorily or consistently shall be reported to the responsible engineer. Tests shall be discontinued pending further instructions.

4.0 ENVIRONMENTAL CONDITIONS

All testing shall be conducted between +50°F and +110°F ambient using MIL-H-5606 hydraulic fluid at a temperature of +70°F to +110°F.

5.0 TEST REQUIREMENTS

5.1 Preliminary Tests

For this series of tests, the test unit shall not be installed on the test fixture assembly. Prior to performance of the following tests, the test unit shall be examined to determine conformance with applicable drawings.

5.1.1 Breakaway Torque: With all ports open and upward and the unit filled with hydraulic fluid, back drive the actuator with a torque wrench adapter on the output shaft. Measure the torque to start the shaft rotating in at least four positions, approximately 90° apart. Also rotate the shaft through several revolutions to make sure the shaft rotates freely and there are no rough spots.

5.1.2 Break-in Run ($P_{c1} > P_{c4}$): With motor ports C2 and C3 interconnected, apply $P_{c1} - P_{c4}$ pressure differential sufficient to cause the output shaft to rotate at 10 RPM. Run the test assembly for at least 1/2-hour. Record $P_{c1} - P_{c4}$ and output shaft speed at the beginning and at the end of the run. The case drain port shall be open to atmosphere during this test and the leakage collected and returned to tank.

5.1.3 Break-in Run ($P_{c4} > Pcl$): Repeat paragraph 5.1.2 above with a $P_{c4} - Pcl$ pressure differential to produce a reverse shaft rotation.

5.1.4 Leakage and Proof Tests

5.1.4.1 C1, C2, C3 and C4 Proof and Leakage: With the motor ports (4) pressurized from a common source (hereinafter referred to as Ps), measure case leakage. Since this is also a proof test, take appropriate precautions to protect personnel in the event of a rupture. Case drain pressure is to be one atmosphere. No external leakage is allowed other than at the shaft seals (2). The test assembly shall be maintained at a given value of Ps for a sufficient period of time (but not less than two minutes) to permit enough fluid to be collected and to provide accurate quantity measurement. Measure and record housing diameter and over-all assembly length prior to test. Measure and record leakage from the case drain port for Ps = 500, 2000, 4000, and 6000 PSIG.

5.1.4.2 Outboard Seal Leakage: With all motor ports blocked, position the test assembly with the shaft vertical and the spline end down. Collect leakage from the outboard seal for case drain pressures of 100, 300 and 500 PSIG.

5.1.4.3 Inboard Seal Leakage: Repeat paragraph 5.1.4.2 with the test assembly inverted to collect the inboard seal leakage.

5.1.4.4 Inspection: Take measurements of the actuator diameter and over-all length and compare with the values recorded prior to proof testing to insure that external distortion or permanent set has not occurred.

5.1.5 Breakaway Torque Recheck: Repeat paragraph 5.1.1 and if results are the same, proceed with paragraph 5.1.6.

5.1.6 Break-in Run ($P_{c1} > P_{c4}$): Repeat paragraph 5.1.2 and if results agree with 5.1.2, proceed with paragraph 5.1.7.

5.1.7 Break-in Run ($P_{c4} > P_{c1}$): Repeat paragraph 5.1.3 and if results agree with 5.1.3, proceed with paragraph 5.1.8.

5.1.8 Disassembly and Inspection: Disassemble the test assembly and visually inspect parts to determine if there has been any distortion, permanent set, damage, or excessive wear. Particular attention should be directed to the assembly bolt lengths and the condition of the commutation plates and orbiter surfaces.

5.1.9 Reassembly and Test: After appropriate action is taken as a result of paragraph 5.1.8, reassemble the test unit. Repeat paragraphs 5.1.1 through 5.1.4.1 (case drain leakage only at Ps = 4000). If results agree with the original values, proceed with paragraph 5.1.10.

5.1.10 Flow Loss Test: By varying supply pressure, slowly increase output shaft speed in the CW direction until 153 RPM is attained. At maximum speed, measure and record actuator flow and C1, C2, C3 and C4 motor pressures. Repeat the test for CCW rotation.

5.2 Static and Cyclic Tests

For these tests, the test assembly shall be installed on the P/N X98609 test fixture assembly that is capable of applying loads up to 80,000 lb-inch at ± 30 degrees output shaft displacement (nominal spring rate of 2667 lb-in/degree). All functional tests shall be conducted with 4000 PSIG supply pressure and 75 PSIG return pressure,unless otherwise specified in a test arrangement as illustrated in Figure 1, and the valves A-C in the parallel mode unless otherwise specified.

5.2.1 Cyclic Displacement: The actuator shall be sinusoidally cycled under load for a minimum of two hours at the following specified conditions:

a) Cycle the actuator 0.5 hour at a frequency of 3.0 HZ and an output amplitude of ± 2 degrees about zero load position.

b) Cycle the actuator 1.5 hours at a frequency of 0.5 HZ and an output amplitude of ± 20 degrees about zero load position.

During cyclic testing, strip record the following parameters at the start and finish of each condition:

. Actuator Flow

. Actuator Differential Pressure

. Actuator Position

. Servovalve Input Current

5.2.2 Displacement Plot: Conduct an X-Y plot of actuator displacement vs. $\Delta P$ at a frequency of .05 HZ or less.

5.2.3 Stall Torque/Case Drain Leakage

Record output displacement and case drain leakage at a constant 4000 PSI differential ($P_{c1} - P_{c4}$ and $P_{c4} - P_{c1}$). At maximum displacement in each direction, measure and record case drain leakage.

5.2.4 Stall Torque/Case Drain Leakage (Series Mode)

Repeat paragraph 5.1.3 with the actuator cylinder lines connected for series operation.

## 6.0 TEST FACILITY REQUIREMENTS

In addition to the fixture of paragraph 5.0, the test facility shall provide..

### 6.1 Instrumentation

Instrumentation shall be provided to monitor and/or record:

a) Actuator motor pressures (50 - 4000 PSIG -- 4 places)

b) Case drain pressure (150 PSIG max.)

c) Output shaft displacement (± 24 degrees max.)

d) Cyclic rate (3 HZ max.)

d) Actuator flow rate (6 GPM max. with load and 45 GPM with no load)

### 6.2 Servovalve

An electrohydraulic servovalve shall be used for controlling actuator velocity.

The valve no-load flow capability shall be a minimum of 10 GPM at 1000 PSI $\Delta$P.

### 6.3 Test System Characteristics

Fluid---------- MIL-H-5606

Fluid Temperature---------- +70°F to +110°F

Ambient Temperature---------- Room

Total Flow-

Unloaded---------- 45 GPM Max.

Loaded---------- 6 GPM Max.

Supply Pressure-

Operating---------- 4000 PSIG Nom.

Proof---------- 6000 PSIG

Return Pressure---------- 75 PSIG Nom.

6.3 Test System Characteristics (Continued)

Actuator Displacement

Unloaded---------- Continuous Rotation

Loaded---------- ± 24 Degrees Max.

Case Drain Pressure---------- 150 PSIG Maximum

Fluid Contamination Control---------- IAW BEPS 1.008, Type II

6.4 Filtration

Supply fluid shall be filtered through a 10-micron pleated paper element filter.

6.5 Test Arrangement

A test circuit and power supply shall be provided as illustrated in Figure 1.

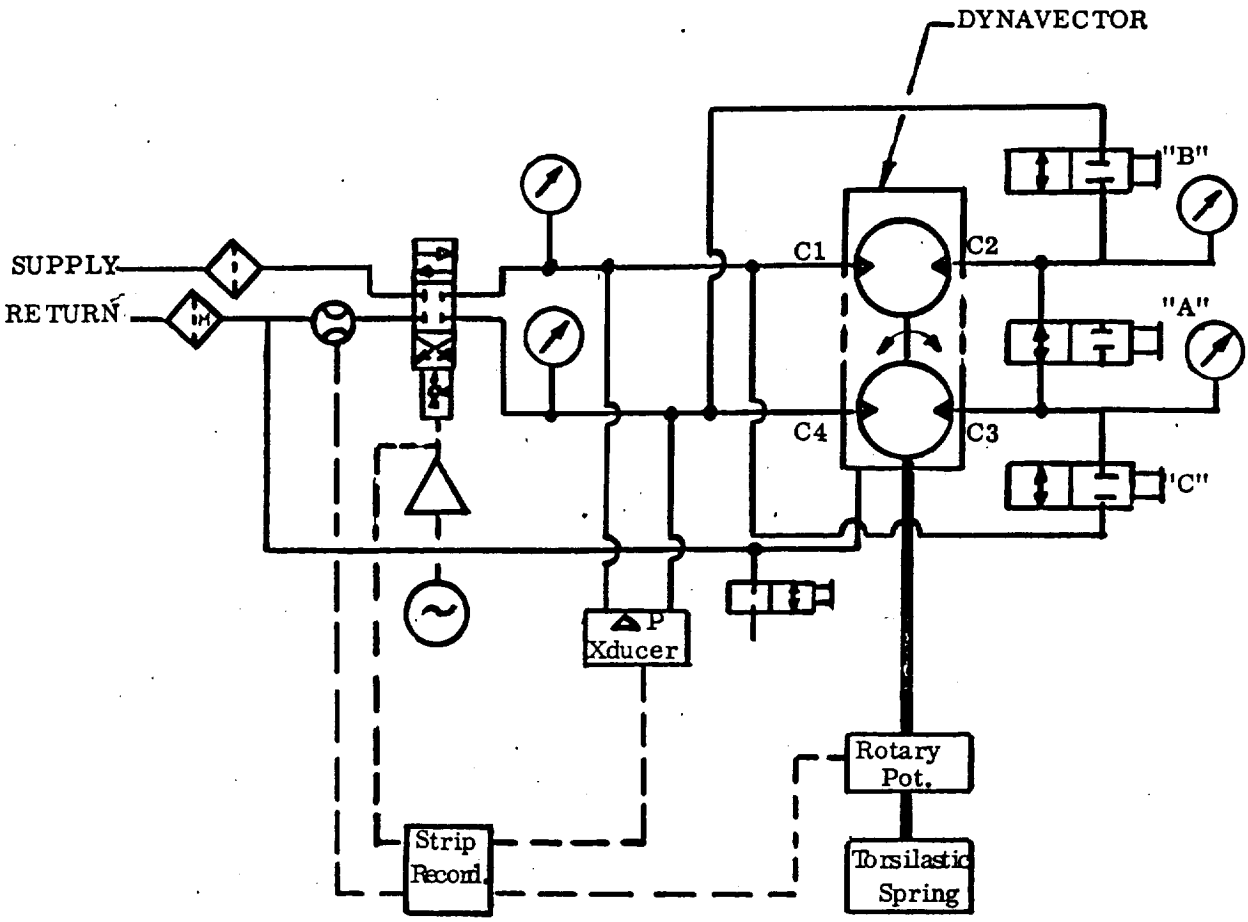


NOTES:
1. Valves A-C shown for series mode operation. For parallel operation, switch all three valves.
2. Valves A-C may be replaced by the displacement changing valve.
3. Operating pressures for supply and return shall be 4000 ± 25 PSIG and 75 ± 25 PSIG, respectively.
4. Hydraulic fluid shall be MIL-H-5606.

FIGURE 1. TEST ARRANGEMENT

| CODE IDENT NO. 77068 | DWG. NO. REPORT 7-3266 |
|---|---|
| | Rev. A SHEET 10 |

THIS DOCUMENT CONTAINS PROPRIETARY INFORMATION, AND SUCH INFORMATION MAY NOT BE DISCLOSED TO OTHERS FOR ANY PURPOSE NOR USED FOR MANUFACTURING PURPOSES WITHOUT WRITTEN PERMISSION FROM THE BENDIX CORPORATION.

APPLICATION

| NEXT ASSY | USED ON |
|---|---|
| | |

REVISIONS

| LTR | DESCRIPTION | DATE | APPROVED |
|---|---|---|---|
| A | Added (series mode) following conditions 4L and 4T on sheet 6.<br>Added drawing numbers to paragraph 9.4, Sheet 10.<br>Added "DSCV" and "DCV" call-outs to Fig. 1, Sheet 11. | 5/12/76 | RKVdP |

| REV STATUS | A | | | | | A | | | | A | A | | | | | | | | | | | | | | | | | |
|---|---|---|---|---|---|---|---|---|---|---|---|---|---|---|---|---|---|---|---|---|---|---|---|---|---|---|---|---|
| OF SHEETS | 1 | 2 | 3 | 4 | 5 | 6 | 7 | 8 | 9 | 10 | 11 | 12 | 13 | 14 | 15 | 16 | 17 | 18 | 19 | 20 | 21 | 22 | 23 | 24 | 25 | 26 | 27 | 28 |

RELEASE STATUS
- ☐ UNLIMITED
- ☐ LIMITED
- ☒ DEVELOPMENTAL EXPERIMENTAL

MATERIAL

CONTRACT NO.

| | | |
|---|---|---|
| PREPARED | R.K. Vanderveldt | 5/13/75 |
| CHECKED | | |
| ENGINEER | R.K. VanderVeldt | 5/23/75 |
| APPROVED | R. Clark | 5/27/75 |
| APPROVED | | |

The Bendix Corporation
Electrodynamics Division
North Hollywood, California

Preceding Page Blank

# DYNAMOMETER TEST PLAN
# POWERED WHEEL DRIVE ACTUATOR

| SIZE | CODE IDENT NO. | DWG NO. |
|---|---|---|
| A | 77068 | REPORT 7-3267 |

SCALE | WT | SHEET 1 OF 12

## TABLE OF CONTENTS


| | | SHEET NO. |
|---|---|---|
| 1.0 | TEST PLAN | 3 |
| 2.0 | TEST LOG DOCUMENTATION | 3 |
| 3.0 | PERFORMANCE DISCREPANCY | 4 |
| 4.0 | ENVIRONMENTAL CONDITIONS | 4 |
| 5.0 | TEST REQUIREMENTS | 4 |
| 5.1 | Preliminary Tests (No-Load) | 4 |
| 5.2 | Statement of Work Test Cycle | 5 |
| 6.0 | POST-DYNAMOMETER FUNCTIONAL TESTS | 8 |
| 6.1 | Breakaway Torque | 8 |
| 6.2 | Leakage | 8 |
| 6.3 | Outboard Seal Leakage | 8 |
| 6.4 | Inboard Seal Leakage | 8 |
| 7.00 | POST-FUNCTIONAL TEST INSPECTION | 9 |
| 8.0 | REASSEMBLY AND TEST | 9 |
| 9.0 | TEST FACILITY REQUIREMENTS | 9 |
| 9.1 | Instrumentation | 9 |
| 9.2 | Requirements | 10 |
| 9.3 | Test Arrangement | 10 |
| 9.4 | Dynamometer and Associated Fixtures | 10 |
| FIG. 1 - TEST ARRANGEMENT | | 11 |
| TABLE 1 - DYNAMOMETER TEST SCHEDULE | | 12 |

## 1.0 TEST PLAN

This test plan defines the room temperature dynamometer testing of the Wheel Drive DYNAVECTOR Assembly, P/N 3311870. The dynamometer tests will be conducted at Bendix Energy Controls Division pursuant to the Statement of Work (SOW) of NASA-Langley Research Center Contract, NAS1-13787, following run-in, static and cyclic tests conducted at Electrodynamics Division pursuant to Report 7-3266.

## 2.0 TEST LOG DOCUMENTATION

A test log shall be compiled for the actuator test program containing the following:

### 2.1 Title Page

Dynamometer Test Log, Powered Wheel Drive Actuator

P/N 3311870, S/N _____

### 2.2 Table of Contents

### 2.3 Section 1.0, Equipment

Specify the following as applicable documents:

a) Test Assembly, Actuator, Powered Wheel, Drawing 3311870.

b) Test Arrangement, Drawing TBD

c) Actual Equipment List

### 2.4 Section 2.0, Calibration Data

List test equipment used and provide appropriate calibration data.

### 2.5 Section 3.0, Performance Data

All data and observations pertaining to the characteristics and performance of the test assembly and equipment shall be contained in this section.

3.0 PERFORMANCE DISCREPANCY

Failure of the test assembly to perform satisfactorily or consistently shall be reported to the responsible engineer. Tests shall be discontinued pending further instructions.

4.0 ENVIRONMENTAL CONDITIONS

All testing shall be conducted between +50°F and +110°F ambient using MIL-H-6083C hydraulic fluid at a temperature of +70°F to +110°F.

5.0 TEST REQUIREMENTS

5.1 Preliminary Tests (No-Load)

For this series of tests, the test assembly shall be installed on the Energy Controls Division's test mandrel (Ref.: Test Arrangement illustrated in Fig. 1) with all clutch components included. However, no dynamometer loading shall be imposed during this series of tests.

5.1.1 Run-in Test ($P_{CA} > P_{CB}$): With the displacement changing valve (DCV) in the series mode configuration, apply $P_{CA} - P_{CB}$ pressure differential sufficient to cause the output shaft to rotate at 10 RPM. Run the test assembly for at least one-half hour. Record $P_{CA} - P_{CB}$ and output shaft speed at the beginning and end of the run.

5.1.2 Run-in Test ($P_{CB} > P_{CA}$): Repeat paragraph 5.1.1 with a $P_{CB} - P_{CA}$ pressure differential to produce a reverse shaft rotation.

5.1.3 Actuator Maximum Speed Run ($P_{CA} > P_{CB}$): With the DCV in the series mode configuration, apply a $P_{CA} - P_{CB}$ pressure differential slowly until shaft rotation speed reaches 153 RPM. At 153 RPM, measure and record $P_{CA} - P_{CB}$.

5.1.4 Actuator Maximum Speed Run ($P_{CB} > P_{CA}$): Repeat paragraph 5.1.3 with a $P_{CB} > P_{CA}$ pressure differential.

5.1.5 Dynamometer Maximum Speed Run: With the system shut-off valve closed and actuator pressures $P_{CA}$ and $P_{CB}$ equal to zero, increase dynamometer speed slowly and verify that the clutch remains disengaged (no actuator rotation) up to the maximum dynamometer speed of 165 mph.

5.1.6 Displacement Changing Function: With the DCV in the parallel mode configuration, apply $P_{CA} - P_{CB}$ pressure differential sufficient to cause the output shaft to rotate at 76.5 RPM. Record PC1 - PC2, PC3 - PC4, $P_{CA} - P_{CB}$ and output shaft speed; then switch the DCV to the series mode configuration. Record PC1 - PC4, $P_{CA} - P_{CB}$ and output shaft speed after stabilization is reached.

5.1.7 Relief Valve Function: With the directional and speed control valve (D and SCV) in the neutral position, the system shut-off valve open, the DCV in the series mode and system pressure at 4000 PSIG, apply dynamometer torque slowly (to back drive the actuator) and observe $|P_{CB} - P_{CA}|$. The relief valve shall switch to the relief mode at $|P_{CA} - P_{CB}| = 4100 \pm 50$ PSIG.

5.1.8 Actuator Maximum Braking $\Delta P$: With the same conditions as paragraph 5.1.7, increase dynamometer speed to 153 RPM or until $|PC4 - PC1|$ equals 4100 PSIG plus the $\Delta P$ recorded in paragraph 5.1.4. Record speed, $|PC4 - PC1|$, $|P_{CB} - P_{CA}|$ and torque.

5.2 Statement of Work Test Cycle

Pursuant to the Statement of Work (SOW), paragraph 3.5.2, Test Envelope, the typical actuator use cycle shall consist of the following conditions:

Landing - Accelerate simulated wheel to 165 mph, slow to 0 mph, engage specified drag, accelerate to 15 mph, activate wheel drive system and engage clutch.

5.2 Statement of Work Test Cycle (Continued)

Condition 1L-Brake to 0 mph from 15 mph (series mode)

Condition 2L-Switch DCV and accelerate to 7.5 mph from 0 mph (parallel mode)

Condition 3L-Switch DCV and accelerate to 15 mph from 7.5 mph (series mode)

Condition 4L-Constant 15 mph speed for remainder of 2.5 mile taxi (series mode)

Condition 1L-Brake to 0 mph from 15 mph (series mode)

Unloading / Loading - Pause and cool for specified interval.

Condition 5T-Reverse direction for 100 yards @ 3 mph (parallel mode)

Condition 2T-Switch DCV and accelerate to 7.5 mph from 0 mph (parallel mode)

Condition 3T-Switch DCV and accelerate to 15 mph from 7.5 mph (series mode)

Condition 4T-Constant 15 mph speed for remainder of 2.5 mile taxi (series mode)

Take-off - Deactivate wheel drive system and disengage clutch, slow to 0 mph, disengage drag, accelerate to 165 mph, slow to 0 mph, pause and cool for specified interval.

The foregoing represents a complete test cycle and shall be performed with a dynamometer drag simulating a grade resistance of 2% or 4% as specified in Table 1. Six complete cycles (as specified in Table 1) shall be performed to demonstrate performance of the actuator in the speed range below 15 mph and to demonstrate freedom from clutch interference at higher speeds. The remainder of the ninety-four test cycles will not include the landing and take-off portions unless test results dictate otherwise.

5.2 Statement of Work Test Cycle (Continued)

During each specified test cycle, the wheel drive hydraulic supply pressure shall be regulated to 4000 ± 25 PSIG and the return pressure regulated to 75 ± 25 PSIG. Strip recordings of the following test parameters shall be made for the first twenty test cycles indicated in Table 1:

- Actuator Torque
- Dynamometer Speed
- Supply-Pressure, $P_{CA}$ or $P_{CB}$
- Return Pressure, $P_{CB}$ or $P_{CA}$
- Motor Chamber Pressure, PC1
- Motor Chamber Pressure, PC2
- Motor Chamber Pressure, PC3
- Motor Chamber Pressure, PC4
- Fluid Inlet Temperature
- Fluid Return Temperature
- System Return Flow Rate
- Motor Case Drain Fluid Temperature

For the remaining eighty test cycles, only the following test parameters shall be continuously recorded:

- Actuator Torque
- Dynamometer Speed
- Supply Pressure
- Return Pressure
- Inlet Fluid Temperature
- Return Fluid Temperature
- Motor Case Drain Fluid Temperature
- System Return Flow Rate

## 6.0 POST-DYNAMOMETER FUNCTIONAL TESTS

Upon completion of dynamometer testing and preliminary approval of the test results by the responsible engineer, the test assembly shall be functionally tested pursuant to the Run-in, Static, and Cyclic Test Plan, Report No. 7-3266, to the extent shown below.

### 6.1 Breakaway Torque

With all ports open and upward and the unit filled with hydraulic fluid, back drive the actuator with a torque wrench adapter on the output shaft. Measure the torque to start the shaft rotating in at least four positions, approximately 90° apart. Also, rotate the shaft through several revolutions to make sure the shaft rotates freely and there are no rough spots.

### 6.2 Leakage

With all motor ports (4) pressurized from a common source (hereinafter referred to as $P_S$), measure case leakage. Case drain pressure is to be one atmosphere. Note any external leakage other than at the two shaft seals. The test assembly shall be maintained at a given value of $P_S$ for a sufficient period of time (but not less than two minutes) to permit enough fluid to be collected and to provide accurate quantity measurement. Record leakage from the case drain port for $P_S$ = 500, 2,000 and 4,000 PSIG.

### 6.3 Outboard Seal Leakage

With the motor ports blocked, position the test assembly with the shaft vertical and the spline-end down. Collect leakage from the outboard seal for case drain pressures of 100, 300, and 500 PSIG.

### 6.4 Inboard Seal Leakage

Repeat paragraph 6.3 with the test assembly inverted to collect inboard seal leakage.

## 7.0 POST-FUNCTIONAL TEST INSPECTION

Upon completion of functional testing and preliminary approval of test results by the responsible engineer, the test assembly shall be visually inspected externally for signs of wear and damage and appropriate photographs made as an aid in recording the signs. The test assembly shall then be disassembled and inspected to evaluate component wear. Appropriate measurements and photographs shall be used to substantiate and record component wear or damage.

## 8.0 REASSEMBLY AND TEST

After appropriate action is taken as a result of paragraph 7.0, reassemble the test unit. Repeat paragraphs 6.2 - 6.4. If the results agree with those of paragraphs 6.2 - 6.4, prepare the unit for delivery to the customer.

## 9.0 TEST FACILITY REQUIREMENTS

### 9.1 Instrumentation

Instrumentation shall be provided to continuously record:

a) Actuator Torque

b) Dynamometer Speed

c) Supply Pressure

d) Return Pressure

e) Motor Pressure, PC1

f) Motor Pressure, PC2

g) Motor Pressure, PC3

h) Motor Pressure, PC4

i) Fluid Inlet Temperature

j) Fluid Return Temperature

k) System Return Flow Rate

l) Motor Case Drain Fluid Temperature

9.2 Requirements

| | |
|---|---|
| Fluid: | MIL-H-6083C |
| Fluid Temperature: | +70°F to +120°F |
| Ambient Temperature: | Room |
| Maximum Flow: | 45 GPM |
| Supply Pressure: | 4000 PSIG Nominal |
| Return Pressure: | 75 PSIG Nominal |
| Case Drain Pressure: | 150 PSIG Maximum |
| Fluid Contamination Control: | NAS1638, Class 5 or Better |
| System Cooling Capability: | 4500 Btu/min for 20-second intervals and 3000 Btu/min for 10-minute intervals. |

9.3 Test Arrangement

A test circuit, pressure gauges, and power supply shall be provided as illustrated in Figure 1.

9.4 Dynamometer and Associated Fixtures

| | |
|---|---|
| Dynamometer Type: | Shaft |
| Flywheel/Clutch Drive Adapter: | Drawing SXE-4490 |
| Test Mandrel and Spacer: | Drawings SXE-4488 and SXC-4489 |
| Dynamometer Inertia | 2513 Slug-$Ft^2$ |
| Drag (Simulated Grade Resist.): | 14,124 to 28,248 Lb-In. |
| Max. Dynamometer Shaft Speed: | 1681 RPM |
| Max. Test Unit Output Torque: | 57,000 Lb-In. |

TABLE 1 - DYNAMOMETER TEST SCHEDULE

| TEST CYCLE NO. | INCLUSIVE SOW TEST CONDITIONS REF. PARA. 5.2 | DATA RECORDING REQMNTS. REF. PARA. 5.2 | % DRAG |
|---|---|---|---|
| 1 THRU 5 | LANDING THROUGH TAKE-OFF | ALL 12 PARAMETERS | 2 |
| 6 THRU 10 | COND. NO. 1L THRU COND. NO. 4T | ALL 12 PARAMETERS | 4 |
| 11 THRU 50 | | ALL EXCEPT MOTOR CHAMBER PRESSURES | 2 |
| 51 THRU 90 | | ALL EXCEPT MOTOR CHAMBER PRESSURES | 4 |
| 91 THRU 95 | | ALL 12 PARAMETERS | 2 |
| 96 THRU 99 | | ALL 12 PARAMETERS | 4 |
| 100 | LANDING THROUGH TAKE-OFF | ALL 12 PARAMETERS | 4 |

Preceding Page Blank

| SIZE | CODE IDENT NO. | DWG NO. |
|---|---|---|
| A | 77068 | REPORT 7-3267 |
| SCALE | REV | SHEET 12 |

# APPENDIX H

## TESTING BASED ON RECOMMENDATION NO. 2

## APPENDIX H

### TEST RESULTS OBTAINED FROM IMPLEMENTATION OF RECOMMENDATION NO. 2

#### GENERAL

Prior to the issuance of this report, it was decided to implement Recommendation No. 2. This implementation consisted of the fabrication of a new Orbiter Ring, P/N 3331954, which differed from the original P/N 3311970 (LE 815429) only in that the commutation porting lands separation was reduced from 0.8140 - 0.8144 to 0.7904 - 0.7900 in. for a total decrease of 0.024 in. normally (reference Figure 84). Also, as part of the implementation, six cams, P/N 3331997, were fabricated to replace six of the P/N 3311972, Spacers, as shown in Figures 85 and H-1.

The reduction of the distance between the commutation metering lands, as explained in Recommendation No. 2, was made to compensate for the commutation metering slot erosion that had occurred. The addition of the cams, also discussed in the same recommendation, was a means of preventing distortion of the Orbiter Ring, which is believed to be the cause of gear disengagement. Although the cams would in effect stiffen the Orbiter Ring, their use was only a convenience for proof and not a final solution, because of the friction imposed by their use. For a future design the Orbiter Ring stiffness must be increased as addressed in Recommendation No. 3 of the basic report.

#### Test Results/Conclusions

The Wheel Drive test unit using the new parts was assembled as shown in Figures 19-25 and installed in the load test set-up as shown in Figure 29. During assembly it was found that it was necessary to reduce the outside diameter of the cams from 0.8110 in. to 0.800 in. to allow the Orbiter Ring to orbit freely.

Results of the testing are shown by Figures H-2 through H-4. As can be seen from the test results, only two test conditions were evaluated. The two conditions were two applied torque values for the stud nuts that control the

Test Results/Conclusions (cont'd)

running clearances between the Orbiter Ring and the Outboard Housing and the Orbiter Ring and the Inboard Housing. The first test run was conducted with 30 lb-in torque on every other of the twelve studs (those containing the original Spacers, P/N 3311972) while the nuts on the other six studs containing the cams were torqued only to 15 lb-in. The second test run was made with an increase of stud nut torque from 30 to 50 lb-in, while maintaining 15 lb-in torque (the highest that prevented excessive breakout torque) on stud nuts for motor chambers containing cams 5.

Figure H-2 shows the torque developed by only one motor, both in the CW and CCW directions. Only one motor was to be used in the beginning, since it was believed discrepancies in the new Orbiter Ring would affect the other motor adversely. The discrepancies were errors in machining which in effect nullified the reduction in the distance between the commutation porting lands for two of the six chambers of one motor and partially nullified the decrease for another chamber. Two things are noteworthy in Figure H-2. First, the output torque developed is better in the CW direction for both values of applied stud nut force and, second, the output torque is better for the lower stud nut torque. The difference in developed output torque may have favored the lesser stud nut loading (which was the first test condition) because of damage that was later discovered and shown in Figures H-5 through H-10.

The reason the stud nut torque was increased was because of excessive case drain leakage as shown in Figure H-3. Note that the leakage was greater in the CCW direction, (the direction with the lower output torque) especially for the higher stud nut torque.

Figure H-4 shows a replot of Figure H-2 with the CW and CCW results averaged for both stud nut torque conditions. Even this unfavorable evaluation

Test Results/Conclusions (cont'd)

indicates a 45 to 55 percent torque efficiency. Although still considerably less than the desired 85 percent, the results are 100 percent improvement over previous results. Besides the improvement in output torque achieved, even with an excessive case drain leakage, the gear mesh did not separate. Although the testing was not sufficient to dispel all doubts, the results do suggest that the stiffening of the Orbiter Ring provided by the six orbiter cams may have prevented mesh separation.

Figures H-5 through H-10 show the damage that was discovered when disassembly was undertaken to relocate the cams from one motor to the other. Damage was so extensive that further testing was considered unproductive. As can be seen, damage occurred in four distinct areas on the Outboard Housing metering surface and three places on the Inboard Housing surface. Corresponding damage occurred on the Orbiter Ring. Three of the four areas on the Outboard Housing surface coincided with those on the Inboard Housing suggesting too much Hertzian stress in these areas, even though the stud nuts were torqued equally for a given motor.

As a result of the damage sustained, it is concluded that the single test assembly fabricated cannot be used for further testing.

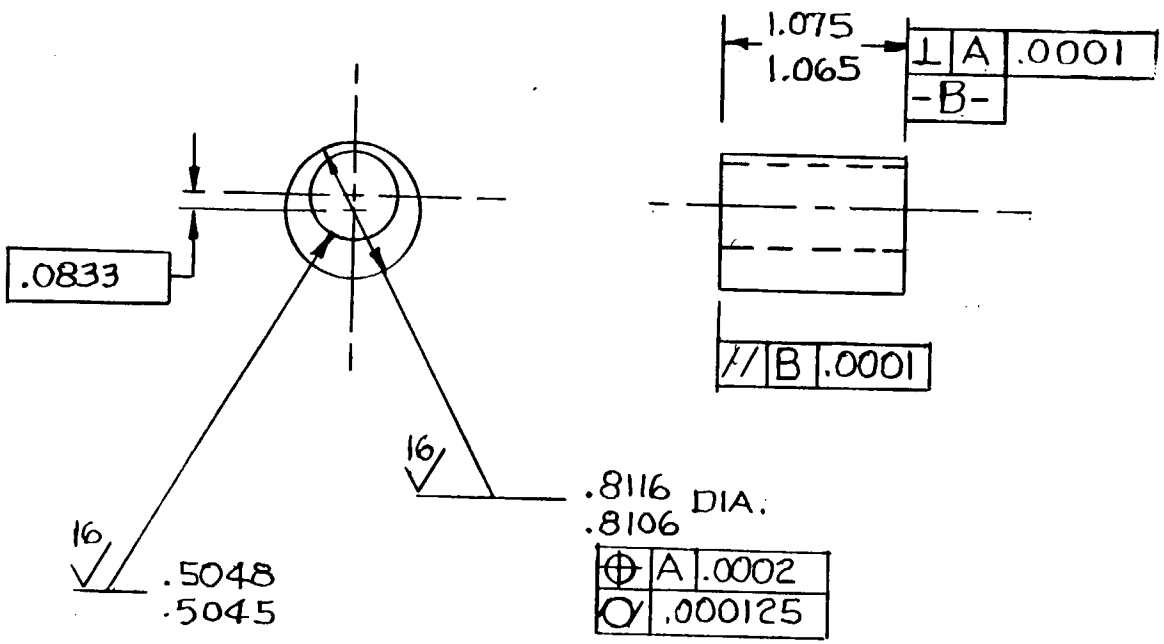


MAT'L: PHOS. BRONZE IAW B139 ALLOY NO. C54400 TEMPER H04 OR ALUM BRONZE IAW ASTM B169 ALLOY NO. 61000 TEMPER H04.

FIGURE H-1 ORBITER CAM
P/N 3331997

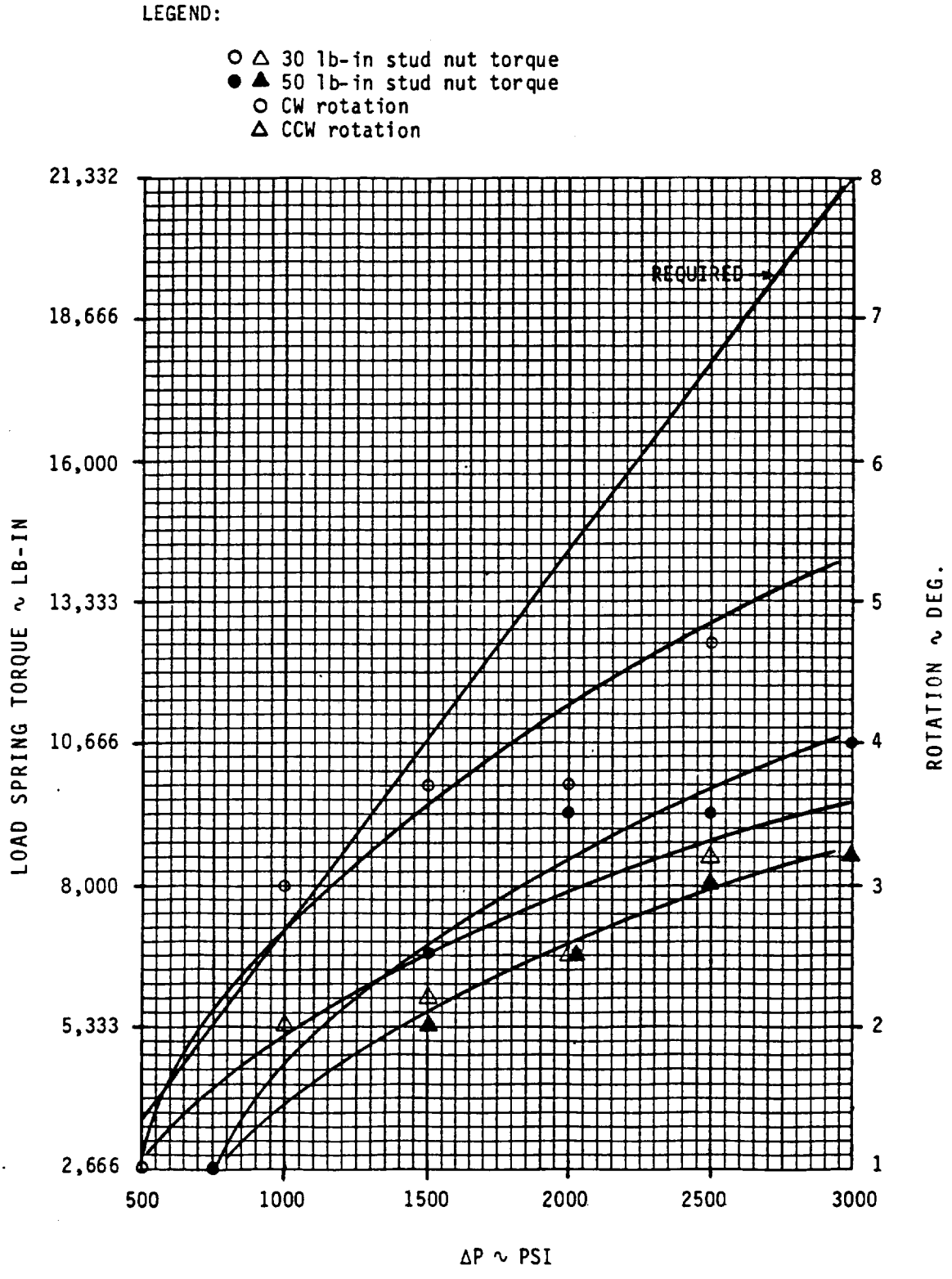


FIGURE H-6 - OUTPUT TORQUE (CW & CCW) VS. DIFFERENTIAL PRESSURE

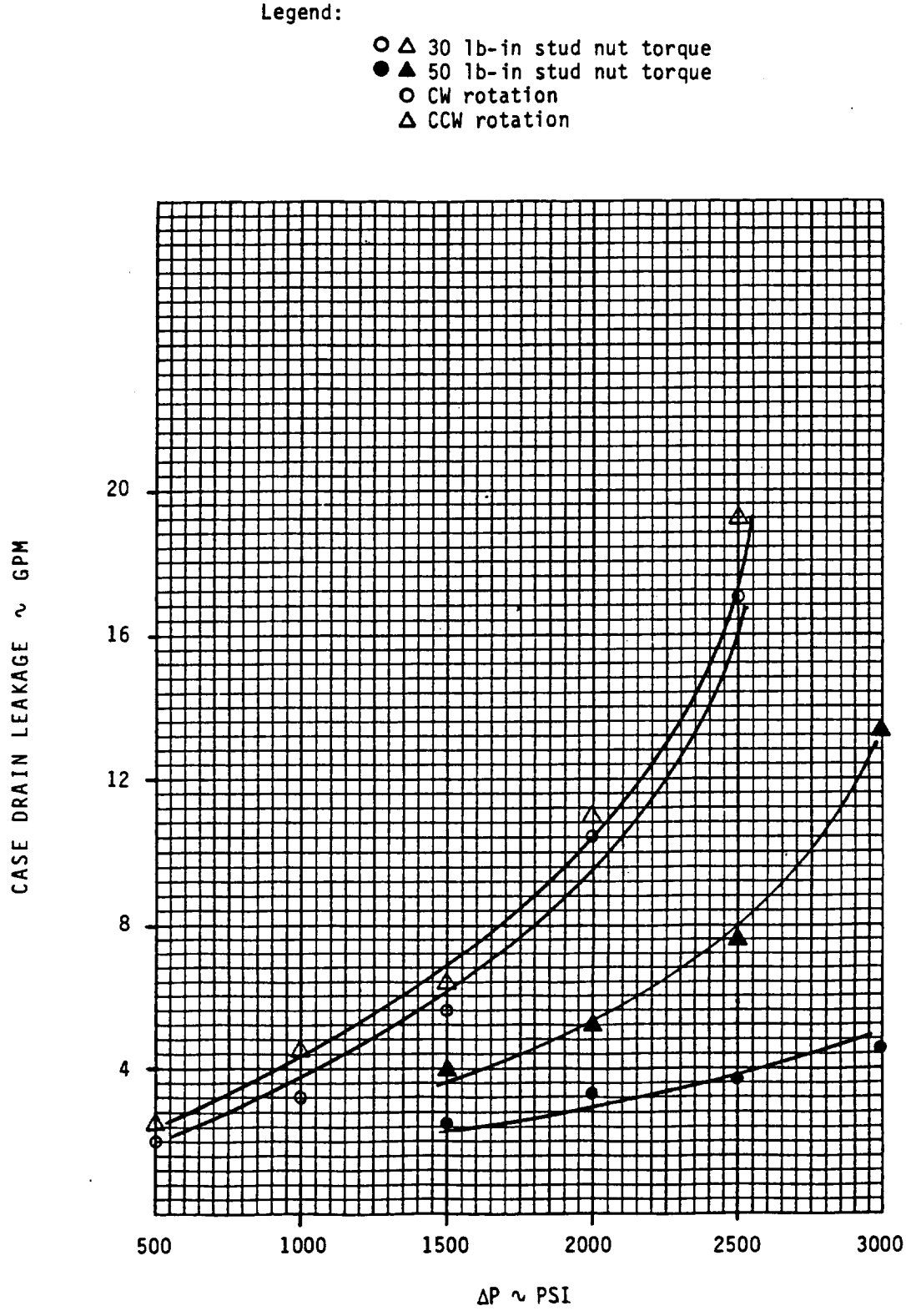


FIGURE H-3 - CASE DRAIN LEAKAGE VS. DIFFERENTIAL PRESSURE

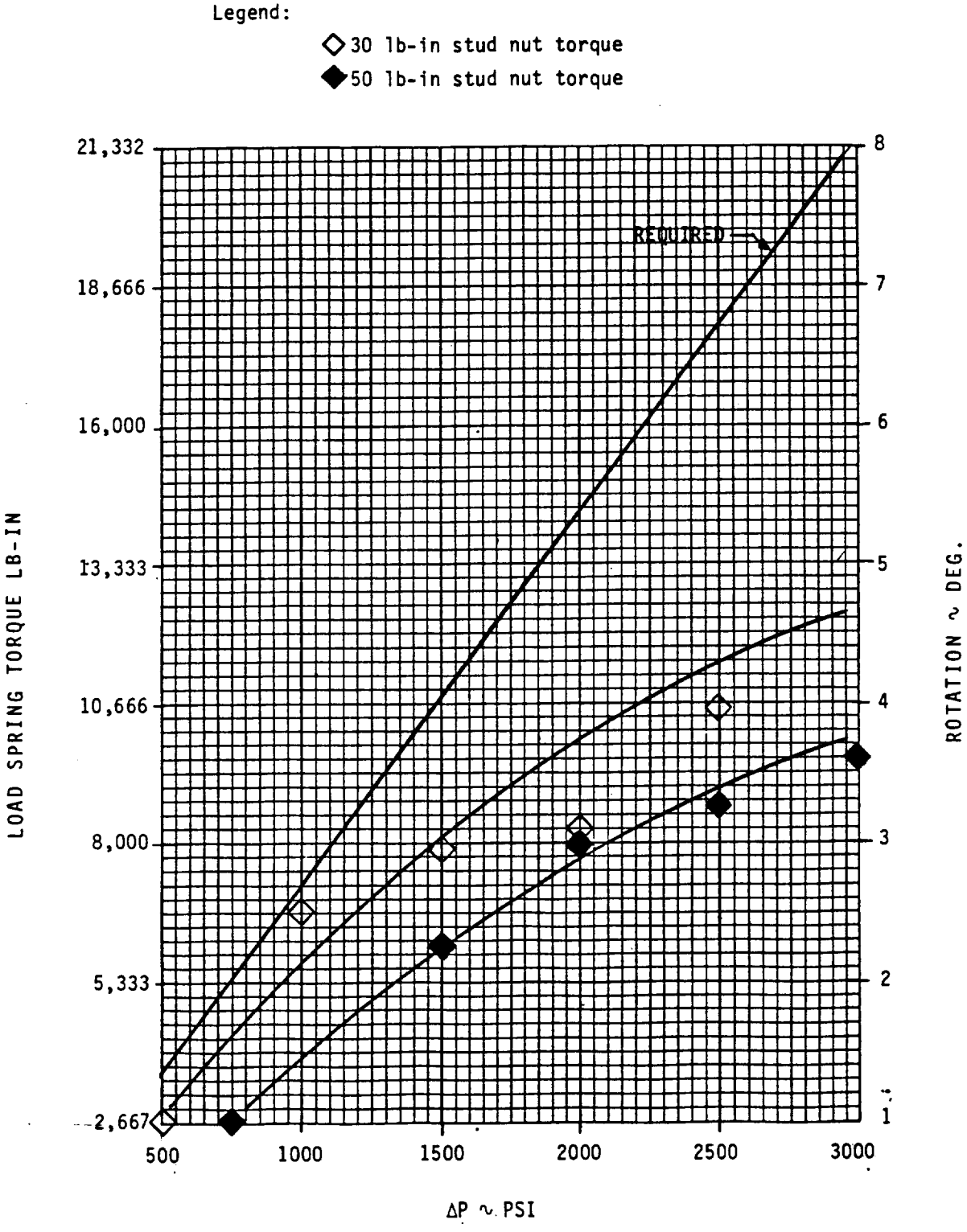


FIGURE H-4 - AVERAGE OUTPUT TORQUE DIFFERENTIAL PRESSURE

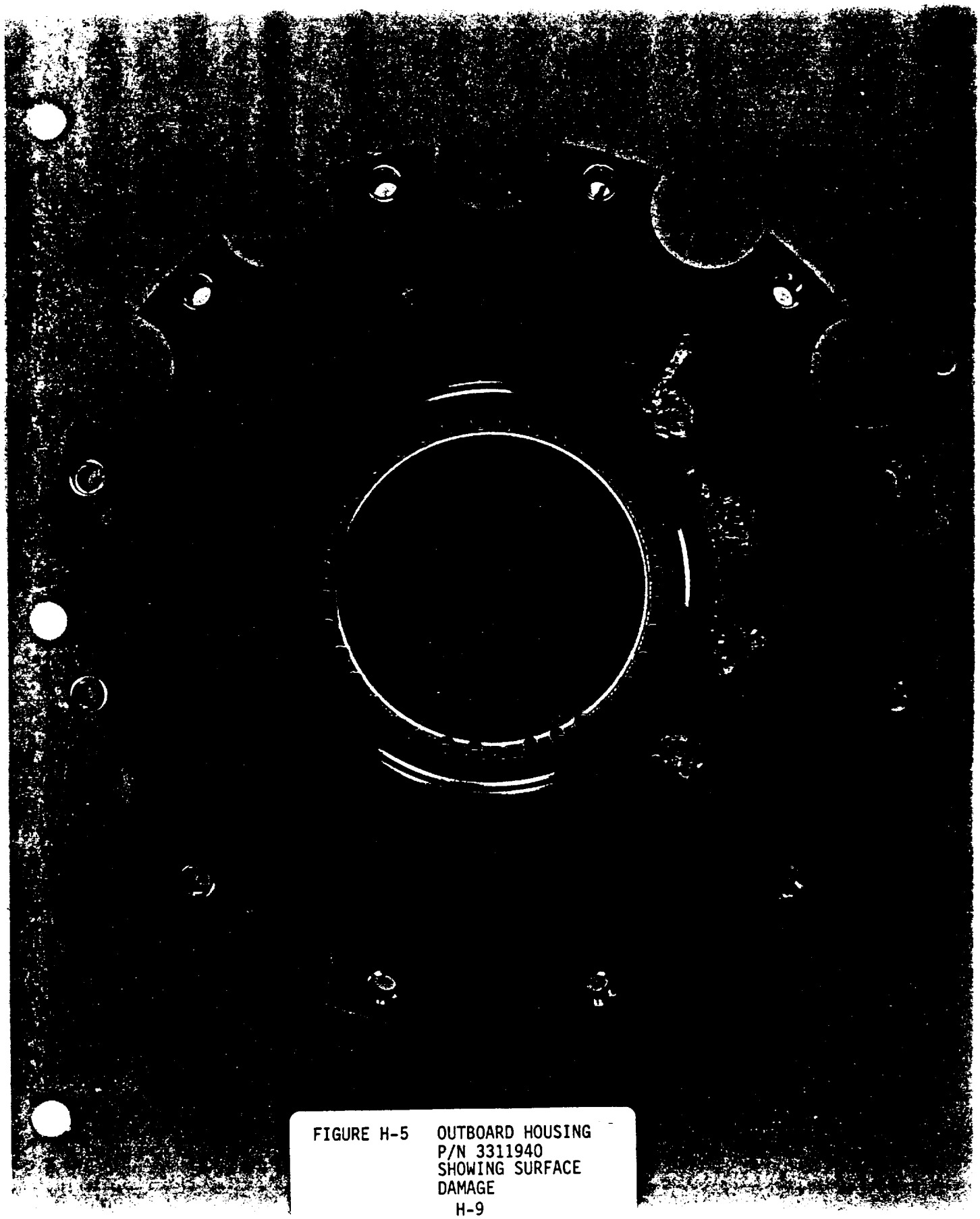

FIGURE H-5 OUTBOARD HOUSING P/N 3311940 SHOWING SURFACE DAMAGE

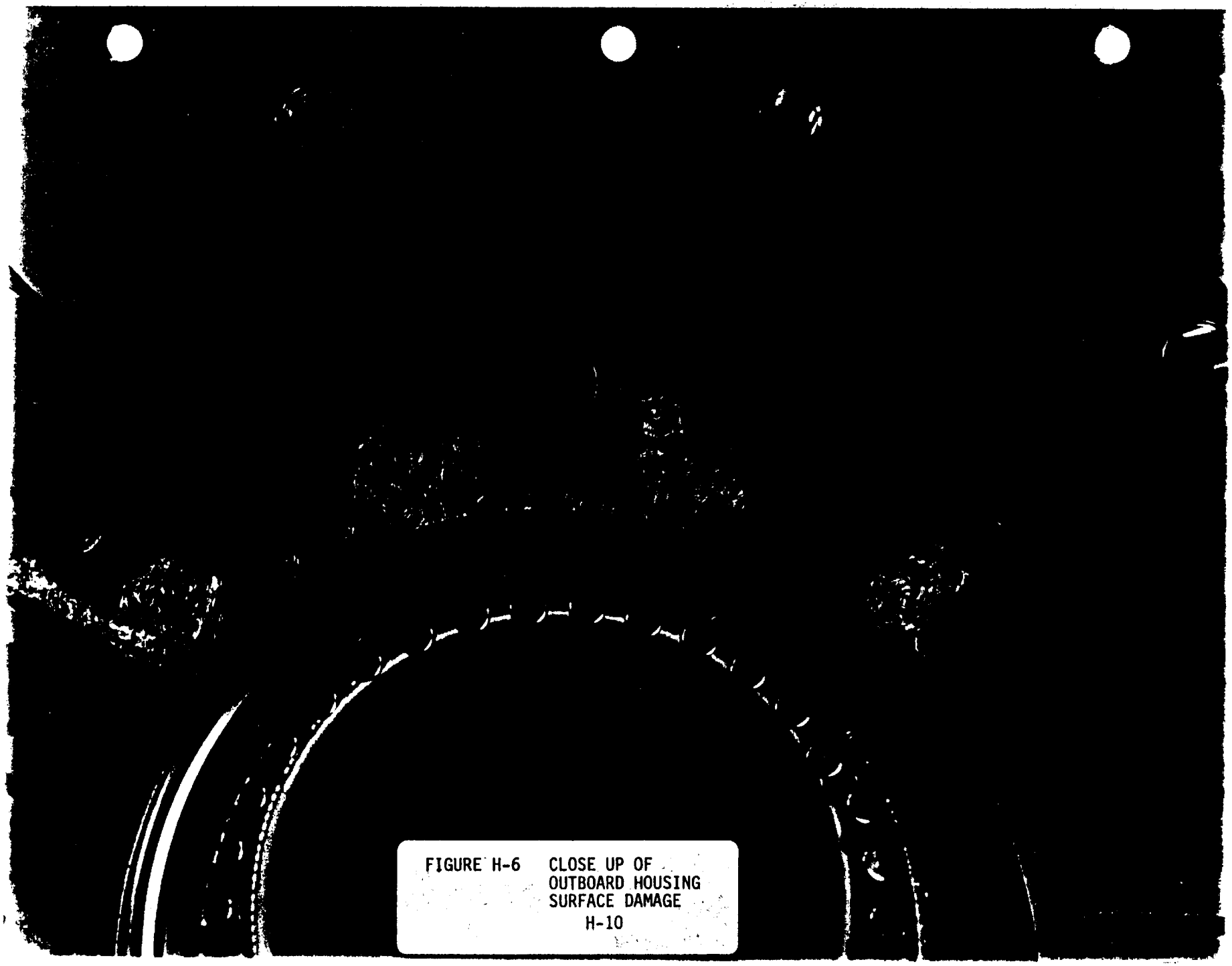

FIGURE H-6 CLOSE UP OF OUTBOARD HOUSING SURFACE DAMAGE

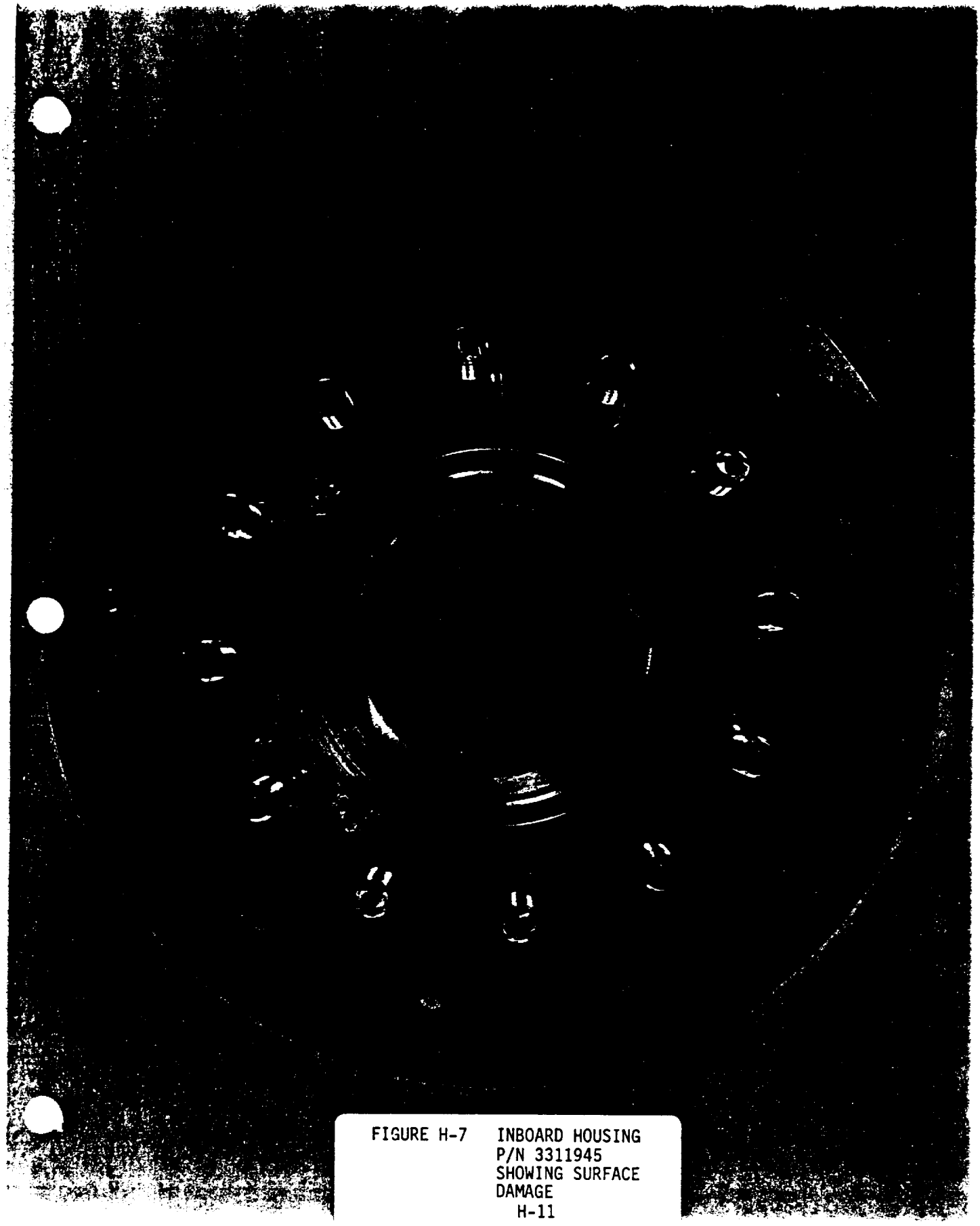

FIGURE H-7 INBOARD HOUSING P/N 3311945 SHOWING SURFACE DAMAGE

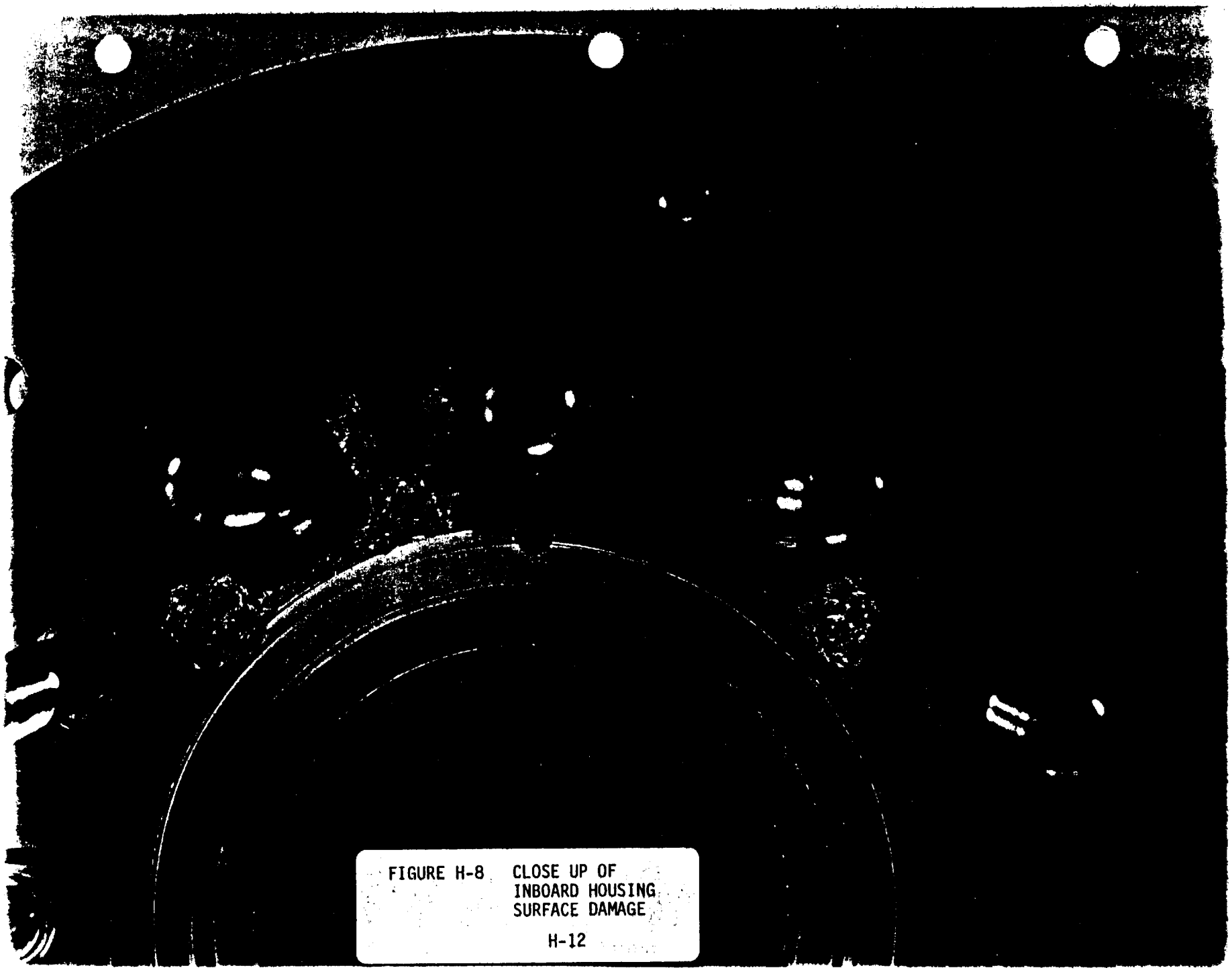

FIGURE H-8 CLOSE UP OF INBOARD HOUSING SURFACE DAMAGE

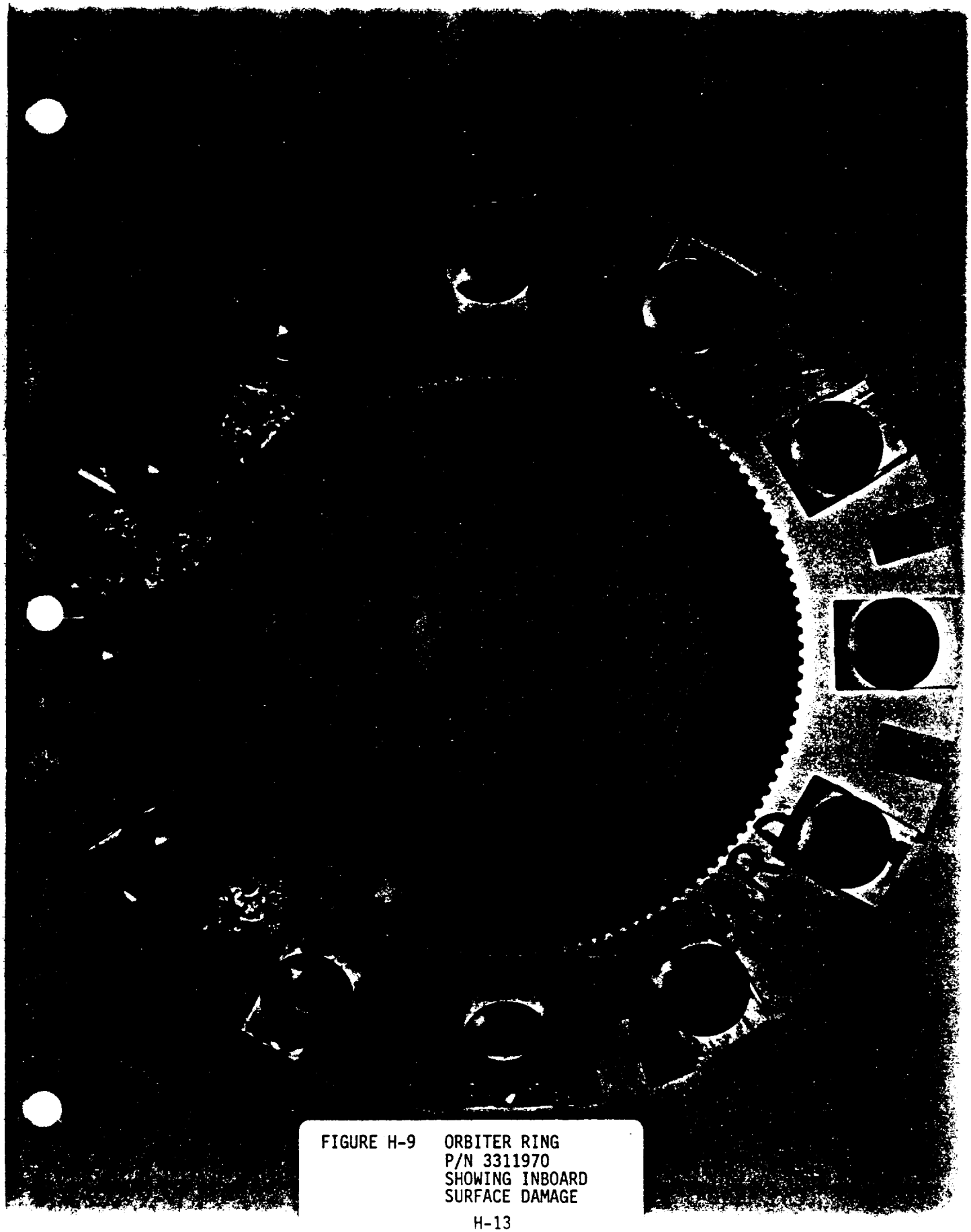

FIGURE H-9 ORBITER RING
P/N 3311970
SHOWING INBOARD
SURFACE DAMAGE

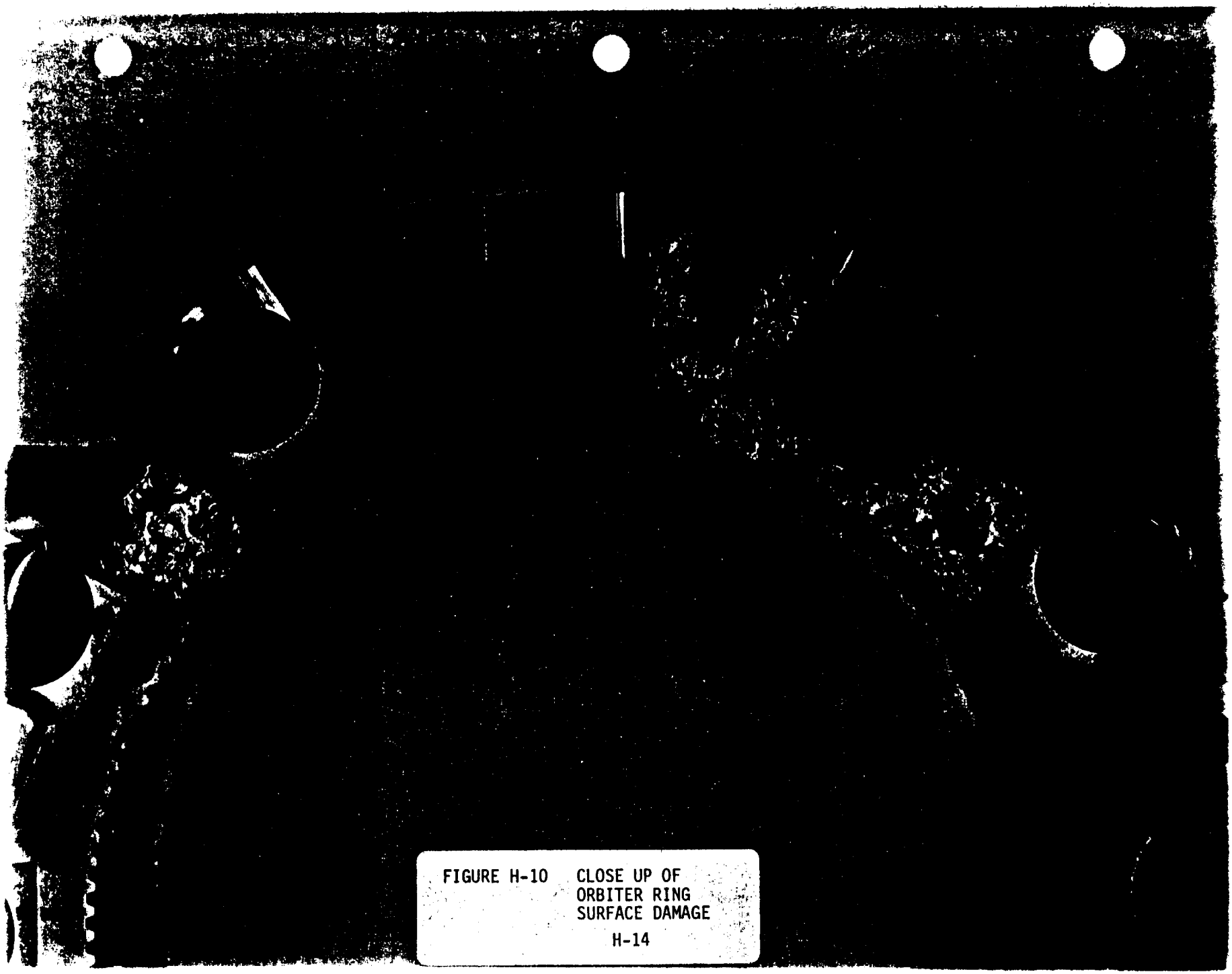

FIGURE H-10 CLOSE UP OF ORBITER RING SURFACE DAMAGE

## REFERENCES


1. Waterman, A. W.: "Energy Conservation Via Airplane Powered Wheels. SAE Paper 751177 Presented at Oct. 8, 1975 Meeting of Committee A-6, Aerospace Fluid Power and Control Technologies (Palm Springs, CA)
2. "Hydraulic Motor Wheels; Aircraft Ground Wheel." British Patent 1290501 issued to Hawker Siddeley Aviation Ltd., Oct. 13, 1969.
3. "Landing Gear Wheel Drive System for Aircraft." Patent applied for by Application No. 208693, Assignee - Curtiss-Wright Corp., Dec. 16, 1971.
4. "Aircraft Wheel Powering Device." United States Patent 3059712 issued to Charles F. Hautau, Oct. 23, 1962.
5. "Airplane Power Dolley." United States patent 3150734 issued to Anderson Dugger, Jr., Sept. 29, 1964.
6. Verge, K. W.; Read, R. G.; and Sikora, N. L.: "Investigation of Rotary Actuation Technique," Air Force Aero Propulsion Laboratory Technical Report AFAPL - TR - 70 - 52, Sept. 1970.
7. Yeaple, F. D.: "Hydraulic and Pneumatic Power and Control," McGraw-Hill Book Co.
8. Roark, R. J.: "Formulas for Stress and Strain," McGraw-Hill Book Co., 1954, Art. 75.
9. Verge, K. W.; Read, R. G.; and Sikora, N. L.: "Investigation of Rotary Actuation Technique," Air Force Aero Propulsion Laboratory Technical Report AFAPL-TR-70-52, Sept. 1970, Appendices J, K, L.
10. Roark, R. J.: "Formulas for Stress and Strain," McGraw-Hill Book Col, 1954, Table XIV, Case 6.
11. Mordkowitz, Aui: "Predicting Service Life for Zero Wear," Machine Design, Vol. 46, No. 1, Jan 10, 1974.

## REFERENCES (Continued)


12. Bayer, R. G.; Shalkey, A. T.; and Wayson, A. R.: "Designing for Zero Wear," Machine Design, Vol.41, No. 1, Jan. 9, 1970.

13. "Military Standardization Handbook - Metallic Materials and Elements for Aerospace Vehicle Structures." Department of Defense MIL-HDBK-5B, Sept. 1971.

14. Moyer, C. A. and McKelvey, R. E.: "A Rating Formula for Tapered Roller Bearings," SAE Paper No. 569B, Sept. 1962.

15. Harold A. Rothbart, Editor-in Chief, Mechanical Design and Systems Handbook, McGraw-Hill Book Co., 1964, Table 12.4.

16. Plastics/Elastomers Reference Issue, Machine Design, Feb. 11, 1971, Pg. 20, Table 4.

17. "Military Standardization Handbook - Metallic Materials and Elements for Aerospace Vehicle Structures," Dept. of Defense MIL-HDBK-5, Vol 1, Table 2.3.1.0 (a - c) and 2.3.1.1.8 (b - d).

18. Monthly Technical Report 7-3273, The Bendix Corp., Electrodynamics Division, July 1975, Contract No. NAS 1-13787, Appendix L.

19. March, 1976, 7-3304 MTR

20. April, 1976, 7-3306 MTR

21. June, 1976, 7-3310 MTR

22. July, 1976, 7-3314 MTR

23. August, 1976, 7-3316 MTR

24. October, 1976, 7-3328 MTR

25. November, 1976, 7-3332 MTR

26. December, 1976, 7-3336 MTR

27. January, 1976, 7-3340 MTR

## REFERENCES (Continued)


28. Roark, "Formulas for Stress and Strain, 3rd Edition, pg. 156.

29. Kenneth E. Binns, "Life Test of a Dynavector Rotary Actuator for Aircraft Hydraulic Systems," Air Force Aero Propulsion Laboratories, Vechicle Power Branch, Aerospace Power Division Report AFAPL-TR-76-58, Oct. 1976.

30. Mark Twyman, "Test of an Electrohydraulic Digital Actuator for Advanced Missle Programs," Aero Propulsion Laboratories, Power Systems Branch, Aerospace Power Division Report AFWAL-TR-80-2001, Feb. 1980.

31. October, 1977, 7-3366 MTR

32. D. R. Cooper and S. R. Bluhm, "Servovalve Spool and Sleeve Material Evaluation," Bendix Electrodynamics Division Report 7-2632, November 1969.